University of Alberta

# Hydrogeological characterization of the Weyburn $CO_2$ project area and Gradient-free inverse conditioning of heterogeneous aquifer models to hydraulic head data

by

K. Daniel Khan ©

A dissertation submitted to the Faculty of Graduate Studies and Research in partial fulfillment of the requirements for the degree of Doctor of Philosophy

Department of Earth and Atmospheric Sciences

Edmonton, Alberta

Fall 2006

Library and
Archives Canada

Published Heritage
Branch

395 Wellington Street
Ottawa ON K1A 0N4
Canada

Bibliothèque et
Archives Canada

Direction du
Patrimoine de l'édition

395, rue Wellington
Ottawa ON K1A 0N4
Canada

*Your file   Votre référence*
*ISBN: 978-0-494-23053-4*
*Our file   Notre référence*
*ISBN: 978-0-494-23053-4*

NOTICE:
The author has granted a non-exclusive license allowing Library and Archives Canada to reproduce, publish, archive, preserve, conserve, communicate to the public by telecommunication or on the Internet, loan, distribute and sell theses worldwide, for commercial or non-commercial purposes, in microform, paper, electronic and/or any other formats.

The author retains copyright ownership and moral rights in this thesis. Neither the thesis nor substantial extracts from it may be printed or otherwise reproduced without the author's permission.

AVIS:
L'auteur a accordé une licence non exclusive permettant à la Bibliothèque et Archives Canada de reproduire, publier, archiver, sauvegarder, conserver, transmettre au public par télécommunication ou par l'Internet, prêter, distribuer et vendre des thèses partout dans le monde, à des fins commerciales ou autres, sur support microforme, papier, électronique et/ou autres formats.

L'auteur conserve la propriété du droit d'auteur et des droits moraux qui protège cette thèse. Ni la thèse ni des extraits substantiels de celle-ci ne doivent être imprimés ou autrement reproduits sans son autorisation.

---

In compliance with the Canadian Privacy Act some supporting forms may have been removed from this thesis.

While these forms may be included in the document page count, their removal does not represent any loss of content from the thesis.

Conformément à la loi canadienne sur la protection de la vie privée, quelques formulaires secondaires ont été enlevés de cette thèse.

Bien que ces formulaires aient inclus dans la pagination, il n'y aura aucun contenu manquant.

Canada

# ABSTRACT

**I.** Pressures and hydraulic heads indicate mostly lateral flow through aquifers in the Weyburn Project area in the north-central Williston Basin. The wide range of TDS (<5 to >350 g/L) is a result of mixing between Ca-SO4 water of meteoric origin, high salinity Na-Cl brines, and hypersaline Ca-Na-Cl brines. The Watrous Fm. separates the deep aquifer systems from a shallow active hydrogeologic system. The Weyburn Field is a good site to store CO2 from a hydrogeological perspective.

New insights and interpretations with respect to the hydrogeology of the Williston Basin include: (1) The absence of Ca-Cl brine compositions in the Mississippian invokes the debated hypothesis of secular variation of global seawater chemistry through geological time; (2) Patterns of brine migration suggest the occurrence of paleo-hydraulic gradients significantly higher than those observed at present; and (3) The oil reservoirs along the Mississippian subcrop are likely not filled to capacity. The anhydritic seal rock facies underlying the subcrop likely failed hydraulically during periods of elevated paleo-fluid pressures.

**II.** The gradient-free calibration method works without the need for expensive or technically-involved computations of sensitivity coefficients of hydraulic head to model grid block permeability. A simple and effective approximation procures a matrix of sensitivity indicators as a substitute for the computation of the Jacobian matrix. Formulation of the minimization problem is based on an approximation of the gradient of the model response with respect to the parameters.

The gradient-free method solves the inversion problem in a similar manner as proven gradient-based calibration methods, but with a straightforward and transparent approach. As a result, some key points are elucidated with respect to inverse conditioning to head data. A calibration data point "samples" a heterogeneity feature when it occurs along a flowline that intersects the feature. The permeability field is adjusted only within sensitive areas, seeding locally-precise permeability perturbations, resulting in consistent identification of key heterogeneities and a corresponding improvement in local precision from conditioning stochastic permeability field realizations to head data.

# ACKNOWLEDGEMENT

I wholeheartedly thank my supervisor, Ben Rostron, for his support throughout my time at the University of Alberta. His generous and trusting support for my endeavors, tempered by enough advisory concern to keep me in check, was invaluable. His enthusiasm as a teacher resulted in my time with him being a continuous learning experience.

The selfless support and guidance I received from the other members of my supervisory committee are also duly acknowledged:

Clayton V. Deutsch encouraged me to exceed myself. He was motivational and inspirational, and he set the standard.

Carl A. Mendoza was always willing to share his extensive knowledge on Hydrogeology, Engineering, and Science on any impromptu occasion.

I thank all of my fellow students in the Hydrogeology Group for their support, assistance, and friendship.

I thank the Petroleum Technology Research Centre, Natural Sciences and Engineering Research Council of Canada, and the Department of Earth and Atmospheric Sciences for the financing needed to conduct the research toward, and complete this dissertation.

I also thank all of the geoscientists at the Subsurface Lab in Regina who worked on the Weyburn $CO_2$ project for their diligent and expert work and enthusiastic assistance.

My Parents, Francine and Farrukh Khan, and my wife Joanna provided me with support that I truly cannot adequately acknowledge. And my children, Hafsa, Hamza, and Zaynab gave me joyous respite.

## TABLE OF CONTENTS

1.0 INTRODUCTION ... 1
1.1 BACKGROUND ... 1
1.2 MOTIVATION ... 2
1.3 RESEARCH OBJECTIVES AND SCIENTIFIC APPROACH ... 4
1.3.1 Hydrogeological characterization of the Weyburn $CO_2$ project area ... 5
1.3.2 Gradient-free inverse conditioning ... 7
1.4 OUTLINE OF THESIS ... 9
1.5 REFERENCES ... 9

2.0 OVERVIEW OF THE HYDROGEOLOGY IN THE IEA GHG WEYBURN $CO_2$ MONITORING AND STORAGE PROJECT AREA: WILLISTON BASIN ... 17
2.1 INTRODUCTION ... 17
2.1.1 Regional Hydrogeological Setting ... 17
2.1.2 Objectives ... 18
2.2 STUDY AREA, DATABASE, AND METHODS ... 18
2.3. RESULTS ... 20
2.3.1 Formation water chemistry ... 20
2.3.2 Driving forces and fluid flow directions ... 21
2.3.3 Vertical pressure gradients ... 23
2.3.4 Aquifer permeabilities, flow velocities, and $CO_2$ Migration ... 24
2.4 IMPLICATIONS FOR $CO_2$ SEQUESTRATION AT WEYBURN ... 27
2.5 CONCLUSIONS ... 28
2.6 REFERENCES ... 29

3.0 COMPOSITIONS AND DISTRIBUTIONS OF FORMATION WATERS IN THE IEA GHG WEYBURN $CO_2$ MONITORING AND STORAGE PROJECT AREA: WILLISTON BASIN ... 43
3.1 INTRODUCTION ... 43

3.2 STUDY AREA AND HYDROGEOLOGICAL FRAMEWORK....44
3.2.1 Previous work....44
3.2.2 Hydrostratigraphy....45
3.3 DATA AND METHODOLOGIES....48
3.4 RESULTS....48
3.4.1 Distribution and composition of formation waters....48
3.4.2 Formation water classification....53
3.4.3 Graphical representation of formation waters....54
3.4.4 Calcium as an indicator species....56
3.5 DISCUSSION....58
3.5.1 Interpretations of the observed distributions of formation waters....59
3.5.2 Implications for anthropogenic activity....63
3.6 CONCLUSIONS....65
3.7 REFERENCES....67

4.0 HYDRODYNAMICS IN THE IEA GHG WEYBURN CO$_2$ MONITORING AND STORAGE PROJECT AREA: WILLISTON BASIN....93
4.1 INTRODUCTION....93
4.2 STUDY AREA AND HYDROGEOLOGICAL FRAMEWORK....94
4.2.1 Previous work....94
4.2.2 Hydrostratigraphy....95
4.3 DATA AND METHODOLOGIES....95
4.3.1 Driving forces on formation waters....96
4.4 RESULTS....97
4.4.1 Potentiometric Analysis....97
4.4.2 Density-corrected driving forces and flow directions....99
4.4.3 Pressure vs. depth analysis....103
4.5 SYNTHESIS AND DISCUSSION....106
4.5.1 Density-related hydrodynamic phenomena....108
4.5.2 Mississippian hydrodynamics and caprock trapping capacities....110
4.6 CONCLUSIONS....114

4.7 REFERENCES ....................116

5.0 APPROXIMATE SENSITIVITY COEFFICIENTS FOR INTEGRATING HYDRAULIC HEAD DATA INTO GEOLOGICAL MODELS ....................139

5.1 INTRODUCTION ....................139

5.1.2 Background: Sensitivity Coefficients ....................140

5.2 METHOD OF ANALYSIS AND RESULTS ....................142

5.2.1 Sensitivity structure ....................143

5.2.2 Approximation of sensitivity coefficients ....................146

5.2.3 Validation of approximate sensitivities ....................148

5.3 DISCUSSION ....................150

5.4 CONCLUSIONS ....................152

5.5 REFERENCES ....................153

6.0 A GRADIENT-FREE APPROACH TO INVERSE CONDITIONING OF HETEROGENEOUS RESERVOIR MODELS TO HYDRAULIC HEAD DATA ....................171

6.1 INTRODUCTION AND BACKGROUND ....................171

6.2 METHODOLOGY ....................174

6.2.1 Gradient-free calibration ....................175

6.3 RESULTS AND DISCUSSION ....................183

6.3.1 Conditioning a single realization ....................184

6.3.2 Conditioning an ensemble of realizations ....................185

6.3.3 Identification of the reference field ....................185

6.3.4 Technological contribution ....................189

6.4 CONCLUSIONS ....................191

6.5 REFERENCES ....................193

7.0 CONCLUSIONS ....................216

7.1 WEYBURN AREA HYDROGEOLOGICAL CHARACTERIZATION ....................216

7.1.1 Scientific and technological contributions ....................218

7.1.2 Recommended areas of future research ....219
7.2 GRADIENT-FREE INVERSE CONDITIONING ....220
7.2.1 Scientific and technological contributions ....222
7.2.2 Recommended areas of future research ....223
7.3 REFERENCES ....224

APPENDIX A: Additional details on methodologies for calculating driving forces on formation waters ....227
APPENDIX B: Additional details on the construction and implementation of the gradient-free algorithm ....234

## LIST OF TABLES

Table 1-1 Storage capacity for three main geological storage options ..........................2
Table 3-1 Chemical compositions of formation water samples ..................................92
Table 6-1 Explanation of deterministic gradient information for a given calibration data location ..........................................................................215
Table 6-2 Explanation of deterministic gradient information for a given calibration data location for the opposite sign on the head mismatch ......215

## LIST OF FIGURES

Figure 2.1 Location map ....................................................................................33
Figure 2.2 Williston Basin stratigraphy and hydrostratigraphic framework adopted for the Weyburn Project geological model ..............................................34
Figure 2.3 Total Dissolved Solids in representative aquifers.......................................35
Figure 2.4 Hydrochemical cross section A-A' ..............................................................36
Figure 2.5 WDF vector maps for Mannville and Midale Aquifers ..............................37
Figure 2.6 Vertical p(d) profiles in the vicinity of the Weyburn Field ........................38
Figure 2.7 Simulated permeability fields and flow velocities in selected aquifers......39
Figure 2.8 Mannville aquifer permeability and flow velocities ...................................40
Figure 2.9 Histogram of local mean flow velocity in Mannville Aquifer....................41
Figure 2.10 WDF and $CO_2$DF Vector map in Midale Aquifer ..........................................42
Figure 3.1 Location map ....................................................................................74
Figure 3.2 Williston Basin stratigraphy and hydrostratigraphic framework adopted for the Weyburn Project geological model ..............................................75
Figure 3.3 Total Dissolved Solids in selected Deep Paleozoic aquifers ......................76
Figure 3.4 Total Dissolved Solids in selected Mississippian aquifers .........................78
Figure 3.5 NW-SE oriented Hydrochemical cross section A-A' ................................80
Figure 3.6 Scatterplot of Total Dissolved Solids versus depth ....................................81
Figure 3.7 Na, K, and Mg plotted versus Total Dissolved Solids................................82
Figure 3.8 %Ca, $\%SO_4$, and $\%HCO_3$ plotted versus Total Dissolved Solids .............83
Figure 3.9 Pentaxial plot devised to display the five principal water types within the study area ....................................................................................84
Figure 3.10 Water samples from (a) Deep Paleozoic Duperow Aquifer, (b) Mississippian Ratcliffe Aquifer ..............................................................85
Figure 3.11 Mesozoic water samples from (a) Newcastle, (b) Mannville, and (c) Jurassic Aquifers..............................................................................86
Figure 3.12 Cationic fraction of Calcium in formation waters of selected Deep Paleozoic and Mississippian aquifers ........................................................87
Figure 3.13 Duperow TDS map showing spatial distribution of water types ................91

Figure 4.1 Location map ....... 123

Figure 4.2 Williston Basin stratigraphy and hydrostratigraphic framework adopted for the Weyburn Project geological model ....... 124

Figure 4.3 Potentiometric surface maps for selected Deep Paleozoic aquifers....... 125

Figure 4.4 Potentiometric surface maps for selected Mississippian aquifers....... 127

Figure 4.5 Potentiometric surface maps of Mesozoic aquifers ....... 129

Figure 4.6 Dip-oriented hydraulic cross section A-A' ....... 130

Figure 4.7 Water Driving Force (WDF) vector maps for selected Deep Paleozoic aquifers....... 131

Figure 4.8 WDF vector maps for selected Mississippian aquifers....... 132

Figure 4.9 Pressure vs. depth profiles ....... 133

Figure 4.10 Schematic hydraulic cross section of the Williston Basin topography-driven flow system....... 134

Figure 4.11 Multiplication surface function used to simulate the effects of paleo-topography ....... 135

Figure 4.12 (a) Potentiometric map of the Winnipegosis Aquifer. (b) Simulated amplified paleo-potentiometric surface ....... 136

Figure 4.13 Simulated paleo-formation water driving force map of the Winnipegosis Aquifer ....... 137

Figure 4.14 Schematic dip-oriented cross-section of Weyburn reservoir geometry....138

Figure 5.1 Flow model domain and flow solution for Model I....... 160

Figure 5.2 (a-d) Map displays of analytical sensitivity coefficients corresponding to the four calibration points in Model I; (e) Permeability field used in flow model ....... 161

Figure 5.3 Frequency histogram of sensitivity coefficients ....... 162

Figure 5.4 (a) Model II: bimodal permeability field; (b) permeability histogram; (c) geobody map ....... 163

Figure 5.5 Hydraulic head solution computed on Model II. ....... 164

Figure 5.6 (a-d) Map displays of sensitivity vectors corresponding to the four calibration points in Model II; (e) Geobody definition outlining

important flow features in model with the well capture flowpaths overlain ....165
Figure 5.7 (a) Depiction of the definition of a streamtube for the computation of approximate sensitivity coefficients; (b) the result delineates streamtubes encompassing potentially sensitive zones of the model for a specific calibration data configuration ....166
Figure 5.8 (a) Approximate sensitivity indicators displayed as sensitivity maps corresponding to (b) the analytical sensitivity coefficients calculated for Model I. ....167
Figure 5.9 (a) Approximate sensitivity indicators displayed as sensitivity maps corresponding to (b) the analytical sensitivity coefficients calculated for Model II. ....168
Figure 5.10 Graphical description of the generation of ln(k) perturbation vectors for the validation of approximate sensitivities using Model I. ....169
Figure 5.11 (a) Scatterplot comparing the linear approximation of hydraulic head against model-calculated heads using the analytically-derived sensitivity coefficients; (b) The same comparison using the approximate sensitivities ....170
Figure 6.1 General flow chart depicting the Sequential Self Calibration (SSC) algorithm with gradient-free method incorporated ....201
Figure 6.2 The process of obtaining approximate sensitivity indicators of head response at four calibration locations to the permeability field ....202
Figure 6.3 Comparison of the parameterization scheme preceding the optimization routine in (a) the original SSC method and (b) the gradient-free approach ....203
Figure 6.4 An example of the parameterization of the optimization to reduce the head mismatch at a specific calibration location ....204
Figure 6.5 Reference permeability field (I) and steady state head solution ....205
Figure 6.6 Results of a synthetic calibration using the gradient-free method ....206
Figure 6.7 Gradient-free calibration progress for a single initial permeability field realization ....207

Figure 6.8 Convergence behaviour of gradient-free conditioning for an ensemble of 20 realizations ....208
Figure 6.9 Reference permeability field (II) used for the demonstration of the types of features that can be consistently identified from a set of calibration head data ....209
Figure 6.10 Gradient-free calibration results shown on five realizations ....210
Figure 6.11 Identification of low-permeability features ....211
Figure 6.12 Controls on the identification of low permeability features by inverse conditioning ....212
Figure 6.13 Partial identification of a high-transmissivity conduit ....213
Figure 6.14 Complete identification of a high-transmissivity conduit ....214
Figure A-1 Crossplot of water density estimates for comparing equations of state ....231
Figure A-2 Crossplots of water density estimates from the two equations of state versus an empirical relation describing density as a function of TDS ....232
Figure A-3 Schematic depicting the analytical calculation of formation water driving force ....233

# 1.0 INTRODUCTION

## 1.1 BACKGROUND

Since the 1992 inception of the United Nations Framework Convention on Climate Change (UNFCCC), $CO_2$ capture and storage has attracted major interest in international policy for emissions reductions. The ultimate objective stated by the UNFCCC is the "stabilization of greenhouse gas concentrations in the atmosphere at a level that prevents dangerous anthropogenic interference with the climate system" (IPCC, 2005). Of the myriad of factors that play into a global international plan for the governance of emissions to achieve the above stated goal, carbon capture and storage (CCS) will play a major role. CCS works by the interplay of locating a $CO_2$ source, applying the appropriate capture technology, and transporting the $CO_2$ to a storage site where it is sequestered. Feasible storage options have been identified as belonging to three types: geological, deep ocean, and mineral carbonation (an industrial process) (IPCC, 2005). Geological storage is attractive primarily because porous geological formations are ubiquitous and have large volumetric capacities; cost-effective means which integrate energy production are potentially available; and the timescales for secure storage of $CO_2$ at an appropriately selected site are potentially long enough to contribute to the above-stated goal of the UNFCCC.

Geological storage options include three main settings: depleted oil and gas fields, saline formations (aquifers), and deep coal seams. The estimated storage capacity of each of these categories is shown in Table (1.1). The most promising of these options are depleted hydrocarbon fields and saline aquifers. The Sleipner project is the flagship project for saline aquifer injection as it is the first commercial-scale project dedicated to $CO_2$ injection into a saline formation (IPCC, 2005). Similarily, the International Energy Agency (IEA) Greenhouse Gas (GHG) Weyburn $CO_2$ monitoring and storage project is the first working example of a $CO_2$ enhanced oil recovery project coupled to a large-scale $CO_2$ sequestration program (Whittaker et al., 2004).

| **Reservoir type** | **Lower estimate of storage capacity (GtCO2)** | **Upper estimate of storage capacity (GtCO2)** |
|---|---|---|
| Oil and gas fields | 675a | 900a |
| Unminable coal seams (ECBM) | 3-15 | 200 |
| Deep saline formations | 1000 | Uncertain, but possibly 104 |

Table 1.1 Storage capacity for three main geological storage options (IPCC, 2005)

*The Weyburn Project*

The principal objective of the Weyburn Project is to demonstrate the capacity of a giant depleted oil field to store anthropogenic $CO_2$ (Preston et al., 2005). The source for the $CO_2$ is the coal gasification facility operated by the Dakota Gasification Company in Beulah, North Dakota. $CO_2$ is concentrated from the emissions stream, compressed and piped to the Weyburn oilfield via a 325 km pipeline connecting the two facilities. The Weyburn field covers an area of approximately 180 $km^2$ with original oil in place estimated at approximately 1.4 billion barrels (222 million $m^3$). It is expected that approximately 20 million tones of $CO_2$ will be left in the reservoir at the end of the project life in 2025.

The success of geological sequestration depends on the efficiency of one or more trapping mechanisms including: structural or stratigraphic trapping; solubility trapping; mineral trapping; and hydrodynamic trapping (Bachu, 2001; IPCC, 2005). The capacity of each of these trapping processes is controlled (or affected by) the subsurface pressure, temperature, and geochemical regime(s). Thus, a comprehensive hydrogeological study has been formally identified as being a key part of any investigation assessing the integrity of a sequestration site (IPCC, 2005).

## 1.2 MOTIVATION

Hydrogeological studies and the development of hydrogeological modeling techniques for assessing the risk of underground waste storage projects have become increasingly important over the last two decades. There are two main objectives of hydrogeological studies in this context: (1) a deterministic assessment of the suitability of the local geological framework to trap the waste introduced into the subsurface, and (2) to provide direct information on key input parameters and ranges of uncertainty in those parameters for risk assessment modeling.

$CO_2$ injection and storage is much like other subsurface waste disposal problems in that risk assessment is contingent upon a diligent geological characterization of the disposal site. The risk of local health, safety, and environmental hazards that may result from escape of $CO_2$ from a storage site (IPCC, 2005, p. 242) must be quantified. In order to do this, system models are built from the results of the detailed geological characterization and hydrogeological analysis. The literature and practice of modeling geological risk at $CO_2$ storage sites is not well-developed; however, it does not need to be developed anew[1], as there is already an extensive body of literature on hydrogeologic conceptualization, model development, and predictive uncertainty analysis around nuclear waste disposal sites (e.g., Neuman and Wierenga, 2003).

A deterministic assessment of the site suitability of a waste disposal site does not resolve the variability and the consequent uncertainty of hydrogeological variables at scales smaller than the data spacing. In particular, characterizing the permeability of aquifers, which are primary natural pathways for the transport of contaminants, and accounting for the uncertainty due to the unknown nature of geological heterogeneity is of paramount importance.

A principle research objective in subsurface fluid flow modeling is to model the heterogeneity in the permeability structure of an aquifer, consistent with direct measurements of permeability *and* state variables (e.g., hydraulic head, tracer concentrations, temperature, etc.).

The problem of integrating measurements of hydraulic head into geological models for aquifer characterization (the groundwater inverse problem) remains an important area despite decades of research. Techniques for solving the inverse problem in hydrogeology have been developed by (Emsellem and de Marsily, 1971; Cooley, 1977; 1979; 1982; 1983; Kitanidis and Vomvoris, 1983; Dagan, 1985; Townley and Wilson, 1985; Carrera and Neuman, 1986; Loaiciga and Marino, 1986; 1987; Woodbury et al., 1987; Dagan and Rubin, 1988; Ahmed and de Marsily, 1989; Gutjahr and Wilson, 1989; Sun and Yeh, 1992; RamaRao et al., 1995; Sun et al., 1995; Yeh and Zhang, 1996; Gomez-Hernandez et al., 1997; Medina and Carrera, 2003) among numerous others. Integrating hydraulic head data into the process of modeling the geological heterogeneity of an aquifer requires solving an inverse problem, where the solution consists of model parameter estimates that are constrained by measurements of the system response. The ultimate goal of inverse flow modeling in this context is to identify important heterogeneities of the distributed parameter field, most often the permeability, of a heterogeneous aquifer or reservoir in order to increase the predictive ability of the model by narrowing the spaces of uncertainty of the response variables.

---

[1] For $CO_2$ storage, extending these hydrogeological methods to the analysis of caprocks is a necessary area to develop in future research.

## 1.3 RESEARCH OBJECTIVES AND SCIENTIFIC APPROACH

Two specific research objectives were undertaken in this work:

1. To characterize the fluid flow regime in the IEA GHG Weyburn $CO_2$ monitoring and storage project area through high-resolution regional mapping in order to identify factors that may affect $CO_2$ storage in the Weyburn oilfield. In particular, the objective was to map hydrodynamic and hydrochemical signatures and to interpret the causal phenomena controlling the observed distributions of fluid pressures and compositions. It was expected that the synthesis of the hydrogeological mapping results would lead to new insights on Williston Basin Hydrogeology because of the incorporation of new data and techniques that have not been adopted in previous studies in the basin.

2. To evaluate the controls on the structure of the sensitivity (Jacobian) matrix containing information on the sensitivity of hydraulic head response to the model parameters representing spatially-variable aquifer permeability. The objective was to devise a means of approximating the Jacobian matrix and develop a calibration algorithm that can use the approximate sensitivity information. The potential reduction in

computational effort that would be offered by circumventing a computation of the Jacobian matrix and the understanding of the controls on model sensitivity with respect to the spatial configuration of the calibration (head) data constituted the motivation for this research.

### 1.3.1 Hydrogeological characterization of the Weyburn $CO_2$ Project Area

Previous hydrogeological studies of the Williston Basin (Hannon, 1987; Toop and Tóth, 1995; Bachu and Hitchon, 1996; Downey, 1984a,b; 1986; Downey et al., 1987; Berg et al., 1994; Busby et al, 1995; DeMis, 1995; LeFever, 1998), among others, have lacked detail in the definition of aquifers and aquitards from the lithologically diverse stratigraphic column. In particular, though not exclusively, the thick Mississippian system of rocks has never been subdivided into individual flow units despite the fact that petroleum geologists have long recognized (at least implicitly) that the Mississippian rocks are not hydraulically uniform. The importance of the Mississippian System for its hydrocarbon resources has resulted in a huge volume of geological and hydrogeological data; and recently, the interest in $CO_2$ EOR/Sequestration projects has brought the need to re-examine old data, integrate newer data, and increase the level of detail from that of overview or screening-type studies.

From a scientific perspective, this work differs from previous regional hydrogeological analysis in the Williston Basin. First, it contains newer (post-1996) data from deep drilling results on the Canadian side of the basin. Second, this study uses previously unavailable geological mapping from the Weyburn project (Whittaker et al., 2004). This enables a much greater hydrostratigraphic resolution, including the separation of the Mississippian aquifer system into constituent aquifers. Third, the estimation of in-situ formation water densities and the calculation of density-corrected driving forces on Williston Basin brines are included here. The observed hydrochemical distributions and the nature of density-dependent flows lead to new interpretations of the paleohydrogeology of the Williston Basin.

### *Scope of work done in relation to results presented*

Chapters 2, 3 and 4 constitute the most comprehensive work in regional hydrogeology in the Williston Basin to date. Together they present only the key results of a detailed hydrogeological analysis of the International Energy Agency (IEA) Greenhouse Gas (GHG) Weyburn CO2 monitoring and storage project area. The full scope of work done for the hydrogeological characterization is not documented in this dissertation.

A large database consisting of over 5300 fluid pressures and formation temperatures and over 8500 formation-water analyses was assembled for this study from a combination of public and private data sources. This was supplemented with petrophysical data from core analyses within key aquifers and over 100 water samples collected from oilfield wellheads. Hydrogeological data were assigned to their respective aquifer units using structural controls based on stratigraphic surfaces that were mapped by a small group of geologists at Saskatchewan Industry and Resources and the North Dakota Geological Survey (Whittaker et al., 2004). This assignment was an iterative procedure which made use of digital grids of elevation differences between the tops and bases of water sample intervals and the stratigraphic surfaces defining aquifers. Details of the procedure are documented in Rostron and Khan (2005).

A total of 137 maps and/or numerical grids of state variables was generated from the hydrogeological data including:

- Formation pressures
- Formation temperatures
- Formation water total dissolved solids concentrations
- Concentrations of individual major ionic constituents ($Na^+$, $Mg^{2+}$, $Ca^{2+}$, $K^+$, $Cl^-$,$SO_4^{2-}$, and $HCO_3^-$) in formation waters
- In-situ formation water densities
- Force vector fields resolving different components and net driving forces on formation fluids
- Formation water velocity fields

The maps presented in Chapters 2, 3, and 4 were synthesized from these components. The full suite of maps and grids are in an unpublished internal report (Rostron and Khan, 2005) completed for the Petroleum Technology Research Council (PTRC) in Regina, Saskatchewan, and are available by request to the PTRC.

### 1.3.2 Gradient-free inverse conditioning

The groundwater inverse problem has been approached from various angles with differing underlying philosophies. It was not the purpose of the work presented in this dissertation to delve into a comparison of these philosophies and approaches from the perspective of inverse theory. The interested reader is referred to the seminal review by McLaughlin and Townley (1996) as an example of a paper with that scope.

The "geostatistical approach" refers to one group of inverse methods which has developed as a result of the need to quantify uncertainty in the input parameters to groundwater flow models. It is widely recognized that heterogeneity plays a critical role in the uncertainty associated with predictive flow and transport models (Kolterman and Gorelick, 1996; de Marsily et al., 2005). Geostatistics is concerned with inferring the structure of spatial correlation of geological attributes modeled as a spatial random function, which is defined as a set of dependent random variables at each location over a study area (Journel and Huijbregts, 1978; Goovaerts, 1997; Deutsch, 2002). The two fundamental concepts of Geostatistics concerning this discussion are estimation and simulation. Estimation aims to obtain a best estimate of the "random" geological variable at an unsampled location in the field. Simulation generates multiple images (realizations) of the random function which reproduce the global multivariate statistics (simulated textures of geological heterogeneity). Similarly, geostatistical inversion methods can be classified as estimation or simulation methods (Medina and Carrera, 2003). The majority of the foundational methods developed in geostatisitical inverse theory have been concerned with estimation (Kitanidis and Vomvoris, 1983; Hoeksema and Kitanidis, 1984, 1985; Dagan, 1985; Carrera and Neuman, 1986a; Rubin and Dagan, 1987) and others. Simulation-based inversion is more recent, originating from methods formalized by Sahuquillo et al. (1992), RamaRao et al. (1995), Gomez-Hernandez et al. (1997), and Capilla et al. (1999). Simulation inversion is based upon generating an ensemble of initial random fields representing the aquifer permeability, with each realization possibly conditioned upon direct permeability measurements and any other variables linearly dependent upon the random variable modeling the permeability, and subsequently perturbing the field[2] in order to minimize the mismatch between measured and model-computed heads (and other state variables). In this way, the model of parametric uncertainty in the aquifer permeability is conditioned upon the head data via *inverse conditioning.*

Inverse conditioning thus refers to a posterior calibration of an ensemble of realizations (i.e., a model of spatial uncertainty) of the permeability field to dynamic data. The conditioning process must somehow address the complex non-linearity between the model response and the model parameters. Although the initial suite of realizations may have been generated conditional to permeability data, in general, they will not result in a simulated reproduction of the available pressure or head measurements, thus resulting in poor predictive ability of the flow models. One major reason for this is because they fail to identify key heterogeneities that affect the flow system response. Inverse conditioning aims to identify the aquifer heterogeneity and consequently narrow the space of uncertainty, as characterized by the flow response over multiple realizations.

The method of inverse conditioning developed in this dissertation utilizes and builds upon the concepts of Sequential Self Calibration (Sahuquillo et al., 1992; Gomez-Hernandez et al., 1997), and pilot points (RamaRao et al., 1995). Sequential Self Calibration (SSC) provided important conceptual advancements in solving the inverse problem in hydrogeology and reservoir characterization (Sahuquillo et al., 1992; Gomez-Hernandez et al., 1997; Capilla et al., 1997; Capilla et al., 1999; Wen et al., 1999).

---

[2] Plausible perturbations lie within uncertainty limits specified by local conditional probabilities obtained by kriging, for example.

## 1.4 OUTLINE OF THESIS

The style of this dissertation is *paper format*, whereby each chapter represents a standalone work. Chapters 2, 3 and 4 present the findings of a detailed hydrogeological characterization of the Weyburn $CO_2$ project area in the Williston Basin. Chapter 2 summarizes the Weyburn project hydrogeological characterization. Chapter 3 summarizes the results of mapping and interpreting the formation water chemistry through the entire succession of deep (> 300 m depth) aquifers within the Weyburn project study area. Chapter 4 synthesizes and explains the hydrodynamic regime of the Weyburn project area.

Chapters 5 and 6 present the development of a *gradient-free* approach to inverse conditioning of stochastic models of aquifer or reservoir permeability. The method is based on an approximate prediction of the sensitivity of hydraulic head to perturbations in the permeability field and an optimization method that determines the search direction via an approximation of the gradient of the objective function to be minimized. In the gradient-free approach — which is the subject of Chapter 6 — parameter sensitivities are predicted, approximately, based on a set of physical criteria. The empirical derivation of these physical criteria is the subject of Chapter 5.

The scope of Chapters 5 and 6 shifts from hydrogeological characterization of the Weyburn project area to general algorithm development related to incorporating hydraulic head data into geostatistical models of aquifer heterogeneity. The method developed in Chapter 6 could have been directly applied to update the geostatistical models of aquifer permeability in Chapter 2, but this was not included in the dissertation because the development of the gradient-free approach to inverse conditioning was the focus of the latter phase of the research conducted toward this dissertation.

## 1.5 REFERENCES

Ahmed, S., de Marsily G., (1989) Co-kriged estimates of transmissivities using jointly water level data. In: M. Armstrong (Ed.), *Geostatistics; Proceedings of the Third*

*International Geostatistics Congress; Volume 2.* (Ed. by M. Armstrong), Kluwer Acad. Publ., Dordrecht, Netherlands. pp. 615-628.

Bachu, S., Hitchon, B., (1996) Regional-scale flow of formation waters in the Williston Basin. *AAPG Bulletin*, 80(2), pp. 248-264.

Bachu, S., (2001) Geological Sequestration of Carbon Dioxide: Applicability and Current Issues. In: L.C. Gerhard, W.E. Harrison, B.M. Hanson (Eds.), Geological Perspectives in Global Climate Change, AAPG Studies in Geology #47 (Ed. by L.C. Gerhard, W.E. Harrison, B.M. Hanson), American Association of Petroleum Geologists, Tulsa,OK. pp. 285-303.

Berg, R.R., DeMis, W.D., Mitsdarffer, A.R., (1994) Hydrodynamic effects on Mission Canyon (Mississippian) oil accumulations, Billings Nose area, North Dakota. *AAPG Bulletin*, 78(4), pp. 501-518.

Busby, J.F., Kimball, B.A., Downey, J.S., (1995) Geochemistry of water in aquifers and confining units of the Northern Great Plains in parts of Montana, North Dakota, South Dakota, and Wyoming. *U.S. Geological Survey Professional Paper 1402-F*, 146p.

Capilla, J.E., Gomez-Hernandez, J.J., Sahuquillo, A., (1997) Stochastic simulation of transmissivity fields conditional to both transmissivity and piezometric data; 2, Demonstration on a synthetic aquifer. *Journal of Hydrology*, 203(1-4), pp. 175-188.

Capilla, J.E., Rodrigo, J., Gomez-Hernandez, J.J., (1999) Simulation of Non-Gaussian Transmissivity Fields Honoring Piezometric Data and Integrating Soft and Secondary Information. *Mathematical Geology*, 31(7), pp. 907-927.

Carrera, J., Neuman, S.P., (1986a) Estimation of aquifer parameters under transient and steady state conditions; 1, Maximum likelihood method incorporating prior information. *Water Resources Research*, 22(2), pp. 199-210.

Carrera, J., Neuman, S.P., (1986b) Estimation of aquifer parameters under transient and steady state conditions; 2, Application to synthetic and field data. *Water Resources Research*, 22(2), pp. 228-242.

Carrera, J., Neuman, S.P., (1986c) Estimation of aquifer parameters under transient and steady state conditions; 2, Uniqueness, stability, and solution algorithms. *Water Resources Research*, 22(2), pp. 211-227.

Cooley, R.L., (1977) A method of estimating parameters and assessing reliability for models of steady state groundwater flow; 1, Theory and numerical properties. *Water Resources Research*, 13(2), pp. 318-324.

Cooley, R.L., (1979) A method of estimating parameters and assessing reliability for models of steady state groundwater flow; 2, Application of statistical analysis. *Water Resources Research*, 15(3), pp. 603-617.

Cooley, R.L., (1982) Incorporation of prior information on parameters into nonlinear regression groundwater flow models; 1, Theory. *Water Resources Research*, 18(4), pp. 965-976.

Cooley, R.L., (1983) Incorporation of prior information on parameters into nonlinear regression ground-water flow models; 2, Applications. *Water Resources Research*, 19(3), pp. 662-676.

Dagan, G., (1985) Stochastic modeling of groundwater flow by unconditional and conditional probabilities; the inverse problem. *Water Resources Research*, 21(1), pp. 65-72.

Dagan, G., Rubin, Y., (1988) Stochastic identification of recharge, transmissivity, and storativity in aquifer transient flow; a quasi-steady approach. *Water Resources Research*, 24(10), pp. 1698-1710.

de Marsily, G., Delay, F., Goncalves, J., Renard, P., Teles, V., Violette, S., (2005) Dealing with spatial heterogeneity. *Hydrogeology Journal*, 13(1), pp. 161-183.

DeMis, W.D., (1995) Effect of cross-basinal hydrodynamic flow on oil accumulations and oil migration history of the Bakken-Madison petroleum system Williston Basin, North America. In: L.D.V. Hunter and R.A. Schalla (Eds), Seventh International Williston Basin Symposium. Montana Geological Society, Billings, Montana, pp. 291-301.

Deutsch, C.V., (2002) *Geostatistical Reservoir Modeling*. Oxford University Press. 384p.

Downey, J.S., (1984a) Hydrodynamics of the Williston Basin in the Northern Great Plains. In: G. Jorgensen Donald, C. Signor Donald (Eds.), *Geohydrology of the Dakota Aquifer*. Natl. Water Well Assoc., Worthington, OH, United States. pp. 92-98.

Downey, J.S., (1984b) Geohydrology of the Madison and associated aquifers in parts of Montana, North Dakota, South Dakota, and Wyoming. *U.S. Geological Survey Professional Paper 1273-G*, 1273-G, 47p.

Downey, J.S., (1986) Geohydrology of bedrock aquifers in the Northern Great Plains in parts of Montana, North Dakota, South Dakota, and Wyoming. *U.S. Geological Survey Professional Paper 1402-E*, 87p.

Downey, J.S., Busby, J.F., Dinwiddie, G.A., (1987) Regional aquifers and petroleum in the Williston Basin region of the United States. In: *1987 Symposium of the Rocky Mountain Association of Geologists* (Ed. by M. Longman), pp. 299-312.

Emsellem, Y., de Marsily, G, (1971) An automatic solution for the inverse problem. *Water Resources Research*, 7(5), pp. 1264-1283.

Gomez-Hernandez, J.J., Sahuquillo, A., Capilla, J.E., (1997) Stochastic simulation of transmissivity fields conditional to both transmissivity and piezometric data; I, Theory. *Journal of Hydrology*, 203(1-4), pp. 162-174.

Goovaerts, P., (1997) *Geostatistics for Natural Resources Evaluation*. Oxford University Press. 496p.

Gutjahr, A., Wilson, J.L., (1989) Co-kriging for stochastic flow models. In: G. de Marsily (Ed.), *The stochastic approach to subsurface flow., 4; 6, Transport in Porous Media* (Ed. by G. de Marsily), D. Reidel Publishing Company, Dordrecht, International. pp. 585-598.

Hannon, N., (1987) Subsurface water flow patterns in the Canadian sector of the Williston Basin. In: *1987 Symposium of the Rocky Mountain Association of Geologists*, pp. 313-321.

Hoeksema, R.J., Kitanidis, P.K., (1984) An application of the geostatistical approach to the inverse problem in two-dimensional groundwater modeling. *Water Resources Research*, 20(7), pp. 1003-1020.

Hoeksema, R.J., P.K, K., (1985) Analysis of the spatial structure of properties of selected aquifers. *Water Resources Research*, 21(4), pp. 563-572.

IPCC, (2005) Special report on carbon dioxide capture and storage prepared by working group III of the Intergovernmental Panel on Climate Change [Metz, B., O. Davidson, H. C. de Coninck, M. Loos, and L. A. Meyer (eds.)]. Cambridge University Press, Cambridge, United Kingdom and NewYork, NY, USA, 442 p.

Journel, A.G., Huijbregts, C.J., (1978) *Mining Geostatistics*. Academic Press, London. 600p.

Kitanidis, P.K., Vomvoris, E.G., (1983) A geostatistical approach to the inverse problem in groundwater modeling (steady state) and one-dimensional simulations. *Water Resources Research*, 19(3), pp. 677-690.

Kolterman, C.E., Gorelick, S.M., (1996) Heterogeneity in sedimentary deposits: A review of structure-imitating, and descriptive processes. *Water Resources Research*, 32(9), pp. 2617-2658.

Lefever, R.D., (1998) Hydrodynamics of formation waters in the North Dakota Williston Basin. In: J.E. Christopher, C.F. Gilboy, D.F. Paterson, S.L. Bend (Eds.), *Eighth Annual Williston Basin Symposium, Special Publication*, pp. 229-237.

Loaiciga, H.A., Marino, M.A., (1986) On solution of the inverse problem for confined aquifer flow via maximum likelihood. *Mathematical Geology*, 18(7), pp. 677-692.

Loaiciga, H.A., Marino, M.A., (1987) Parameter estimation in groundwater: classical, Bayesian, and deterministic assumptions and their impact on management policies. *Water Resources Research*, 23(6), pp. 1027-1035.

McLaughlin, D., Townley, L.R., (1996) A reassessment of the groundwater inverse problem. *Water Resources Research*, 32(5), pp. 1131-1161.

Medina, A., Carrera, J., (2003) Geostatistical inversion of coupled problems: dealing with computational burden and different types of data. *Journal of Hydrology*, 281(4), pp. 251-264.

Neuman, S.P., Wierenga, P.J., (2003) A comprehensive strategy of hydrogeologic modeling and uncertainty analysis for nuclear facilities and sites. U.S. Nuclear Regulatory Commission Office of Nuclear Regulatory Research, Washington, DC. 239 p.

Preston, C., Monea, M., Jazrawi, W., Brown, K., Whittaker, S., White, D., Law, D., Chalaturnyk, R., Rostron, B., (2005) IEA GHG Weyburn $CO_2$ monitoring and storage project. *Fuel Processing Technology*, 86, pp. 1547-1568.

RamaRao, B.S., Lavenue, A.M., de Marsily, G., Marietta, M.G., (1995) Pilot point methodology for automated calibration of an ensemble of conditionally simulated transmissivity fields; 1, Theory and computational experiments. *Water Resources Research*, 31(3), pp. 475-493.

Rostron, B.J., Khan, D.K., (2005) Final report Task 2.2.1: Regional hydrogeology of the Weyburn CO2 project area, Petroleum Techonolgy Research Centre, Regina, SK. 176p.

Rubin, Y., Dagan, G., (1987) Stochastic identification of transmissivity and effective recharge in steady groundwater flow; 1, Theory. *Water Resources Research*, 23(7), pp. 1185-1192.

Sahuquillo, A., Capilla, J.E., Gomez Hernandez, J.J., Andreu, J., (1992) Conditional simulation of transmissivity fields honoring piezometric data. In: B.a. Cabrera (Ed.), *Hydraulic Engineering Software IV, Fluid Flow Modeling, II, Elsevier Applied Science* (Ed. by B.a. Cabrera), Elsevier. pp. 201-214.

Sun, N.Z., Yeh, W.W.G., (1992) A stochastic inverse solution for transient groundwater flow; parameter identification and reliability analysis. *Water Resources Research*, 28(12), pp. 3269-3280.

Sun, N.Z., Jeng, M.C., Yeh, W.W.G., (1995) A proposed geological parameterization method for parameter identification in three-dimensional groundwater modeling. *Water Resources Research*, 31(1), pp. 89-102.

Toop, D.C., Toth, J., (1995) Hydrogeological characterization of formation waters using ionic ratios, south-central Saskatchewan. In: *7th International Williston Basin Symposium* (Ed. by L.D.V. Hunter, R.A. Schalla), Montana Geological Society, Billings, Montana. pp. 313-319.

Townley, L.R., Wilson, J.L., (1985) Computationally efficient algorithms for parameter estimation and uncertainty propagation in numerical models of groundwater flow. *Water Resources Research*, 21(1), pp. 1851-1860.

Wen, X.H., Capilla, J.E., Deutsch, C.V., Gomez-Hernandez, J.J., Cullick, A.S., (1999) A program to create permeability fields that honor single-phase flow rate and pressure data. *Computers & Geosciences*, 25, pp. 217-230.

Whittaker, S., Rostron, B.J., Khan, D., Hajnal, Z., Qing, H., Penner, L., Maathuis, H., Goussev, S., (2004) IEA GHG Weyburn $CO_2$ monitoring & storage project summary report 2000-2004. In: *Seventh International Conference on Greenhouse Gas Control Technologies*, *1* (Ed. M. Wilson, M. Monea), Petroleum Technology Research Centre. pp. 15-69.

Woodbury, A.D., Smith, L., Dunbar, W.S., (1987) Simultaneous inversion of hydrogeoloic and thermal data; 1, Theory and application using hydraulic head data. *Water Resources Research*, 23(8), pp. 1586-1606.

Yeh, T.C.J., Zhang, J., (1996) A geostatistical inverse method for variably saturated flow in the vadose zone. *Water Resources Research*, 32(9), pp. 2757-2766.

# 2.0 OVERVIEW OF THE HYDROGEOLOGY IN THE IEA GHG WEYBURN $CO_2$ MONITORING AND STORAGE PROJECT AREA: WILLISTON BASIN*

## 2.1 INTRODUCTION

Disposal of anthropogenically-produced $CO_2$ by injection into saline aquifers or oilfields (either abandoned or producing) has been termed geological storage, or sequestration (IPCC, 2005). Geological sequestration appears to be a viable means of reducing global $CO_2$ emissions. The IEA Weyburn $CO_2$ Monitoring and Storage Project is a comprehensive study investigating the viability of geological sequestration of $CO_2$ in the Weyburn oilfield in Saskatchewan, Canada.

Sequestration involves the segregation of $CO_2$ from the biosphere for a target time frame. The success of geological sequestration thus depends on the efficiency of one or more different trapping mechanisms including: structural or stratigraphic traps, solubility trapping, mineral trapping, and hydrodynamic trapping (Bachu, 2001). Each of the aforementioned trapping mechanisms depends on the subsurface pressure, temperature, and geochemical regime(s). Thus, hydrogeology is a cornerstone of any investigation assessing the integrity of a sequestration site (IPCC, 2005).

### 2.1.1 Regional Hydrogeological Setting

The study area is located in the northeastern part of the Williston Basin (Figure 2.1). Regionally, the hydrogeology and hydrochemistry of the Williston Basin has been widely studied, with examples from the Canadian side of the basin [Hannon, 1987; Bachu and Hitchon, 1996), the American portion (Downey at al., 1987), and on a basin-wide scale (Benn and Rostron, 1998). Previous studies have concluded that flow of formation waters generally occurs from the south-southwest to north-northeast across the basin. This cross-basin flow is thought to occur in response to a regional hydraulic gradient created by topographic elevation differences, approximately 1000 m on average, between major aquifer outcrop areas at opposite edges of the basin. Meteoric waters are thought to enter the basin at elevated aquifer outcrops along the south, southwest and western basin flanks and are driven toward the basin center, as suggested by very fresh formation waters in the basal aquifers [Bachu and Hitchon, 1996; Benn and Rostron, 1998] with meteoric isotopic signatures (Rostron and Holmden, 2003). In the deepest portions of the basin, meteoric waters mix with saline brines (Iampen and Rostron, 2000) and the resulting mixtures are displaced up dip from the basin centre onto the northeast basin flank (Downey at al., 1987). This cross-basinal flow system is thought to have originated relatively recently in the history of the basin, with the current boundary conditions set up in Eocene times in association with the onset of the Laramide Orogeny.

---

* A version of this chapter was published as: Khan, D.K., Rostron, B.J., (2004) Regional Hydrogeological Investigation Around The IEA Weyburn CO2 Monitoring And Storage Project Site. In: *Proceeding of the 7th International Conference on Greenhouse Gas Control Technologies* (GHGT-7), Sept. 5-9, 2004, Vancouver, Canada, v.I, pp. 741-750. Volume 1: Peer-Reviewed Papers and Plenary Sessions, Elsevier, UK.

### 2.1.2 Objectives

The objective of the regional hydrogeological mapping component of the IEA Weyburn CO2 Monitoring and Storage Project was to characterize the natural hydraulic regime of the sedimentary succession in the study area in order to examine the impact of fluid flow on CO2 storage and to define the necessary boundary conditions for the risk analysis (RA) system models. The initial hypothesis that we set out to verify was that the Weyburn field and the encompassing geological framework is a good location to store injected $CO_2$. The primary goal of the hydrogeological analysis was thus to identify the directions and rates of formation fluid flow through water-transmitting strata (aquifers). Other objectives included: the location of any preferential pathways for cross-formational fluid flow, the assessment of the competence of low permeability confining strata (aquitards), a hydrochemical characterization of each aquifer; and the provision of hydrogeological data (e.g., pressures, temperatures, porosities, and permeabilities) for predictive modeling of $CO_2$ sequestration performance for environmental risk assessment.

## 2.2 STUDY AREA, DATABASE, AND METHODS

An area encompassing approximately 50,000 km$^2$ of the Williston Basin was examined for this study (Figure 2.1). The regional hydrogeological characterization area is bounded by meridians 102-106W and parallels 48.5-50.5N, and is slightly larger (an additional 50 km to the west) than the 200 by 200 km block centered on the Weyburn

Field, which was adopted for the Weyburn Project geosphere characterization (Whittaker et al., 2004).

A hydrogeological database of over 5300 fluid pressures and formation temperatures, and over 8500 formation-water analyses was assembled from public and private data sources. This was supplemented with petrophysical data from core analyses in key aquifers and over 100 privately collected wellhead water samples. The geological framework for the hydrogeological study was re-mapped from public well data by Saskatchewan Industry and Resources and the North Dakota Geological Survey. Geological mapping procedures and results are described in Whittaker et al. (2004).

Hydraulic and hydrochemical data were assigned to their respective named aquifer units and then tested against structural controls provided by the geological mapping. Where aquifer nomenclature was incomplete or vague (e.g., "Mississippian Aquifer"), data were assigned to individual aquifers through a series of "interval tests". Data spanning multiple aquifers were removed from the mapped data. Following these procedures, and after examination of data distributions and preliminary hydrogeological results, a hydrostratigraphic framework consisting of 18 major aquifers and 13 major aquitards was developed (Figure 2.2). Data were dealt with on an individual aquifer basis and later recombined for cross-section construction.

All data were carefully screened using automated and manual techniques. Only quality pressure data with full Horner-type extrapolations (Horner, 1951) were used. Each pressure measurement was screened for production-influenced pressure drawdown using a quantitative index accounting for radial proximity of a drill stem test (DST) to production/injection wells and the duration of production/injection (Alkalali, 2002). Chemical data were screened to remove non-representative data (e.g., mixtures, drilling mud filtrates, spent acid-fracture fluids, injection waters) using automated techniques (e.g., Hitchon and Brulotte, 1994) supplemented by manual inspection.

Pressure data were used for pressure versus depth (p[d]) profiles and converted into potentiometric surfaces and hydraulic cross-sections. Variable-density flow effects are significant in many aquifers and procedures for identifying and dealing with these effects are discussed in the following section. Hydrochemical data were mapped as individual ions, ion ratios, and as Total Dissolved Solids (TDS). In this manner all geological and hydrogeological data were synthesized into a regional picture of fluid flow in the study area.

## 2.3 RESULTS

### 2.3.1 Formation water chemistry

Geochemical mapping revealed large variations in water chemistry (both composition and TDS) within, and between, the aquifers in the study area. These variations are evident in TDS patterns shown from typical aquifers in each of the three main aquifer groups: Deep Paleozoic (e.g., Birdbear Aquifer, Figure 2.3d); Mississippian (e.g., Midale Aquifer, Figure 2.3c); and Mesozoic (e.g., Jurassic and Mannville Aquifers, Figures 2.3b,a). Vertical variations in TDS are visible in a typical TDS cross-section (Figure 2.4).

In Deep Paleozoic aquifers, TDS patterns have a similar overall character, with fresh waters (TDS <5 g/L) occurring in the west and north of the map area, Na-Cl brines with intermediate TDS (100 to 300 g/L) occupying the central area, and Ca-Na-Cl brines (TDS >300 g/L) in the south and east map areas. Salinity systematically increases within each aquifer toward the deeper part of the basin without a clear dependence on stratigraphic depth (Figure 2.4). Fresh waters (TDS <5 g/L) are Ca-SO4 type and represent meteoric waters that have penetrated to depth and have migrated considerable distances from their presumed points of entry along the south and western flanks of the Williston Basin. The degree of penetration of these fresh waters into the Paleozoic rocks within the study area decreases with depth (Figure 2.4). Concentrated brines are Ca-Na-Cl type waters with Ca occurring in equal, or higher reactive concentrations than Na, reflecting an origin as evaporatively concentrated seawater (Hanor, 1994). Intermediate TDS waters (10 to 100 g/L) constitute various mixing-type hydrochemical facies between the aforementioned water types, and are best characterized as Na-SO4 type waters. The 25-50 g/L contour interval marks the transition between significantly different water chemistries and is interpreted to be a mixing zone between invading fresh waters and more "connate" brines. The width and position of this transition zone varies between aquifers (Figures 2.3a,b, 2.4). Mississippian aquifers have a similar range of TDS values and exhibit similar TDS distributions as the underlying Paleozoic aquifers (e.g., Midale Aquifer, Figure 2.3c). Of particular interest to the Weyburn CO2 Project is the steep salinity gradient (from <50 to >150 g/L) within the Midale and Frobisher Aquifers across the Weyburn Field (Figures 2.3b, 2.4). Invading fresher waters mix to transition-type Na-SO4 waters across the field. Hydrochemical facies (e.g., Ca-SO4, Na-Cl, and Ca-Na-Cl types) and interpreted origin of waters in Mississippian aquifers are the same as for the Deep Paleozoic aquifers. Although waters in Mississippian aquifers have similar chemical compositions and origins, the spatial distribution of water types is variable between each aquifer (e.g., Figure 2.4) indicating differences in aquifer hydraulics.

Formation fluids in Mesozoic aquifers are markedly different from the underlying aquifer groups (Figures 2.3a,b, 2.4). TDS are generally much lower with maximum values up to 85 g/L (Figure 2.3b) and typical values between 10-50 g/L (Figure 2.4). There is no consistent spatial pattern of TDS between the Mesozoic aquifers. Na-HCO3 waters comprise the dominant water type in all of the Mesozoic aquifers, in contrast to the Paleozoic aquifers in which this water type does not occur. These characteristics suggest an active flow regime comprised of formation waters of predominantly meteoric origin. Indeed, the most relevant difference between the Mesozoic aquifers and the underlying Mississippian aquifers is the absence of brines (TDS >100 g/L) in any of the Mesozoic aquifers within the study area (e.g., Figures 2.3a,b, 2.4).

### 2.3.2 Driving forces and fluid flow directions

Directions of regional formation water flow were determined using potentiometric surfaces obtained from pressure measurements in each aquifer. This discussion is limited to flow directions in the aquifer receiving $CO_2$ (Midale Aquifer, Figure 2.5b) and a typical Mesozoic aquifer above it (Mannville Aquifer, Figure 2.5a). Flow patterns of formation waters are normally interpreted from gradients of equivalent freshwater hydraulic head (*EFWH*), with flow toward lower values of *EFWH* (e.g., Figure 2.5b). However, the presence of saline brines, and thus the potential for significant density-related flow effects ~~in the~~ Mississippian and Deep Paleozoic aquifers, complicates the process of determining flow directions.

In aquifers with significant spatial variations in formation water density, a parallel approach of mapping *EFWH* and calculating point estimates of density-corrected water driving forces *WDF* was used. A detailed description of the theory (Davies, 1987; Bachu, 1995) and the process (Alkalali, 2002; Alkalali and Rostron, 2003) is included in Appendix (A). In short, density related flow effects become significant where the aquifer slope increases, density (i.e., TDS) increases, gradient of *EFWH* decreases, or a combination of the preceding factors occurs. In order to account for significant density related flow effects, the *WDF* was calculated on a discretized grid in each aquifer. In-situ formation water densities were calculated using an equation of state (Appendix A). The *WDF* was calculated by adding a buoyancy correction to the gradient of *EFWH* (Davies, 1987; Alkalali and Rostron, 2003). Flow directions are indicated by the direction of the *WDF* vectors, and an indication of the magnitude of the driving force is given by the length of the *WDF* vector (Figure 2.5).

In Deep Paleozoic aquifers (not shown) EFWH values range from over 1000 m in the south to less than 600 m in the northeast. Hydraulic gradients ranging in magnitude between 0.1 to 7 m/km, with an average value of about 1 m/km, drive formation waters across the study area in a generally northeasterly direction. Individual aquifers exhibit similar trends in magnitude and gradient of *EFWH*, with little dependence on aquifer depth. Formation water densities are generally high in the Deep Paleozoic aquifer group (e.g., Figure 2.3d) and large areas of intense density flow reversals are common, where the WDF deviates strongly from the driving force predicted by the hydraulic gradient, resulting in down dip basin-inward flows.

Within Mississippian aquifers (e.g., Midale Aquifer, Figure 2.5b), hydraulic heads have similar trends to the underlying Deep Paleozoic aquifers. The average direction of formation water flow in the Midale Aquifer is diverted to the east-southeast in the vicinity the Weyburn Field (Figure 2.5b). The eastward-deflected flow is attributed to the hydraulic barrier created by the Watrous Aquitard at the Midale subcrop. Hydraulic gradients are generally comparable to other Paleozoic aquifers except for local areas with gradients up to 20 m/km in the east (Figure 2.5b). Locally high gradients in *EFWH* indicate the existence of barriers to lateral flow. Density-corrected driving force vectors within the Midale Aquifer indicate that flow directions are correctly represented by *EFWH* in the west, due to low TDS in that portion of the aquifer (Figure 2.3c). Water driving forces are deflected down dip in the south half of the Weyburn Field as increasingly dense brines and a southward-increasing structural gradient become important controls on flow (Figure 2.5b). The steep salinity gradient across the Weyburn Field in the Midale Aquifer marks the approximate position of this transition to buoyancy-dominated flows. Other Mississippian aquifers show similar patterns of fluid flow.

In the Mesozoic aquifers, average water flow directions are more variable between aquifers. Magnitudes of hydraulic gradients are also lower than those observed in the underlying aquifer groups. Flow directions in the Jurassic Aquifer (not shown) are directed north-northeast, similar to the underlying Mississippian aquifers. Within the Mannville Aquifer, hydraulic heads vary from over 650 m in the west, to values less than 500 m in the east-northeast, driving fluid flow in a generally east to west direction (Figure 2.5a). In the Newcastle Aquifer (not shown) fluids are flowing south to north, following the elongate orientation of the permeable Newcastle sand body (Figure 2.7a). The absence of dense brines in the Mesozoic aquifers (e.g., Figure 2.3a) permits the use of potentiometric surface maps alone to delineate lateral formation water flow directions (Figure 2.5a).

### 2.3.3 Vertical pressure gradients

Vertical pressure profiles indicate the presence or absence of a vertical component to the hydraulic gradient, which cannot be quantified from potentiometric surface maps. Two pressure versus depth (p[d]) profiles in the vicinity of the Weyburn Field area (Figure 2.6) reveal important elements of the hydraulic regime through the entire section at Weyburn. First and overall, there is no significant vertical component to flow in the Deep Paleozoic and Mississippian aquifers, as all pressure data fall along the nominal hydrostatic gradient (Figures 2.6a,b). In this case, a hydrostatic vertical pressure gradient indicates a lack of vertical flow; in other words, formation water flow is almost entirely horizontal in these units. Second, within the Weyburn Field, most of the Mississippian data are slightly overpressured (Figure 2.6a, 1.36-1.53 km depth). The origin of these overpressures is ambiguous; they could indicate minor isolation of that portion of the aquifer, or reflect the pressurization effects of water injection. In any case, these data fall along a single hydrostatic gradient, indicating that water flow through the reservoir zone is predominantly horizontal. Third, east of the Weyburn Field, p[d] data show a change in slope or an apparent break between the Midale Aquifer and the Watrous Aquitard (Figure 2.6b). If these were both permeable units, the change in slope would indicate an upward component of flow. However, given the relatively low permeability of the Watrous Aquitard, the more likely interpretation of the break in the p[d] profile is a hydraulic discontinuity between the Mississippian (Midale Aquifer) and the Mesozoic (Jurassic Aquifer). Finally, Mesozoic aquifers are normally- to underpressured (Figure 2.6a,b, <1.25 km depth) which, in the area east of the Weyburn Field (Figure 2.6b), results in a superhydrostatic vertical pressure gradient between the Jurassic and Mannville Aquifers of 13.7 MPa/km. This indicates that upward flow is occurring locally in the shallower aquifers overlying the sequestration horizon.

### 2.3.4 Aquifer permeabilities, flow velocities, and $CO_2$ Migration

Formation water fluxes and velocities were estimated by combining mapped *WDF* with conditional simulations of aquifer permeabilities, consistent with permeability estimates from DST's, and a constant average porosity field based on core data (Figure 2.7). Spatially-variable dynamic viscosity of formation water was accounted for in the calculation of the equivalent hydraulic conductivity field using the following relation:

$$v(u) = \frac{-k(u)\rho_0 g}{\mu_0}\frac{\mu_0}{\mu(u)}[\nabla EFWH], \tag{2.1}$$

where $u$ is a location vector and the subscript $_0$ signifies the reference state for freshwater at standard temperature and pressure for,

| | |
|---|---|
| $v$ | formation water velocity; |
| $k$ | scalar-valued (isotropic) block absolute permeability; |
| $\rho$ | density of water; |
| $g$ | gravitational acceleration; |
| $\mu$ | dynamic fluid viscosity. |

Note that in Equation (2.1) viscosity is the only state variable assumed to be spatially variable as a function of formation temperature. This is because temperature has the largest effect on equivalent hydraulic conductivity. The calculation of point-wise dynamic viscosity is done using the following equation of state (Chierici, 1994, p. 38):

$$\mu(T,C)(m\text{Pa s}) = \left(1 + 2.765 \text{ x } 10^{-3} C\right) \exp\left[11.987 - 5.943 \text{ x } 10^{-2} T + 6.422 \text{ x } 10^{-5} T^2\right] \tag{2.2}$$

where $T$ is temperature in degrees K and $C$ is TDS in kg m$^{-3}$. Spatial grids of formation temperatures are obtained by interpolating temperature measurements from long-duration drill stem tests with large fluid recovery. Density in the Mesozoic aquifers varies only by minor amounts and has a relatively negligible effect on the equivalent hydraulic conductivity, and so it is assumed to be constant over the domain in the application of Equation (2.1). This assumption permits the use of *EFWH* to compute the driving force in Equation (2.1). If a similar approach were taken in aquifers where density varies significantly, such as in the Paleozoic system, density would be calculated over the area and *WDF* would be used in place of *EFWH*, as described in the preceding section.

Conditional geostatistical simulation (Deutsch and Journel, 1998) of regional aquifer permeability fields was used to generate heterogeneous permeability fields. These permeability fields honour DST-derived permeability estimates and reproduce the spatial covariance between the scattered permeability data in four key aquifers (Figures 2.7 and 2.8). The permeability data have an intrinsic variance related to the sample support volume (the scale of the data), which necessarily decreases as the data are made to inform larger volumes. A DST in the moderate transmissivity formations in the study area may have a radius of investigation of 15–30 m, so scaling of the permeability histogram and variogram (Kupfersberger et al., 1998; Oz et al., 2002) is necessary to get the correct variance at the model scale (cells of 3150 x 2600 m were used in Figures 2.7 and 2.8). The upscaled variogram models have an extended range and a decreased nugget effect, as short scale variability in the permeability data cannot be resolved at regional mapping scales. The theory and practice applied in this study, as well as the program used to perform the scaling are found in Oz et al. (2002).

Sequential simulation can produce reasonable representations of the spatial structure of heterogeneous permeability fields. A single realization of Mannville Aquifer permeability (Figure 2.8) reveals the presence of areally-extensive, high-conductivity channels, which is consistent with geological interpretation (Christopher, 2003). Calculated point groundwater velocities (via Equation 2.1) in these channels may approach 50 m/yr (Figure 2.8).

If a "map" of the permeability field is desired, a criterion for selecting a single realization is a minimized mismatch between observed and model-calculated hydraulic heads. However, selecting a single realization does not take advantage of a stochastic approach in the presence of correlated data and a model of the spatial correlation between the data locations. For example, the formation-water flow velocity in the Mannville Aquifer overlying the sequestration target horizon was identified as a key parameter in risk assessment. Quantifying the uncertainty in the local mean velocity (i.e., the average velocity over a specified area [subdomain] within the study area) in the Mannville Aquifer over the area of the Weyburn Field (Figure 2.8) was desired for this reason. The uncertainty in local mean velocity is dependent on the spatial configuration of the data, and may be calculated through conditional simulation by obtaining the local average velocity in the Weyburn Field area from an ensemble of realizations (Figure 2.9).

Driving force calculations were carried out to predict the directions of lateral migration of separate phase (supercritical or gaseous) $CO_2$ in key aquifers. $CO_2$ densities at aquifer conditions were estimated using a tabulated solution for an equation of state for $CO_2$ by Altunin (1975), after the implementation by Pruess (2004). The in-situ $CO_2$

density was then combined with the *WDF* to calculate the trajectory of stringers of separate-phase $CO_2$ migrating through each aquifer (e.g., Midale Aquifer, Figure 2.10). In general, formation water flow has a small effect on separate-phase $CO_2$ migration because $CO_2$ is driven primarily by strong buoyant forces acting in the direction of the local structural gradient (Figure 2.10).

## 2.4 IMPLICATIONS FOR $CO_2$ SEQUESTRATION AT WEYBURN

Regional mapping of the deep hydrogeology at the Weyburn $CO_2$ Monitoring and Storage Project area reveals two main hydraulic regimes in the study area: a lower regime, consisting of the Deep Paleozoic and Mississippian aquifer groups, and an upper regime made up of the Mesozoic aquifer group. There is significant variability in water chemistry and pressure distributions between and within the two hydraulic regimes, and all individual aquifers in the section (e.g., Figures 2.3, 2.4), and in general, all aquifer flow is predominantly laterally confined within regionally continuous aquifer units.

Hydrogeological characteristics of the injection zone (Midale Aquifer) in the Weyburn Field are highly variable chemically (e.g., Figure 2.3c) and hydrodynamically (Figure 2.5b). Within the Weyburn Field, relatively low hydraulic gradients drive flow sluggishly (<1 m/yr) through the water zone in the Midale Aquifer, with flow roughly parallel to the subcrop (Figure 2.5b). South and east of the Weyburn Field, density-driven flows drive formation waters down dip and inward into the basin (Figure 2.5b). The Midale Aquifer is effectively separated from the overlying Jurassic Aquifer by the competent Watrous Aquitard. Although in direct contact with the Mississippian aquifers, the overlying Mesozoic aquifer system exhibits markedly different chemical characteristics (e.g., Figures 2.3, 2.4), fluid flow directions , and flow rates (Figure 2.7).

Hydrogeological conditions at the Weyburn $CO_2$ Monitoring and Storage Project site appear favourable for $CO_2$ sequestration. First, vertical pressure profiles indicate negligible vertical flow in the Midale Aquifer at Weyburn, which is consistent with the interpretation that formation waters are flowing horizontally along the subcrop through the relatively high-permeability aquifer. Second, hydrochemistry of the Mesozoic aquifer group further supports the lack of vertical flow from the underlying Mississippian aquifers. The absence of brines in the Mesozoic section supports the interpretation that there are no major vertically continuous heterogeneities in the Watrous Aquitard allowing cross-flow upward from the Mississippian aquifers along the subcrop trend. Finally, within this study area there are regions where down dip flows create favourable sites for hydrodynamic trapping of $CO_2$.

Results of the hydrogeological mapping have several implications for other aspects of the Weyburn $CO_2$ Project. First, based on the analysis of the entire flow system, it is justified to limit the system model and risk assessment studies to the Mississippian and Mesozoic aquifer groups because there is little, if any, contribution to fluid flows from the underlying Deep Paleozoic aquifers. Second, the steep gradient in TDS (<50 to >150 g/L) and chemical composition of formation waters (Ca-Na-$SO_4$ waters mixing to Na-Cl brines) should be accounted for in geochemical modeling of $CO_2$-water-rock interaction (Pruess and Garcia, 2002) and wellbore cement degradation models in the field. Finally, formation water flow in the Mesozoic aquifers will be a sensitive parameter to scenario modeling in $CO_2$ sequestration performance predictions due to predicted flow velocities as high as 10 m/yr. High flow rates are advantageous to geological sequestration because the more vigorous the flow rate, the greater an aquifer's capacity to absorb $CO_2$; but on the other hand, $CO_2$ will disperse over greater distances with time.

## 2.5 CONCLUSIONS

Regional mapping of the deep hydrogeology at the Weyburn CO2 Monitoring and Storage Project area demonstrates: 1) A strong regional aquitard (Watrous) separates the deep hydrogeological system, including the Midale Aquifer, from a shallow (1000 to 300 m depth) hydrogeologic system characterized by lower salinities, higher permeability aquifers, and faster flowing formation waters. There is no evidence for regional flow of formation waters from the Midale Aquifer across the Watrous Aquitard into the upper aquifers within the project area. The Watrous Aquitard should serve as an excellent primary seal for $CO_2$ injected into the Midale reservoir at the Weyburn Field. 2) Low flow velocities (<1 m/yr) and favourable (horizontal) flow directions in the Midale Aquifer prevent formation water flow from acting as an effective transport agent, thus hydrodynamically trapping injected $CO_2$. 3) The steep salinity gradient (TDS <50 to >150 g/L) across the $CO_2$ injection area must be accounted for in geochemical modelling and risk assessment. 4) The deep hydrogeological regime beneath the reservoir may be neglected in order to simplify the RA system models. 5) High flow velocities in overlying aquifers (1-10 m/yr) are important input parameters to the system model for scenario analysis of any $CO_2$ leakage into overlying horizons.

Classical hydrogeological mapping techniques coupled with novel analytical methods used here demonstrate that the Weyburn site is a good site to store $CO_2$ from a fluid flow perspective. These hydrogeological techniques can be used to identify other sites for $CO_2$ sequestration, and are applicable to geological storage site characterization in sedimentary basins worldwide.

## 2.6 REFERENCES

Alkalali, A., (2002) *Petroleum hydrogeology of the Nisku Aquifer*. Unpublished M.Sc. thesis, University of Alberta, Edmonton, Alberta.

Alkalali, A., Rostron, B.J., (2003) Basin-scale analysis of variable-density groundwater flow: Nisku Aquifer, Western Canadian Sedimentary Basin. *Journal of Geochemical Exploration*, 78-79, pp.313-316.

Altunin, V.V., (1975) *Thermophysical properties of carbon dioxide*. Publishing House of Standards, Moscow.

Bachu, S., (1995) Flow of variable-density formation water in deep sloping aquifers: review of methods of representation with case studies. *Journal of Hydrology*, 164, pp. 19-38.

Bachu, S., Hitchon, B., (1996) Regional-scale flow of formation waters in the Williston Basin. *AAPG Bulletin*, 80(2), pp. 248-264.

Bachu, S., (2001) Geological Sequestration of Carbon Dioxide: Applicability and Current Issues. In: L.C. Gerhard, W.E. Harrison, B.M. Hanson (Eds.), Geological Perspectives in Global Climate Change, AAPG Studies in Geology #47 (Ed. by L.C. Gerhard, W.E. Harrison, B.M. Hanson), American Association of Petroleum Geologists, Tulsa,OK. pp. 285-303.

Benn, A.A., Rostron, B.J., (1998) Regional hydrochemistry of Cambrian to Devonian aquifers in the Williston basin, Canada-USA. In: J.E. Christopher, C.F. Gilboy, D.F. Paterson, S.L. Bend (Eds.), *Eighth International Williston Basin Symposium, Special Publication*, pp. 238-246.

Chierici, G.L., (1994) *Principles of petroleum reservoir engineering*. Springer-Verlag, Berlin; New York. 430 p.

Christopher, J.E., (2003) Jura-Cretaceous Success Formation and Lower Mannville Group of Saskatchewan, Saskatchewan Industry and Resources, Regina, SK. 128p.

Davies, P.B., (1987) Modeling areal, variable-density, ground-water flow using equivalent freshwater head - analysis of potentially significant errors. In: *Solving Ground Water Problems With Models, 2*, National Water Well Association, Denver, Colorado. pp. 888-903.

Deutsch, C.V., Journel, A.G., (1998) *GSLIB, Geostatistical software library and users guide*. Oxford University Press, New York, Oxford. 369p.

Downey, J.S., Busby, J.F., Dinwiddie, G.A., (1987) Regional aquifers and petroleum in the Williston Basin region of the United States. In: *1987 Symposium of the Rocky Mountain Association of Geologists* (Ed. by M. Longman), pp. 299-312.

Hannon, N., (1987) Subsurface water flow patterns in the Canadian sector of the Williston Basin. In: *1987 Symposium of the Rocky Mountain Association of Geologists*, pp. 313-321.

Hanor, J.S., (1994) Origin of saline fluids in sedimentary basins. In: *Geofluids: Origin, Migration and Evolution of Fluids in Sedimentary Basins* (ed. J. Parnell) Geological Society Special Publication 78, pp. 151-174.

Hitchon, B., Brulotte, M., (1994) Culling criteria for "standard" formation water analyses. *Applied Geochemistry*, 9, pp. 637-645.

Horner, D.R., (1951) Pressure build-up in wells. *Proceeding Third World Petroleum Congress*, Section 2, pp. 503-521.

IPCC, (2005) Special report on carbon dioxide capture and storage prepared by working group III of the Intergovernmental Panel on Climate Change [Metz, B., O. Davidson, H. C. de Coninck, M. Loos, and L. A. Meyer (eds.)]. Cambridge University Press, Cambridge, United Kingdom and NewYork, NY, USA, 442 p.

Iampen, H.T., Rostron, B.J., (2000) Hydrogeochemistry of pre-Mississippian brines, Williston Basin, Canada-USA. *Journal of Geochemical Exploration*, 69-70, pp. 29-35.

Kupfersberger, H., Deutsch, C.V., Journel, A.G., (1998) Deriving Constraints on Small-Scale Variograms due to Variograms of Large-Scale Data. *Mathematical Geology*, 30(7), pp. 837-852.

Oz, B., Deutsch, C.V., Frykman, P., (2002) A visualbasic program for histogram and variogram scaling. *Computers & Geosciences*, 28(1), pp. 21-31.

Pruess, K., (2004) Numerical simulation of CO2 leakage from a geologic disposal reservoir, including transitions from super- to subcritical conditions, and boiling of liquid CO2. *SPE Journal*, 9(2), pp. 237-248.

Pruess, K., Garcia, J., (2002) Multiphase flow dynamics during CO2 disposal into saline aquifers. *Environmental Geology*, 42, pp. 282-295.

Rostron, B.J., Holmden, C., (2003) Regional variations in oxygen isotopic compositions in the Yeoman and Duperow aquifers, Williston basin (Canada-USA). *Journal of Geochemical Exploration*, 78-79, pp. 337-341.

Whittaker, S., Rostron, B.J., Khan, D., Hajnal, Z., Qing, H., Penner, L., Maathuis, H., Goussev, S., (2004) IEA GHG Weyburn $CO_2$ monitoring & storage project summary report 2000-2004. In: *Seventh International Conference on Greenhouse Gas Control Technologies, 1* (Ed. M. Wilson, M. Monea), Petroleum Technology Research Centre. pp. 15-69.

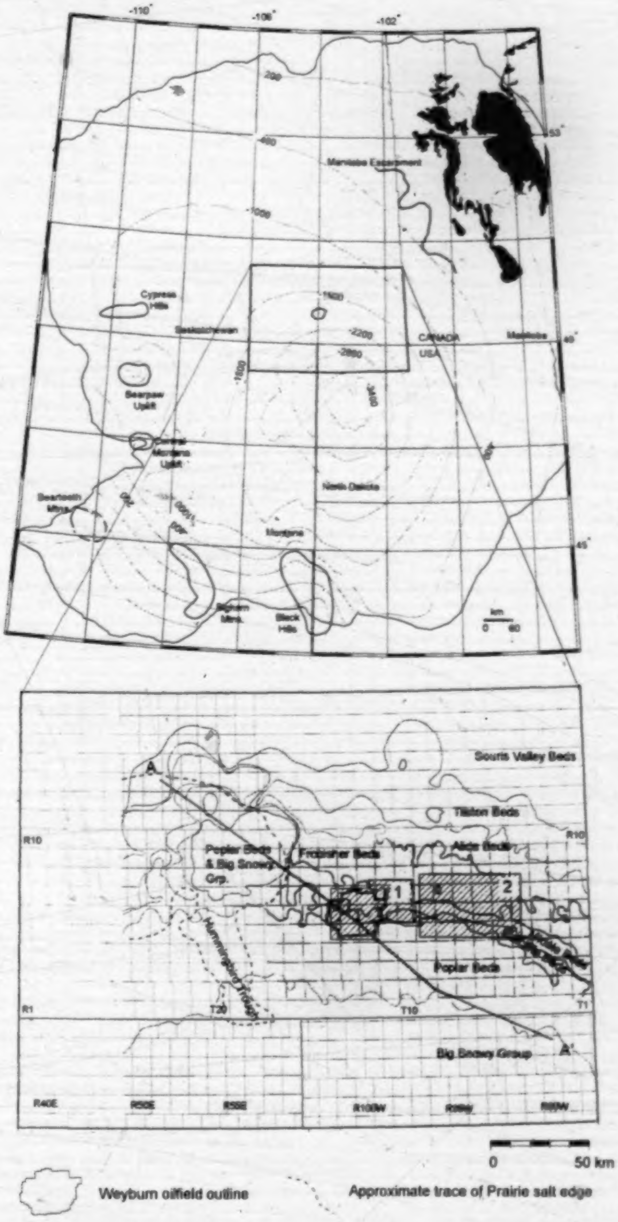
-110°
-106°
-102°
53°
49°
45°
200
400
-1000
-1600
-1800
-2200
-2800
-3400
Manitoba Escarpment
Cypress Hills
Saskatchewan
Manitoba
CANADA
USA
Bearpaw Uplift
Central Montana Uplift
Beartooth Mtns.
North Dakota
Montana
Bighorn Mtns.
Black Hills
km
0 60
Souris Valley Beds
Tilston Beds
Alida Beds
Frobisher Beds
Poplar Beds & Big Snowy Grp.
Poplar Beds
Big Snowy Group
A
A'
1
2
3
R10
R1
T20
T10
T1
R40E
R50E
R55E
R100W
R99W
R89W
0
50 km
Weyburn oilfield outline
Approximate trace of Prairie salt edge

Figure 2.1. Composite reference map of study area set within the Williston Basin. Large area shows overall basin structure (structure contours on top of Ordovician Red River Formation) and major tectonic elements. Inset shows Weyburn Project map area and the slightly smaller geological characterization area (shaded area) including Mississippian subcrop map. Numbered blocks (hatched) are locations of data used to construct pressure-depth profiles.

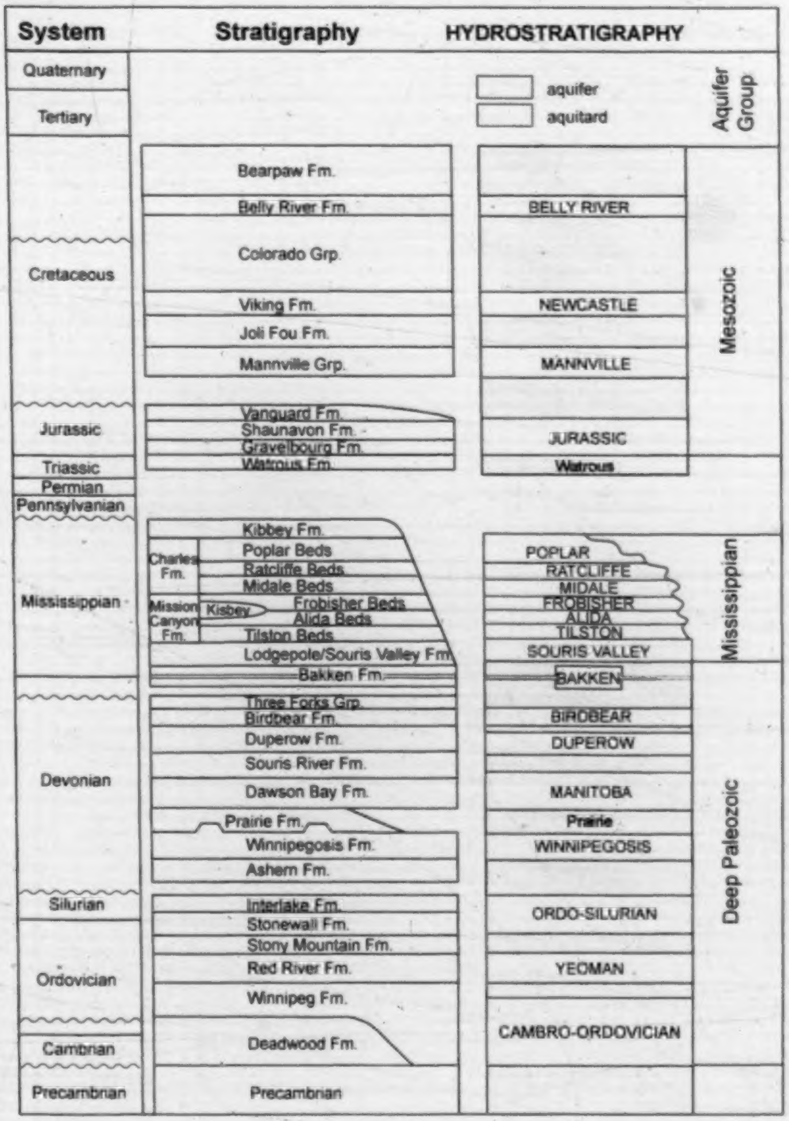
System
Stratigraphy
HYDROSTRATIGRAPHY
Quaternary
Tertiary
aquifer
aquitard
Aquifer Group
Bearpaw Fm.
Belly River Fm.
BELLY RIVER
Cretaceous
Colorado Grp.
Viking Fm.
NEWCASTLE
Joli Fou Fm.
Mannville Grp.
MANNVILLE
Mesozoic
Jurassic
Vanguard Fm.
Shaunavon Fm.
Gravelbourg Fm.
JURASSIC
Triassic
Watrous Fm.
Watrous
Permian
Pennsylvanian
Kibbey Fm.
Poplar Beds
POPLAR
Charles Fm.
Ratcliffe Beds
RATCLIFFE
Mississippian
Midale Beds
MIDALE
Mission Canyon Fm.
Kisbey
Frobisher Beds
FROBISHER
Alida Beds
ALIDA
Tilston Beds
TILSTON
Mississippian
Lodgepole/Souris Valley Fm.
SOURIS VALLEY
Bakken Fm.
BAKKEN
Three Forks Grp.
Birdbear Fm.
BIRDBEAR
Duperow Fm.
DUPEROW
Souris River Fm.
Devonian
Dawson Bay Fm.
MANITOBA
Prairie Fm.
Prairie
Winnipegosis Fm.
WINNIPEGOSIS
Ashern Fm.
Deep Paleozoic
Silurian
Interlake Fm.
Stonewall Fm.
ORDO-SILURIAN
Stony Mountain Fm.
Ordovician
Red River Fm.
YEOMAN
Winnipeg Fm.
Cambrian
Deadwood Fm.
CAMBRO-ORDOVICIAN
Precambrian
Precambrian

Figure 2.2. Williston Basin stratigraphy and hydrostratigraphic framework adopted for the Weyburn Project geological model (Whittaker et al., 2004).

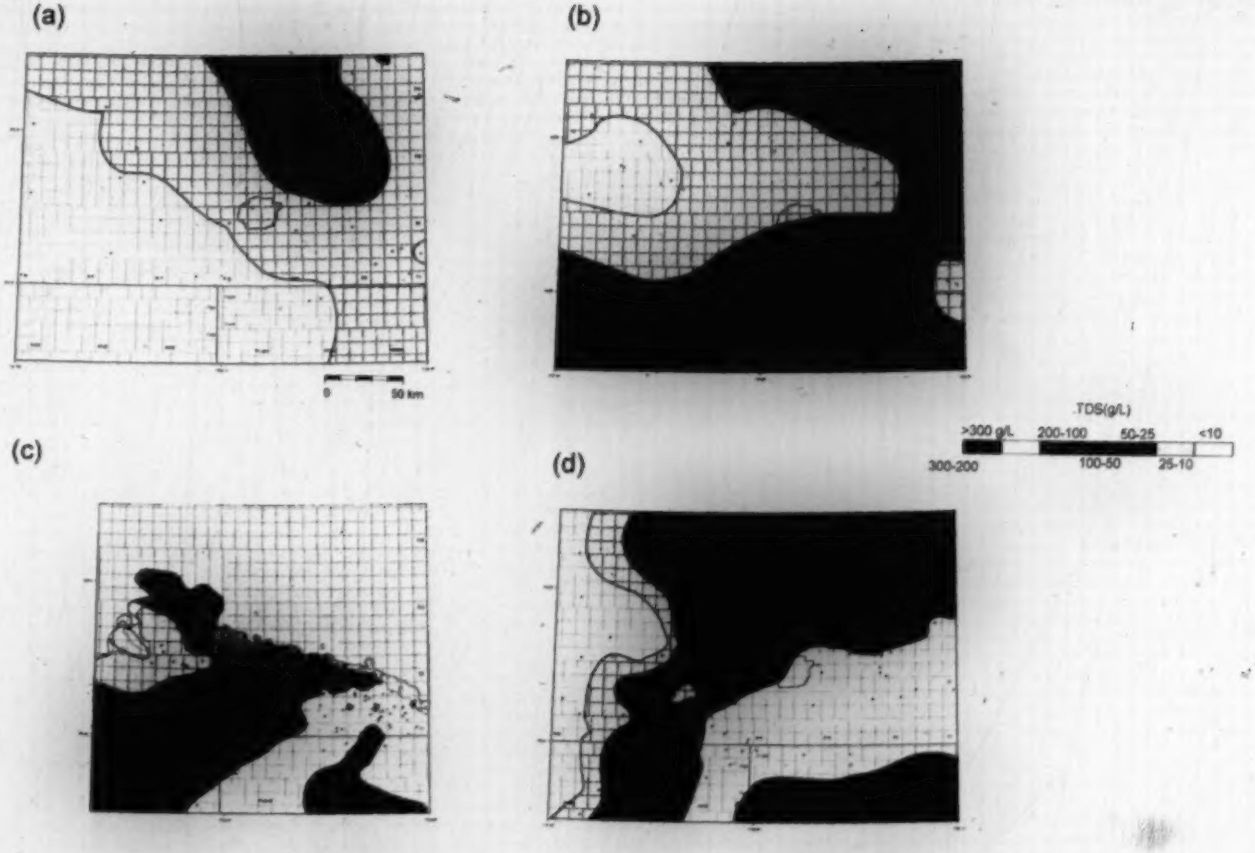
(a)
(b)
(c)
(d)
0
50 km
TDS(g/L)
>300 g/L
300-200
200-100
100-50
50-25
25-10
<10

Figure 2.3. (a) TDS in Manville Aquifer; (b) Jurassic Aquifer; (c) Midale Aquifer; and (d) Birdbear Aquifer. Crosses indicate data points.

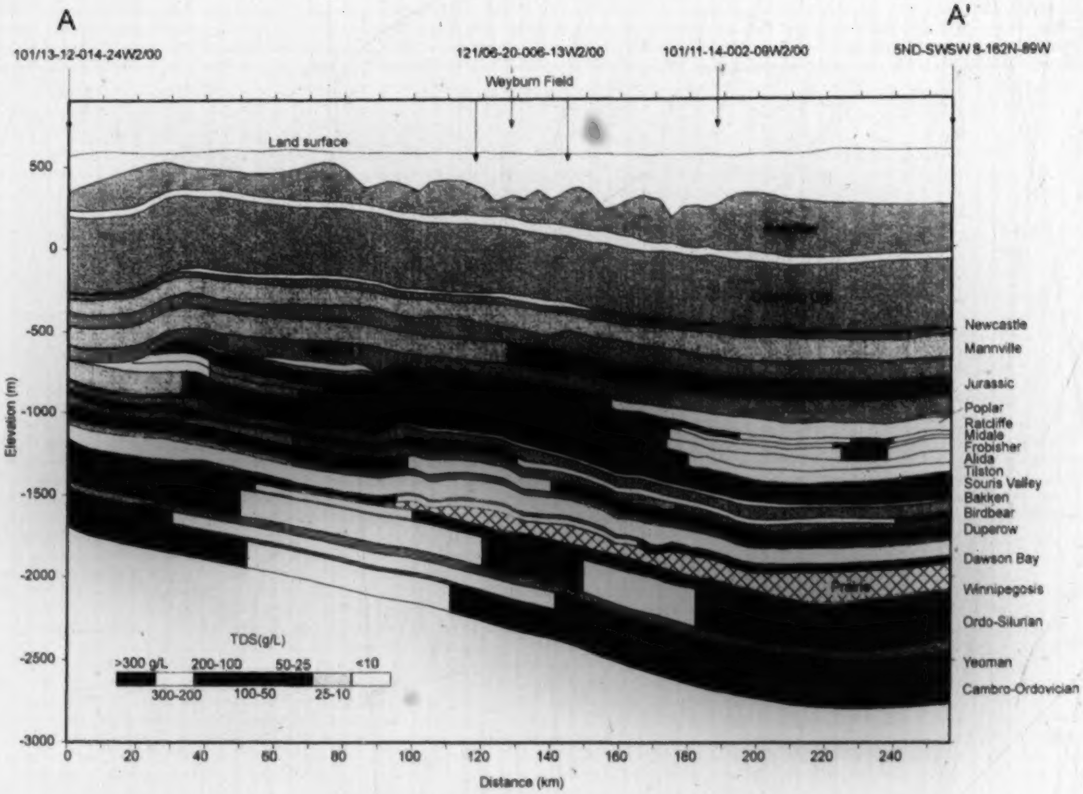
A
A'
101/13-12-014-24W2/00
121/06-20-006-13W2/00
101/11-14-002-09W2/00
5ND-SWSW 8-162N-89W
Weyburn Field
Land surface
Elevation (m)
500
0
-500
-1000
-1500
-2000
-2500
-3000
Distance (km)
0
20
40
60
80
100
120
140
160
180
200
220
240
Newcastle
Mannville
Jurassic
Poplar
Ratcliffe
Midale
Frobisher
Alida
Tilston
Souris Valley
Bakken
Birdbear
Duperow
Dawson Bay
Winnipegosis
Prairie
Ordo-Silurian
Yeoman
Cambro-Ordovician
TDS(g/L)
>300 g/L
300-200
200-100
100-50
50-25
25-10
<10

Figure 2.4. NW-SE oriented cross section A-A' (see Figure 2.1 for line of section).

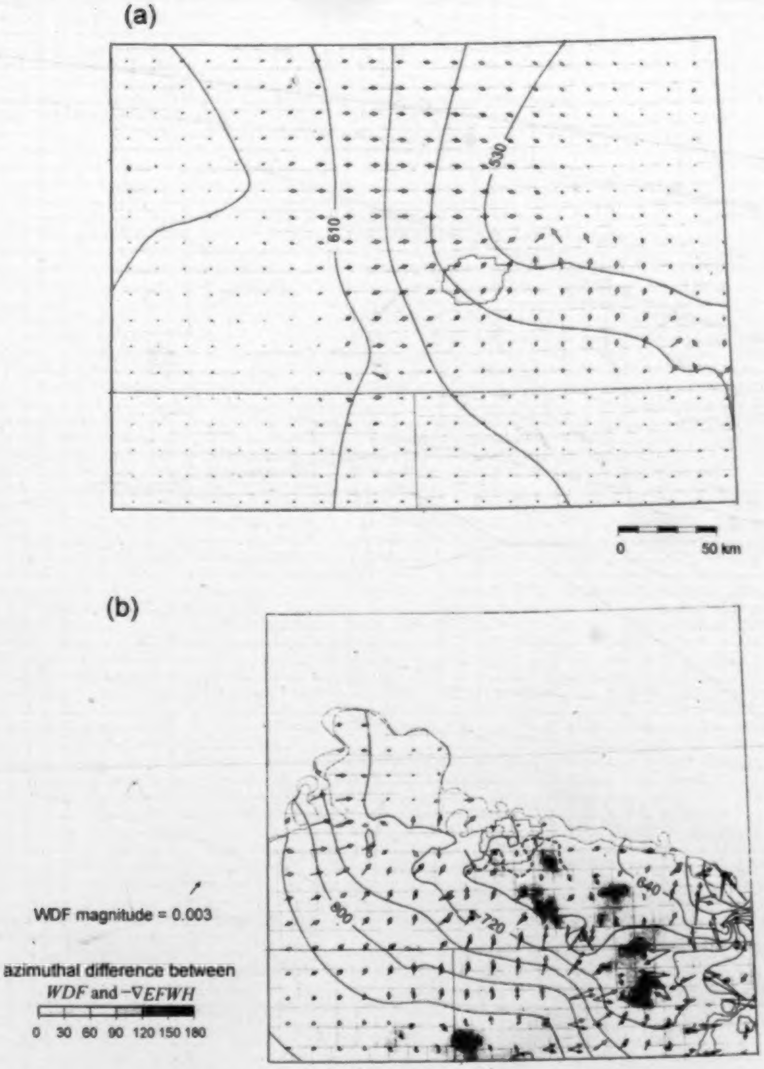
(a)
610
530
0
50 km
(b)
800
720
640
WDF magnitude = 0.003
azimuthal difference between
WDF and −∇EFWH
0 30 60 90 120 150 180

Figure 2.5. WDF vector maps for selected aquifers: a) Mannville, b) Midale. Negative gradient of *EFHW* is indicated by grey-coloured vectors and density-corrected *WDF* vectors are black. Vector scale is linear.

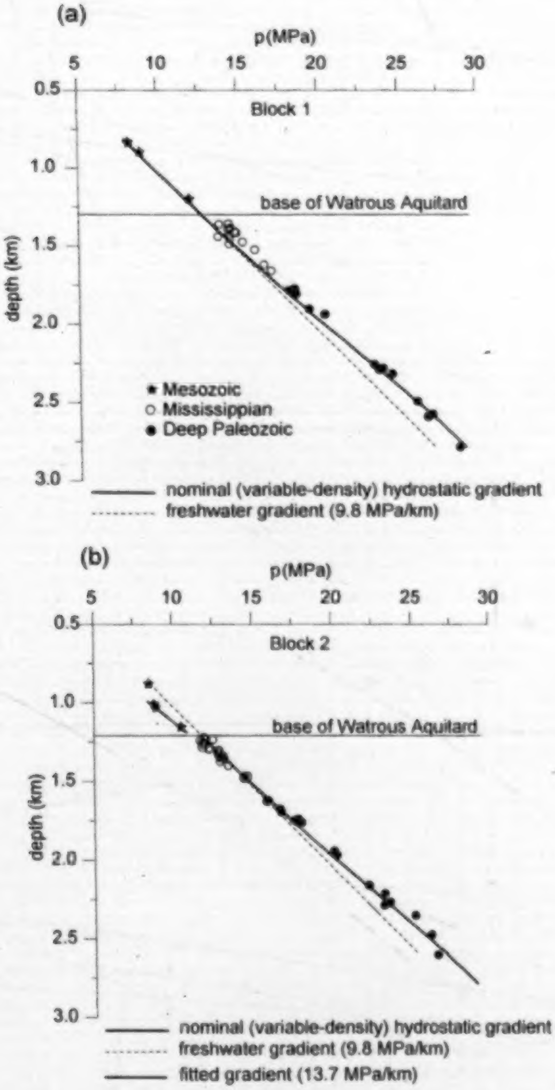

Figure 2.6 (a) p[d] profile in the Weyburn Field, and (b) east of the Weyburn Field area (locations in Figure 2.1)

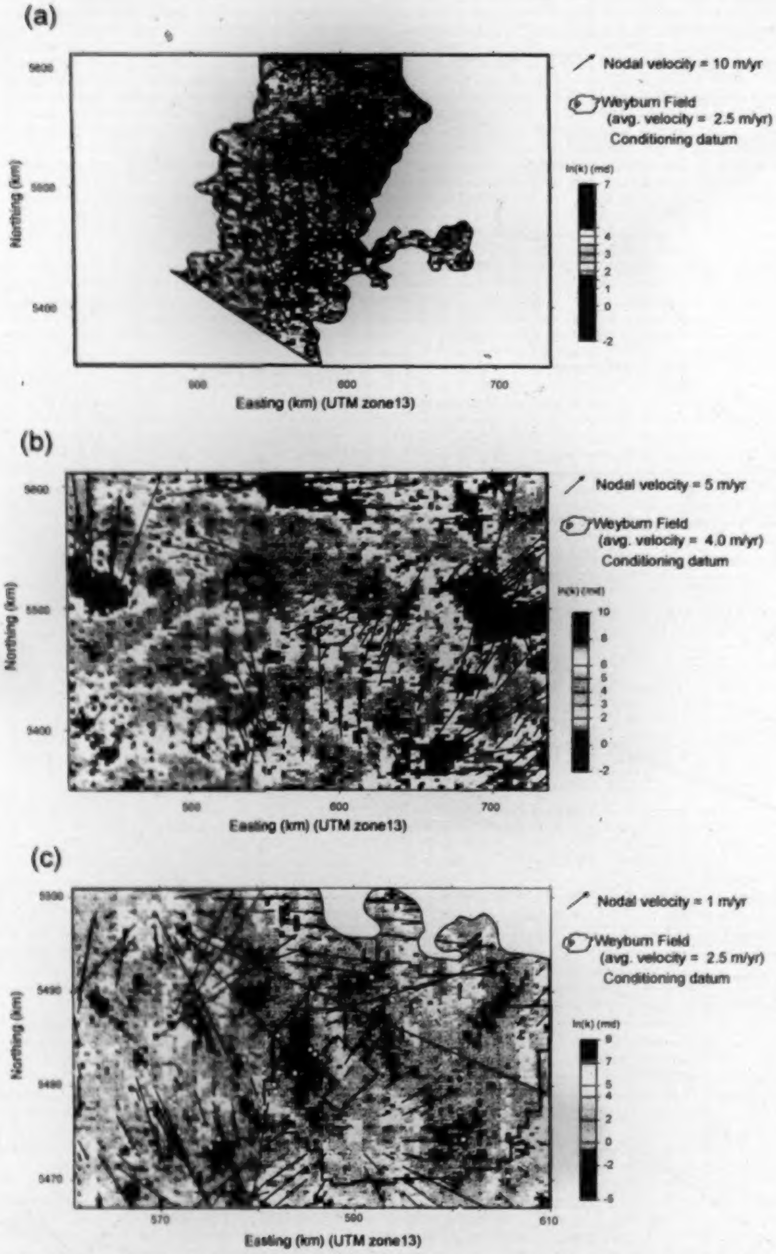
(a)
Nodal velocity = 10 m/yr
Weyburn Field
(avg. velocity = 2.5 m/yr)
Conditioning datum
ln(k) (md)
7
4
3
2
1
0
-2
Northing (km)
5600
5500
5400
500
600
700
Easting (km) (UTM zone13)
(b)
Nodal velocity = 5 m/yr
Weyburn Field
(avg. velocity = 4.0 m/yr)
Conditioning datum
ln(k) (md)
10
8
6
5
4
3
2
0
-2
Northing (km)
5600
5500
5400
500
600
700
Easting (km) (UTM zone13)
(c)
Nodal velocity = 1 m/yr
Weyburn Field
(avg. velocity = 2.5 m/yr)
Conditioning datum
ln(k) (md)
9
7
5
4
2
0
-2
-5
Northing (km)
5500
5490
5480
5470
570
590
610
Easting (km) (UTM zone13)

Figure 2.7. Realizations of aquifer permeability fields in (a) Viking; (b) Jurassic; and (c) Midale Aquifers. Note that (a) and (b) are over the entire study area and (c) is over a much smaller area centered on the $CO_2$ injection area within the Weyburn Field. Scales vary according to individual legends.

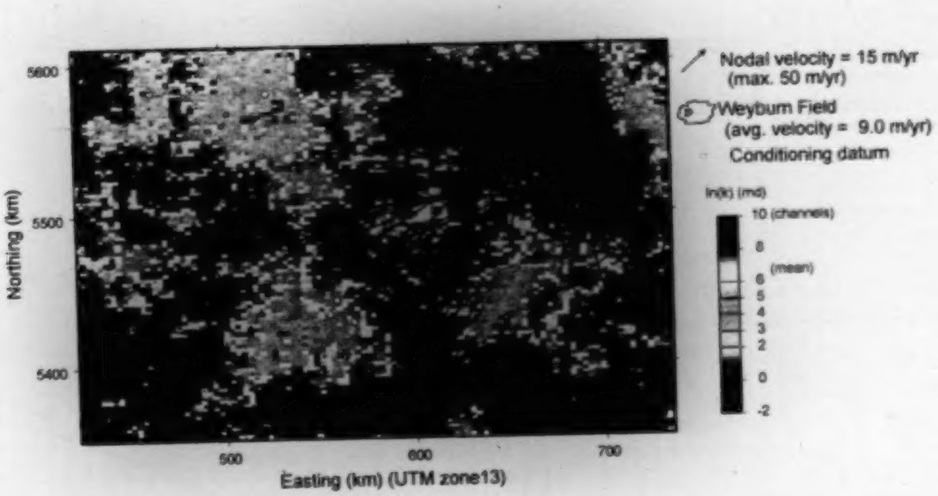
Nodal velocity = 15 m/yr
(max. 50 m/yr)
Weyburn Field
(avg. velocity = 9.0 m/yr)
Conditioning datum
ln(k) (md)
10 (channels)
8
(mean)
6
5
4
3
2
0
-2
5600
5500
5400
Northing (km)
500
600
700
Easting (km) (UTM zone13)

Figure 2.8. Single realization of Mannville Aquifer permeability field and groundwater velocities. Local mean velocity in the Weyburn Field area for this realization is 9 m/yr. Points represent DST locations.

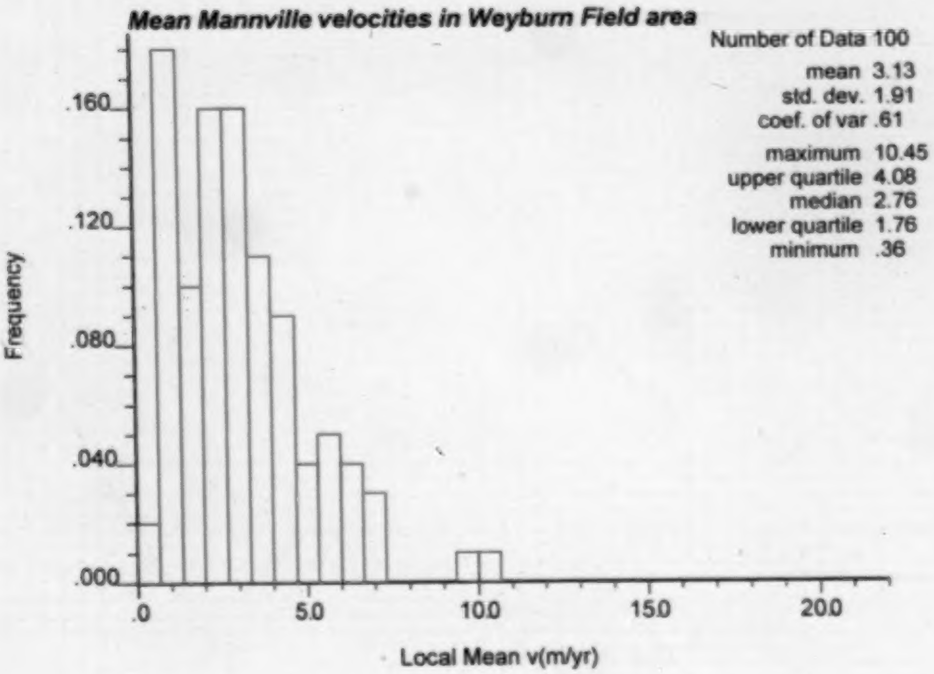

Figure 2.9. Histogram of the local mean groundwater flow velocity in the Mannville Aquifer from 100 realizations over the Weyburn Field area.

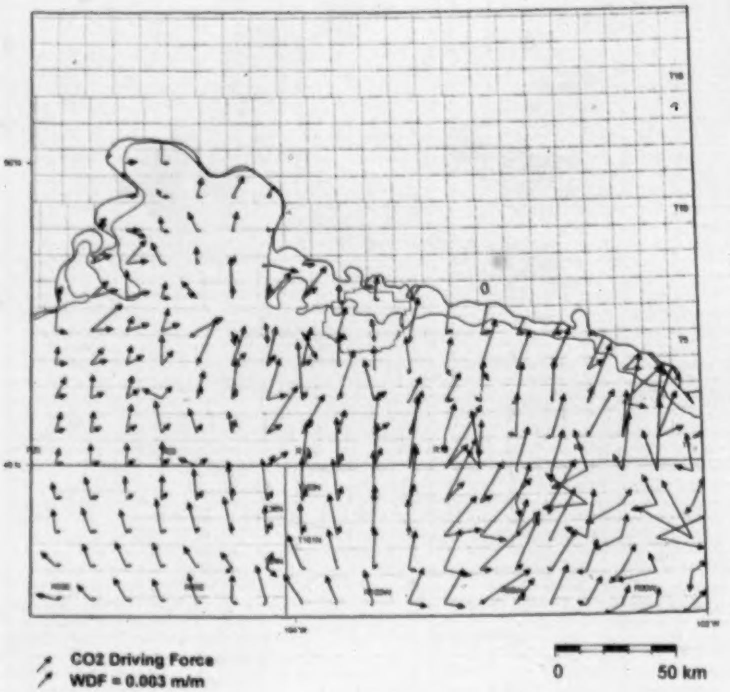
CO2 Driving Force
WDF = 0.003 m/m
0
50 km

Figure 2.10. WDF (black vectors) and CO2 Driving force field (red vectors) predicted within the Midale Aquifer.

# 3.0 COMPOSITIONS AND DISTRIBUTIONS OF FORMATION WATERS IN THE IEA GHG WEYBURN $CO_2$ MONITORING AND STORAGE PROJECT AREA: WILLISTON BASIN*

## 3.1 INTRODUCTION

The composition, classification, and distribution of subsurface brines in sedimentary basins has been of interest to scientists for decades (e.g., Sulin, 1946; Chebotarev, 1955; Clayton et al., 1966; Collins, 1975; McCaffrey et al., 1987; Hanor, 1994; Lowenstein et al., 2003). Formation waters record events and processes occurring throughout the evolution of sedimentary basins and classifying formation water types and comparing hydrochemical patterns is fundamental to hydrogeological mapping for delineating patterns of regional flow [Back, 1961; Tóth, 1984]. The interpretive keys to hydrochemical mapping are: an understanding of the origin of the chemical species dissolved in formation waters, and the inference of the mechanisms that have caused their subsequent redistribution in the flow system.

The motivation for this work was threefold: First, hydrochemical mapping was an integral part of the detailed analysis of the geological framework conducted for the IEA GHG Weyburn $CO_2$ monitoring and storage project (Whittaker et al., 2004; Preston et al., 2005). Carbon dioxide sequestration, in the form of geological storage, involves the injection of anthropogenic $CO_2$ into saline aquifers or oilfields (Socolow, 2005). Prediction of the storage potential of the geological framework is contingent upon understanding the nature of long-term natural fluid migration in the area, which, in turn, depends on interpretations drawn from mapping the hydrochemical distributions of formation waters. Second, previous hydrochemical and hydrogeological studies in the Williston Basin require updating and lack important details: They are missing a wealth of recent data, which has since become available as a result of deep drilling for petroleum exploration (Haidl, et al., 1996), most previous studies lack relevant hydrostratigraphic detail — particularly in the Mississippian System; and previous studies have not accounted for the effects of density gradients on the flows of formation waters (see Chapter 4). Thus, by mapping and characterizing the formation water chemistry through the entire succession of deep (> 300 m depth) aquifers within the study area, we expected to gain new insights into the present (and past) hydrogeology of the Williston Basin.

---

* A version of this chapter has been submitted to the journal *Geofluids*, Blackwell Publishing, and is expected to be published with the title shown by authors: D.K. Khan and B.J. Rostron.

## 3.2 STUDY AREA AND HYDROGEOLOGICAL FRAMEWORK

The area under consideration encompasses an approximately 70,000 km$^2$ cross-border region of the Williston Basin, bounded by meridians 102-106W and parallels 48.5-50.5N (Figure 3.1). The study area is offset slightly north of the basin's depocentre, situated beneath North Dakota. Maximum depths to Precambrian crystalline basement within the area are at approximately 3800 m. Structure contours in Figure 3.1 represent the elevation of the top of the Red River Formation (Ordovician), which approximates the overall geological structure of the basin.

A 100 km radius around the Weyburn oilfield was the formally-defined study area for the geological characterization component of the Weyburn Project (Whittaker et al., 2004). The hydrogeological study was done over a slightly larger area, extending an additional 50 km to the west (Figure 3.1), to include additional hydrochemical data. Mississippian aquifer maps, however, cover only the smaller geological characterization area because the Mississippian hydrostratigraphic framework depends on data from the detailed geological work done for the Weyburn Project in the smaller study area.

### 3.2.1 Previous work

The hydrogeology and hydrochemistry of the Williston Basin has been widely studied, with examples from the Canadian side of the basin (Hannon, 1987; Toop and Tóth, 1995; Bachu and Hitchon, 1996), the American portion (Downey, 1984a,b; 1986; Downey et al., 1987; Berg et al., 1994; Busby et al, 1995; DeMis, 1995; LeFever, 1998), and on a basin-wide scale (Benn and Rostron, 1998). Previous hydrogeological studies have concluded that formation waters generally flow from the S-SW to N-NE across the basin (e.g., Downey, 1984a,b; Hannon, 1987; Demis, 1995; Bachu and Hitchon, 1996). This cross-basin flow is thought to occur in response to a regional hydraulic gradient created by topographic elevation differences, approximately 1000 m on average, at opposite edges of the basin. Meteoric waters are thought to enter the basin at uplifted aquifer outcrops along the south, southwest and western basin flanks (Figure 3.1) and are driven to depth, as indicated by very fresh formation waters in the Paleozoic aquifers (Busby et al., 1995; Hitchon, 1996; Benn and Rostron, 1998) with meteoric isotopic signatures (Rostron and Holmden, 2003). Saline formation waters are thought to discharge along the low-elevation Paleozoic aquifer outcrops along the Canadian Shield (Figure 3.1). It has been suggested that these discharging waters are likely mixed with refluxing Pleistocene-age glacial meltwater (Grasby and Betcher, 2002). Deep basin brines are known to exist in the central area of the basin and are displaced from the basin centre, somewhat updip onto the Northeast basin flank (Downey, 1984a,b;1986). This cross-basinal flow system is thought to have originated relatively recently, with the current hydraulic boundary conditions initiated at the onset of the Laramide orogeny and reaching peak hydrodynamics in the Early Tertiary (DeMis, 1995). Present-day hydrodynamics cause tilted oil-water contacts in oil fields, and result in brine inflows which threaten subsurface potash mining operations (DeMis, 1995; Wittrup and Kyser, 1990).

All previous hydrogeological studies of the Williston Basin have lacked detail in the definition of flow units (aquifers and aquitards), from the lithologically diverse stratigraphic column. In particular, though not exclusively, the thick Mississippian System of rocks has never been subdivided into individual flow units despite the fact that petroleum geologists have long recognized (at least implicitly) that the Mississippian rocks are not hydraulically uniform. The importance of the Mississippian System for its hydrocarbon resources has resulted in a huge volume of geological and hydrogeological data; and recently, the interest in $CO_2$ EOR/Sequestration projects constitutes a need to re-examine this data in greater detail.

### 3.2.2 Hydrostratigraphy

To examine the hydrochemistry of the study area, geologic strata must be regrouped into hydraulically-similar flow units: aquifers, which are relatively transmissive strata or groups of strata; and aquitards, which are of relatively low permeability. The classification of a stratum or a group of strata as either an aquifer or an aquitard is based largely on the purpose of study and the time scales of the processes under consideration (Tóth, 1995). Availability of data also plays a role in the construction of the hydrostratigraphic framework.

A hydrostratigraphic framework consisting of 19 major aquifers and 13 major aquitards was developed for this study (Figure 3.2). The hydrostratigraphic framework consists of three major aquifer systems: Deep Paleozoic, Mississippian, and Mesozoic.

There exists a large body of literature on the geology of the Williston Basin so only brief geological descriptions of the aquifers and some of the aquitards are provided here. Further details of the geology and stratigraphy in the study area can be found elsewhere (e.g., Whittaker et al, 2004 and references therein).

### *Deep Paleozoic Aquifers*

The hydrostratigraphic subdivision of the pre-Mississippian Paleozoic strata follows from that devised by Benn and Rostron (1998), and used in subsequent studies by Iampen and Rostron (2000), and Rostron and Holmden (2003). Several aquifers are mapped within what have previously been considered thick confining aquitards (Downey, 1984; 1986; Downey et al., 1987; Busby et al., 1995), or undifferentiated aquifer systems (Bachu and Hitchon, 1996). This aquifer group consists of eight major aquifers and several intervening aquitards, each comprised of one or more formations forming of variable thickness, lithology and distribution (Figure 3.2). Readers are referred to Whittaker et al., (2004) for a detailed description of the constitutive geology of the hydrostratigraphic section.

### *Mississippian Aquifers*

The Mississippian System was divided into seven aquifers based on the formal stratigraphic subdivisions adopted in Canada (Sask. Geol. Soc., 1956) (Figure 3.2). This geologically intuitive approach to hydrostratigraphy was adopted for the Mississippian

System because of the following: Thick stratigraphic successions within the Mississippian Beds form shallowing-upward cycles of peritidal deposits — for example, the Midale Beds (hosting the Weyburn oilfield) consist of relatively porous and permeable limestone and dolostone layers capped by dense anhydrites formed in very shallow to periodically exposed evaporitic environments (Whittaker et al, 2004). Thus, cycles of alternating and regionally continuous high and low porosity/permeability layers occur throughout the Mississippian strata in the northeast portion of the Williston Basin. Major cyclic successions are often defined by depositional surfaces used as markers to subdivide the Mississippian System stratigraphically (Fuzesy, 1983).

### *Mesozoic Aquifers*

Three aquifers were mapped within the Mesozoic System, which is a thick package of predominantly fine-grained, low-permeability siliclastics (Figure 3.2). At the base of the Mesozoic System are the mudstones and siltstones of the Watrous Formation that form the Watrous Aquitard. The Watrous is a regionally-continuous aquitard that separates the underlying Deep Paleozoic and Mississippian aquifer systems from the Mesozoic aquifer system. The Gravelbourg Formation and overlying Shaunavon Formation form a package of permeable carbonates and sandstones, comprising the Jurassic Aquifer, directly overlying the Watrous aquitard. Sandstones of the Cretaceous-aged Mannville Group and unconformable undifferentiated permeable Jurassic sands at the base of the Mannville Group, form the Mannville Aquifer, which is the most prolific aquifer in the section. A thin sandstone between the shales of the Joli Fou Formation and the base of the overlying Bearpaw Formation comprises the Newcastle (Viking) Aquifer. The uppermost Belly River Aquifer was identified (Figure 3.2), but not mapped, due to an extreme paucity of data within the study area.

Tertiary and Quaternary-aged strata were not included in this study. The Weyburn Project included these potable water-bearing strata as part of the "biosphere" (Whittaker et al., 2004), the base of which formed the top boundary of the geological section under consideration herein.

## 3.3 DATA AND METHODOLOGIES

A hydrogeological database of over 5300 fluid pressures and formation temperatures and over 8500 formation-water analyses was assembled for this study from a combination of public and private data sources. This was supplemented with petrophysical data from core analyses within key aquifers and over 100 water samples collected from oilfield wellheads. Only the results of the hydrochemical data processing are presented in this paper.

Stratigraphic surfaces were mapped by geologists at Saskatchewan Industry and Resources and the North Dakota Geological Survey and made available for the study through the Weyburn Project (Whittaker et al., 2004). Hydrogeological data were assigned to their respective aquifer units using structural controls provided by the geological mapping. This assignment was an iterative procedure which made use of digital grids of elevation differences between the tops and bases of water sample intervals and the stratigraphic surfaces defining aquifers.

Screening of non-representative water chemistry data was based roughly on culling criteria developed in previous studies (Hitchon and Brulotte, 1994). These criteria were modified to give consideration to significant differences in formation water chemistry between the Williston and Alberta Basins, such as fresh Ca-Na-$SO_4$ type waters with low Na/Ca and high Na/Cl ratios and high $K^+$ brines within the Williston Basin. The data culling process was iterative, and largely manual, due to the highly variable compositions of formation waters in the study area.

## 3.4 RESULTS

### 3.4.1 Distribution and composition of formation waters

*Total Dissolved Solids*

Total Dissolved Solids (TDS) is a measure of the sum of dissolved ionic constituents of pore waters and it is therefore a bulk parameter that is useful for obtaining a broad overview of a groundwater flow system. It is relatively easily to measure with little possibility for major analytical error, or at least it is easy to perform quality assessment by a simple charge balance between the major anions and cations: namely, $HCO3^{-}$,$SO4^{2-}$, $Cl^{-}$, $Mg^{2+}$, $Ca^{2+}$, $K^{+}$, and $Na^{+}$. TDS may be regarded as a first-order estimate of the extent of interaction of the pore fluids with the surrounding rock framework due to a number of physio-chemical processes (Chebotarev, 1955; Tóth, 1984; Hanor 1994). It is therefore possible to obtain a qualitative estimate of the residence time, or age, of different waters in a groundwater flow system via TDS.

Formation waters within the study area range between 2 and 438 g/L TDS. Maps (Figures 3.3, 3.4) and cross-sections (Figure 3.5) in this chapter use a variable contour interval that tends to illustrate significant changes in formation-water composition across isoconcentration lines.

In Deep Paleozoic and Mississippian aquifers the TDS ranges from a fresh water classification (< 5 g/L) to that of brines (>100 g/L; Carpenter, 1978). Fresh waters occur in all aquifers along the western portions of the study area (Figures 3.3, 3.4) with the apparent exception of the two deepest aquifers: the Cambro-Ordovician and the Yeoman (Figure 3.3e,f). Both of these aquifers do contain fresh waters (Benn and Rostron, 1998), but to the west of the current study area. All of the Deep Paleozoic and Mississippian aquifers contain brines, with salinity increasing systematically along a directional trend from the fresher waters in the west toward brines occupying the basin centre. The highest values of TDS within the study area, frequently over 300 g/L, are found in the southeast (Figures 3.3, 3.4).

Mesozoic aquifers have a much smaller range of TDS. In the Mannville and Newcastle aquifers, maximum TDS values of 40 and 20 g/L, respectively, are found (e.g., Figure 3.5) with an almost constant distribution of TDS across the study area (not shown). The highest values of TDS in the Mesozoic aquifer system — up to 85 g/L — are found in the Jurassic aquifer along the southern edge of the study area, at greatest depths within the Mesozoic system (Figure 3.5).

There are a number of consistent patterns of TDS observed within the study area: First, in the west, with increasing elevation there is a systematic increase in the total area occupied by fresh waters (Figures 3.3, 3.4, and 3.5). Second, brackish to saline waters within the 25-100 g/L interval mark a transition zone between significantly different water chemistries. The longitudinal axis (parallel to isoconcentration lines) of this zone shifts progressively eastward and rotates northward in subsequently shallower aquifers (Figure 3.3). In Mississippian aquifers, this transition zone consistently aligned along a northeasterly axis (Figure 3.4). Finally, there is relatively poor correlation between TDS and depth, which is an exception rather than the norm (Hanor, 1994). For example, a plot of TDS versus depth (Figure 3.6) shows a modest correlation in the shallowest depth ranges — between 500 and 1100 m, which is generally the depth range of the Mesozoic aquifer system — and a trend of increasing TDS with depth past 3000 m in the deep basin; otherwise, there is almost no correlation between TDS and depth in the study area. This is due to the similarity in TDS distribution and range within the individual aquifers of the Deep Paleozoic and Mississippian systems.

### *Major Ions*

Typically, there are predictable relationships between TDS and formation water compositions in terms of their individual major ionic constituents, as seen in datasets from sedimentary basins worldwide (Hanor, 1994), and the same holds true within the Williston Basin. The major ions routinely reported in formation water sample reports are: $Na^+$, $Ca^{2+}$, $K^+$, and $Mg^{2+}$, $Cl^-$, $SO4^{2-}$, and $HCO^{3-}$. For convenience, the valence of these ions is dropped from notation for the remainder of the discussion.

Chloride (Cl) is the dominant anion in almost every water sample and is linearly proportional to TDS for the entire dataset (not shown). Indeed, TDS, as shown in Figures 3.3 through 3.5, is a proxy of the spatial distribution of Cl.

Sodium (Na) and TDS are linearly related below 300 g/L, beyond which Na concentrations drop sharply in the Deep Paleozoic aquifers (Figure 3.7a). Halite saturation occurs at approximately 300 g/L (Hanor, 1994), which generally explains the observed behaviour, but there are several brine samples with high Na, as predicted by the linear trend, despite having TDS in excess of 330 g/L (Figure 3.7a). Mississippian samples, as a group, do not show this characteristic downward hook in Na concentration, other than a few data points which are within typical scatter (Figure 3.7b). The Mesozoic sample data display a linear relationship between Na and TDS over a relatively small range of TDS (Figure 3.7c).

Potassium (K) and Magnesium (Mg) both increase with increasing TDS in an exponential fashion for the Deep Paleozoic sample set, rising sharply beyond TDS of 300 g/L (Figure 3.7d,g)[1]. This characteristic rise in the concentration of these cations mirrors the drop in Na described above. In the Mississippian data, just as the distinct drop in Na is not observed, nor is there a clear sharp rise in K and Mg, although there is considerable the scatter in the data (Figure 3.7e,h). Potassium and Mg are minor constituents in Mesozoic formation waters (Figure 3.7f,i).

Scatter in the data increases with increasing TDS in all plots (Figure 3.7). It is possible to plot subordinate or "scanning" curves off of a main functional relationship describing the variation of an ionic species with TDS. This suggests that formation waters within the study area have intermediate compositions due to mixing between waters of low and high TDS.

For the remaining major ions, it is more informative to examine them as percentages of the total equivalent reacting values compared to their respective ionic charge group (Figure 3.8).

Calcium (Ca) is generally the dominant cation in brines with TDS exceeding 300 g/L in the Deep Paleozoic aquifers (Figure 3.8a), which is consistent with the observed drop in Na (Figure 3.7a). There is a characteristic U-shape to the dependence between Ca and

---

[1] There are several samples showing a $K^+$ value of zero. These samples do contain K, but it has not been reported.

TDS in the deep Paleozoic aquifers (Figure 3.8a). The fresh waters within the Deep Paleozoic system are also dominated by Ca, where it accounts for up to 70% of the total cations, and drops to 15% in samples around 25 g/L TDS (Figure 3.8a). Between approximately 35 g/L to 300 g/L TDS, Ca accounts for no more than about 10% of cations in the Deep Paleozoic aquifers. In contrast, in the Mississippian aquifers, Ca can account for up to 35% of the cations throughout the range of TDS (Figure 3.8a). What is most intriguing about the Mississippian sample set is that the highest TDS brines have low percentage Ca, with Na remaining the dominant cation in the most concentrated brines (Figure 3.7b). Indeed, the brines in the Mississippian aquifers are markedly different from the Deep Paleozoic brines in this respect. Conversely, fresh waters in the Mississippian aquifers are virtually identical in composition to those in the Deep Paleozoic aquifers, being dominated by Ca at the lowest TDS values, with Ca replaced by Na as TDS increases (Figure 3.8a,b). Finally, with the exception of three samples from the Jurassic Aquifer, fresh waters in the Mesozoic aquifers are generally low in Ca (<10%, Figure 3.7c), and are thus unlike the fresh waters in the two deeper aquifer groups (Figure 3.7a,b). The cationic fraction of Ca is a variable that explains a great deal about the relationship between the water types in the study area, and its role as an indicator species will be covered at the end of this section.

Brines in the study area have less than 10% Sulphate ($SO_4$) (Figure 3.8d,e). Although invisible on the arithmetic scale used in the plots, the main difference between the Deep Paleozoic and Mississippian aquifer groups is that around 300 g/L TDS, $SO_4$ drops off sharply in the Deep Paleozoic aquifers to values less than 0.1%. Sulphate is the dominant anion in the fresh waters (Figure 3.8d,e,f), and remains characteristically elevated in brackish waters having TDS < 35 g/L in the Deep Paleozoic and Mississippian aquifers (Figure 3.8d,e). The freshest waters have Ca as the complementary dominant cation, whereas brackish waters are dominated by Na. Similarly, High-$SO_4$ waters from the Mesozoic aquifers similarly have a dominant cation component of either Ca or Na. Mesozoic samples with $SO_4$ exceeding 40% of the total anions (Figure 3.8f) are from the Jurassic Aquifer exclusively. These few samples from the Jurassic aquifer — which were noted in the preceding paragraph as having Ca as the dominant cation — are compositionally identical to the fresh waters of the two deeper aquifer systems, and are atypical of the majority of Mesozoic formation waters.

Bicarbonate ($HCO_3$) exceeds 15% of the total anions in fresh waters from the Mesozoic aquifer system (Figure 3.8i), and these $HCO_3$-type waters occur in the Mannville and Newcastle aquifers only. The majority of fresh waters sampled within the Mesozoic aquifer group are of a distinctly different composition than fresh waters from the Deep Paleozoic and Mississippian aquifers, as noted above, and further suggested by characteristically elevated $HCO_3$ (Figure 3.8g-i).

### 3.4.2 Formation water classification

In order to use formation water chemistry as an interpretive tool, it is necessary to deduce the principal chemical compositions that most succinctly explain the observed variation. There are five distinct water compositions that can be differentiated by major ion chemistry within the study area:

*Type 1: $Ca$-$SO_4$*

Type 1 waters are characterized by very low TDS (< 5 g/L), Ca in excess of 40% of total cations, and $SO_4$ greater than 50% of anions (Figure 3.8). It is actually a Ca-Na-$SO_4$ type, but for clarity, the ubiquitous Na cationic component is dropped for the discussion. This water type is akin to the types of Williston Basin recharge-area waters identified by Busby et al. (1995). Its chemical character is the result of relatively short residence time (i.e., rapid flow) and relatively low reactivity with halite-free rocks along the flowpath from the recharge area(s) to the depths of the basin, as shown in Figures (3.3-3.5). These fresh waters are supersaturated with respect to anhydrite and gypsum as well as calcite and dolomite, based on an equilibrium speciation calculation using PHREEQC (Parkhurst, 1995). The position and extent of the fresh water plume entering the Williston Basin has been shown to correspond well to a large salt-free area of the basin where the Prairie Evaporite is absent (Benn and Rostron, 1998).

*Type 2: Na-Cl*

Na-Cl brines span a broad range of TDS with Ca and $SO_4$ concentrations accounting for less than 10 % of their respective ionic charge group (Figure 3.8a,b,d,e). Brines of this compositional group occur over the majority of the study area.

*Type 3: Ca-Cl*

Type 3 waters are brines with a dominant Ca cationic component. The composition is more completely expressed as Ca-Na-Cl, but as with Type 1 waters, the Na is dropped from the descriptor for convenience. These brines differ from the Type 2 brines in that Ca occurs in excess of 40% of the dissolved cations (Figure 3.8a), and the other major cations represent significant fractions of the total dissolved species.

*Type 4: Na-$HCO_3$*

This fresh water type differs from the Type 1 waters found in the Paleozoic aquifers in that it is relatively $HCO_3$ -enriched (>20% of anions) and Ca-poor (<10% of cations). Type 4 waters are only found stratigraphically above the Jurassic Aquifer.

*Type 5: Na-$SO_4$*

This water type has TDS less than 100 g/L. It is intermediate in salinity as well as composition. This type represents the principal chemical composition of the waters within the brackish water transition zone, occurring approximately between TDS contours of 25 to 100 g/L (Figures 3.3 and 3.4). The Type 5 composition is interpreted to be the result of mixing between Type 1 Ca-$SO_4$ fresh waters and Type 3 Na-Cl brines, as discussed in the following section.

### 3.4.3 Graphical representation of formation waters

A clear discussion on formation water classification requires some graphic mean of displaying distinct compositional classes. Trilinear plots, such as the Piper plot (Piper, 1944), have been used to separate sample data into distinct hydrochemical facies (Back, 1960; 1961). We found the Piper plot, as well as other ternary diagrams to be unsatisfactory in clearly displaying the principal water types interpreted from this data set. Stiff diagrams, which make use of distinct polygonal shapes, are better for classifying formation waters having a large range of compositional variation, but use absolute ion concentrations, which were already found to be less informative than normalized values in distinguishing between distinct compositions for this data set. We devised a customized plot based on a small number of key variables explaining the variation of the water types found in the study area.

A pentaxial plot displays the water samples as characteristic polygonal shapes based on five principal axes with a normalized scale from 0 to 1 (Figure 3.9): (1) TDS normalized to the range of the entire dataset; ratios between (2) $Ca^{2+}$, (3) $SO_4^{2-}$, and (4) $HCO_3^-$ and their respective charge group; and (5) The ratio of Ca to Na, normalized to the range of the dataset.

Selected type samples corresponding to the five principal water types are plotted on Figure 3.9. In general, the *vertical height* of a polygon along the TDS Norm axis indicates the concentration of dissolved solids on a relative scale. The *horizontal width* of a polygon indicates the relative importance of Ca in describing the cationic composition of a formation water sample (e.g., Type 3; Figure 3.9). Conversely, dominance of Na over Ca is implicit by the horizontal constriction of a polygon; for example, the Type 2 Na-Cl brines. A *downward point* indicates the presence of significant $SO_4$ or $HCO_3$, corresponding to Type 4 or Type 5 waters, respectively (Figure 3.9).

The plots are useful for looking at a large number of analyses as well as plotting type samples. For example, waters from the Deep Paleozoic Duperow Aquifer — which is compositionally representative of the entire Deep Paleozoic system — fall between three end members (Figure 3.10a), such that all of the samples plot within one of the characteristic polygons defining water Types 1 to 3 (Figure 3.9). This would support an interpretation that many of the samples are compositionally a mixture of two (or more) of the principal water types found in this aquifer system.

The Mississippian formation water compositions, as represented by the Ratcliffe Aquifer data (Figure 3.10b), are subtly different from the Deep Paleozoic waters (Figure 3.10a). The most conspicuous difference is the absence of Type 3 high-Ca brines from the Mississippian data.

The water types found in the Mesozoic aquifers cannot be shown by a single representative plot. Despite having a smaller range of TDS and major ionic concentrations (Figures 3.5-3.8), the Mesozoic Aquifer group is more variable with respect to overall chemical compositions between individual aquifers than what is observed from the deeper aquifer groups (Figure 3.11). Bicarbonate-enriched samples, corresponding to Type 4 waters (Figure 3.9), characterize the uppermost Mannville and Newcastle aquifers (Figure 3.11 a,b). Samples from the Mannville Aquifer are fresh to brackish Na-$HCO_3$ and Na-$SO_4$ compositions (Figure 3.11b), the former being the only water type sampled in the overlying Newcastle sand (Figure 3.11a). Mannville Aquifer formation waters have a hybrid compositional character, with chemistries somewhere between those of the subjacent Jurassic Aquifer and the overlying Newcastle Aquifer (Figure 3.11). The Jurassic Aquifer is characterized by a small number of Type 1 Ca-$SO_4$ waters, with the majority of samples represented by the Type 5 Na-$SO_4$ composition (Figure 3.11c), some of which are highly enriched in sulfate compared to the Type 5 waters observed in the deep Paleozoic and Mississippian aquifers.

Na-$HCO_3$ (Type 4) waters are not found in either the Mississippian or the Deep Paleozoic Aquifers. Conversely, the Type 2 and 3 brines characterizing the deep aquifer groups are absent from the Mesozoic aquifers. The only chemical signature that is common between the deeper groups and the Mesozoic aquifer group is the Type 1 Ca-$SO_4$ fresh water, and it is limited to the Jurassic aquifer (Figure 3.11c) which is the deepest of the Mesozoic aquifers.

### 3.4.4 Calcium as an indicator species

The cationic fraction of Ca is a key variable in illustrating the relationship between the water types in the study area. High-Ca waters, with Ca in excess of 30 percent of total cations, occur at opposite ends of the TDS scale (Figure 3.8a). These waters are found within two regions of the study area in the Deep Paleozoic aquifers (Figure 3.12a-f):

1. The high-Ca waters found along the western area in the Devonian aquifers (Figure 3.12a,b) correspond to fresh Type 1 waters (Figure 3.3). Although it appears that the Type 1 water occurs only within the Devonian aquifers, the fresh waters which occur in the other Deep Paleozoic aquifers (Figure 3.3) are mixed with the pure Type 1 waters which occur to the west of the study area).

2. High-Ca waters occurring along the southern to southwestern limits of the maps (Figure 3.12a-f) are indicative of Type 3 Ca-Cl brines.

In the Mississippian system, the fresh waters in the west (Figure 3.4) are also associated with the high-Ca Type 1 water type (Figure 3.12g-l), although the study area limits and a paucity of wells drilled in this area obscure a clear delineation from the data. Nonetheless, the elevated Ca concentrations in the west-northwest are diagnostic (Figure 3.12h,k,l). In stark contrast to the Deep Paleozoic Aquifers, however, there is no indication of Type 3 brines in the Mississippian aquifers in the deep basin within the south-southwest of the study area (compare Mississippian aquifers of Figure 3.12g-l with Deep Paleozoic aquifers of Figure 3.12a-f).

The only occurrence of high-Ca brine is in an isolated pod at the subcrop of the Poplar Aquifer in the east of the study area (Figure 3.12g). The brines in this location of the Poplar Aquifer are quite low in TDS (Figure 3.4a), so this water type is anomalous and does not represent the Type 3 brine composition. In fact, the Poplar Aquifer is quite different from the rest of the Mississippian flow units as indicated by pressure anomalies (see Chapter 4). The presence of several minor evaporite layers in this shallowest part of the Mississippian depositional sequence likely interrupts hydraulic continuity, leading to minor isolation of different zones sampled in the aquifer making it difficult to interpret the pressure and hydrochemical anomalies present within the Poplar aquifer within the framework of the larger study area.

## 3.5 DISCUSSION

The formation waters identified in the study area punctuate a gradational compositional variation that spans nearly the entire range of TDS that has been observed in formation waters throughout the world's sedimentary basins. The hydrochemical classification derived for this work is an interpretive scheme which is specific to the study area; it is formulated to explain specific elements of the hydrogeological system based on hydrochemistry. The compositional variation could be broken down using a more general classification scheme, such as that proposed by Hanor (1994), who states that formation waters can be divided into three groups:

1. Waters with dominant anions other than Cl, typically having TDS less than 10 g/L
2. Cl-dominated, halite unsaturated waters with TDS between 10 g/L to 300 g/L
3. Cl-dominated, halite saturated waters with TDS in excess of 300 g/L with Ca and K being characteristically dominant cations

Each of these major compositional groups records or reflects events and processes in sedimentary basins.

Fresh waters record geologically-recent recharge by meteoric waters; and, when observed at great depths, they indicate hydraulic continuity of the rock framework of sedimentary basins. Type 1 Ca-$SO_4$ waters found within the Deep Paleozoic and Mississippian aquifer systems of the current study area have been identified as having meteoric isotopic signatures (Bailey et. al., 1973; Rostron and Holmden, 2003).

Sodium-Cl brines are perhaps the most frequently-encountered formation water compositions. These are formed equally plausibly from evaporated seawater or by groundwater evolution, from recharge at the earth's surface to a point downgradient along a deep regional flowpath (Chebotarev, 1955; Tóth, 1984). It is possible to distinguish between these two origins based on major and trace ion chemistry.

Type 2 (Na-Cl) and Type 3 (Ca-Cl) Williston Basin brines have previously been differentiated using Na-Cl-Br systematics (Iampen and Rostron, 2000). Type 2 brines within the study area are likely the product of halite dissolution, as they have major ion chemistry that is inconsistent with evaporated seawater (McCaffrey et al., 1997). Type 3 brines appear to be residual seawater (Iampen and Rostron, 2000), but with discrepancies in major ion composition that are not easily explained by starting from a composition of modern seawater, nor is their composition easily explained by rock-water interaction (Lowenstein et al., 2003). Type 3 brines may record complex mineral-buffered reaction paths (Carpenter, 1978), or they may more simply — in terms of a chemical explanation — reflect the composition of paleo-seawaters which have had a different composition than modern seawater (Horita et al., 2001). The north-central Williston Basin is an area of a confluence between all three of the major compositional groups of formation waters.

### 3.5.1 Interpretations of the observed distributions of formation waters

The similarity in TDS patterns between the Deep Paleozoic and Mississippian aquifers (Figures 3.3 and 3.4) suggests large-scale hydrodynamic control. One possible interpretation is that efficient vertical mixing, due to weak intervening aquitards, causes compositional homogenization of formation waters. This was postulated by Hitchon (1996) for the aquifers of the Deep Paleozoic aquifer system. Analysis of vertical pore pressure variations indicates that cross-formational flow is relatively insignificant in the study area (see Chapter 4), so it is difficult to assess the competence of the intervening aquitards. In any case, the interpretation made here is that the similarity in composition and distribution of formation waters between aquifers within the Deep Paleozoic system, and between the aquifers of the Mississippian system, is instead the result of predominantly lateral mixing — advective and/or diffusive — between water Types 1,2, and 3.

Formation water flow through the deep aquifer systems within the study area is much like a parallel electrical circuit. As with the hydrochemical distributions, the fluid potentials within individual aquifers are markedly similar. This is a due to common recharge and discharge areas — specifically, their average topographic elevations —

between all of the aquifers of the two deeper systems, and the location of study being situated in the midline area (Tóth, 1978) of the flow system, where flow is predominantly horizontal (see Chapter 4).

### *Hydrodynamic Mixing*

The spatial relationship between the water types within the study area in the aquifers of the Deep Paleozoic system can be summarized by plotting selected samples along a transect parallel to the TDS gradient (Figure 3.13). Sample compositions are listed in Table (3-1). The fresh Type 1 waters occur in the west map area (Figure 3.13; sample 1). The Na-$SO_4$ Type 5 waters occur within TDS contours between 10-50 g/L (Figure 3.13; sample 2), with the $SO_4$ component decreasing as TDS increases (Figure 3.8b). These waters occur within the transition zone between Type 1 waters to Type 2 Na-Cl brines. It was straightforward to match the Type 5 composition of sample 2 (Figure 3.13) with an equilibrium mixing model starting from solutions with the compositions of samples 1 and 4 (Figure 3.13) using PHREEQC (Parkhurst, 1995). Progressing in the direction of increasing TDS from the location of sample 2, Cl becomes dominant over $SO_4$ and Na replaces Ca as the dominant cation (Figure 3.13; sample 3), indicating the transition to Na-Cl brines (Figure 3.13; sample 4). Hypersaline Na-Cl brines occupy the central study area (Figure 3.13, sample 5). Type 3 high-Ca brines are found at the end of the sampling transect, towards the south, in the area of maximum TDS (Figure 3.13, sample 7). This systematic pattern of water chemistries is similar, between all of the deep Paleozoic aquifers.

The chemical distribution of brines is influenced by hydrodynamics and mixing. Although present-day flow is sluggish due to high brine densities, elevated paleo-hydraulic gradients would have effectively mixed end-member brines within the Williston Basin (see Chapter 4). It is not straightforward to model mixing between these hypersaline brines. The ionic strengths of these solutions is at, or exceeding the upper limit of the range of applicability of the Pitzer (1987) model, which is the only available choice for modeling the behaviour of electrolyte solutions of very high (up to 6 mol/kg) ionic strengths (Langmuir, 1997). The gradational nature of the compositional variation between Type 2 and Type 3 brines observed within the study area (Figure 3.13; samples 5,6,7) the nature of the scatter in the ion versus TDS plots (e.g., Figure 3.7a), and the patterns in the pentaxial plots (Figure 3.10a), clearly indicate mixing between these end-member brines.

The majority of brines classified as Type 3 in this study are not truly representative of the end-member Ca-Cl brine type in the basin. The outlier in Figures (3.6-3.8), which plots at a TDS value of 438 g/L, is a more likely type candidate. This sample, taken during a drill stem test in the Devonian Dawson Bay Formation in the CAN HUNTER TABLELAND 6-27-2-9 well, is a brine from a relatively isolated porous and permeable zone of otherwise low permeability, evaporite-rich strata. Jensen et al. (2006) report a number of samples -- most likely from the same zone -- with end-member Type 3 Ca-Cl compositions, with TDS upward of 525 g/L, to the north and east of the current study area, in the Potash mining districts of Saskatchewan. The rest of the samples classified as Type 3 in this study area from better regional aquifers and reflect mixing and dilution with Na-Cl brines.

### *Paleohydrogeological interpretations*

The sequence of dominant ionic species observed in formation waters along the transect of Figure 3.13) is reminiscent of the well-known Chebotarev sequence (Chebotarev, 1955). In this case, however, the ionic progression is probably the result of a nesting of timescales, rather than groundwater evolution along a single, temporally-continuous flow path. The sharp interface between the fresh Type 1 waters and saline brines (Figures 3.3 and 3.4) is a gradational hydrochemical contact between waters of possibly vastly different ages. The fresh water within the study area spans the age of the present day flow system, and the Type 2 Na-Cl brines east of the brackish transition zone may be much older.

As an example, it is of interest to consider the timing of dissolution of the Prairie Formation salt in the Williston Basin. The edge of the Prairie salt occurs in the west of the study area (Figures 3.1 and 3.5) corresponding to what is commonly referred to as the

Hummingbird Trough area (Holter, 1969). The plume of fresh Type 1 water is approximately coincident with the edge of the salt in the study area (Figure 3.3), and has been shown to correlate well with the salt-free area at the basin scale (Benn and Rostron, 1998). There is, however, no reason to assert that the relatively recent fresh water recharge is responsible for removal of the salt. Thickening of the Triassic-Jurassic-aged Lower Watrous Formation over the present-day edge of the Prairie Formation salt suggests syndepositional removal of the underlying Prairie Formation salt, or depositional infilling of the depression formed by the structural sag of the entire pre-Mississippian – post-Devonian salt sequence due to subsurface salt dissolution during the period of subaerial exposure and erosion of the post-Mississippian unconformity (Figure 3.5). The latter scenario seems correct since there is anomalous preservation of rocks from the Poplar Beds and Big Snowy Group in an outlier which is coincident with the salt-free area (Figure 3.1). This suggests that removal of the Prairie salt began in response to formation water flow events (i.e., fresh water recharge) which are as old as late Mississippian.

The absence of Type 3 brines in the Mississippian aquifers merits comment. From the TDS distribution and geological compositions of the aquifer systems, we would not expect any significant differences in brine chemistry between the deep Paleozoic and Mississippian aquifers (Figures 3.3 and 3.4). But the Ca concentrations in the brines above 300 g/L TDS are markedly different between the two aquifer groups, with an apparent absence of Type 3 brines from the Mississippian system (Figures 3.7,3.8; Figure 3.12). It is possible that Type 3 brines do exist within the Mississippian aquifers to the south of the study area in the deep basin. We may simply have missed sampling any Type 3 brines in the Mississippian aquifers, or dilution due to mixing with Na-Cl (Type 2) brines may have resulted in a subdued chemical signature of high-Ca brines sampled within the Mississippian system in the study area.

It is also possible that there are no high-Ca Type 3 brines within the Mississippian aquifers anywhere within the Williston Basin because they were never there. Proponents of the hypothesis of secular variation of global seawater chemistry through geologic time assert that the variability in brine chemistry observed in basins reflects changes in the composition of the parent seawater, rather than hydrogeological processes (Horita et al., 2002). Lowenstein et al. (2003) present a case for an evaporated-paleoseawater origin of sedimentary Ca-Cl brines which were formed during periods when seawater chemistry was highly enriched in Ca compared to modern seawater. They suggest that during most of the Mississippian, however, seawater had the composition of modern seawater. In this case it should be expected that formation waters sourced from subaerially evaporated seawater within Mississippian strata should have entirely different major ion chemistry than their pre-Mississippian counterparts.

Further sampling and analysis of formation waters in the Mississippian aquifers to the south of the study area is needed in order to make a conclusion about the presence or absence of Type 3 brines in the Mississippian aquifers of the Williston Basin. A pervasive absence of Ca-Cl brines in the entire Mississippian aquifer system would be important evidence supporting the hypothesis that global seawater has varied between $Ca\text{-}Cl_2$ and $Mg\text{-}SO_4$ compositions through time (e.g., Lowenstein et al., 2003).

### 3.5.2 Implications for anthropogenic activity

The Mississippian subcrop in Canada within the study area forms a prolific hydrocarbon play, with the Weyburn field alone containing an estimated 1.4 billion barrels of oil in place ($223 \times 10^6 m^3$) (Kent et al., 1988). Hydrocarbon exploration and the recent interest in $CO_2$ sequestration coupled to enhanced oil recovery makes it worth commenting on some implications of this study with respect to these activities.

*$CO_2$ Sequestration*

Of particular interest to the Weyburn $CO_2$ Project is the steep salinity gradient across the Weyburn field within the Midale Aquifer and the underlying Frobisher Aquifer (Figures 3.4 and 3.5). $CO_2$ introduced into a brackish water aquifer of TDS between 1 and 10 g/L is twice as soluble as in a brine aquifer (TDS > 100 g/L) (Pruess and Garcia, 2002). The steep salinity gradient in the Midale Aquifer across the Weyburn field (Figure 3.4) will therefore exert some control on $CO_2$ solubility in formation waters. Long-term

$CO_2$ storage volumetrics in the Weyburn reservoir and/or the underlying Midale aquifer should therefore account for variable brine salinity.

The Mesozoic aquifer system is important to the Weyburn $CO_2$ Project because these aquifers overlie the Mississippian beds and the Midale Aquifer (Figure 3.2), which is the injection target. Vertical upward leakage of $CO_2$ from the Midale aquifer into the Mesozoic aquifers via well bores or natural fluid-flow pathways is a concern to public safety. There are two interpretations with respect to the hydrochemistry of the Mesozoic Aquifers that are directly relevant to $CO_2$ sequestration in the Mississippian aquifers:

(1) There are no brines in the Mesozoic aquifers (Figure 3.5). A simple force balance approach (Bond and Cartwright, 1970) indicates that the present-day vertical hydraulic gradients between the Mississippian aquifer system and the overlying Jurassic Aquifer are sufficient to displace Mississippian brines upward across the Watrous aquitard. The absence of brines in the Jurassic aquifer therefore suggests that the Mesozoic aquifer group tends toward hydraulic separation from the underlying Mississippian aquifer group within the study area. This is corroborated by fluid pressures and fluid potentials which indicate that, in the central study area, the Mississippian subcrop is a competent hydraulic barrier (see Chapter 4).

It was noted that there are a few samples of Type 1 fresh waters from the Jurassic aquifer. Fluid potentials in the Jurassic (see Chapter 4) are very similar in character to the underlying Deep Paleozoic and Mississippian aquifers, and very different from the overlying Mannville and Newcastle aquifers. This is again attributed to common hydrologic boundary conditions; stratigraphically-equivalent rocks that form Jurassic aquifer in the current study area crop out in the same recharge areas as the Paleozoic aquifers (Darton, 1906). As a result, the plume of Type 1 fresh water occurs within the Jurassic aquifer as well, thus explaining this common hydrochemical signature with the deeper aquifer systems, as opposed to vertical leakage across the Watrous Aquitard in the western study area.

(2) The hydrochemical signature of the Mesozoic aquifer group strongly suggests vertical mixing between the Mesozoic aquifers due to leakage across intervening aquitards. The interpretation of vertical mixing due to cross-formational flow in the Mesozoic system is based on the transitional nature of chemical signatures between adjacent aquifers (Figure 3.11), as well as from pore pressure data (see Chapter 4). This has implications to environmental risk assessment, where the concern is how efficiently $CO_2$ will be transported vertically upward toward the biosphere if $CO_2$ injected into the underlying Mississippian aquifer system migrates into the Mesozoic aquifers.

*Hydrocarbon exploration and crude gravity*

The hydrochemical patterns identified in this study could be useful in petroleum exploration because of the spatial correlation between water chemistry and oil quality. Bailey et al. (1973) link the alteration of Mississippian hosted crude oils within the current study area to the processes of water washing and associated bacterial degradation. They identified brackish $Na-SO_4$ type waters — (Type 5 in this study) — with a meteoric isotopic signature, changing to Na-Cl brines eastward along the Mississippian subcrop. Crude oil gravity covaried between 15 to 35 API. They concluded that meteoric waters degraded the oils trapped along the Mississippian subcrop creating heavier, more sulfurous crudes. It is now well known among oil industry professionals that the quality of oils along the Canadian Mississippian subcrop play in Saskatchewan varies, and the abruptness of the variation is often unexpected. Detailed delineation of the extent of freshwater invasion in individual Mississippian reservoir horizons, shown for the first time in this study (Figure 3.4), is therefore useful information for explorationists in predicting oil quality.

## 3.6 CONCLUSIONS

This chapter summarizes the results of an analysis of hydrochemical data that was conducted as part of the hydrogeological characterization of the Weyburn $CO_2$ project area.

Five distinct formation water compositions are identified on the basis of major ion chemistry: (1) Ca-$SO_4$ fresh waters, (2) Na-$SO_4$ brackish waters, (3) Na-Cl brines, (4) Ca-Cl brines, and (5) Na-$HCO_3$ fresh waters.

Deep Paleozoic (i.e., pre-Mississippian) and Mississippian aquifers contain fresh Ca-$SO_4$ waters, intermediate salinity Na-$SO_4$ waters, Na-Cl brines, and Ca-Cl brines. These four types of formation waters, within a limited area of the Williston Basin, effectively represent the entire range of compositional variation found within the formation waters of the world's sedimentary basins.

The distribution of formation water types within the study area is predictable and consistent between individual aquifers of each aquifer group. This style of "homogeneous heterogeneity" indicates large-scale control by hydrodynamics on the distribution and interaction between waters of vastly differing ages and origins.

Confined or horizontal flow and lateral advective and diffusive mixing between formation waters is occurring in the Deep Paleozoic and Mississippian aquifer systems. The Mesozoic aquifer group contains no brines and is dominated by brackish to fresh Na-$SO_4$ and Na-$HCO_3$ waters. Vertical mixing between formation waters is evident from compositional trends within the Mesozoic aquifer group. An entirely different flow system is operative in the Mesozoic aquifer group, as is apparent from the contrasting style of hydrochemical variation to what is observed in the deeper aquifer systems.

The distribution of the formation water compositional types that have been identified is the result of a nesting of paleoflow systems of different absolute times and time scales through the history of the evolution of the Williston Basin. Recently influxed meteoric waters with a Ca-$SO_4$-dominated major ion chemistry represent the most recent development in the hydrodynamics of the basin. The distribution of Ca-Cl type brines (or mixing types close to this composition) may record the redistribution of connate waters by formation water flow in the Williston Basin. In using the term "connate", we do mean to imply that Ca-rich brine compositions within the Deep Paleozoic aquifers may reflect the compositions of ancient Paleozoic seawater. The absence of high Ca- brines in the Mississippian aquifers could provide support to the hypothesis that global seawater chemistry has varied throughout geologic time.

With respect to industrial and economic interests: (1) the steep salinity gradient across the Weyburn field within the Midale aquifer has implications to the solubility of $CO_2$ in formation water in the Weyburn oilfield; (2) the lack of brines above the Watrous Aquitard in the Mesozoic aquifers suggest that in the study area, the Paleozoic and Mesozoic aquifers are effectively hydraulically separated; (3) the compositional variation in the Mesozoic aquifer system indicates cross-formational flow, which has implications for environmental risk assessment concerned with the transport of $CO_2$; and, (4) The detailed mapping of the formation water types is a valuable exploration tool for hydrocarbons along the Mississippian subcrop. In particular, the delineation of the fresh waters which are thought to control the degree of biodegradation observed in Mississippian crudes.

## 3.7 REFERENCES

Bachu, S., Hitchon, B., (1996) Regional-scale flow of formation waters in the Williston Basin. *AAPG Bulletin*, 80(2), pp. 248-264.

Back, W., (1960) Origin of hydrochemical facies of ground water in the Atlantic Coastal Plain. In: *21st International Geological Conference, Part I*, Copenhagen. pp. 87-95.

Back, W., (1961) Techniques for mapping of hydrochemical facies. *United States Geological Survey Prof. Paper 424-D*, pp. 380-382.

Bailey, N.J.L., Krouse, H.R., Evans, C.R., Rogers, M.A., (1973) Alteration of crude oil by waters and bacteria - evidence from geochemical and isotope studies. *AAPG Bulletin*, 57, pp. 1276-1290.

Benn, A.A., Rostron, B.J., (1998) Regional hydrochemistry of Cambrian to Devonian aquifers in the Williston basin, Canada-USA. In: J.E. Christopher, C.F. Gilboy, D.F. Paterson, S.L. Bend (Eds.), *Eighth International Williston Basin Symposium, Special Publication*, pp. 238-246.

Berg, R.R., DeMis, W.D., Mitsdarffer, A.R., (1994) Hydrodynamic effects on Mission Canyon (Mississippian) oil accumulations, Billings Nose area, North Dakota. *AAPG Bulletin*, 78(4), pp. 501-518.

Bond, D.C., Cartwright, K., (1970) Pressure observations and water densities and their relation to problems in gas storage. *Journal of Petroleum Technology*, 22, pp. 1492-1498.

Busby, J.F., Kimball, B.A., Downey, J.S., (1995) Geochemistry of water in aquifers and confining units of the Northern Great Plains in parts of Montana, North Dakota, South Dakota, and Wyoming. *U.S. Geological Survey Professional Paper 1402-F*, 146p.

Carpenter, A.B., (1978) Origin and chemical evolution of brines in sedimenatry basins. *Oklahoma Geological Survey Circular* 79, pp. 60-77.

Chebotarev, I.I., (1955) Metamorphism of natural waters in the crust of weathering, 1. *Geochemica et Cosmochimica Acta*, 8, pp.22-48, 137-170, 198-212.

Clayton, R.N., Friedman, I., Graf, D.L., Mayeda, T.K., Meents, W.F., Shimp, N.F., (1966) The origin of saline formation waters 1. Isotopic composition. *Journal of Geophysical Research*, 71(16), pp. 3869-3882.

Collins, A.G., (1975) *Geochemistry of oilfield waters*. Elsevier Sci. Publ. Co.

Darton, N.H., (1906) Geology of the Bighorn Mountains. *U.S. Geological Survey Professional Paper 51*, 129p.

DeMis, W.D., (1995) Effect of cross-basinal hydrodynamic flow on oil accumulations and oil migration history of the Bakken-Madison petroleum system Williston Basin, North America. In: *Seventh International Williston Basin Symposium* (Ed. by L.D.V. Hunter, R.A. Schalla), Montana Geological Society, Billings, Montana. pp. 291-301.

Downey, J.S., (1984a) Hydrodynamics of the Williston Basin in the Northern Great Plains. In: G. Jorgensen Donald, C. Signor Donald (Eds.), *Geohydrology of the Dakota Aquifer*. Natl. Water Well Assoc., Worthington, OH, United States. pp. 92-98.

Downey, J.S., (1984b) Geohydrology of the Madison and associated aquifers in parts of Montana, North Dakota, South Dakota, and Wyoming. *U.S. Geological Survey Professional Paper 1273-G*, 1273-G, 47p.

Downey, J.S., (1986) Geohydrology of bedrock aquifers in the Northern Great Plains in parts of Montana, North Dakota, South Dakota, and Wyoming. *U.S. Geological Survey Professional Paper 1402-E*, 87p.

Downey, J.S., Busby, J.F., Dinwiddie, G.A., (1987) Regional aquifers and petroleum in the Williston Basin region of the United States. In: *1987 Symposium of the Rocky Mountain Association of Geologists* (Ed. by M. Longman), pp. 299-312.

Fuzesy, L.M., (1983) Correlation and Subcrops of the Mississippian Strata in Southeastern and South-Central Saskatchewan, Saskatchewan Energy and Mines, Regina. *Report 51*. 63p.

Grasby, S.E., Betcher, R.N., (2002) Regional hydrogeochemistry of the carbonate rock aquifer, southern Manitoba. *Can. J. Earth Sci.*, 39, pp. 1053-1063.

Haidl, F., Kreis, L.K., Dancsok, E.F.R., (1996) New oil discoveries in Ordovician Red River Strata, southeastern Saskatchewan. In: *Summary of Investigations 1996*, Saskatchewan Industry and Resources, Regina, SK, Canada. pp. 136-144.

Hannon, N., (1987) Subsurface water flow patterns in the Canadian sector of the Williston Basin. In: *1987 Symposium of the Rocky Mountain Association of Geologists*, pp. 313-321.

Hanor, J.S., (1994) Origin of saline fluids in sedimentary basins. In: *Geofluids: Origin, Migration and Evolution of Fluids in Sedimentary Basins* (ed. J. Parnell) Geological Society Special Publication 78, pp. 151-174.

Hitchon, B., Brulotte, M., (1994) Culling criteria for "standard" formation water analyses. *Applied Geochemistry*, 9, pp. 637-645.

Hitchon, B., (1996) Rapid evaluation of the hydrochemistry of a sedimentary basin using only standard formation water analyses: example from the Canadian portion of the Williston Basin. *Applied Geochemistry*, 11, pp. 789-795.

Holter, M.E., (1969) The Middle Devonian Prairie Evaporite of Saskatchewan. Saskatchewan Department of Mineral Resources. Report 123. 134p.

Horita, J., Zimmerman, H., Holland, H.D., (2002) Chemical evolution of seawater during the Phanerozoic: Implications from the record of marine evaporites. *Geochimica et Cosmochimica acta*, 66(21), pp. 3733-3756.

Iampen, H.T., Rostron, B.J., (2000) Hydrogeochemistry of pre-Mississippian brines, Williston Basin, Canada-USA. *Journal of Geochemical Exploration*, 69-70, pp. 29-35.

Jensen, G.K.S., Rostron, B.J., Duke, M.J.M., Holmden, C., (2006) Bromine and stable isotopic profiles of formation waters from potash mine-shafts, Saskatchewan, Canada. *Journal of Geochemical Exploration*, 89(1-3), pp. 170-173.

Kent, D.M., Haidl, F.M., MacEachern, J.A., (1988) Mississippian oilfields in the northern Williston Basin. In: S.M. Goolsby, M.W. Longman (Eds.), *Occurrence and petrophysical properties of carbonate reservoirs in the Rocky Mountain region*, Rocky Mt. Assoc. Geol, Denver, CO. pp. 381-418.

Kent, D.M., Thomas, P., Heck, T., (2004) Geological mapping of the Mississippian strata in southeastern Saskatchewan, northwestern North Dakota, and Northeastern Montana. In: *Summary of Investigations 2004, 1*, Saskatchewan Industry and Resources, Regina, SK, Canada. 10 p.

Langmuir, D., (1997) *Aqueous Environmental Geochemistry*. Prentice Hall.

Lefever, R.D., (1998) Hydrodynamics of formation waters in the North Dakota Williston Basin. In: J.E. Christopher, C.F. Gilboy, D.F. Paterson, S.L. Bend (Eds.), *Eighth Annual Williston Basin Symposium, Special Publication*, pp. 229-237.

Lowenstein, T.K., Hardie, L.A., Timofeeff, M.N., Demicco, R.V., (2003) Secular variation in seawater chemistry and the origin of calcium chloride basinal brines. *Geology*, 31(10), pp. 857-860.

MacCaffrey, M.A., Lazar, B., Holland, H.D., (1987) The evaporation path of seawater and the coprecipitation of Br- and K+ with halite. *Journal of Sedimentary Petrology*, 57(5), pp. 928-937.

Parkhurst, D.L., (1995) Users guide to PHREEQC - A computer program for speciation, reaction-path, advective-transport, and inverse geochemical calculations. *U.S. Geological Survey Water Resources Inv. Rept. 95-4227*.

Piper, A.M., (1944) A graphic procedure in the geochemical interpretation of water-analyses. *American Geophysical Union*, 25, pp. 914-923.

Pitzer, K.S., (1987) Thermodynamic model for aqueous solutions of liquid-like density. In: I.S.E. Carmichael, H.P. Eugster (Eds.), *Thermodynamic modeling of geological materials: Minerals, fluids, and melts, Reviews in Mineralogy*, Min. Soc. Am. pp. 97-142.

Preston, C., Monea, M., Jazrawi, W., Brown, K., Whittaker, S., White, D., Law, D., Chalaturnyk, R., Rostron, B., (2005) IEA GHG Weyburn $CO_2$ monitoring and storage project. *Fuel Processing Technology*, 86, pp. 1547-1568.

Pruess, K., Garcia, J., (2002) Multiphase flow dynamics during $CO_2$ disposal into saline aquifers. *Environmental Geology*, 42, pp. 282-295.

Rostron, B.J., Holmden, C., (2003) Regional variations in oxygen isotopic compositions in the Yeoman and Duperow aquifers, Williston basin (Canada-USA). *Journal of Geochemical Exploration*, 78-79, pp. 337-341.

Socolow, R.H., (2005) Can we bury global warming? In: *Scientific American, 293*, pp. 49-55.

Sulin, V.A., (1946) Vody neftyanykh mestorozhdeniy v sisteme prirodnykh vod (The position of petroleum deposit waters in the system of natural waters). In: *State Sci.-Tech. Press for Petroleum and Solid Fuel Lit.* ; Moscow-Leningrad ; SUN ; USSR, 96p.

Toop, D.C., Toth, J., (1995) Hydrogeological characterization of formation waters using ionic ratios, south-central Saskatchewan. In: *7th International Williston Basin Symposium* (Ed. by L.D.V. Hunter, R.A. Schalla), Montana Geological Society, Billings, Montana. pp. 313-319.

Tóth, J., (1978) Gravity-induced cross-formational flow of formation fluids, Red Earth region, Alberta, Canada: Analysis, patterns, evolution. *Water Resources Research*, 14(5), pp. 805-843.

Tóth, J., (1984) The role of gravity flow in the chemical and thermal evolution of ground water. In: *First Canadian/American Conference on Hydrogeology; Practical Applications of Groundwater Geochemistry* (Ed. by B. Hitchon, E.I. Wallick), National Water Well Association, Banff, Alberta, Canada. pp. 3-39.

Tóth, J., (1995) Hydraulic continuity in large sedimentary basins. *Hydrogeology Journal*, 3(4), pp. 4-16.

Whittaker, S., Rostron, B.J., Khan, D., Hajnal, Z., Qing, H., Penner, L., Maathuis, H., Goussev, S., (2004) IEA GHG Weyburn $CO_2$ monitoring & storage project summary report 2000-2004. In: *Seventh International Conference on Greenhouse Gas Control Technologies, 1* (Ed. M. Wilson, M. Monea), Petroleum Technology Research Centre. pp. 15-69.

Wittrup, M.B., Kyser, T.K., (1990) The petrogenesis of brines in Devonian potash deposits of western Canada. *Chemical Geology*, 82, pp. 103-128.

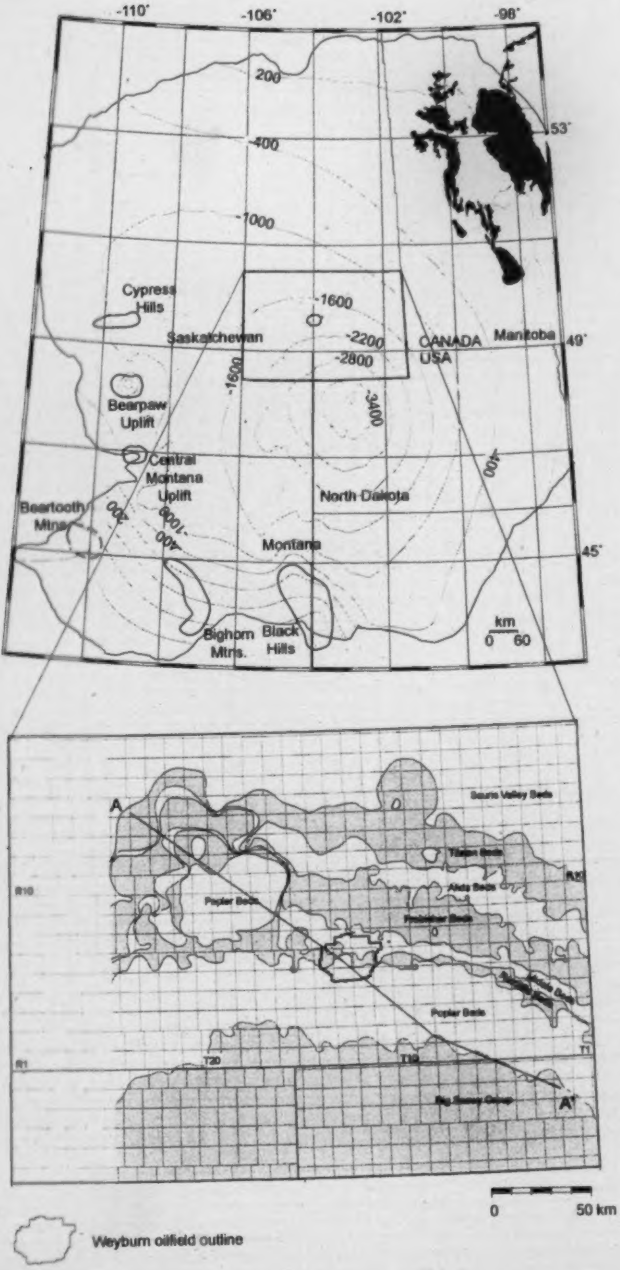
-110°
-106°
-102°
-98°
200
-400
-1000
-1600
-2200
-2800
-3400
-1600
-400
53°
49°
45°
Cypress Hills
Saskatchewan
CANADA
USA
Manitoba
Bearpaw Uplift
Central Montana Uplift
Beartooth Mtns.
North Dakota
Montana
Bighorn Mtns.
Black Hills
km
0 60
200
1000
400
A
A'
Souris Valley Beds
Tilston Beds
Alida Beds
Frobisher Beds
Poplar Beds
Poplar Beds
Big Snowy Group
R10
R1
R10
T20
T10
T1
0 50 km
Weyburn oilfield outline

Figure 3.1. Composite reference map of study area set within the Williston Basin. Large area shows overall basin structure (structure contours on top of Ordovician Red River Formation) and major tectonic elements. Inset shows Weyburn Project map area and the slightly smaller geological characterization area (shaded area) including Mississippian subcrop map (after Kent et al., 2004).

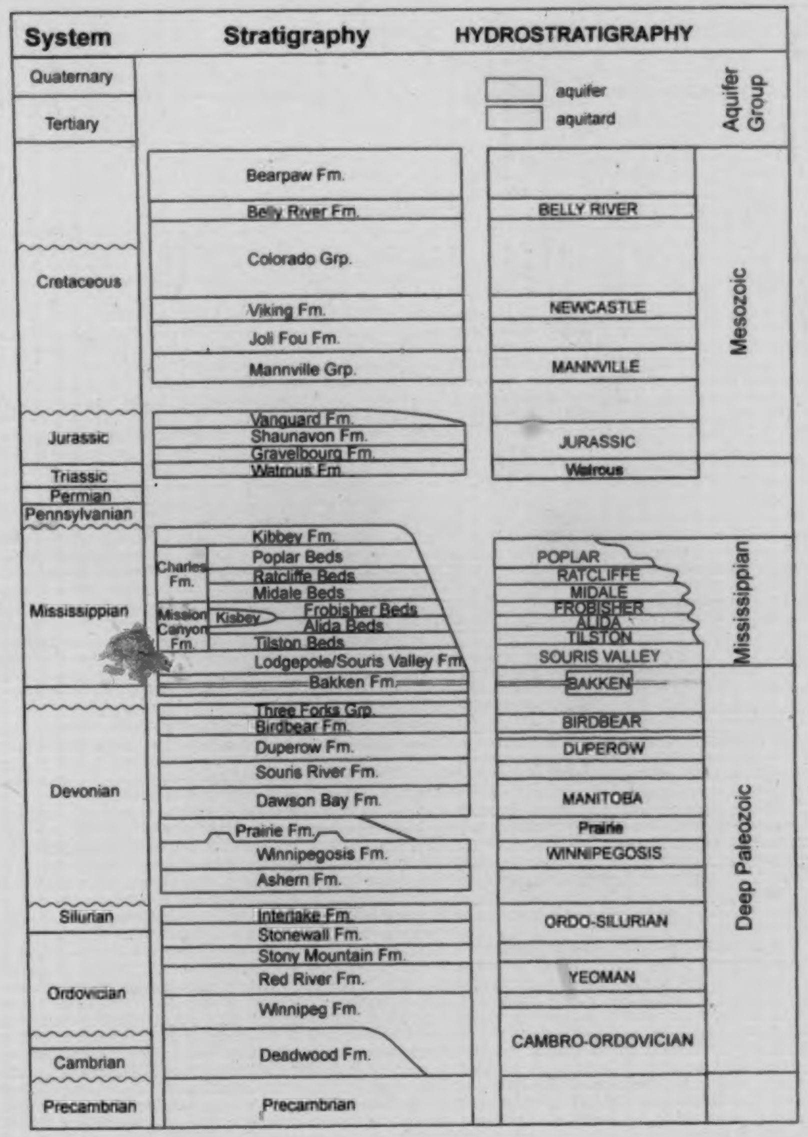
System
Stratigraphy
HYDROSTRATIGRAPHY
aquifer
aquitard
Aquifer Group
Quaternary
Tertiary
Cretaceous
Jurassic
Triassic
Permian
Pennsylvanian
Mississippian
Devonian
Silurian
Ordovician
Cambrian
Precambrian
Bearpaw Fm.
Belly River Fm.
Colorado Grp.
Viking Fm.
Joli Fou Fm.
Mannville Grp.
Vanguard Fm.
Shaunavon Fm.
Gravelbourg Fm.
Watrous Fm.
Kibbey Fm.
Charles Fm.
Poplar Beds
Ratcliffe Beds
Midale Beds
Mission Canyon Fm.
Kisbey
Frobisher Beds
Alida Beds
Tilston Beds
Lodgepole/Souris Valley Fm
Bakken Fm.
Three Forks Grp.
Birdbear Fm.
Duperow Fm.
Souris River Fm.
Dawson Bay Fm.
Prairie Fm.
Winnipegosis Fm.
Ashern Fm.
Interlake Fm.
Stonewall Fm.
Stony Mountain Fm.
Red River Fm.
Winnipeg Fm.
Deadwood Fm.
Precambrian
BELLY RIVER
NEWCASTLE
MANNVILLE
JURASSIC
Watrous
POPLAR
RATCLIFFE
MIDALE
FROBISHER
ALIDA
TILSTON
SOURIS VALLEY
BAKKEN
BIRDBEAR
DUPEROW
MANITOBA
Prairie
WINNIPEGOSIS
ORDO-SILURIAN
YEOMAN
CAMBRO-ORDOVICIAN
Mesozoic
Mississippian
Deep Paleozoic

Figure 3.2. Williston Basin stratigraphy and hydrostratigraphic framework adopted for the Weyburn Project geological model (Whittaker et al., 2004).

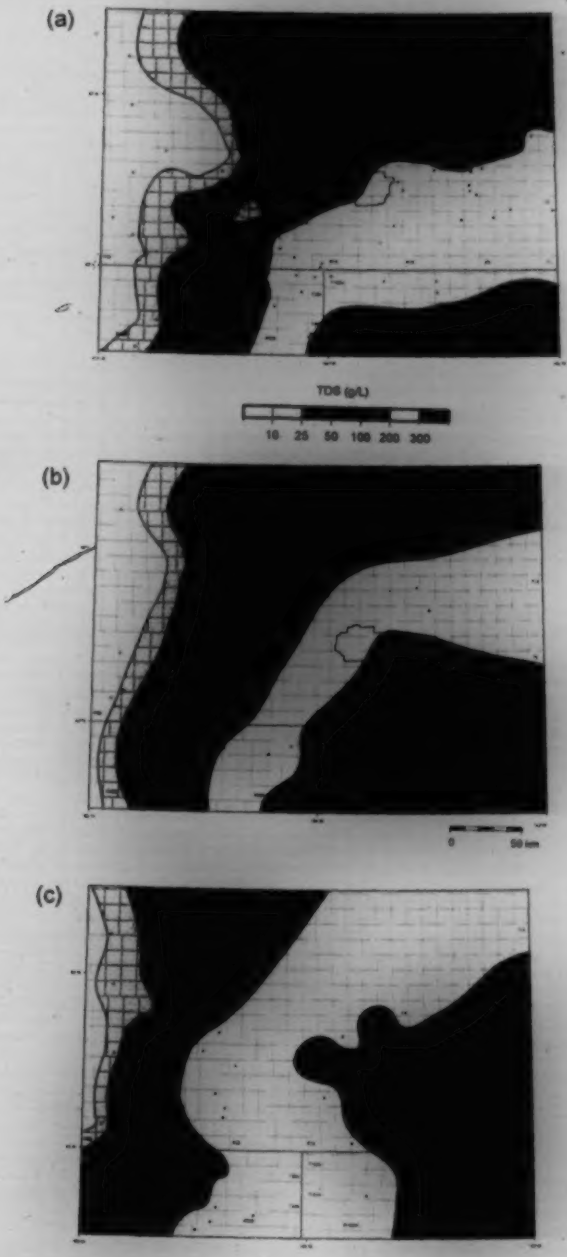
(a)
TDS (g/L)
10
25
50
100
200
300
(b)
0
50 km
(c)

Figure 3.3. Total Dissolved Solids in selected Lower Paleozoic aquifers: a) Birdbear, b) Duperow, c) Winnipegosis. Crosses indicate data points.

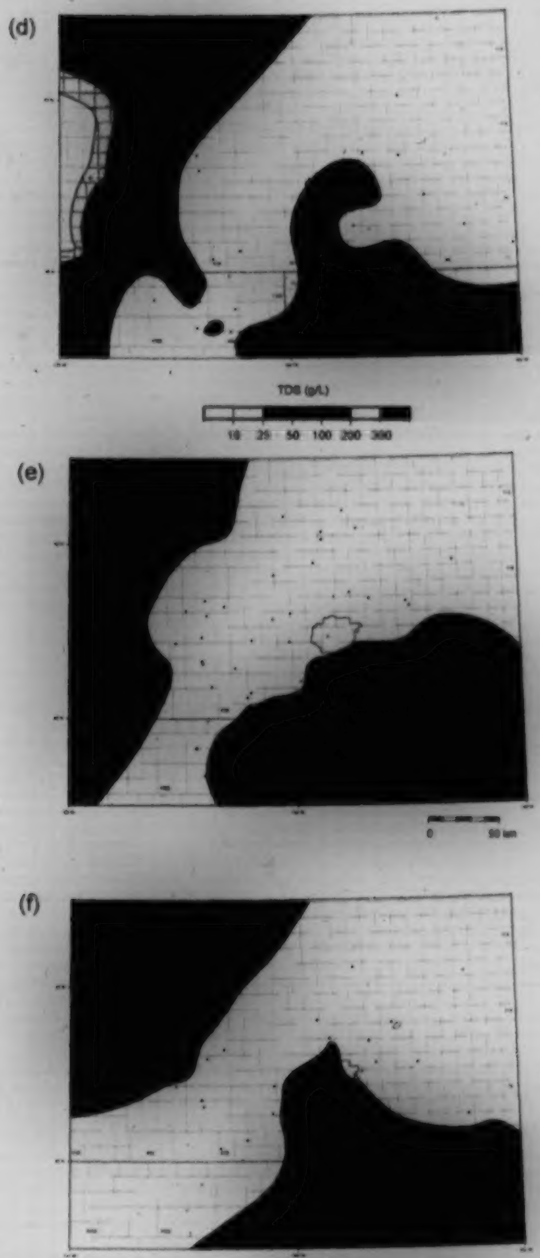
(d)
TDS (g/L)
10 25 50 100 200 300
(e)
0 50 km
(f)

Figure 3.3: (continued) Total Dissolved Solids in selected Lower Paleozoic aquifers: d) Ordo-Silurian, e) Yeoman, and f) Cambro-Ordovician. Crosses indicate data points.

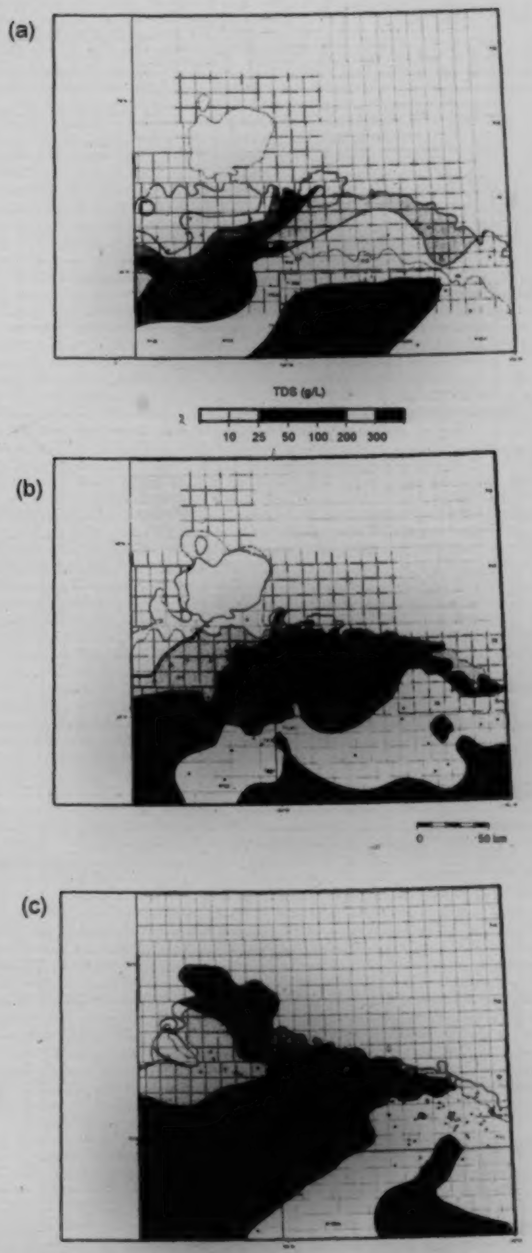
(a)
TDS (g/L)
10 25 50 100 200 300
(b)
0 50 km
(c)

Figure 3.4. Total Dissolved Solids in selected Mississippian aquifers: a) Poplar, b) Ratcliffe, c) Midale. Crosses indicate data points.

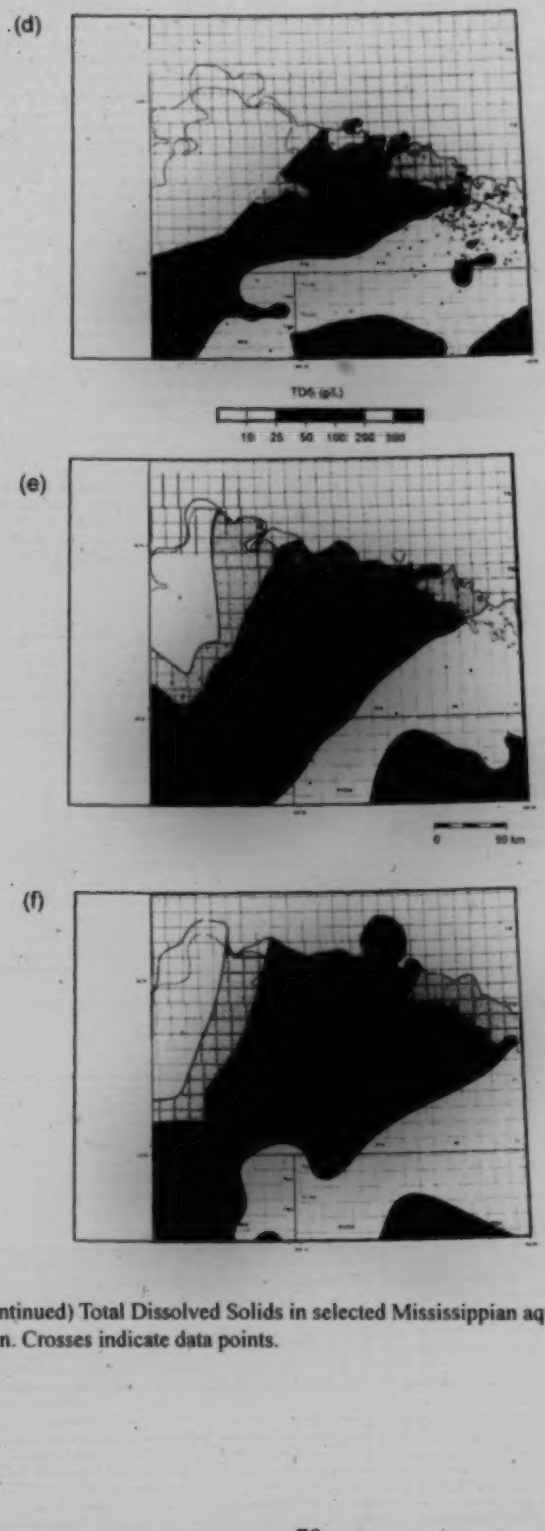
(d)
TDS (g/L)
10 25 50 100 200 300
(e)
0
50 km
(f)

Figure 3.4. (continued) Total Dissolved Solids in selected Mississippian aquifers: d) Frobisher, e) Alida, f) Tilston. Crosses indicate data points.

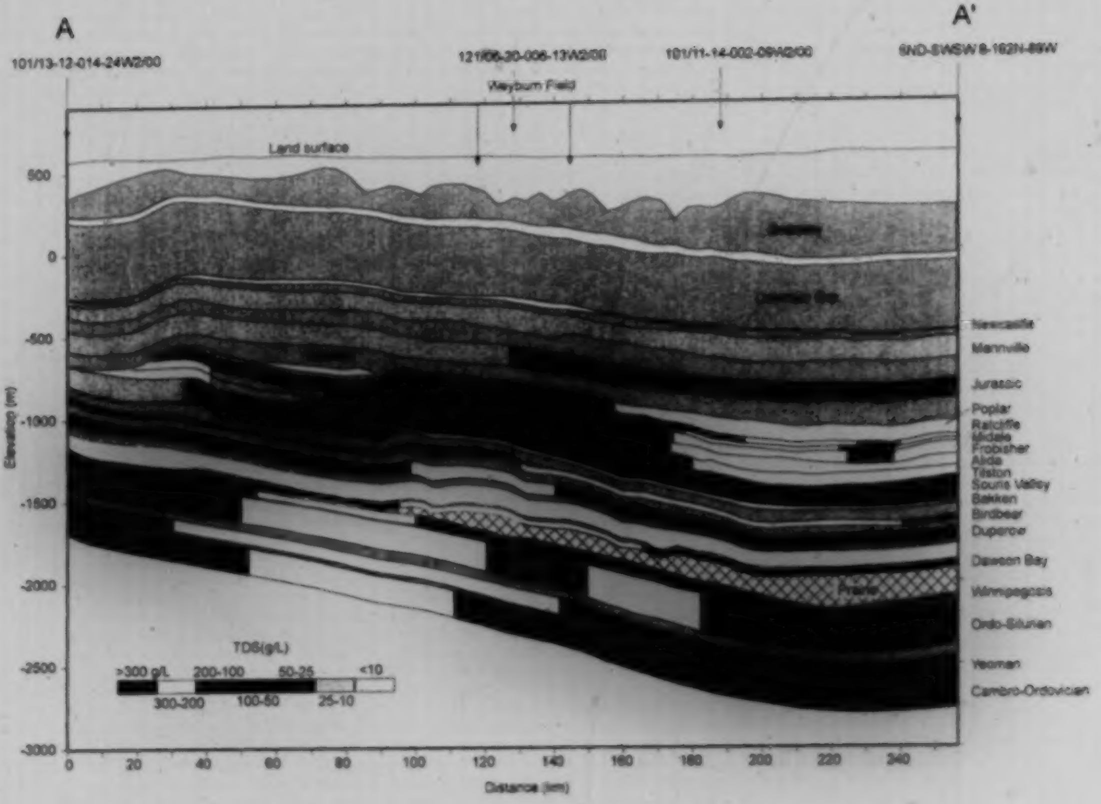
A
A'
101/13-12-014-24W2/00
121/06-30-006-13W2/00
101/11-14-002-09W2/00
SND-SWSW 8-162N-89W
Weyburn Field
Land surface
500
0
-500
-1000
-1500
-2000
-2500
-3000
Elevation (m)
0
20
40
60
80
100
120
140
160
180
200
220
240
Distance (km)
Newcastle
Mannville
Jurassic
Poplar
Ratcliffe
Midale
Frobisher
Alida
Tilston
Souris Valley
Bakken
Birdbear
Duperow
Dawson Bay
Winnipegosis
Ordo-Silurian
Yeoman
Cambro-Ordovician
Prairie
TDS(g/L)
>300 g/L
300-200
200-100
100-50
50-25
25-10
<10

Figure 3.5. NW-SE oriented cross section A-A' (see Figure 3.1 for line of section).

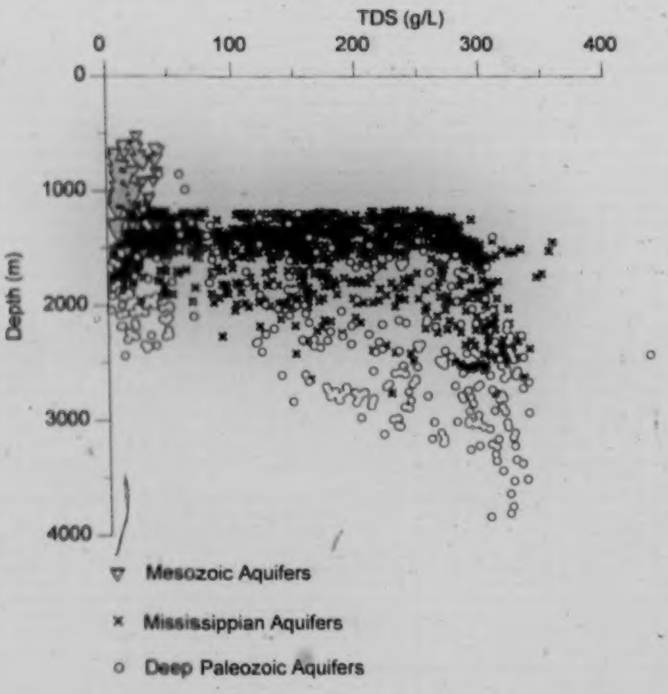

Figure 3.6. Scatterplot of Total Dissolved Solids versus depth for the entire dataset

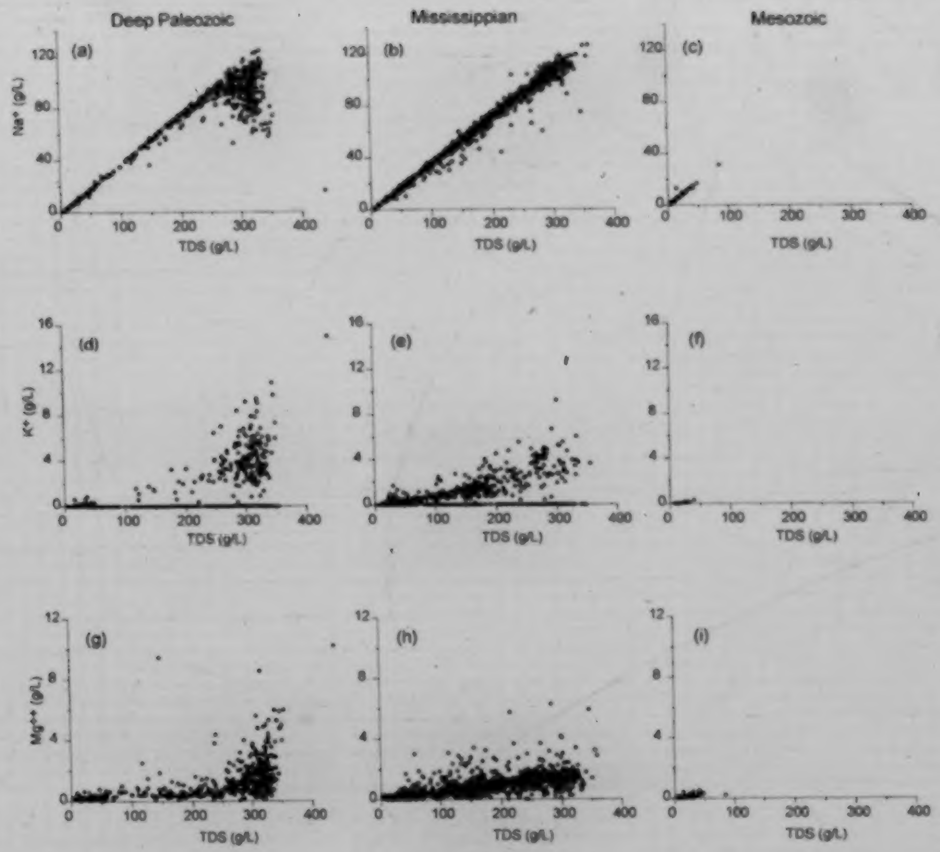

Figure 3.7. (a,b,c) Na, (d,e,f) K, and (g,h,i) Mg plotted versus Total Dissolved Solids for the three aquifer groups, columnwise.

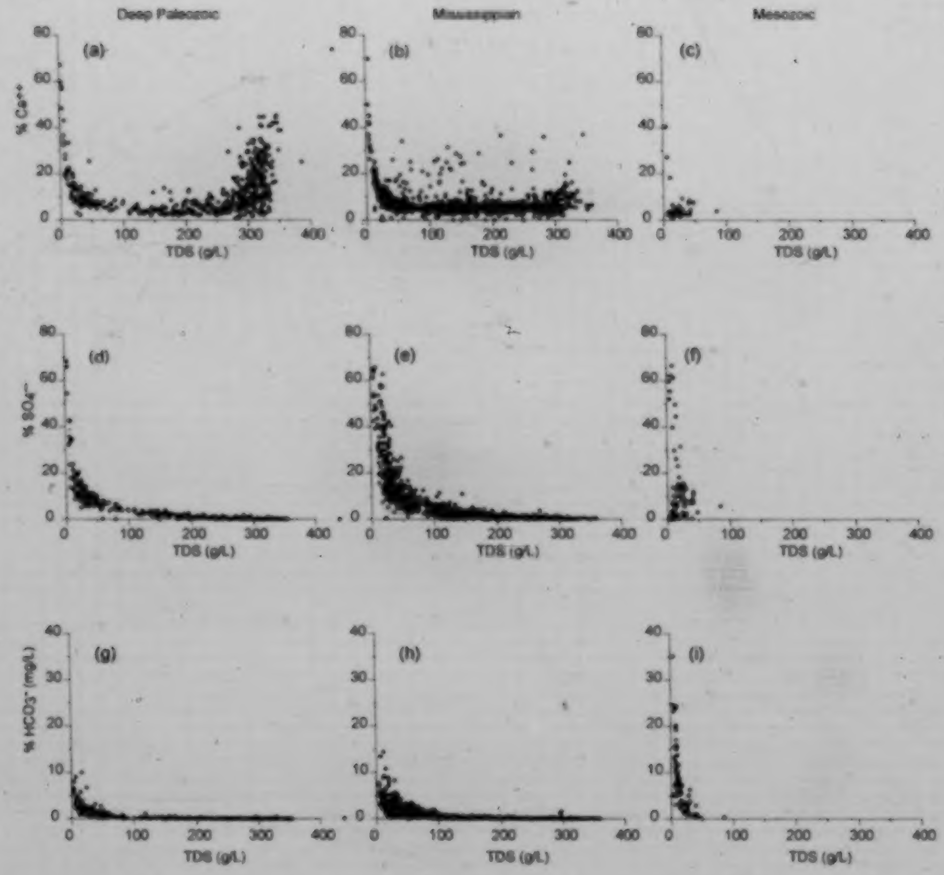

**Figure 3.8. (a,b,c) %Ca, (d,e,f) %SO4, and (g,h,i) %HCO3 plotted versus Total Dissolved Solids for the three aquifer groups, columnwise.**

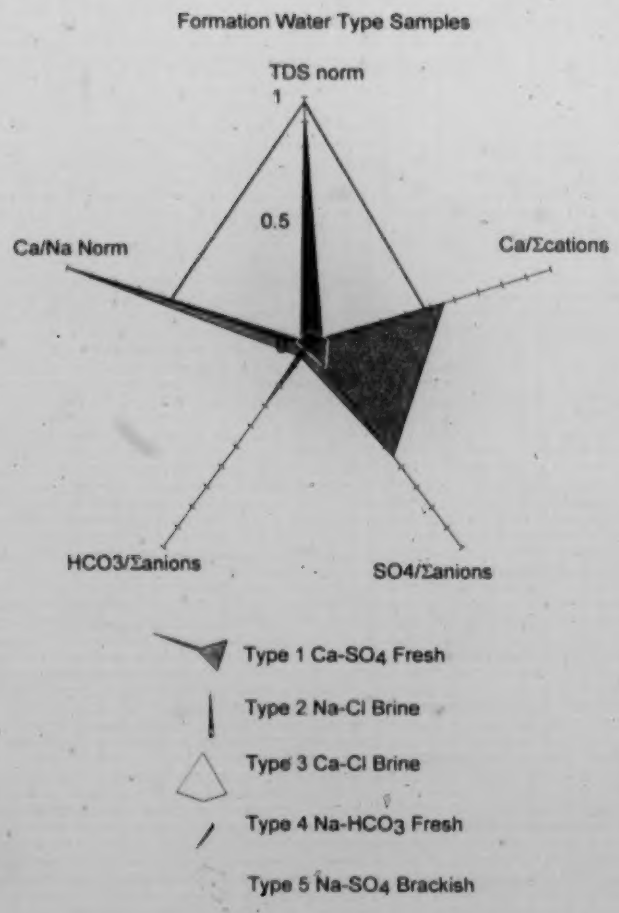

Figure 3.9. Pentaxial plot devised to display the five principal water types within the study area.

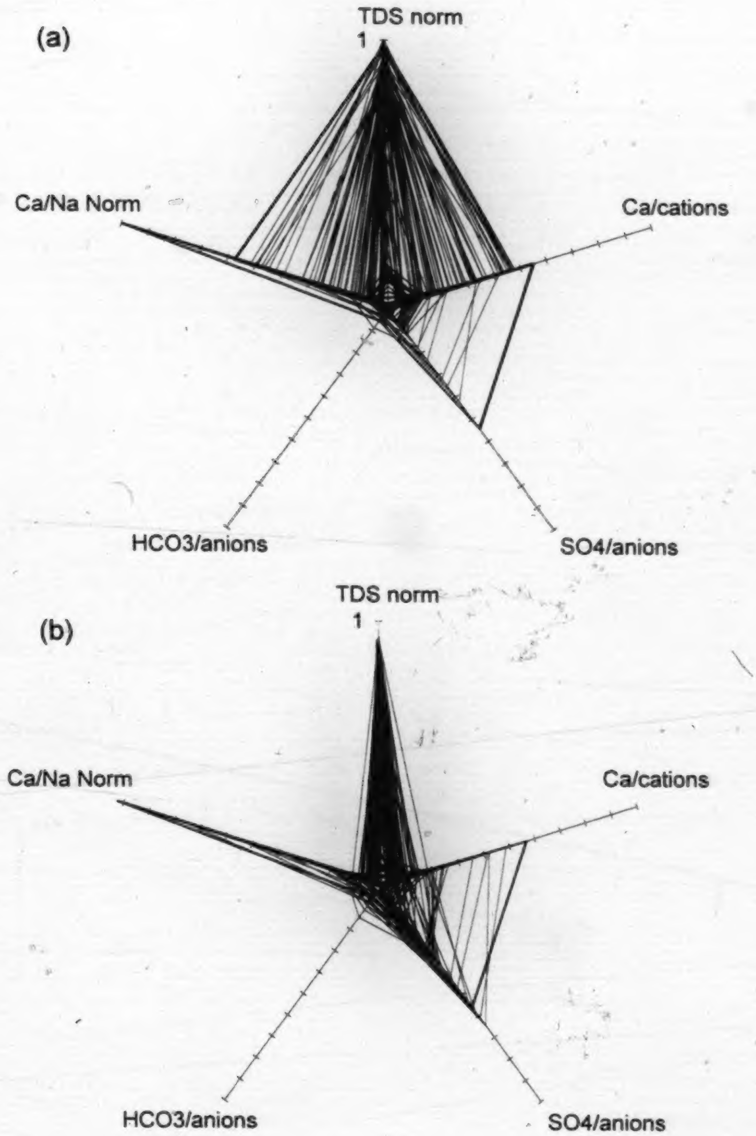

Figure 3.10. (a) Water samples from (a) Deep Paleozoic Duperow Aquifer, (b) Mississippian Ratcliffe Aquifer. Bold polygons indicate representative, or end-member types.

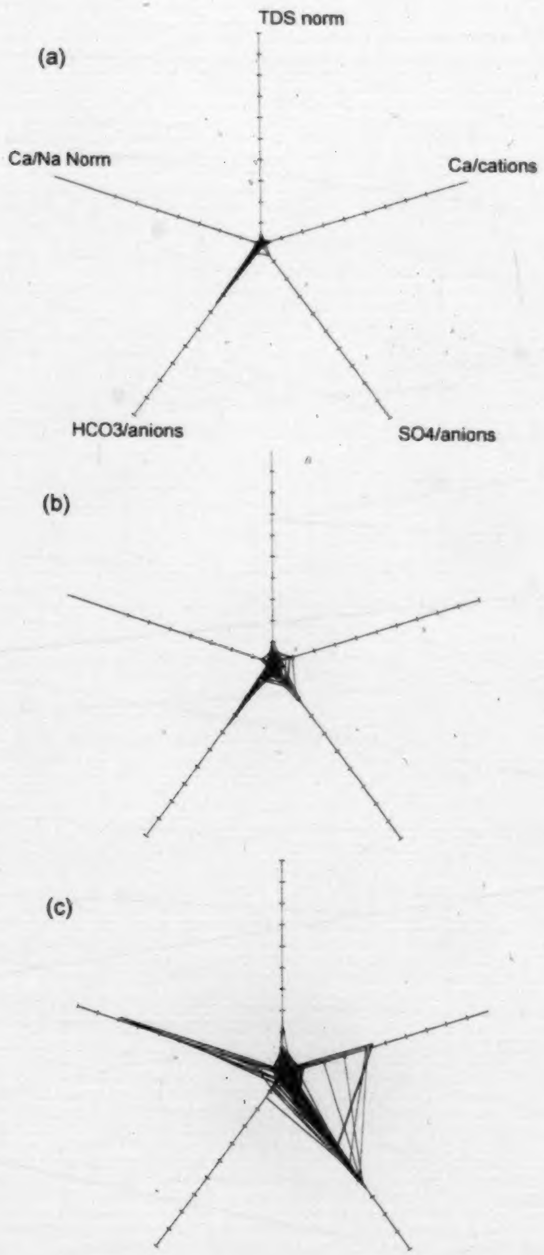

Figure 3.11. Mesozoic water samples from (a) Newcastle, (b) Mannville, and (c) Jurassic Aquifers.

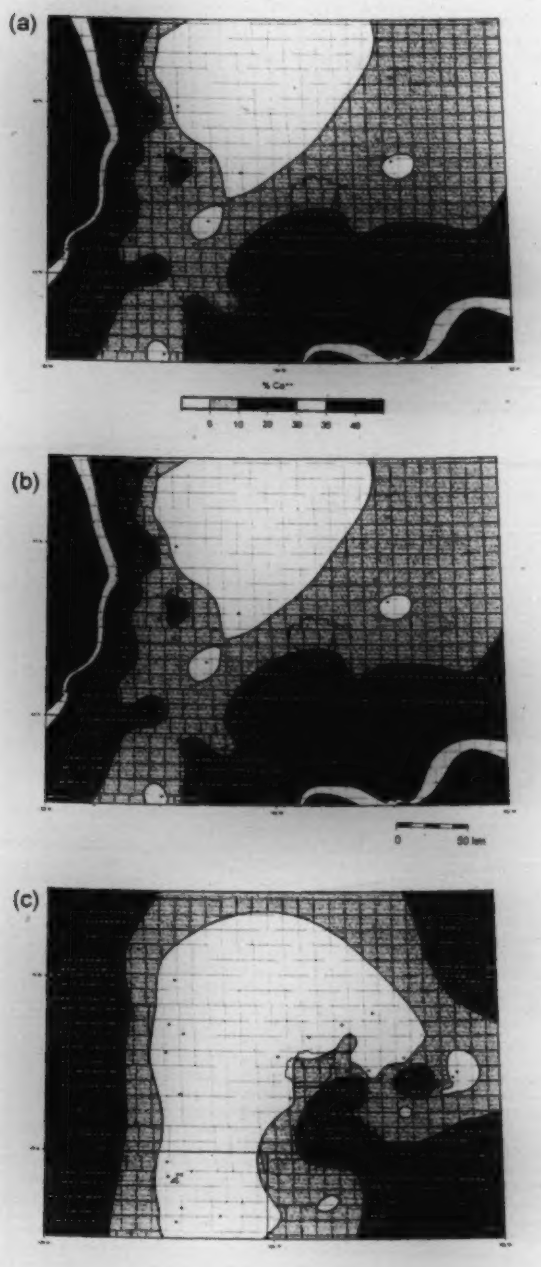
(a)
% Ca++
5
10
20
30
35
40
(b)
0
50 km
(c)

Figure 3.12. Cationic fraction of Calcium in formation waters of selected Deep Paleozoic aquifers: a) Birdbear, b) Duperow, and c) Winnipegosis.

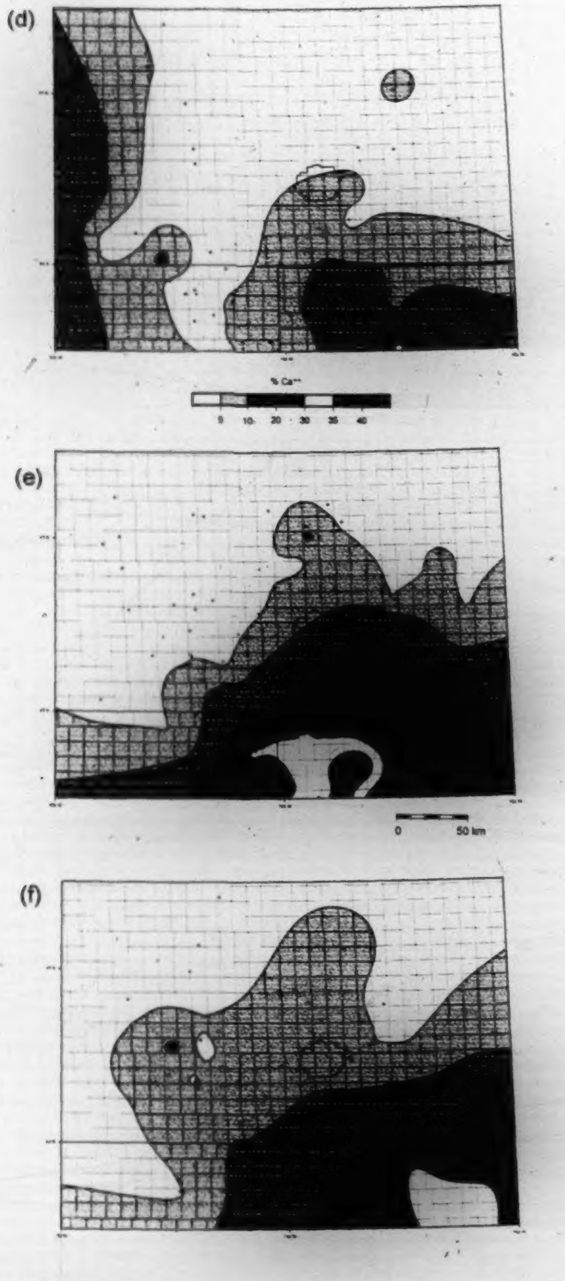
(d)
% Ca++
5
10
20
30
35
40
(e)
0
50 km
(f)

Figure 3.12. (continued) Cationic fraction of Calcium in formation waters of selected Deep Paleozoic aquifers: d) Ordo-Silurian, e) Yeoman, and f) Cambro-Ordovician.

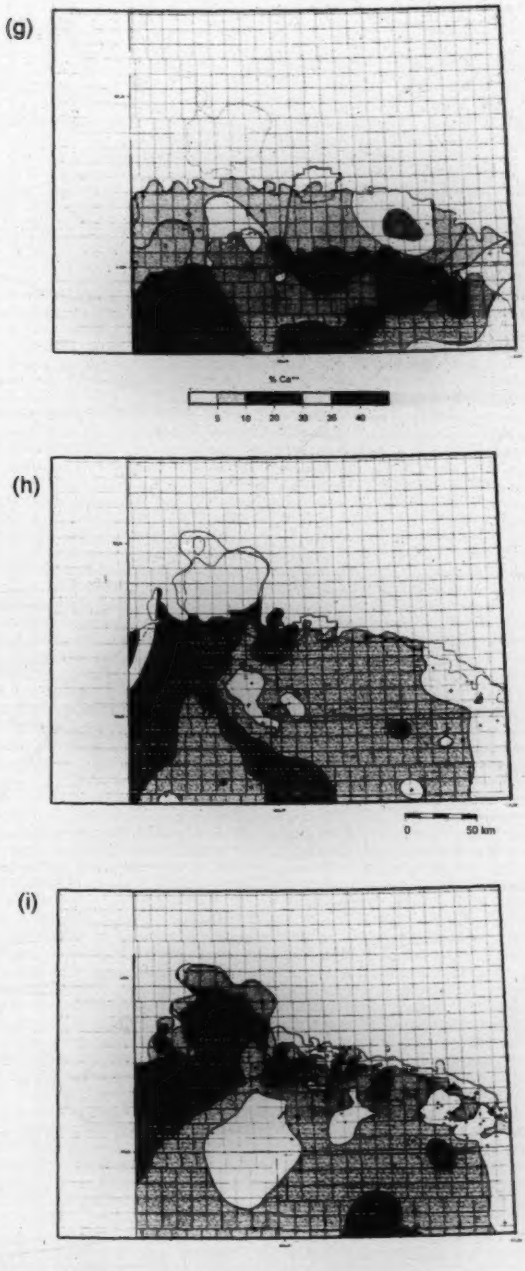
(g)
% Ca++
5
10
20
30
35
40
(h)
0
50 km
(i)

Figure 3.12. (continued) Cationic fraction of Calcium in formation waters of selected Mississippian aquifers: g) Poplar, h) Ratcliffe, and i) Midale.

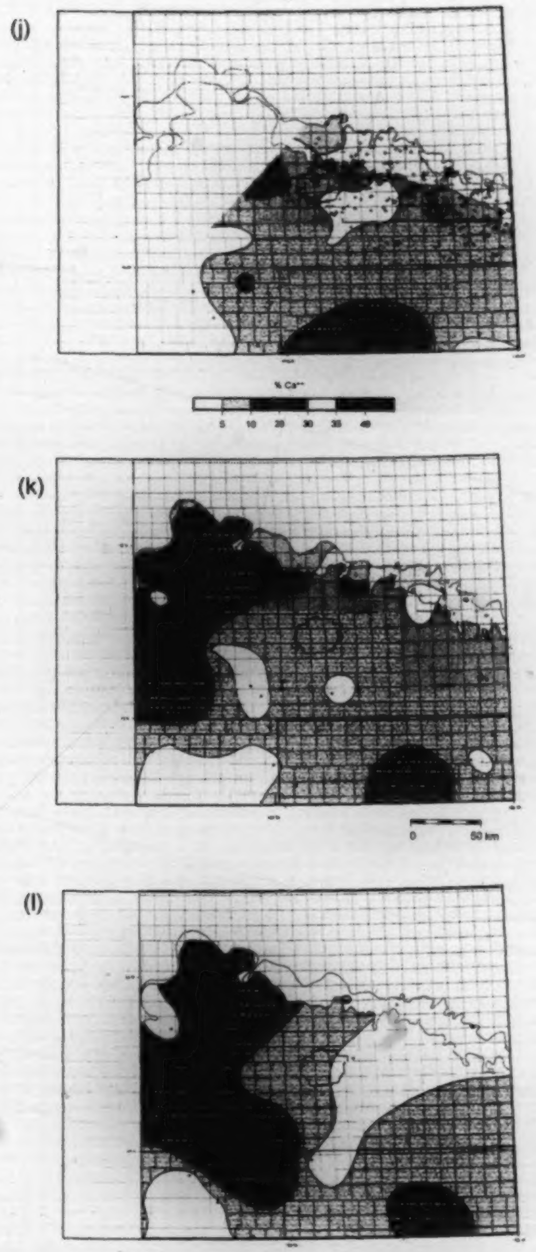
(j)
% Ca++
5
10
20
30
35
40
(k)
0
50 km
(l)

Figure 3.12. (continued) Cationic fraction of Calcium in formation waters of selected Mississippian aquifers: j) Frobisher, k) Alida, and l) Tilston.

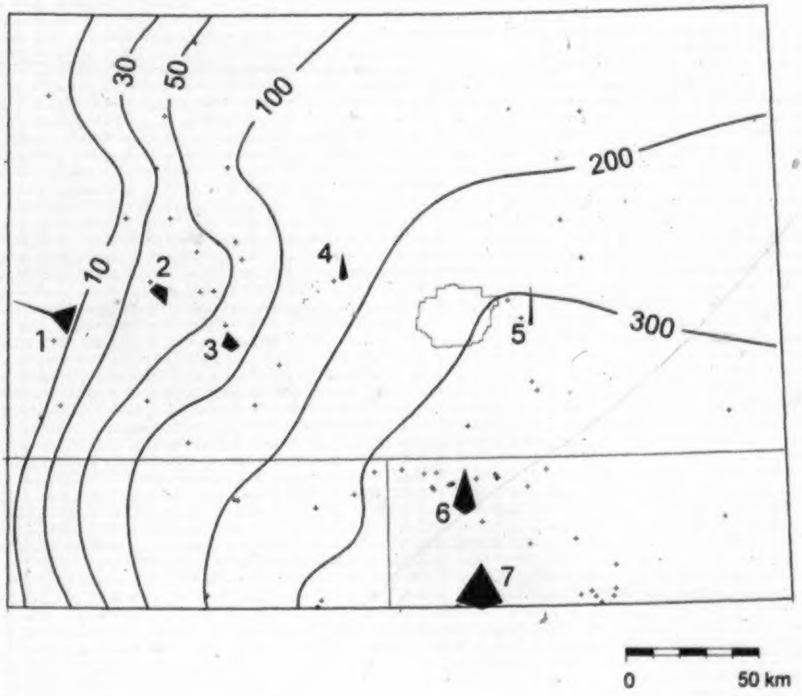
10
30
50
100
200
300
1
2
3
4
5
6
7
0
50 km

Figure 3.13. Duperow TDS map showing spatial distribution of water types (see Figure 3.9 for reference). Selected type samples are shown by their corresponding symbol — as plotted on a pentaxial plot — with the corresponding water analyses shown in tabular format in Table (3-1).

| Sample No. | TDS($gL^{-1}$) | Na+K($mgL^{-1}$) | Ca | Mg | Cl | $SO_4$ | $HCO_3$ | Type |
|---|---|---|---|---|---|---|---|---|
| 1 | 4.3 | 418 | 732 | 140 | 600 | 2198 | 218 | 1 |
| 2 | 35.1 | 12097 | 1099 | 231 | 18034 | 3329 | 322 | 5 |
| 3 | 50.0 | 17209 | 1386 | 315 | 27000 | 3457 | 630 | 5-2 |
| 4 | 157.6 | 58673 | 2106 | 408 | 93000 | 2973 | 395 | 2 |
| 5 | 286.5 | 107067 | 4080 | 640 | 173000 | 1467 | 275 | 2 |
| 6 | 335.8 | 97570 | 31265 | 1287 | 205296 | 289 | 159 | 2-3 |
| 7 | 347.0 | 64444 | 57915 | 5900 | 219000 | 110 | 0 | 3 |

Table 3-1. Chemical compositions of formation water samples posted on Figure 3.13

# 4.0 HYDRODYNAMICS IN THE IEA GHG WEYBURN $CO_2$ MONITORING AND STORAGE PROJECT AREA: WILLISTON BASIN[*]

## 4.1 INTRODUCTION

A detailed characterization and analysis of the hydrodynamic regime in a large area located in the north-central Williston Basin provides new insights on the hydrogeology of the basin. The purpose of this study was twofold: (1) to quantify the driving forces and characterize the hydrodynamic regimes acting on formation waters in the study area; and (2) hydrodynamic analysis was an integral part of the characterization of the geological framework conducted for the IEA GHG Weyburn CO2 monitoring and storage project (Whittaker et al., 2004; Preston et al., 2005).

The principal objective of the Weyburn Project is to demonstrate the capacity of a giant depleted oil field to store anthropogenic $CO_2$. Subsurface $CO_2$ storage or sequestration involves the segregation of CO2 from the biosphere for a time frame long enough to contribute to a stabilization of the increasing atmospheric concentrations of $CO_2$ observed today (Socolow, 2005). The success of geological sequestration depends on the efficiency of one or more trapping mechanisms including: structural or stratigraphic traps, solubility trapping, mineral trapping, and hydrodynamic trapping (Bachu, 2001). The capacity of each of these trapping processes is controlled (or affected by) the subsurface pressure, temperature, and geochemical regimes. Thus, a comprehensive hydrogeological study is a cornerstone of any investigation assessing the integrity of a sequestration site (IPCC, 2005).

The synthesis of the results presented herein and in any similar hydrogeological analysis provides the basis, in the form of boundary and initial conditions, for numerical simulations as a part of risk analysis (e.g., Zhou et al., 2004), which are required for the screening and approval stages by regulatory frameworks designed for $CO_2$ storage projects (Tsang et al., 2001). The methodology presented may be useful to others intending to perform characterizations of other $CO_2$ sequestration projects in the future.

---

[*] A version of this chapter has been submitted to the journal *Geofluids*, Blackwell Publishing, and is expected to be published with the title shown by authors: D.K. Khan and B.J. Rostron.

However, the results of this work and the accompanying chapter (see Chapter 3) contribute to the understanding of the hydrogeology of the Williston Basin as a whole.

From a scientific perspective, this study differs from any previous regional hydrogeological analysis in the Williston Basin. First, it contains newer (post-1996) data from deep drilling results on the Canadian side of the basin. Second, this study used previously unavailable geological mapping from the Weyburn project (Whittaker et al., 2004). This enabled a much greater hydrostratigraphic resolution, including the separation of the Mississippian aquifer system into constituent aquifers. This paper includes the first attempt at mapping the detail of the hydraulics of distinct horizons within the Mississippian strata, which are of greatest importance to economic and environmental interests at this time. Third, the estimation of in-situ formation water densities and the calculation of density-corrected driving forces on Williston Basin brines are included here. Our interpretation of the patterns of density-dependent flows leads to new interpretations of the paleohydrogeology of the Williston Basin.

## 4.2 STUDY AREA AND HYDROGEOLOGICAL FRAMEWORK

An area encompassing approximately 50,000 km$^2$ of the Williston Basin was examined for this study (Figure 4.1). The regional hydrogeological characterization area is bounded by meridians 102-106W and parallels 48.5-50.5N, and is slightly larger (an additional 50 km to the west) than the 200 by 200 km block centered on the Weyburn Field, which was adopted for the Weyburn Project geosphere characterization (Whittaker et al., 2004).

### 4.2.1 Previous work

Regionally, formation water flow in the Williston Basin has been widely studied, with examples from the Canadian side of the basin (Hannon, 1987; Bachu and Hitchon, 1996) and the American portion (Downey, 1984a,b; 1986; Downey et al., 1987). Previous studies have concluded that flow of formation waters generally occurs from the S-SW to N-NE across the basin. This cross-basin flow is thought to occur in response to a regional hydraulic gradient created by topographic elevation differences, approximately 1000 m on average, between major aquifer outcrop areas at opposite edges of the basin. This cross-basinal flow system is thought to have originated relatively recently in the history of the basin, with the current boundary conditions set up in Eocene times in association with the Laramide orogeny (DeMis, 1995) when the flanks of the basin within the Rocky Mountain foreland were uplifted (Dickinson et al., 1988).

### 4.2.2 Hydrostratigraphy

To examine the hydrodynamics of the study area, geologic strata must be regrouped into hydraulically-similar flow units: aquifers, which are relatively transmissive strata or groups of strata; and aquitards, which are of relatively low permeability. The classification of a stratum or a group of strata as either an aquifer or an aquitard is based largely on the purpose of study and the time scales of the processes under consideration (Tóth, 1995). Availability of data also plays a role in the construction of the hydrostratigraphic framework.

A hydrostratigraphic framework consisting of 19 major aquifers and 13 major aquitards was developed (Figure 4.2) in conjunction with the Weyburn Project geological model (Whittaker et al., 2004). These 18 major aquifers were combined into three major groups for discussion: 1) Deep Paleozoic, 2) Mississippian, and 3) Mesozoic aquifer groups. Further details on the geology and hydrostratigraphic subdivision are included in Chapter 2.

## 4.3 DATA AND METHODOLOGIES

A hydrogeological database of over 5300 fluid pressures and formation temperatures and over 8500 formation-water analyses was assembled from public and private data sources. Hydraulic and hydrochemical data were assigned to their respective named aquifer units and then tested against structural controls defined by geological mapping completed by Saskatchewan Industry and Resources and the North Dakota Geological

Survey (Whittaker et al., 2004). Stratigraphic surfaces were mapped by geologists at Saskatchewan Industry and Resources and the North Dakota Geological Survey and made available for the study through the Weyburn Project (Whittaker et al., 2004). Hydrogeological data were assigned to their respective aquifer units using structural controls provided by the geological mapping. This assignment was an iterative procedure which made use of digital grids of elevation differences between the tops and bases of water sample intervals and the stratigraphic surfaces defining aquifers.

All data were carefully screened using automated and manual techniques. Formation-pressure data came from drill stem tests. Only quality pressure data with full Horner-type extrapolations (Horner, 1951) were used. Each pressure measurement was screened for production-influenced pressure drawdown by calculating the cumulative drawdown on the potentiometric surface due to of any number of pumping or injection wells within a specified radial distance from a fluid pressure sample. This allows the objective removal of anomalous pressure data which are the result of fluid production or injection, and which do not reflect the pseudo-steady state potentiometric surface. The method used is based on the description of the Interference Index (Tóth and Corbet ,1986; Rostron, 1994).

### 4.3.1 Driving forces on formation waters

Formation water flows in sedimentary basins are driven by topographic relief, buoyancy, sediment compaction, erosional unloading, and other processes resulting in hydrodynamic pore pressure gradients (Neuzil, 1995; Ingebritsen and Sanford, 1998). In mature sedimentary basins, where deformational processes have largely ceased and cross-basin topographic relief is present, the fluid potential gradient due to the elevation differences between major aquifer recharge and discharge areas tends to dominate the flow driving force regime (Tóth, 1978; Garven, 1995). The effects of any of the other processes may, however, locally dominate the net driving force on formation fluids.

It is generally accepted that the cross-basinal flow of formation waters in the Williston Basin is a result of elevation differences between areas of recharge at aquifer outcrops in the Southern to Western basin flanks, and discharge areas along the Canadian Shield in the northeast. Density-dependent flows of brines in the Williston Basin have been postulated (Downey, 1984a,b, 1986; Downey at al., 1987); however, there has been little quantitative analysis of buoyant flows in the Williston Basin.

The approach taken to quantifying the fluid driving forces in the study area was based on this conceptual model — that regionally topography-driven flow is heterogeneously modified by lateral density gradients. The methodology thus consisted of three steps: 1) generate potentiometric surface maps for each aquifer in order to estimate hydraulic gradients, 2) estimate spatially-variable, in-situ formation water densities to estimate the density gradients causing buoyant flows, 3) analytically calculate the net point driving-force vectors resulting from the combined hydraulic and density gradients to quantify the fluid driving force field in each aquifer. A computer program developed by Alkalali and Rostron (2003) was used to perform this task.

Such a methodology, which is based on potentiometric analysis, can provide a complete assessment of only the horizontal component of the fluid driving force field. The vertical component was assessed by pressure versus depth analysis, considering a stratified variable-density fluid column at the location of a pressure-depth profile, where necessary.

Details on each of these methodology components are presented in Appendix A.

## 4.4 RESULTS

### 4.4.1 Potentiometric Analysis

In the Deep Paleozoic aquifers, hydraulic heads range from over 1000 m in the south to less than 600 m in the northeast (Figure 4.3). Hydraulic gradients range in magnitude between 0.1 to 7 m/km, with an average of about 1 m/km. Hydraulic head decreases across the study area in a generally northeasterly direction. The potentiometric surfaces of the aquifers in the Deep Paleozoic group are overall quite similar, indicating little dependence between fluid potentials and depth.

Within the Mississippian aquifers, hydraulic heads exhibit similar trends to the underlying Deep Paleozoic aquifer group (Figure 4.4). Hydraulic heads vary from over 850 m in the south-southwest to less than 600 m in the northeast. Hydraulic gradients are generally comparable to other Paleozoic aquifers except for local areas with gradients up to 20 m/km in the east (Figure 4.4a-c); these locally high gradients in hydraulic heads indicate the existence of competent barriers to lateral flow.

In the Mesozoic aquifers, potentiometric surfaces are very different between individual aquifers, unlike what is observed in the deeper groups (Figure 4.5). Hydraulic gradients are also lower than those observed in the underlying aquifer groups. These characteristics imply significant differences in the hydraulics of the Mesozoic aquifer group compared to the underlying units.

Flow directions inferred from hydraulic gradients in the Jurassic Aquifer (Figure 4.5c) are directed north-northeast, similar to the underlying Mississippian and Deep Paleozoic aquifers. Hydraulic gradients in the Jurassic Aquifer range from less than 0.5 m/km to 7 m/km, with an average magnitude of 1.1 m/km.

Within the Mannville Aquifer, hydraulic heads vary over a relatively small range from over 650 m in the west, to values less than 500 m in the east-northeast, with hydraulic gradients driving fluid flow in a generally east to west direction (Figure 4.5b). Hydraulic gradients in the Mannville aquifer vary between 0.2 and 4 m/km, with a regional average of 0.8 m/km. The patterns in the potentiometric surface map of the Mannville aquifer, with locally high gradients toward the centre of the study area, are interpreted to be caused by the regional flow cutting across the predominantly north-south orientation of the regional permeability anisotropy (Khan and Rostron, 2004), which is due to large north-south trending channels of thick sands within the Mannville aquifer (Christopher, 2003).

In the Newcastle Aquifer flow is from south to north, following the elongate orientation of the permeable Newcastle sand body (Figure 4.5a). Hydraulic gradients average approximately 0.8 m/km in the Newcastle aquifer.

A vertical hydraulic cross section displays the vertical variation of hydraulic head. It shows similarities and differences in the hydraulics between the aquifer groups, as well as several anomalies (Figure 4.6). The Deep Paleozoic aquifers appear very similar with respect to hydraulic head patterns. However, notable exceptions include the Manitoba Aquifer, which appears to be relatively underpressured, and the Bakken Aquifer which is overpressured in the south (maximum heads of 1780 m) (Figure 4.3a). The terms under- and over-pressured are used here in a qualitative sense to describe apparent relative anomalies in the values of hydraulic head for an arbitrary vertical line through the section. Considering that the pore pressures in the majority of the section are close to hydrostatic (discussed below), these qualitative terms are a proxy for the strict quantitative use of the descriptors.

A broad relative low in hydraulic heads (700-500 m) is apparent in the Mississippian System between the Ratcliffe to Alida Aquifers.

The Jurassic aquifer appears similar to the Mississippian aquifers with respect to hydraulic head patterns. However, the shallower Mesozoic aquifers are quite different, with lower heads overall, and what appear to be abnormally low hydraulic heads in the north and northeast (heads < 500 m) (Figure 4.6).

### 4.4.2 Density-corrected driving forces and flow directions

The relative importance of buoyant forces to the net driving force field on formation waters is controlled by the interplay between aquifer structural gradient, water density, and the gradient of hydraulic head (Davies, 1987). Density-driven flows become significant as the aquifer slope increases, density (i.e., TDS) increases, and the gradient of hydraulic head decreases. The effects of buoyant forces on formation water flow in the Williston Basin have not previously been quantified.

The absence of dense brines in the Mesozoic aquifers (see Chapter 3) permits the use of potentiometric surface maps alone to estimate lateral formation water flow directions (Figure 4.5).

High formation-water densities in the Deep Paleozoic aquifer group result in large areas of density flow reversals. The term "flow reversals" refers to areas characterized by down-dip (i.e., southerly directions in these maps), basin-inward flows where formation waters tend to "sink" toward points of lower structural elevation, opposing the ubiquitous updip-directed driving force due to the hydraulic gradients.

Vector maps are used to show the azimuthal difference between the orientations of the driving force field due to the hydraulic gradient, *-grad h*, and that due to the resultant net water driving force, *WDF*, after accounting for the combined effect of formation-water density and structural dip of the aquifer (Davies, 1987; Alkalali and Rostron, 2003) (Figure 4.7). Assuming an isotropic permeability field, the direction of formation water flow is correctly predicted by the density-corrected *WDF*. In the vector maps of Figures (4.7 and 4.8), potentiometric surface contours are overlain on shaded contours, with the shading indicating the degree of azimuthal divergence between *-grad h* (indicated by grey-coloured vectors) and the density-corrected *WDF* (black vectors). At locations of density flow reversals within the study area, the azimuthal divergence between *-grad h* and the density-corrected *WDF* exceeds 90°.

Within the upper section of the Deep Paleozoic aquifer group, as shown by the Duperow Aquifer (Figure 4.7a), there is a correspondence over most of the study area between locations of significant density flows and relaxations in the hydraulic gradient (all shaded areas in Figure 4.7a). In these locations, the updip-directed *-grad h* is insufficient to counter the downdip-directed buoyancy force, resulting in density flow reversals, where the *WDF* is oriented in a down-dip (southerly) direction. Other pronounced occurrences of flow reversals related to low hydraulic gradients are observed in the northeast corner [T1-10,R10-17, Sask. (refer to Figure 4.1 for Survey grid labels)] of the study area in the Duperow, Winnipegosis, and Yeoman Aquifers (Figure 4.7 a,b,c), where the azimuthal divergence between *-grad h* and the density-corrected *WDF* approaches 180°.

In the southeast of the study area, high formation water densities exert significant control on the *WDF* and corresponding flow directions within most of the Deep Paleozoic aquifers. For example, in the southeast corner of the Winnipegosis Aquifer map (R95W-90W, North Dakota), despite moderately high hydraulic gradients, the effects of density flows are intense, as indicated by azimuthal divergences between *-grad h* and density-corrected *WDF* vectors exceeding 90° (Figure 4.7b).

Within the Cambro-Ordovician aquifer, there is a large elliptically-shaped area in the southeast (centered at T159N, R93W, North Dakota) with azimuthal divergences up to 180°. This area corresponds to the joint occurrence of relatively high structural dip (sloping toward the basin centre to the south), a relaxation in the hydraulic gradient, and formation waters with densities in excess of 1170 kg m-3 (Figure 4.7d).

However, high hydraulic gradients in the southeast corner of the Red River Aquifer (R95W - 100W, North Dakota) overcome the buoyancy force completely such that flow is driven predominantly by the potentiometric gradient, as indicated by nearly parallel orientation of *-grad h* and the *WDF* vectors (Figure 4.7c).

Within the Mississippian system, the interplay between local variability in the hydraulic gradient and formation-water densities results in quite different hydrodynamic regimes between individual Mississippian aquifers (Figure 4.8). This is the first time the Mississippian aquifers in the Williston Basin have been characterized with vertical detail as a succession of separate aquifers, as opposed to a single aquifer system, and that density-corrected flow directions have been calculated.

Density-corrected *WDF* vectors in the western part of the study area in the Midale and Frobisher Aquifers are oriented parallel with *-grad h* (Figure 4.8c,d). Flow directions are controlled strictly by the hydraulic gradient in the western portions of these aquifers due to the occurrence of relatively fresh formation waters (see Chapter 3 ).

Flow along the Midale and Frobisher subcrop between the Weyburn field and the western edge of the study area is oriented roughly parallel to the subcrop trend, indicating that the subcrop is a competent barrier to fluid flow in this part of the Mississippian system (Figure 4.8c,d).

Water driving forces are deflected down dip in the south half of the Weyburn oilfield within the Midale Aquifer (Figure 4.8c) as increasingly dense brines and a southward-increasing structural gradient become important controls on flow. The steep salinity gradient across the Weyburn oilfield in the Midale Aquifer (see Chapter 3) marks the approximate position of this transition to buoyancy-dominated flows, as indicated by a dashed line in the vicinity of the Weyburn field in Figure (4.8c).

The area of density-dependent flows in the Ratcliffe Aquifer is confined to the south of the study area (North Dakota), and controlled primarily by high formation-water densities and steepening structural gradients toward the south (Figure 4.8b). A lack of data in the east-central area (blanked map area - Figure 4.8b) precludes confirmation that formation water flows in the vicinity of the Ratcliffe Aquifer subcrop are oriented in an easterly direction, parallel to the subcrop, as seen in the Midale and Frobisher Aquifers (Figure 4.8c,d). But this is likely considering that the Ratcliffe Beds, like the Midale and Frobisher Beds, are capped by evaporitic lithofacies which directly underlie the Watrous aquitard at the unconformity surface (Kent et al., 2004).

A large potentiometric trough in the central part of the study area (centered at T3,R17, Sask.) within the Poplar Aquifer results in the area being dominated by basin-inward density flows due to very low potentiometric gradients (0.03 to 0.3 m/km) (Figure 4.8a). The anomalies in the potentiometric surface of the Poplar aquifer, as well as hydrochemical anomalies (see Chapter 3) indicate that the Poplar Aquifer is characterized by a very different hydrodynamic regime from the rest of the Mississippian system. The likely cause for the observed anomalies is that the Poplar Beds contain several continuous evaporite layers throughout their vertical thickness (Kent et al., 2004). Internal vertical heterogeneity may result in sampling of pressures and chemistries from different zones which are in poor hydraulic communication with one another. In this case, taking the data to represent a single aquifer unit may result in anomalous pressure and chemistry distributions of over the map area. This is the likely cause for the apparent localized low-pressure zone centered on the closed low in the potentiometric surface in the west-central area of the Poplar Aquifer. There are sufficient data to support the presence of this anomaly (8 DST's - Figure 4.3a), but the cause of the underpressuring is not known.

### 4.4.3 Pressure vs. depth analysis

Density-corrected WDF maps only account for the driving forces on formation waters which are oriented parallel to the confining or bounding surfaces of the aquifers. The presence and direction of a vertical component to the hydraulic gradient may be inferred from a plot of pore pressure versus depth (Toth, 1978). Ideally a pressure-depth [p(d)] profile would be constructed from simultaneous measurements of pressure along a continuous vertical transect (e.g., repeat formation tester). In practice, for regional data sets consisting primarily of exploratory drill stem tests, p(d) profiles are constructed from data within optimally-sized local areas. Optimal block size balances adequate data needed to construct a reasonably continuous p(d) plot over a given stratigraphic interval, against an area small enough to minimize the effects of aquifer heterogeneity and topographic relief (Tóth and Almasi, 2001).

Vertical flow was assessed using seven p(d) profiles over the study area. Figure (4.1) shows the locations of blocks used to construct these p(d) profiles. The blocks are numbered according to the corresponding p(d) profile in Figure (4.9). Vertical changes in formation water density were accounted for by calculating a density-weighted nominal hydrostatic pressure gradient. Weighting was based on the thicknesses of the stratigraphic intervals assumed to contain formation water of a constant density, with density transitions assumed to occur within aquitards. The nominal hydrostatic gradient is therefore not constant with depth (e.g., Figure 4.9a).

Two p(d) profiles (Figure 4.9a,b) in the vicinity of the Weyburn oilfield area (Figure 4.1; Blocks 1 and 2) indicate that there does not appear to be any significant vertical component to formation water flow through the entire hydrostratigraphic section. Pore pressures throughout the Deep Paleozoic and Mississippian aquifers plot along the nominal hydrostatic gradient. Within the Weyburn oilfield (Figure 4.1; Block 1), most of the Mississippian data indicate a slight overpressuring (Figure 4.9a; 1.36 - 1.53 km depth). The origin of the overpressures is ambiguous; it could be a minor isolation of that portion of the aquifer, or, more likely, the effects of water injection, which has been part of the production operations in the field since shortly after discovery in 1954. The scatter in the Mississippian pressure data is to be expected from the age of many of the drill stem tests (ca. 1952-1988) and the accuracy of pressure recorders from the older tests (Olson, 1967). In any case, fitting a pressure gradient to the Mississippian data shows that the pressure gradient is parallel to the nominal gradient (Figure 4.9a), suggesting that water flow beneath the oil column is predominantly horizontal.

East of the Weyburn oilfield (Figure 4.1; Block 2), there is an apparent break in the pressure profile between the Mississippian and the Mesozoic across the Watrous Aquitard (Figure 4.9b; 1.16 to 1.21 km depth). The unconformity surface terminating the Mississippian System is underlain by a heavily diagenetically-altered zone over a large part of the study area, including the location of the Weyburn oilfield, in which porosity is almost completely occluded (Whittaker et al., 2004). It is therefore likely that the observed break in the p(d) profile represents a hydraulic discontinuity equivalent to about 715 kPa at this location. The Mesozoic pressure data indicate underpressuring and upward flow (i.e., a superhydrostatic gradient) between the Jurassic and Mannville aquifers (Figure 4.9b; 1.04 to 1.16 km depth) directly east (Figure 4.1; Block 2), as well as to the north [Figure 4.1; Block 3] of the Weyburn oilfield (p(d) not shown).

In the northeast of the study area (Figure 4.1;Block 4), all of the pressure data spanning the interval between the Mesozoic Newcastle Aquifer to the Deep Paleozoic Birdbear Aquifer are underpressured (Figure 4.9c; 0.71 - 1.42 km depth). Pressures in the Mississippian Souris Valley and Tilston Aquifers appear to fall along a superhydrostatic vertical pressure gradient (11.4 MPa/km), indicating upward movement of formation waters across the Watrous Aquitard. Since it is possible to fit a single superhydrostatic pressure gradient through the pressure data from the Mesozoic aquifers down to the deep Paleozoic Duperow Aquifer, this implies vertical hydraulic continuity through the entire stratigraphic section above the Prairie Aquitard (Figure 4.2) and a significant vertically-upward component to bulk flow in the northeast of the study area (Figure 4.9c).

In the south-central study area (Figure 4.1; Block 5), pressure data spanning the Mississippian to Yeoman Aquifers scatter tightly about the nominal hydrostatic gradient (Figure 4.9d), indicating a negligible vertical component to flow (i.e., predominantly horizontal flow).

Pressure data in the west of the study area (Figure 4.1; Block 6) appear to fall along superhydrostatic pressure gradients (Figure 4.9e). The data in this p(d) profile are located on the edge of a regional freshwater plume recharging the Paleozoic aquifers in the basin (Benn and Rostron, 1998, see Chapter 3). A single superhydrostatic gradient (11.5 MPa/km) fits the data spanning the Ordo-Silurian to Manitoba Aquifers, and a second superhydrostatic gradient (13.8 MPa/km) may be fit to a shallower group of data in the Devonian Duperow and Birdbear aquifers. All of the data in this profile are from three wells, each with several recent drill stem tests along the same borehole, so increased confidence in the observed deviations from the nominal gradient is warranted. Given the confidence in the prediction of the formation water density in this area (freshwater) and the collocated pressure data, it is reasonable to conclude a significant upward component to flow in the western study area between this interval in the Deep Paleozoic aquifer group.

## 4.5 SYNTHESIS AND DISCUSSION

The fluid dynamic parameters presented here enable a synthesis of the hydrodynamic regime within the study area, as well as extrapolation beyond the current study area, and with respect to the paleohydrogeology of the Williston Basin.

To a first order, the observations outlined in the preceding sections are consistent with the classic model for topography-driven cross-basinal flow of formation waters (Tóth, 1978). The study area falls within the end of the basin midline region and the beginning of the discharge region, where flow directions are horizontal to mildly vertically upward, respectively (Figure 4.10). Vertical p(d) profiles indicate sub-horizontal flow with a tendency of upward cross-formational flow.

Flow is largely horizontal in the majority of the study area. Hydraulic heads within the Deep Paleozoic and Mississippian aquifers (Figures 4.3 and 4.4) show no significant dependence on depth. The hydraulic head at a given location reflects the elevation of, and the distance from the recharge areas of the basin. For example, the average value of hydraulic head of approximately 1000 m in the southwest map area within the Deep Paleozoic and Mississippian aquifers reflects the topographic elevation of the Black Hills and/or uplifts in central Montana, less the amount of head lost along the flowpath to frictional resistance. The effects of transient adjustment to the denudation of the uplifted recharge areas (Tóth and Millar, 1983) are not reflected in the hydraulic head distributions within the aquifers.

Pressure-depth analysis reveals that a significant upward vertical component to formation water flow exists in two regions: (1) the northeast of the map area (Figure 4.1; Block 4), in the aquifers above the Prairie salt Aquitard (Figure 4.9c; < 1.6 km depth), and (2) the western area (Figure 4.1, Block 6; Figure 4.9e), coincident with the occurrence of fresh formation waters at the edge of a regional plume of recharging meteoric waters and the absence of the Prairie Aquitard (see Chapter 3). The absence, or the inconsequence of the Prairie Aquitard is the common factor promoting vertical hydraulic continuity in these areas and pronounced cross-formational flow.

In the northeast area (Block 4), underpressures and superhydrostatic gradients (Figure 4.9c) indicate pressure drainage and upward flow, respectively. "Pressure drainage" refers here to the efficient equilibration of the hydraulic heads in an aquifer to values approaching the average elevation of a distal discharge area at the land surface. High transmissivity aquifers connected to such a discharge area results in efficient hydraulic connection to atmospheric pressures at points quite distant from the area of discharge. An analogous situation was reported by Tóth (1978) in the Alberta Basin. The result is pore pressures significantly lower than hydrostatic.

Hydraulic heads in the northeast of the study area in the Mesozoic Jurassic and Mannville aquifers are approximately 400 m. Jurassic and Cretaceous rocks, which are stratigraphically and lithologically equivalent to the rocks that form the highly transmissive Jurassic and Mannville aquifers within the study area, crop out along the Manitoba escarpment (Figure 4.1) at elevations of approximately 350-300 m. Underpressuring is most pronounced in the Mesozoic aquifers, but the pressure drawdown causes underpressuring extending down to the Deep Paleozoic aquifers (Figure 4.9c). The upward discharge of formation waters inferred from the continuous superhydrostatic pressure gradient on the p(d) plot of Figure (4.9c) indicates hydraulic communication across the Watrous aquitard from the Deep Paleozoic and lower Mississippian (Souris River and Tilston) aquifers toward zones of low hydraulic head (< 500 m) within the overlying Mesozoic aquifers (Figure 4.6). Thinning of the Watrous and Vanguard Aquitards (Figure 4.2) in the Mesozoic System in the northeast (Figure 4.6) contributes to the widespread pressure drainage by promoting efficient vertical hydraulic communication. Other factors enhancing vertical hydraulic communication include: 1) lack of evaporitic lithofacies in the Souris River and Tilston Aquifers along the Mississippian subcrop trend in the north-northeast, and 2) being in a location that is approaching the Williston Basin discharge region (Figure 4.10).

In the western area (Figure 4.1; Block 6), invading fresh waters are being diverted upward in a relatively restricted area. The interpretation of upward flow of fresh waters in this area is consistent with that of Downey (1984a,b); that the invading fresh waters recharging the Williston Basin are directed upward and around the dense brines in the basin center.

### 4.5.1 Density-related hydrodynamic phenomena

The density flow reversals shown warrant further investigation. Mapping out local pockets of buoyancy-dominated flows is useful, for example, in petroleum exploration, where the net hydrodynamic force influencing petroleum migration trajectories and trapping capacities is very different from what is estimated from the pressure field alone (Barson et al., 1998). But the mere fact that large areas of downdip density flows exist provides important clues to the hydrodynamic and associated geologic history of the Williston Basin.

It is well-known that the brines in the deep Paleozoic and Mississippian aquifers in the central Williston Basin are displaced updip toward the northeast flank of the basin (e.g., Downey, 1984a,b; 1986; Downey at al., 1987). It has not previously been recognized that these brines are sinking back toward the basin center by density-dominated flows. It was thought that the present-day hydrodynamic regime controls the displacement of the central Williston Basin "brine slug". Previous workers proposed that the displaced position of the brines was maintained in a static position, or driven slowly northeastward from the basin center by the ubiquitous updip -directed potentiometric driving force in the Deep Paleozoic and Mississippian aquifer systems (Downey 1984a,b,1987; Bachu and Hitchon, 1996). Results shown here provide a different explanation. The observation that the dense brines occur at locations where they are gravitationally unstable indicates that such locations have been positions where the brines rested in gravitational equilibria when hydraulic gradients were sufficient to displace the brines updip and overcome the tendency to sink back toward lower elevations in the basin. In other areas where the present hydraulic gradient is sufficient to counter, or balance this tendency to flow back down dip to a position of static equilibrium, the brines continue to move slowly updip, or stagnate in place, respectively.

In summary, rather than a model where recharging waters are pushing brines updip to their present position, we would argue that the brines were displaced from the basin center by greater (paleo) hydraulic gradients and that they are now moving back to equilibrium positions, toward the depocenter of the basin.

To illustrate this, we performed a simple calculation using the data from the Winnipegosis aquifer (Figure 4.7b) as an example. The first step was to create a plausible configuration of the elevated potentiometric surface and the resultant hydraulic gradients within this aquifer that would have existed during peak hydrodynamics. Erosion rate estimates in the Black Hills suggest that approximately 2100 metres of Phanerozoic sediments were removed in a period of 6 to 7.5 million years (Lisenbee and DeWitt, 1993). This equates to a threefold increase in the topographic elevation difference across the basin from what it is today. We simulated the effect of this magnified cross-basin relief on the configuration of the potentiometric surface of the Winnipegosis aquifer.

A discretized grid spanning the geographic extent of the Williston Basin was populated with a spatially-variable multiplication factor ranging from a value of 3.0 at the locations of major uplifts to a value of 1.0 along the Precambrian shield outcrops in Canada. This multiplication surface decayed from the maximum values with an exponential character (Figure 4.11). The domain was cropped to the region coincident with the study area and multiplied by the potentiometric surface grid of the Winnipegosis aquifer to yield a simulated paleo-potentiotiometric surface (Figure 4.12).

The WDF vector analysis was done on this simulated potentiometric surface map to yield a plausible realization of the formation water driving force distribution that would have existed during the period of peak hydrodynamics. As expected, almost all of the areas characterized by unstable density flows at present (shaded areas) show sufficiently increased hydraulic gradients to drive the brines updip toward the N-NE (compare Figure 4.7b with Figure 13). Shaded contours in Figure (4.13) are the same as in Figure (4.7b), but in Figure (4.13), the shading may simply be interpreted as the relative degree of gravitational instability of the brines in the present-day flow system. Note that in all of the shaded areas, brines would have been flowing updip to the northeast under increased paleo-driving forces. In the southeast (R95W), the inability to significantly change the direction of brine migration is due to uncertainty in the actual shape of the surface to apply in the simulation, and/or the need for increased paleo-topography. Although beyond the scope of this study, a sensitivity analysis modeled after the preceding exercise provides a way to constrain estimates of the amount and rates of erosion in the Williston Basin.

Paleomagnetic studies (Cioppa, 2003) have indicated the influx of a chemically-reducing fluid into the Watrous Aquitard, sourced from the underlying Mississippian aquifers. This event is dated at latest Cretaceous to earliest Tertiary time. This is an alternate line of evidence which supports the proposed paleo-hydrodynamic model suggested herein. Although today's hydraulic gradients are insufficient to breach the hydraulic barrier along the Mississippian subcrop in the area of the Weyburn oilfield, fluid pressures during the peak hydrodynamic phase appear to have been sufficient to force large-scale leakage into the Watrous Formation, as discussed further below.

### 4.5.2 Mississippian hydrodynamics and caprock trapping capacities

A detailed characterization of the Mississippian aquifer group was a primary objective of this study because of the relevance to the Weyburn $CO_2$ project and to future $CO_2$ storage projects along the Mississippian subcrop in Canada. Mapping reveals two important aspects of the hydrodynamics in the Mississippian aquifer system. First, the flow of formation waters along the subcrop edge is oriented subparallel to the subcrop, rather than updip, in the majority of the map area within the Midale, Frobisher, and Alida Aquifers (Figure 4.8). This suggests that a large portion of the subcrop of these aquifers within the study area has extremely low permeability and causes flow to be redirected along the hydraulic boundary coincident with the subcrop. In the case of the Midale Aquifer, the hydraulic barrier at the subcrop is enhanced by the diagenetic occlusion of porosity due to extensive anhydritization and micritization of the carbonate beds (Kendall, 1975; Kent, 1987, Whittaker at al., 2004). Second, there appears to be little to no vertical component to the hydraulic gradient in the Mississippian aquifers in the vicinity of the Weyburn oilfield (Figure 4.9a,b). With the exception of the northeast area (Figure 4.1; Block 4), where there appears to be upward cross-formational flow from the lower Mississippian strata (Figure 4.9c), there appears to be very poor hydraulic communication between the Mississippian aquifers and the Mesozoic aquifers within the study area.

These two characteristics of the Mississippian hydrodynamics are positive aspects for $CO_2$ sequestration operations. However, a quantitative assessment of the trapping capacity of the caprock(s) in question, including the effects of hydrodynamics, is necessary for risk assessment for any $CO_2$ sequestration project.

The reservoir geometry at Weyburn is shown in Figure 4.14. The oil is trapped stratigraphically within the Midale Beds by a combination of reservoir top and floor seals formed by the Midale and Frobisher Evaporites, respectively. The Midale Evaporite is usually assumed to be the reservoir seal, but the updip limit of the Midale Beds beneath the unconformity is also part of the seal. Directly underlying the unconformity surface is a tight anhydritized, or diagenetically altered zone (Whittaker et al., 2004). The altered zone could be considered the ultimate sealing lithofacies at Weyburn before fluids reach the base of the Watrous Aquitard from the Midale Beds (Figure 4.14). This dense, anhydritized dolostone likely behaves similarly, hydraulically and geomechanically, to the massive anhydrite of the Midale Evaporite.

Li et al. (2005) report breakthrough capillary pressures[1] of approximately 30 MPa for the Midale Evaporite for a N2-brine fluid system. For a $CO_2$-brine system, due to much a lower interfacial tension, breakthrough capillary pressures for the Midale Evaporite were measured between 9-11 MPa. Li et al. (2005) state that the value for the interfacial tension of the Weyburn oil-brine fluid system could be several times higher than the interfacial tension of 21 mN $m^{-1}$ for the $CO_2$-brine system. Capillary pressure scaling relationship (Watts, 1987) cannot be used here to obtain a value for the breakthrough pressure to oil since the interfacial tension of the oil-brine system has not been measured, nor the contact angles between any of the fluids and the reservoir rock. However, based on qualitative information about the relative interfacial tensions, it is likely that the capillary breakthrough pressure of the Midale Evaporite for oil is higher than 11 MPa. These are extremely large values for the pressure differential needed between the immiscible fluid phases to have leakage of the seal. The height of the hydrocarbon column that would be needed to achieve this pressure differential is obtained from hydrostatics:

---

[1] Breakthrough pressure is the relevant quantity to describe capillary membrane leakage, where leakage occurs as a result of breaching a path of sufficiently large interconnected pore throats, rather than minimum entry or displacement capillary pressure, which occurs when the first (largest) pore throat is breached at the rock-fluid interface.

$$p_c = (\rho_w - \rho_o) g h_o \qquad (3.1)$$

where g is the gravitational acceleration and ho is the height of the oil column. For a capillary pressure of 9 MPa — the lower bound breakthrough pressure measured for the Midale Evaporite — and assuming average water and oil phase densities of 1050 kg $m^{-3}$ and 870 kg $m^{-3}$ at Weyburn, an oil column of over 5100 m would be needed to breach the capillary membrane formed by the Midale Evaporite. This is likely also true of the dense anhydritized zone below the unconformity.

In the case that such unrealistic oil columns are needed to cause capillary membrane failure, one might consider a hydraulic seal model (Watts, 1987). For a hydraulic seal, a cap rock with extremely high capillary entry pressures fails upon hydraulic fracturing, or wedging open of existing fractures upon exceeding a threshold stress value (Watts, 1987). This threshold stress, for an unfractured hydraulic seal, occurs when the pore fluid pressure exceeds the minimum effective horizontal stress ($S_{Hmin}$) on the caprock plus the tensile strength of the rock (Watts, 1987). After fractures have developed in the caprock, leakage will involve wedging open pre-existing fractures, so the tensile strength of the rock can be neglected.

The Weyburn caprock is almost undoubtedly fractured at present (Zhou et al., 2004). Fracturing within the reservoir itself is well-documented (McLellan et al., 1992; Beliveau et al., 1993). McLellan et al. (1992) report a lower bound estimate for the minimum horizontal in-situ stress gradient in the Weyburn-Midale field area of approximately 14 kPa/m. At a mean reservoir depth of 1450 m, this amounts to a $S_{Hmin}$ value of approximately 20.3 MPa. Pore pressures in the water zone of the Weyburn reservoir are between 14.4 to 14.9 MPa (Figure 4.9a). The additional fluid pressure exerted by the buoyant oil column is obtained by adding the value of the capillary pressure at the top of the oil column calculated from Equation (3.1). Considering a 200 m vertical oil column at Weyburn, the excess fluid pressure amounts to only 353 kPa. The total fluid pressure exerted at the top of the oil accumulation is therefore only between 14.8 and 15.2 MPa, which is insufficient to open pre-existing fractures in the cap rock. This means that the Weyburn reservoir is probably not filled to capacity, and that the trapping of the oil column can be explained solely by the hydraulic seal formed by the Midale Evaporite and the altered zone at the updip limit of the Midale Beds.

The traps along the Mississippian subcrop are probably not filled to capacity. It is possible however, that the observed oil columns reflect the caprock trapping capacities that existed during peak hydrodynamics when water pressures would have been significantly higher, possibly resulting in breaching of the top seals along the Mississippian subcrop. In this case, failure of the caprock and leakage into the overlying Ratcliffe Beds and the Watrous Aquitard could have occurred if the fluid pressures in the Midale Aquifer exceeded the value of $S_{Hmin}$. A calculation for the Midale Aquifer, analogous to what was presented in the previous section, revealed that water pressures at peak hydrodynamics could have easily exceeded the estimated value of $S_{Hmin}$ at the Weyburn reservoir depth (20.3 MPa).

The inferred influx of chemically-reducing fluids based on the paleomagnetic study (Cioppa, 2003) mentioned in the preceding section also suggests that the Mississippian subcrop was leaky during peak hydrodynamics in the Williston Basin.

Finally, the prospects for $CO_2$ storage in the oil pools along the Mississippian subcrop play appear to be good based on the above discussion, with the geological risk[2] seemingly quite low. In the case of the Weyburn $CO_2$ Project, an average $CO_2$ density of 630 kg $m^{-3}$ was calculated based on a tabulated solution for an equation of state by Altunin (1975), after the implementation by Pruess (2004), using the pressure and temperature conditions in the Weyburn oilfield. Assuming an average brine density of 1050 kg $m^{-3}$ and a minimum breakthrough pressure for $CO_2$ of 9 MPa (Li et al., 2005), the maximum $CO_2$ column height that could be trapped considering a capillary membrane model for the Weyburn caprock is well over 2000 m based on Equation (3.1).

However, a hydraulic seal model is more likely considering the presence of fractures in the caprock. Li et al. (2005) reported some low values (2-4 MPa) for gas breakthrough pressures in the Midale Evaporite samples which they attribute to microfractures in the caprock. Field-scale fractures could thus significantly lower the capillary sealing capacity of the Midale Evaporite to supercritical $CO_2$. A hydraulic seal model for the Weyburn caprock and analogues along the Canadian Mississippian subcrop may be a better (and more conservative) model.

## 4.6 CONCLUSIONS

This paper presented a detailed hydrodynamic study of the Weyburn $CO_2$ Project area in the Williston Basin in order to identify hydrodynamic phenomena which may be relevant to the long-term storage capacity of $CO_2$ for the purpose of carbon sequestration. The results were interpreted in a holistic perspective, adding to, and updating the current understanding of the present-day and paleo-hydrogeology of the Williston Basin.

The Weyburn CO2 Project area, located in the north-central Williston Basin, straddles the midline and discharge regions of the cross-basin topography-driven flow system. Consequently, formation water flows tend to be sub-horizontal, parallel to aquifer confining surfaces, in the majority of the study area with the tendency toward upward-directed cross-formational flow.

---

[2] The geological risk considers only the natural state of the system and does not consider engineering risks such as wellbore leakage and stress changes due to water/$CO_2$ injection operations (Rutqvist and Tsang, 2002) or due to long-term fluid production and reservoir pressure drawdown.

Potentiometric analysis indicates an overall similarity in the fluid potentials between individual aquifers of the two major Paleozoic aquifer systems. This is due to the large scale control of the topography-driven cross-basinal hydrodynamic drive on formation waters. Potentiometric surfaces in the Mesozoic aquifer system reflect a different flow system — particularly above the Jurassic aquifer — and suggest that modifications of the system boundaries control flow in the Mesozoic. A specific instance of this is the interpreted connection between the low-elevation outcrops of the Mesozoic rocks along the Manitoba escarpment and resultant large-scale underpressuring observed within the study area in the Mesozoic System.

The flow of brines in the Williston Basin is characterized by complex local variability of force regimes resulting in a range of scenarios from sluggish updip flow, driven by the potentiometric gradient, to strong density flows driving brines back down structural dip against the driving force imposed by the potentiometric gradient.

Increased paleo-topographic elevation differences across the Williston Basin during Late Cretaceous to early Tertiary time resulted in significantly higher hydraulic gradients than those observed in the present flow system. The Paleozoic brines were displaced from the central basin under correspondingly higher potentiometric gradients and the updip flow of the brines was sustained during this period of peak hydrodynamics. The transient relaxation of this effect results in the density flow reversals observed today.

Detailed analysis of Mississippian hydrodynamics shows that the Mississippian system is indeed highly variable and should not be lumped together as one aquifer for hydrogeological analysis. The Mississippian subcrop is a competent hydraulic barrier in the majority of the study area within the Alida, Frobisher, and Midale Aquifers. Cross-formational flow from the Mississippian system to the overlying Mesozoic aquifers occurs more readily in the Tilston and Souris Valley Aquifers, due in part to the absence of evaporitic lithofacies capping the sequences that form these lower Mississippian Beds.

It is likely that the Alida, Frobisher, and Midale Aquifer subcrops within the study area that today effectively prevent or retard the upward flow of formation waters from the Mississippian was leaky during peak hydrodynamics in the late Cretaceous-Early Tertiary. Leakage would have occurred by wedging open pre-existing fractures due to fluid pressures in excess of the minimum in-situ stress in the Weyburn field.

Storage of injected $CO_2$ in the oil reservoirs along the Mississippain subcrop appears to be feasible given the high capillary breakthrough pressures calculated for the sealing lithofacies at the location of the Weyburn Field (Li et al., 2005). However, given that a fracturing is known to exist in the Weyburn reservoir, and, by extension, the Midale caprock, a hydraulic seal model, where breakthrough pressures are governed by capillary leakage through fractures may be a better (and more conservative) model.

## 4.7 REFERENCES

Adams, J.J., Bachu, S., (2002) Equations of state for basin geofluids: algorithm review and intercomparison for brines. *Geofluids*, 2(4), pp.257-271.

Alkalali, A., Rostron, B.J., (2003) Basin-scale analysis of variable-density groundwater flow: Nisku Aquifer, Western Canadian Sedimentary Basin. *Journal of Geochemical Exploration*, 78-79, pp.313-316.

Altunin, V.V., (1975) *Thermophysical properties of carbon dioxide*. Publishing House of Standards, Moscow.

Bachu, S., (1995) Flow of variable-density formation water in deep sloping aquifers: review of methods of representation with case studies. *Journal of Hydrology*, 164, pp. 19-38.

Bachu, S., Hitchon, B., (1996) Regional-scale flow of formation waters in the Williston Basin. *AAPG Bulletin*, 80(2), pp. 248-264.

Bachu, S., (2001) Geological sequestration of carbon dioxide: Applicability and current issues. In: L.C. Gerhard, W.E. Harrison, B.M. Hanson (Eds.), *Geological Perspectives in Global Climate Change*, *AAPG Studies in Geology #47* (Ed. by L.C. Gerhard, W.E. Harrison, B.M. Hanson), American Association of Petroleum Geologists, Tulsa,OK. pp. 285-303.

Barson, D., Rakhit, K., Myers, T., Powers, N., Poletto, C., (1998) A new look at tilted oil/water contacts in the Williston Basin, *Saskatchewan Geological Society Special Publication No. 13*, pp. 226-228.

Batzle, M., Wang, Z., (1992) Seismic properties of pore fluids. *Geophysics*, 57, pp. 1396-1408.

Bekele, E.B., Rostron, B.J., Person, M.A., (2003) Fluid pressure implications of erosional unloading, basin hydrodynamics and glaciation in the Alberta Basin, Western Canada. *Journal of Geochemical Exploration*, pp. 78-79, 143-147.

Beliveau, D., Payne, D.A., Mundry, M., (1993) Waterflood and $CO_2$ flood of the fractured Midale field. *Journal of Petroleum Technology*, Sept. 1993, pp. 881-887.

Benn, A.A., Rostron, B.J., (1998) Regional hydrochemistry of Cambrian to Devonian aquifers in the Williston basin, Canada-USA. In: J.E. Christopher, C.F. Gilboy, D.F. Paterson, S.L. Bend (Eds.), *Eighth International Williston Basin Symposium*, *Special Publication*, pp. 238-246.

Chierici, G.L., (1994) *Principles of petroleum reservoir engineering*. Springer-Verlag, Berlin; New York. 430 p.

Christopher, J.E., (2003) Jura-Cretaceous Success Formation and Lower Mannville Group of Saskatchewan, Saskatchewan Industry and Resources, Regina, SK, 128 p.

Cioppa, M.T., (2003) Magnetic evidence for the nature and timing of fluid migration in the Watrous Formation, Williston Basin, Canada: a preliminary study. *Journal of Geochemical Exploration*, 78-79, pp. 349-354.

Davies, P.B., (1987) Modeling areal, variable-density, ground-water flow using equivalent freshwater head - analysis of potentially significant errors. In: *Solving Ground Water Problems With Models, 2*, National Water Well Association, Denver, Colorado. pp. 888-903.

DeMis, W.D., (1995) Effect of cross-basinal hydrodynamic flow on oil accumulations and oil migration history of the Bakken-Madison petroleum system Wiliston Basin, North America. In: *Seventh International Williston Basin Symposium* (Ed. by L.D.V. Hunter, R.A. Schalla), Montana Geological Society, Billings, Montana. pp. 291-301.

Dickinson, W.R., Snyder, W.S., (1978) Plate tectonics of the Laramide Orogeny. In: V. Mathews (Ed.), *Laramide folding associated with basement block faulting, Geological Society of America Memoir*, pp. 355-366.

Downey, J.S., (1984a) Hydrodynamics of the Williston Basin in the Northern Great Plains. In: G. Jorgensen Donald, C. Signor Donald (Eds.), *Geohydrology of the Dakota Aquifer*. Natl. Water Well Assoc., Worthington, OH, United States. pp. 92-98.

Downey, J.S., (1984b) Geohydrology of the Madison and associated aquifers in parts of Montana, North Dakota, South Dakota, and Wyoming. *U.S. Geological Survey Professional Paper 1273-G*, 1273-G, 47 p.

Downey, J.S., (1986) Geohydrology of bedrock aquifers in the Northern Great Plains in parts of Montana, North Dakota, South Dakota, and Wyoming. *U.S. Geological Survey Professional Paper 1402-E*, 87 p.

Downey, J.S., Busby, J.F., Dinwiddie, G.A., (1987) Regional aquifers and petroleum in the Williston Basin region of the United States. In: *1987 Symposium of the Rocky Mountain Association of Geologists* (Ed. by M. Longman), pp. 299-312.

Garven, G., (1995) Continental-scale groundwater flow and geologic processes. *Annual Review of Earth and Planetary Sciences*, 23, pp. 89-117.

Haidl, F., Kreis, L.K., Dancsok, E.F.R., (1996) New oil discoveries in Ordovician Red River Strata, southeastern Saskatchewan. In: *Summary of Investigations 1996*, Saskatchewan Industry and Resources, Regina, SK, Canada. pp. 136-144.

Hannon, N., (1987) Subsurface water flow patterns in the Canadian sector of the Williston Basin. In: *1987 Symposium of the Rocky Mountain Association of Geologists*, pp. 313-321.

Horner, D.R., (1951) Pressure build-up in wells. *Proceeding Third World Petroleum Congress*, Section 2, pp. 503-521.

IPCC, (2005) Special report on carbon dioxide capture and storage prepared by working group III of the Intergovernmental Panel on Climate Change [Metz, B., O. Davidson, H. C. de Coninck, M. Loos, and L. A. Meyer (eds.)]. Cambridge University Press, Cambridge, United Kingdom and NewYork, NY, USA, 442 p.

Ingebritsen, S.E., Sanford, W.E., (1998) *Groundwater in geologic processes*. Cambridge University Press. 341 p.

Kendall, (1975) Anhydrite replacements of gypsum (satin-spar) veins in the Mississippian caprocks of southeastern Saskatchewan. *Can. J. Earth Science*, 12, pp. 1190-1195.

Kent, D.M., (1987) Mississippian Facies, Depositional history, and oil occurrences in Williston Basin, Manitoba and Saskatchewan. In: *1987 Symposium of the Rocky Mountain Association of Geologists*, pp. 157-170.

Kent, D.M., Thomas, P., Heck, T., (2004) Geological mapping of the Mississippian strata in southeastern Saskatchewan, northwestern North Dakota, and northeastern Montana. In: *Summary of Investigations 2004, 1*, Saskatchewan Industry and Resources, Regina, SK, Canada. 10 p.

Khan, D.K., Rostron, B.J., (2004) Regional hydrogeological investigation around the IEA Weyburn $CO_2$ monitoring and storage project site. In: *Proceeding of the 7th International Conference on Greenhouse Gas Control Technologies* (GHGT-7), Sept. 5-9, 2004, Vancouver, Canada, v.I, Volume 1: Peer-Reviewed Papers and Plenary Sessions, Elsevier, UK. pp. 741-750.

Li, S., Dong, M., Li, Z., Huang, S., Qing, H., Nickel, E., (2005) Gas breakthrough pressure for hydrocarbon reservoir seal rocks: implications for the security of long-term $CO_2$ storage in the Weyburn field. *Geofluids*, 5(4), pp. 326-334.

Lisenbee, A.L., DeWitt, E., (1993) Laramide evolution of the Black Hills uplift. In: S. A.W., J.R. Steidtmann, S.M. Roberts (Eds.), *Geology of Wyoming, Geological Survey of Wyoming Memoir*, pp. 374-412.

McLellan, P.J., Lawrence, K.H., Cormier, K.W., (1992) A multiple-zone acid stimulation treatment of a horizontal well, Midale, Saskatchewan. *Journal of Canadian Petroleum Technology*, 31, pp. 71-82.

Minerals Diversified Services, Inc., (2005) MDS Williston Basin Map. Minerals Diversified Services, Inc., Bismarck ND.

Neuzil, C.E., (1995) Abnormal pressures as hydrodynamic phenomena. *American Journal of Science*, 295, pp. 742-786.

Olson, C.C., (1967) Technical advancement four decades of D.S.T. In: *8th Ann. SPWLA Logging Symposium*, Denver. pp. 1-11.

Preston, C., Monea, M., Jazrawi, W., Brown, K., Whittaker, S., White, D., Law, D., Chalaturnyk, R., Rostron, B., (2005) IEA GHG Weyburn $CO_2$ monitoring and storage project. *Fuel Processing Technology*, 86, pp. 1547-1568.

Pruess, K., (2004) Numerical simulation of $CO_2$ leakage from a geologic disposal reservoir, including transitions from super- to subcritical conditions, and boiling of liquid $CO_2$. *SPE Journal*, 9(2), pp. 237-248.

Rostron, B.J., (1994) A new method for culling pressure data used in hydrodynamic studies. In: *AAPG annual convention, 1994, Annual Meeting Abstracts - American Association of Petroleum Geologists and Society of Economic Paleontologists and Mineralogists*, pp. 247.

Rowe, A.M., Chou, J.C.M., (1970) Pressure–volume–temperature–concentration relation of aqueous NaCl solutions. *Journal of Chemical Engineering Data*, 15, pp. 61-66.

Rutqvist, J., Tsang, C., (2002) A study of caprock hydromechanical changes associated with CO2-injection into a brine formation. *Environmental Geology*, 42, pp. 296-305.

Socolow, R.H., (2005) Can we bury global warming? In: *Scientific American, 293*, pp. 49-55.

Tóth, J., (1978) Gravity-induced cross-formational flow of formation fluids, Red Earth region, Alberta, Canada: Analysis, patterns, evolution. *Water Resources Research*, 14(5), pp. 805-843.

Tóth, J., Millar, R.F., (1983) Possible effects of erosional changes of the topographic relief on pore pressures at depth. *Water Resources Research*, 19(6), pp. 1585-1597.

Tóth, J., Corbet, T.F., (1986) Post-Paleocene evolution of regional groundwater flow-systems and their relation to petroleum accumulations, Taber area, southern Alberta, Canada. *Bulletin of Canadian Petroleum Geology*, 34(3), pp. 339-363.

Tóth, J., (1995) Hydraulic continuity in large sedimentary basins. *Hydrogeology Journal*, 3(4), pp. 4-16.

Tóth, J., Almasi, I., (2001) Interpretation of observed fluid potential patterns in a deep sedimentary basin under tectonic compression: Hungarian Great Plain, Pannonian Basin. *Geofluids*, 1, pp. 11-36.

Watts, N.L., (1987) Theoretical aspects of cap-rock and fault seals for single- and two-phase hydrocarbon columns. *Marine and Petroleum Geology*, 4, pp. 274-307.

Whittaker, S., Rostron, B.J., Khan, D., Hajnal, Z., Qing, H., Penner, L., Maathuis, H., Goussev, S., (2004) IEA GHG Weyburn $CO_2$ monitoring & storage project summary report 2000-2004. In: *Seventh International Conference on Greenhouse Gas Control Technologies, 1* (Ed. M. Wilson, M. Monea), Petroleum Technology Research Centre. pp. 15-69.

Zhou, W., Stenhouse, M., Sheppard, M., Walton, F., (2004) IEA GHG Weyburn $CO_2$ monitoring & storage project summary report 2000-2004. In: *Seventh International Conference on Greenhouse Gas Control Technologies, 1* (Ed. M. Wilson, M. Monea), Petroleum Technology Research Centre. pp. 211-268.

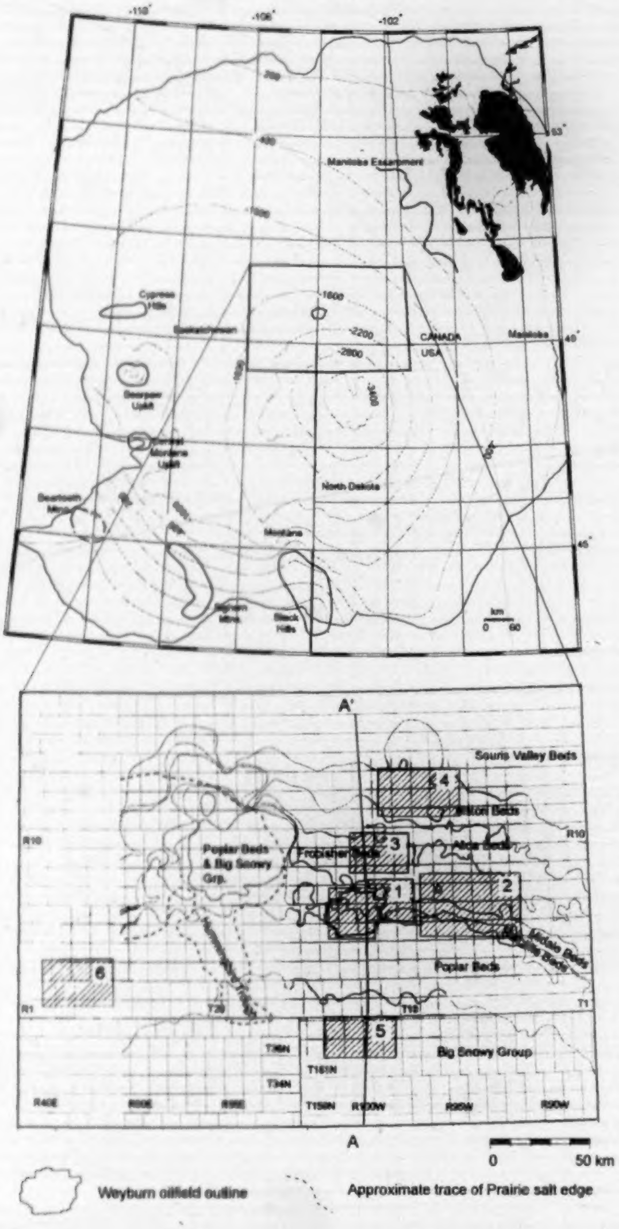
-110°
-106°
-102°
53°
49°
45°
Manitoba Escarpment
Cypress Hills
Saskatchewan
CANADA
USA
Manitoba
Sweetgrass Uplift
Central Montana Uplift
Beartooth Mtns.
North Dakota
Montana
Bighorn Mtns.
Black Hills
km
0 60
-1600
-2200
-2800
-3400
A'
Souris Valley Beds
4
Tilston Beds
Alida Beds
Frobisher Beds
3
Poplar Beds & Big Snowy Grp.
1
2
Midale Beds
Ratcliffe Beds
Poplar Beds
6
5
Big Snowy Group
R10
R1
T1
T20
T36N
T161N
T34N
T159N
R40E
R100W
R90W
A
0
50 km
Weyburn oilfield outline
Approximate trace of Prairie salt edge

Figure 4.1. Composite reference map of study area set within the Williston Basin. Large area shows overall basin structure (structure contours on top of Ordovician Red River Formation) and major tectonic elements. Inset shows Weyburn Project map area and the slightly smaller geological characterization area (shaded area) including Mississippian subcrop map (after Kent et al., 2004). Numbered blocks (hatched) are locations of data used to construct pressure-depth profiles.

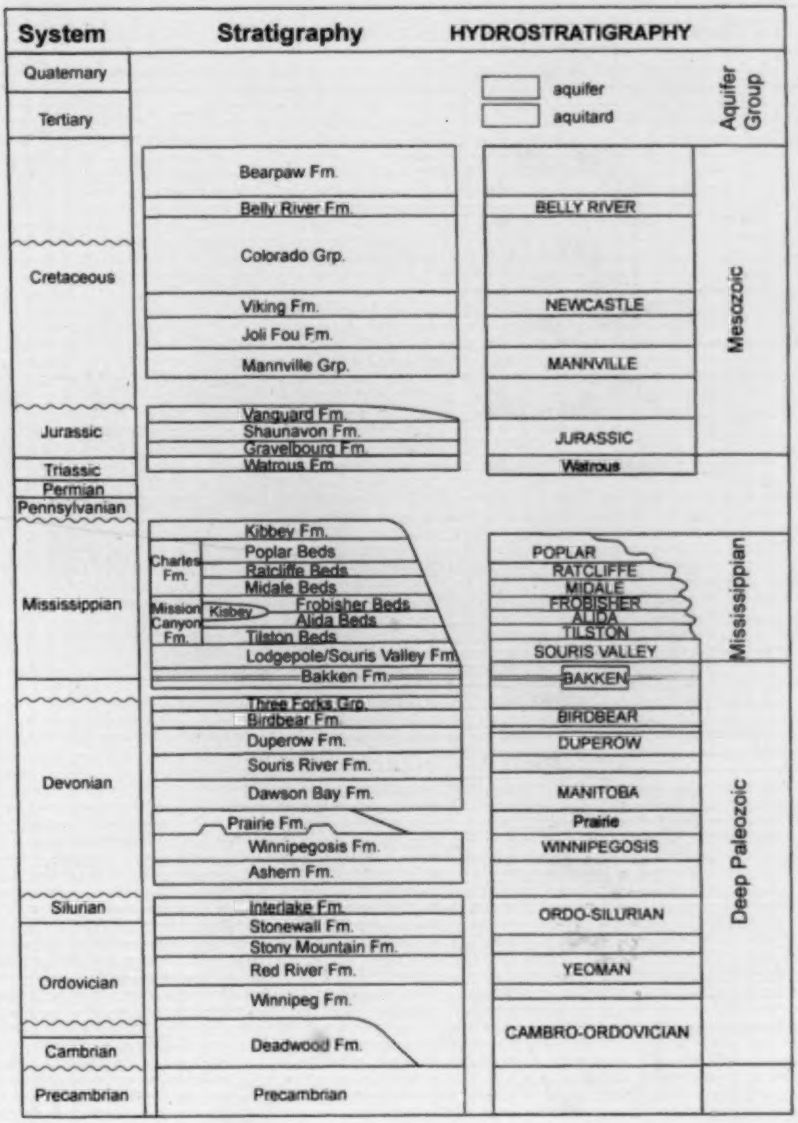
System
Stratigraphy
HYDROSTRATIGRAPHY
Quaternary
Tertiary
aquifer
aquitard
Aquifer Group
Bearpaw Fm.
Belly River Fm.
BELLY RIVER
Cretaceous
Colorado Grp.
Viking Fm.
NEWCASTLE
Joli Fou Fm.
Mannville Grp.
MANNVILLE
Mesozoic
Jurassic
Vanguard Fm.
Shaunavon Fm.
Gravelbourg Fm.
JURASSIC
Triassic
Watrous Fm.
Watrous
Permian
Pennsylvanian
Kibbey Fm.
Charles Fm.
Poplar Beds
Ratcliffe Beds
Midale Beds
Mississippian
Mission Canyon Fm.
Kisbey
Frobisher Beds
Alida Beds
Tilston Beds
Lodgepole/Souris Valley Fm
POPLAR
RATCLIFFE
MIDALE
FROBISHER
ALIDA
TILSTON
SOURIS VALLEY
Mississippian
Bakken Fm.
BAKKEN
Three Forks Grp.
Birdbear Fm.
BIRDBEAR
Duperow Fm.
DUPEROW
Devonian
Souris River Fm.
Dawson Bay Fm.
MANITOBA
Prairie Fm.
Prairie
Winnipegosis Fm.
WINNIPEGOSIS
Ashern Fm.
Deep Paleozoic
Silurian
Interlake Fm.
ORDO-SILURIAN
Stonewall Fm.
Stony Mountain Fm.
Ordovician
Red River Fm.
YEOMAN
Winnipeg Fm.
Cambrian
Deadwood Fm.
CAMBRO-ORDOVICIAN
Precambrian
Precambrian

Figure 4.2. Williston Basin stratigraphy and hydrostratigraphic framework adopted for the Weyburn Project geological model (Whittaker et al., 2004).

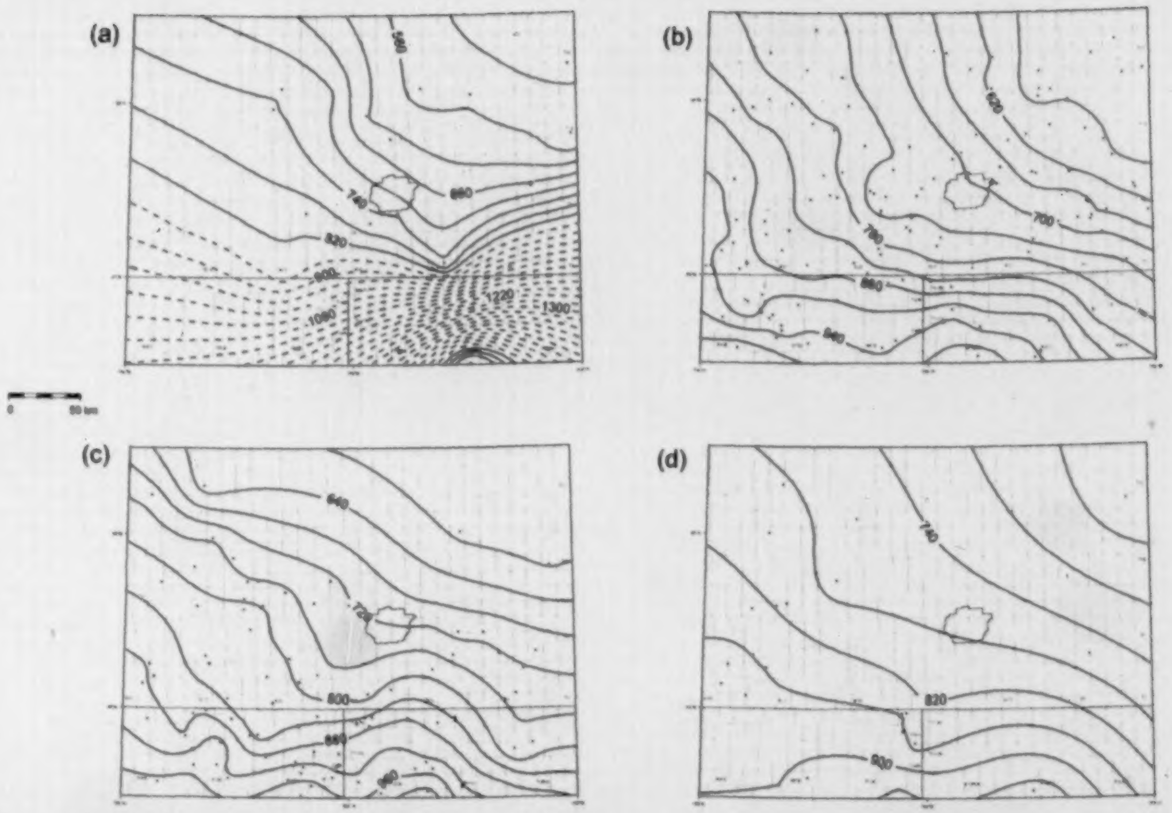
(a)
580
660
740
820
900
1060
1220
1300
(b)
620
700
780
860
940
0
50 km
(c)
640
720
800
880
960
(d)
740
820
900

Figure 4.3. Potentiometric surface maps for selected Deep Paleozoic aquifers: a) Bakken, b) Birdbear, c) Duperow, and d) Manitoba. Crosses indicate locations of culled DST pressure data.

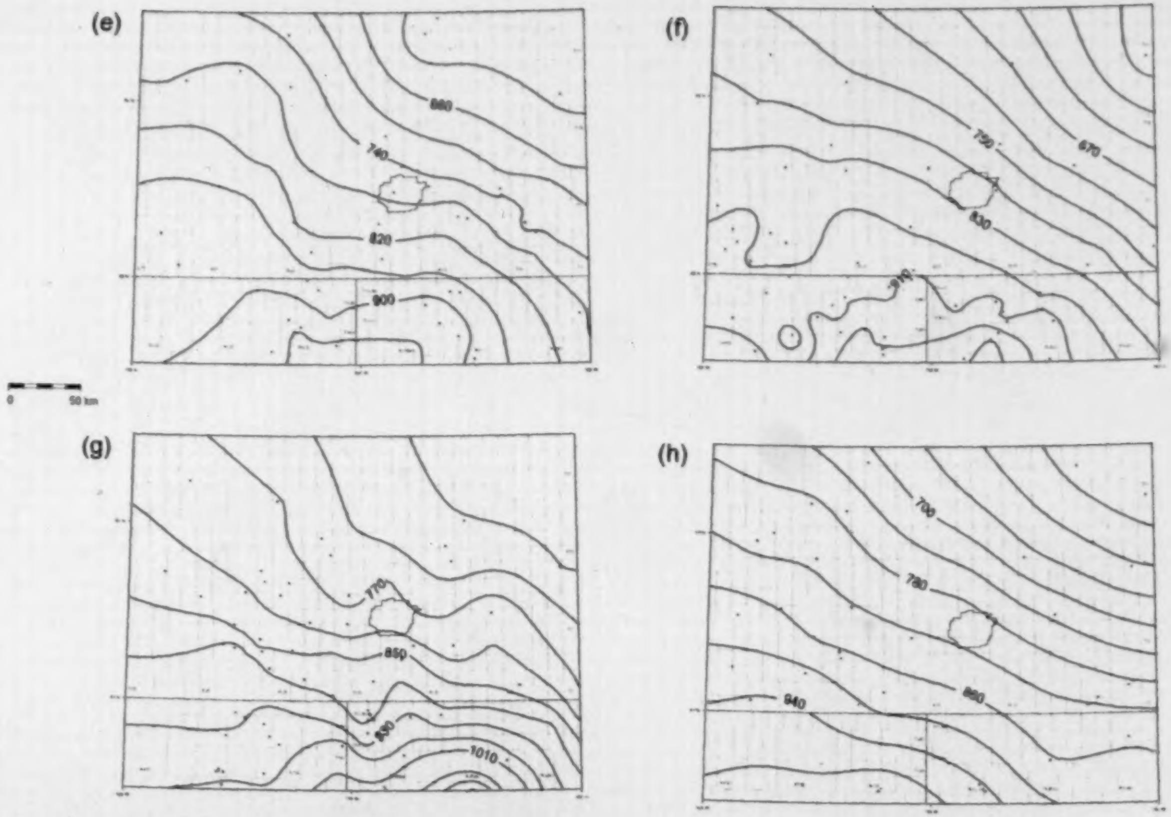
(e)
660
740
820
900
(f)
750
670
830
910
0
50 km
(g)
770
850
930
1010
(h)
700
780
860
940

Figure 4.3. (continued) Potentiometric surface maps for selected Deep Paleozoic aquifers: e) Winnipegosis, f) Ordo-Silurian, g) Yeoman, and h) Cambro-Ordovician. Crosses indicate locations of culled DST pressure data.

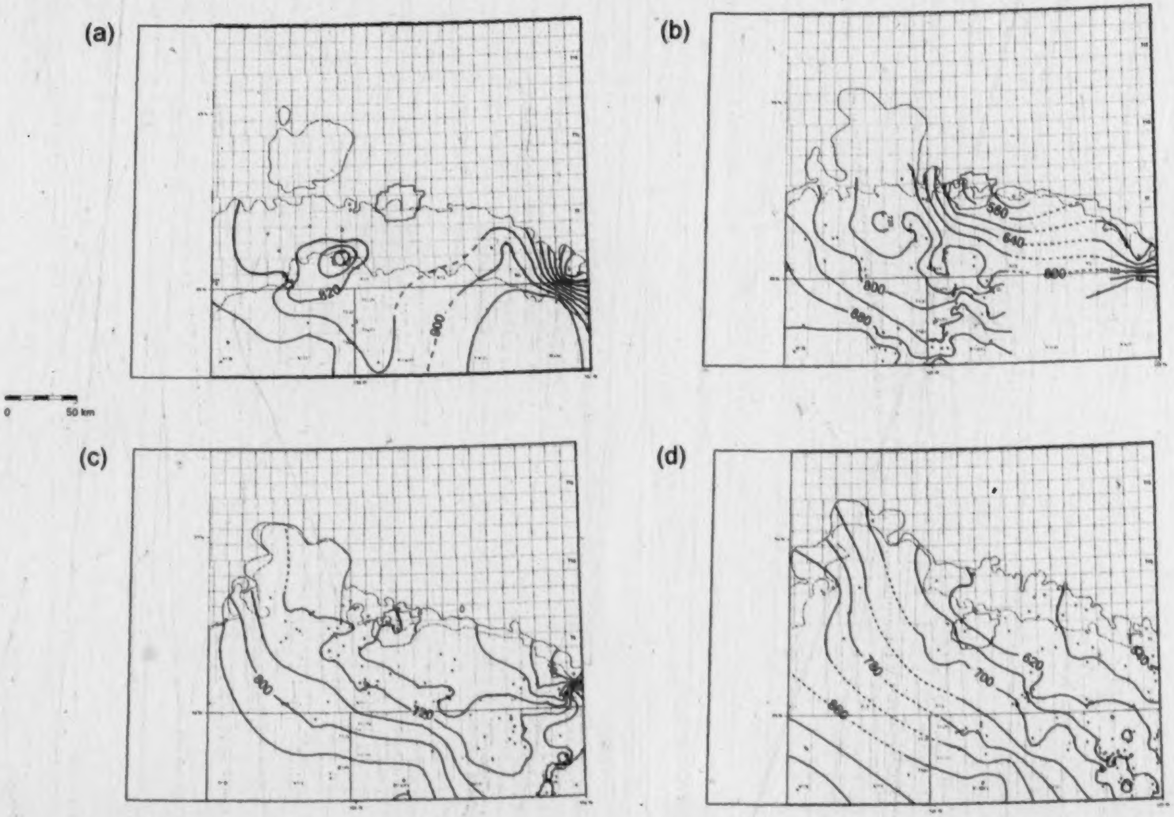
(a)
820
900
(b)
560
640
800
880
0
50 km
(c)
800
720
(d)
600
620
700
780
860

Figure 4.4. Potentiometric surface maps for selected Mississippian aquifers: a) Poplar, b) Ratcliffe, c) Midale, and d) Frobisher. Crosses indicate locations of culled DST pressure data.

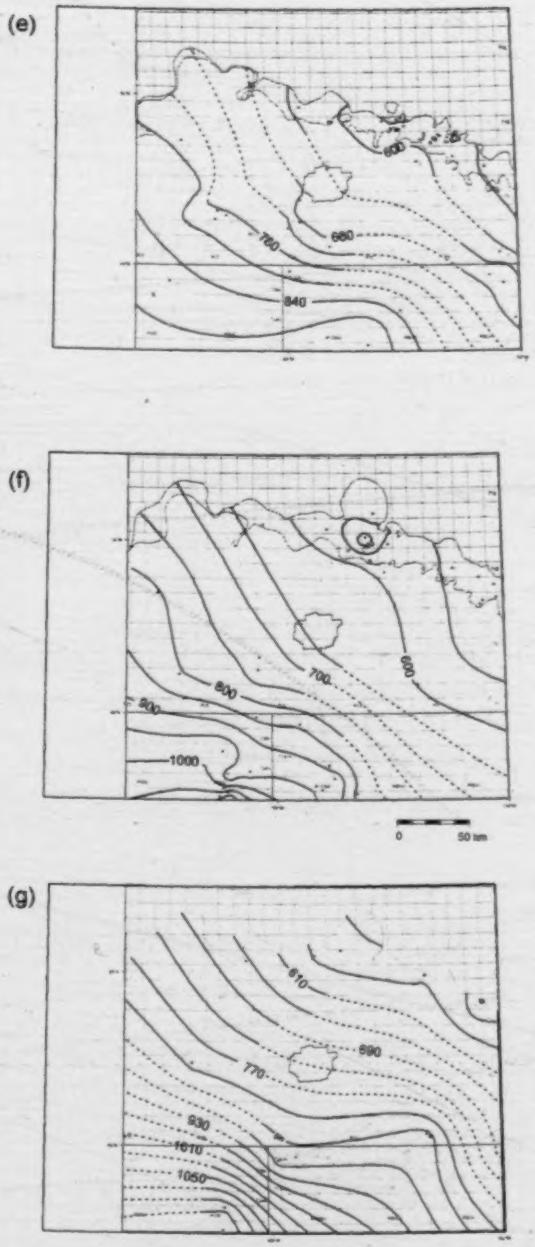
(e)
600
680
760
840
(f)
600
700
800
900
1000
0
50 km
(g)
610
690
770
930
1010
1050

Figure 4.4. (continued) Potentiometric surface maps for selected Mississippian aquifers: e) Alida, f) Tilston, and g) Souris Valley.

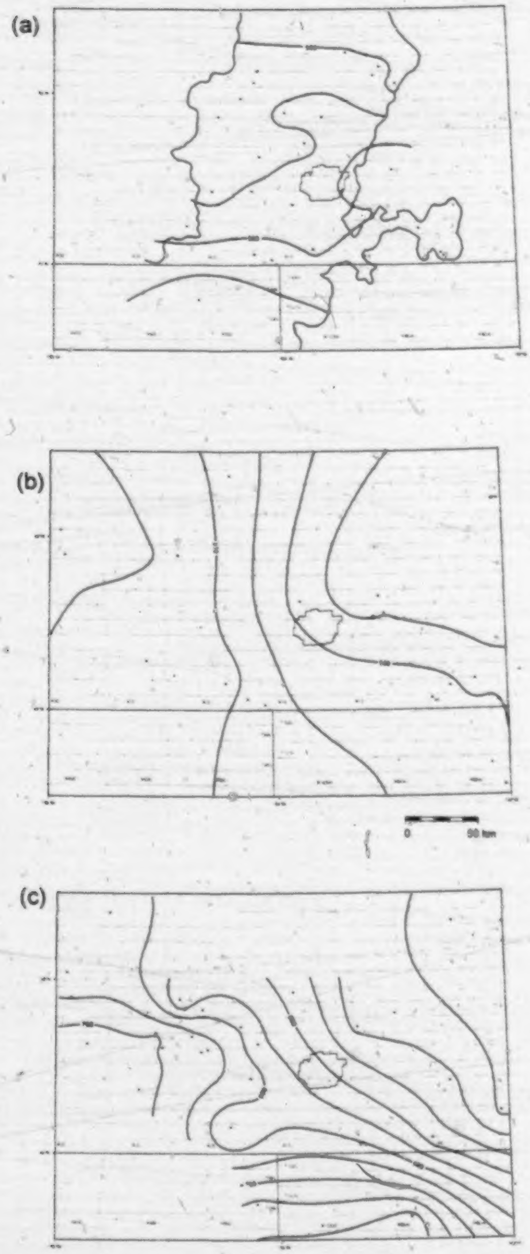

Figure 4.5. Potentiometric surface maps for selected Mesozoic aquifers: a) Newcastle (black line indicates limit of permeable Newcastle sand body), b) Mannville, and c) Jurassic.

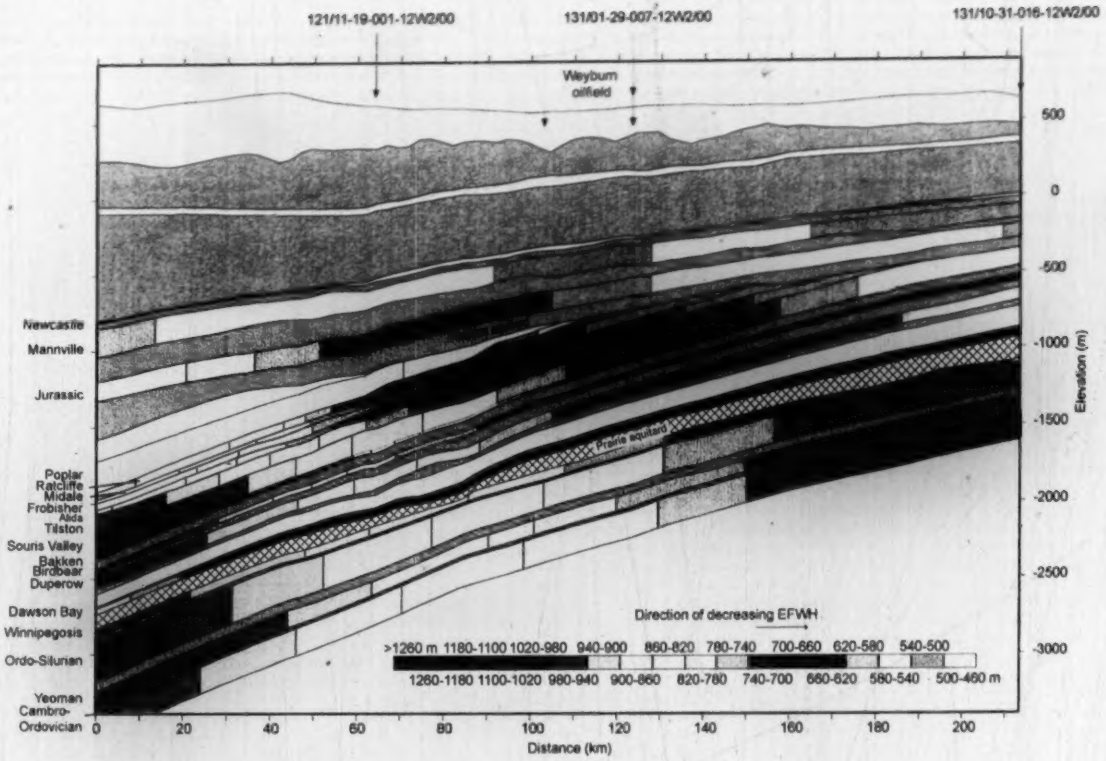
121/11-19-001-12W2/00
131/01-29-007-12W2/00
131/10-31-016-12W2/00
Weyburn oilfield
Newcastle
Mannville
Jurassic
Poplar
Ratcliffe
Midale
Frobisher
Alida
Tilston
Souris Valley
Bakken
Birdbear
Duperow
Dawson Bay
Winnipegosis
Ordo-Silurian
Yeoman
Cambro-Ordovician
Prairie aquitard
Direction of decreasing EFWH
>1260 m 1180-1100 1020-980 940-900 860-820 780-740 700-660 620-580 540-500
1260-1180 1100-1020 980-940 900-860 820-780 740-700 660-620 580-540 500-460 m
0
20
40
60
80
100
120
140
160
180
200
Distance (km)
500
0
-500
-1000
-1500
-2000
-2500
-3000
Elevation (m)

Figure 4.6. Hydraulic cross section A-A' (Refer to Figure 4.1 for line of section). Aquitards are shaded or cross-hatched. Well UWI numbers along the top indicate the locations of wells used to tie the section.

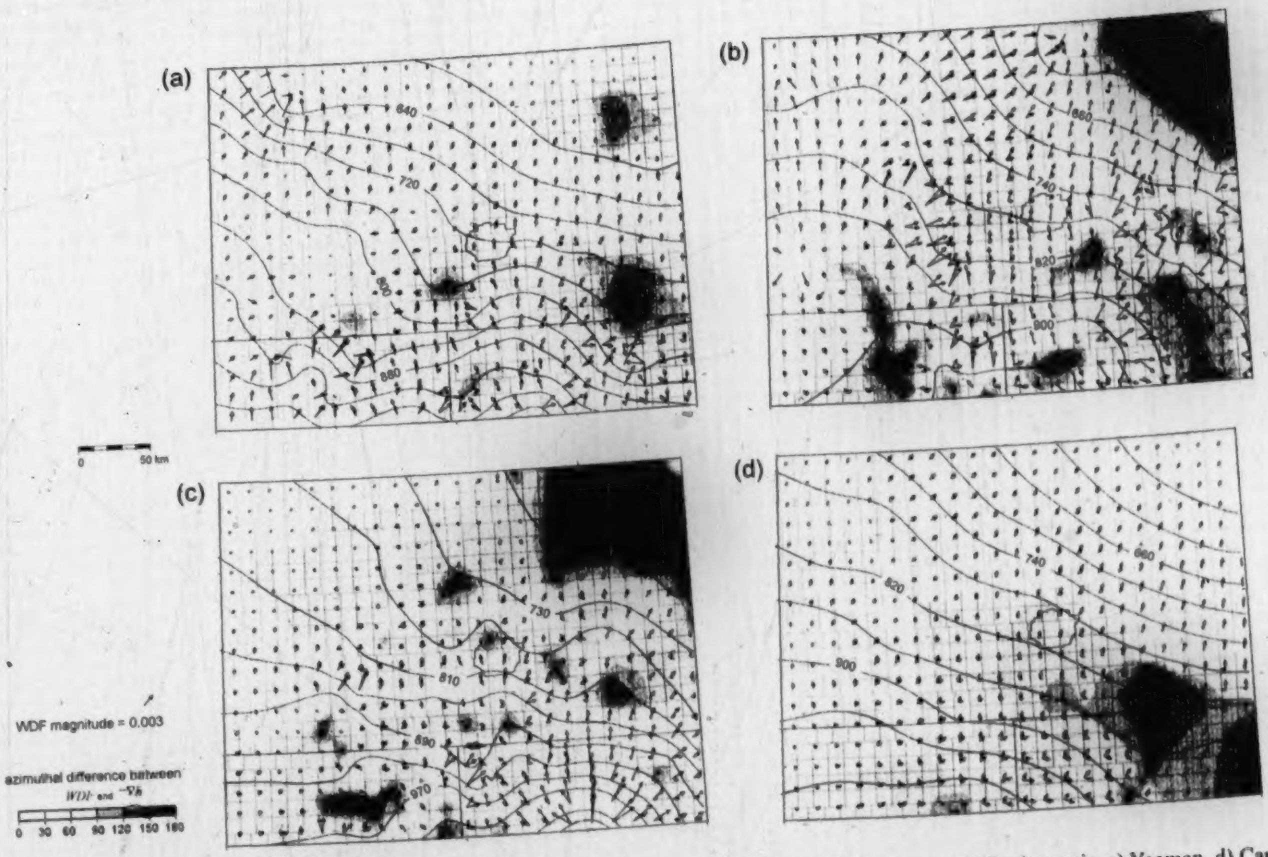
(a)
640
720
800
880
(b)
660
740
820
900
(c)
730
810
890
970
(d)
660
740
820
900
0
50 km
WDF magnitude = 0.003
azimuthal difference between WDF and −∇h
0 30 60 90 120 150 180

Figure 4.7. Water Driving Force (WDF) vector maps for selected Deep Paleozoic aquifers: a) Duperow, b)Winnipegosis, c) Yeoman, d) Cambro-Ordovivian. *-grad h* indicated by grey-coloured vectors and density-corrected WDF vectors are black. Vector scale is linear.

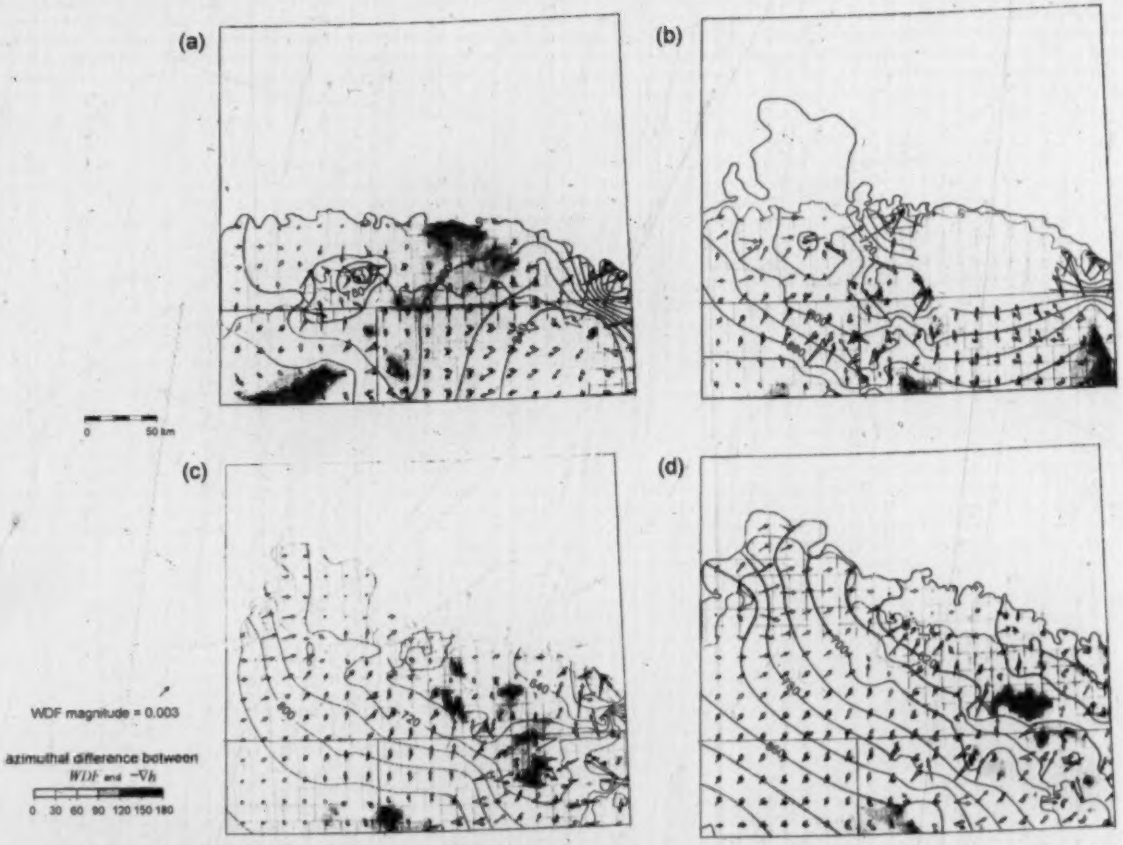
(a)
(b)
(c)
(d)
0
50 km
WDF magnitude = 0.003
azimuthal difference between
$WDF$ and $-\nabla h$
0 30 60 90 120 150 180

Figure 4.8. Water driving force (WDF) vector maps for selected Mississippian aquifers: a) Poplar, b) Ratcliffe, c) Midale, d) Frobisher. *-grad h* indicated by grey-coloured vectors and density-corrected WDF vectors are black. Vector scale is linear.

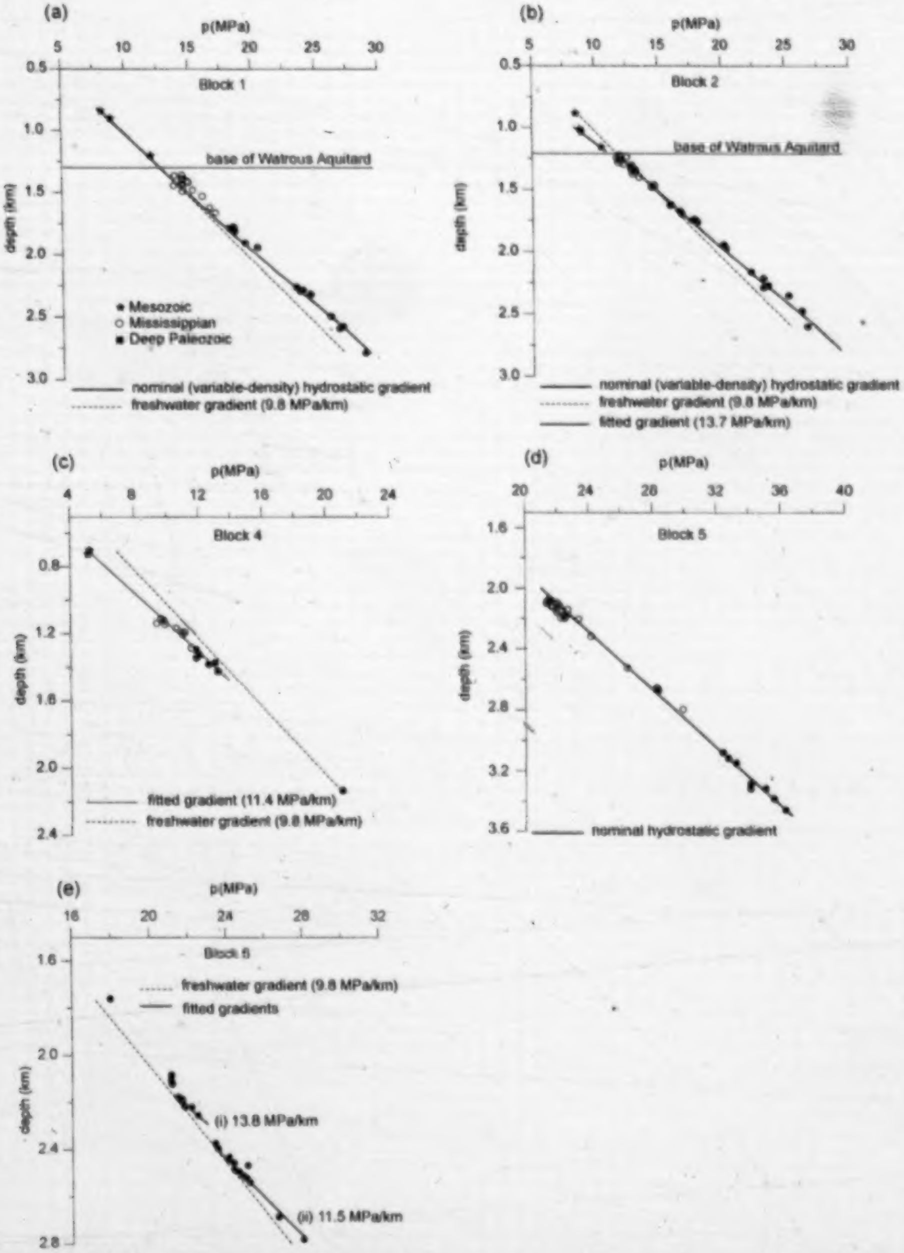

Figure 4.9. Pressure vs. depth profiles (areas shown in Figure 3.1): a) Block 1; pressure data fall along the nominal hydrostatic gradient despite some overpressures observed in the upper Mississippian data; b) Block 2 ; pressure data fall along the nominal hydrostatic gradient except data from the Mesozoic Jurassic and Mannville aquifers, which are underpressured and fit a superhydrostatic gradient; c) Block 4; underpressuring and is observed between the Deep Paleozoic to Mesozoic aquifers with pressure data falling along a common superhydrostatic gradient; d) Block 5; pressure data fall along the nominal hydrostatic gradient; and e) Block 6; data from the Deep Paleozoic aquifers plot along superhydrostatic pressure gradients.

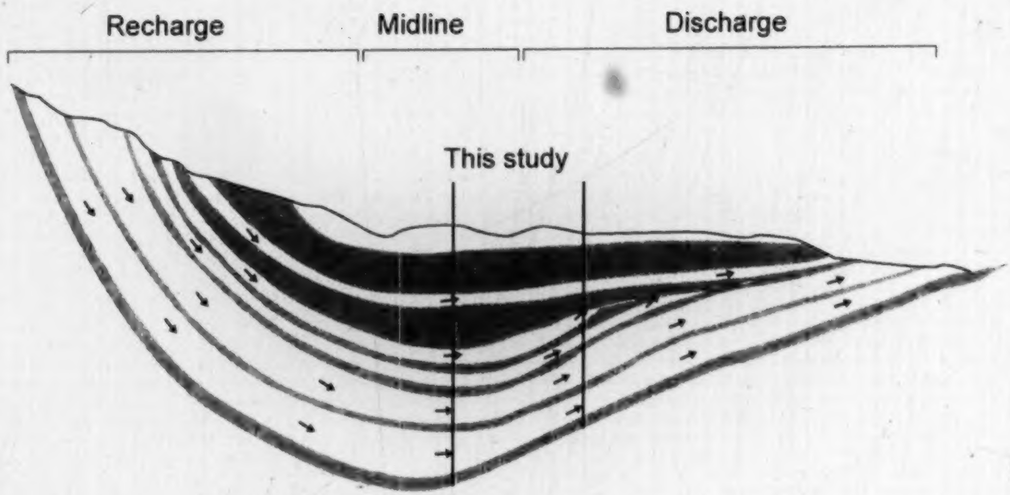
Recharge
Midline
Discharge
This study

Figure 4.10. Schematic hydraulic cross section of the Williston Basin topography-driven flow system showing the position of the study area within the context of regional recharge (flow away from the land surface), midline (horizontal flow), and discharge (flow toward from the land surface) regions. (Modified after DeMis, 1995)

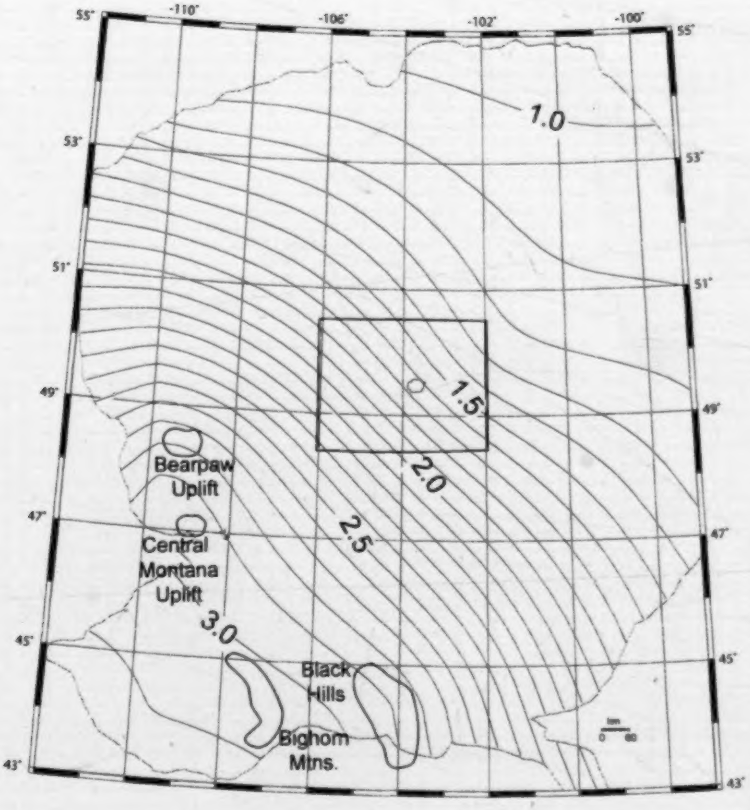
55°
-110°
-106°
-102°
-100°
55°
53°
53°
51°
51°
49°
49°
47°
47°
45°
45°
43°
43°
1.0
1.5
2.0
2.5
3.0
Bearpaw
Uplift
Central
Montana
Uplift
Black
Hills
Bighorn
Mtns.
km
0 80

Figure 4.11. Contour map of the surface used to amplify the potentiometric gradient in the Winnipegosis aquifer to simulate the effects of paleo-topography. Numeric values indicate the multiplication factor applied to the potentiometric surface maps. The operation was performed only within the study area (outlined at centre).

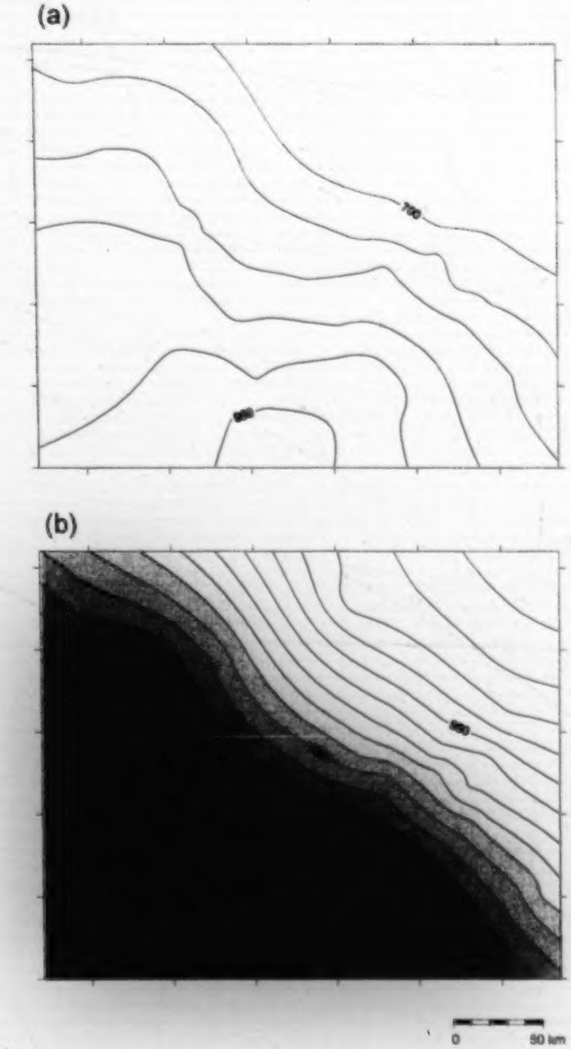

Figure 4.12. (a) Potentiometric map of the Winnipegosis Aquifer. (b) Simulated amplified potentiometric surface representing paleo-potentiometric surface during peak hydrodynamics.

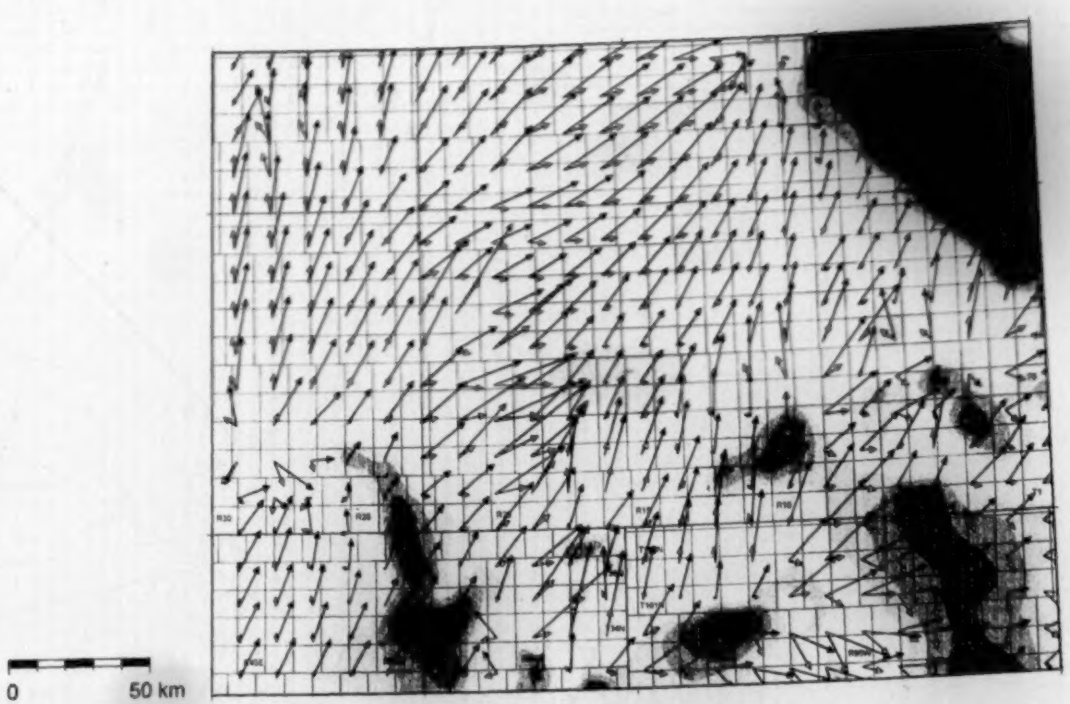

Figure 4.13. Simulated paleo-formation water driving force map of the Winnipegosis Aquifer. Simulated paleo-WDF vectors (black) compared with present-day WDF field (grey). Shading may be interpreted as relative degree of gravitational instability of the brines in the present-day flow system. Note that in all of these areas, brines would have been flowing updip to the northeast under increased paleo-driving forces – in areas where this does not appear to be the case, it is reasonable to dismiss this as uncertainty not addressed in the modelling.

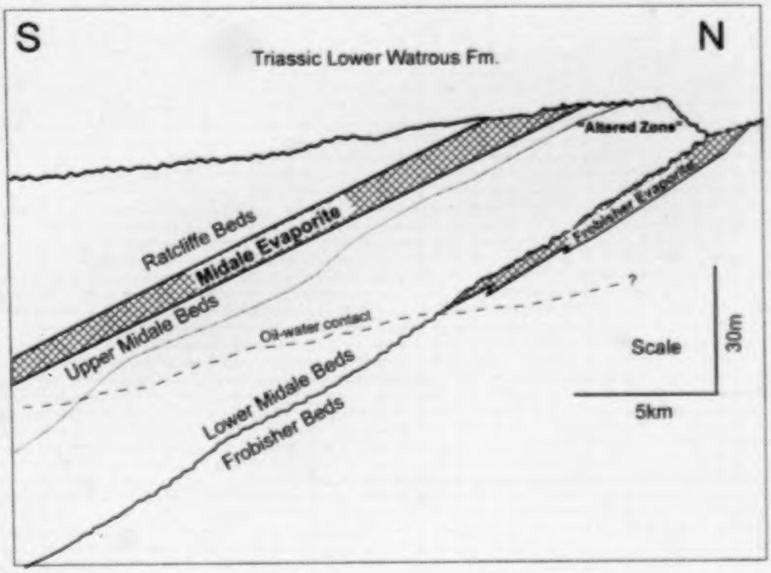
S
N
Triassic Lower Watrous Fm.
"Altered Zone"
Ratcliffe Beds
Midale Evaporite
Upper Midale Beds
Frobisher Evaporite
?
Oil-water contact
Lower Midale Beds
Frobisher Beds
Scale
30m
5km

Figure 4.14. Schematic dip-oriented cross-section of Weyburn reservoir geometry (modified from Whittaker et al., 2004).

# 5.0 APPROXIMATE SENSITIVITY COEFFICIENTS FOR INTEGRATING HYDRAULIC HEAD DATA INTO GEOLOGICAL MODELS

## 5.1 INTRODUCTION

The problem of integrating measurements of hydraulic head into geological models for aquifer characterization (the groundwater inverse problem) remains an important area despite decades of research. Techniques for solving the inverse problem in hydrogeology have been developed by (Emsellem and de Marsily, 1971; Cooley, 1977; 1979; 1982; 1983; Kitanidis and Vomvoris, 1983; Dagan, 1985; Townley and Wilson, 1985; Carrera and Neuman, 1986; Loaiciga and Marino, 1986; 1987; Woodbury et al., 1987; Dagan and Rubin, 1988; Ahmed and de Marsily, 1989; Gutjahr and Wilson, 1989; Sun and Yeh, 1992; RamaRao et al., 1995; Sun et al., 1995; Yeh and Zhang, 1996; Gomez-Hernandez et al., 1997; Medina and Carrera, 2003) among numerous others. The hydraulic head data represent measurements of the response of a flow system to perturbations imposed on that system (i.e., whether the natural system or the flow model representing it). The perturbations may be imposed by stresses such as pumping and injection or by the (possibly changing) nature of the boundary conditions of the flow system. Integrating hydraulic head data into the process of modeling the geological heterogeneity of an aquifer requires solving an inverse problem, where the solution consists of model parameter estimates that are constrained by measurements of the system response. The ultimate goal of inverse flow modeling in this context is to infer — or attempt to identify important features of — the distributed parameter field representing the permeability of a heterogeneous aquifer.

A major challenge of inverse modeling is related to non-uniqueness of the solution — where the solution is some parameter set that reproduces the measured response — and instabilities associated with this non-uniqueness, or more generally, with an ill-posed mathematical problem (Neuman, 1973, Deitrich et al, 1989; Carrera and Neuman, 1986a; Yeh, 1986; McLaughlin and Townley, 1996; Carrera et al., 2005). Early research tended to focus on understanding and dealing with these difficulties and is summarized in reviews by Carrera and Neuman, (1986a) Yeh (1986); Ginn and Cushman (1990), McLaughlin and Townley (1996); and de Marsily et al. (2000), among others. More recent research has focused on technological advancements, or ways to make the computations more efficient (e.g., Wen et al., 2002; Medina and Carrera, 2003).

At the heart of inverse modeling is the identification of sensitive parameters, that is, the parameters that most significantly affect the model response. An assessment of the sensitivity of model response with respect to the model parameters is required in order to make educated updates to the model for an efficient calibration. In addition, the modeler learns a great deal about the model structure from parameter sensitivity, and may use the information gleaned from a sensitivity analysis to assess the reliability of the model and the parameter estimates.

The scope of this chapter is the sensitivity of hydraulic head in an aquifer model to the distributed parameter field representing the aquifer permeability. Despite an extensive body of literature on obtaining sensitivity coefficients as a key aspect to solving inverse flow problems (e.g., Dogru and Seinfeld, 1981; Sykes et al., 1985; Carrera et al., 1990; 2005; Oliver, 1994, Chu et al., 1995, Carrera et al., 1997; Landa et al., 1997; Medina and Carrera, 2003), little attention has been paid to their structure in relation to the permeability field and the flow model. Thus, the objective of this study is to identify the controls on the spatial structure of sensitivity coefficients of head to the permeability field. Specifically: How can one predict which cells are sensitive with respect to a given calibration data location? A related question we address is: How can we obtain a fast and adequate approximation of the sensitivity matrix for flow model calibration or inversion problems?

### 5.1.2 Background: Sensitivity Coefficients

Sensitivity coefficients are the partial derivatives of the model response at a specified location with respect to a parameter change. Here we consider the sensitivity of hydraulic head at measurement location $j$ to a change in the logarithm of permeability at model cell $i$. The complete matrix of sensitivities, otherwise called the Jacobian matrix, may be expressed as:

$$\mathbf{J} = \{s_{i,j}\} = \frac{\partial h_j}{\partial \ln(k)_i}, \qquad i = 1,\ldots N; j = 1,\ldots m \tag{5.1}$$

where $h$ is hydraulic head at a specific calibration data location, which may be a function of time, and $k$ is absolute permeability at a model cell.

Automated calibration procedures rely on sensitivity coefficients to guide the calibration of the model parameter estimates. Perhaps the most common approach is to use iterative or indirect procedures, recasting the inverse problem as a parameter optimization problem. Sensitivity coefficients are used to determine the search direction within the parameter space that results in an improved match between the calibration (dynamic) data and the model response (Carrera et al., 2005). The computation of sensitivity coefficients has always been a limiting factor in the practicality of automated calibration algorithms (Carrera et al., 1990).

The biggest advantage to using automatic calibration procedures over manual trial-and-error approaches is the potential reduction in professional hours spent. A disadvantage that prevents their widespread use is that automated methods require highly-specialized computer codes and users often take a "black box" approach. Insights that should be obtained from a formal sensitivity analysis, such as the recognition of important regions within the model that dominate the solution, may be lost, despite the fact that the Jacobian matrix has been calculated and used for the inversion. The modeler should know where and how calibration is likely to affect the parameter estimates. This information is contained in the sensitivity coefficients (Equation 5.1).

Sensitivity coefficients are rarely used directly by modelers; rather, they are typically used by a computer code in the formulation of a minimization problem (see Chapter 6). However, a map of sensitivities of the hydraulic head at a given calibration data location to changes in the permeability at each grid block in the model would be useful. Such a map can be obtained by plotting the vector corresponding to one row of the Jacobian matrix

$$s_{i,j}(x,y) = \left\{ \frac{\partial h_j}{\partial \ln(k)_i} \right\} \tag{5.2}$$

where sensitivity, *s(x,y)*, is a function of model cell location, here in two-dimensional Cartesian space. In the following examples, sensitivity maps reveal how the flow model controls the structure of the sensitivity coefficients.

## 5.2 METHOD OF ANALYSIS AND RESULTS

A 1000 m x 1000 m square domain was discretized as a 50 x 50 grid using a uniform cell size of 20 m x 20 m. The permeability field was generated by an unconditional sequential Gaussian simulation using an anisotropic semivariogram consisting of a single spherical structure with maximum and minimum range parameters of 600 m and 160 m, respectively maximum continuity at an azimuth of 45 degrees. The permeability histogram was lognormally distributed with a ln($k$) mean and variance of 6.0 and 3.0, respectively.

A hydraulic head of 100 m was specified for every boundary cell. The flow equations were solved in steady state to obtain an equilibrium drawdown of the potentiometric surface (Figure 5.1). A specified flux node (a sink) was located at the center of the domain, plus four calibration points spaced at a distance of approximately 280 m from the sink forming a "five-spot" pattern. These nodes are taken as locations in the model for which we have calibration data.

Sensitivity coefficients were calculated using the direct derivation method for the purpose of studying their spatial structure. The direct derivation method involves calculating derivatives of the flow equations with respect to the parameters. A set of equations is obtained which is analogous in form to the original flow equations, with the independent variables being the desired parameter sensitivity coefficients (Yeh, 1986;

Gomez-Hernandez et al., 1997). The computer code of Wen et al. (1999) was used for this study, specifying every cell in the model as a parameter, and modifying the code to output the sensitivity coefficients (Equations 5.1 and 5.2) to a file to plot sensitivity maps. These sensitivity coefficients are obtained through a numerical implementation of an analytical formulation, so hereinafter they are referred to as analytical sensitivities.

### 5.2.1 Sensitivity structure

Figure (5.2) consists of sensitivity maps corresponding to the four vectors described by Equation (5.2) for the corresponding four calibration points. The following characteristics of the spatial structure of the sensitivity coefficients are noted:

1. *A limited number of grid cells have large sensitivity.* The distinction between significant and negligible sensitivity when examining the empirical results (Figure 5.2) was initially subjective. The colour map (Figure 5.2) was adjusted such that any node with a sensitivity coefficient greater or less than one standard deviation from the zero mean (Figure 5.3) was considered sensitive. Although there may be a non-zero sensitivity coefficient at a given location, it is clear from the distribution of sensitivity coefficients (Figures 5.2 and 5.3) that the model response at a given location is predominantly controlled by a small fraction of the parameter field area.

2. *There is a systematic pattern to the sign of the sensitivities.* The sign on a sensitivity coefficient is controlled by the location of the corresponding $i^{th}$ model cell within the flowfield with respect to the $j^{th}$ calibration point. If the flow at a grid cell is directed toward the calibration point, the sign of the sensitivity with respect to permeability is positive (Figure 5.2). In the opposite case that flow is directed away from the calibration location, the sign is negative. This is intuitive. For example: if a model cell is located upgradient from a calibration point, an increase in permeability at that upgradient model cell contributes to an increase in flow toward the calibration location and a corresponding increase in hydraulic head at the calibration location. In this case the sensitivity is positive (Equation 5.1). Conversely, an increase in permeability at a model cell located downgradient from the calibration location will contribute to a draining off of fluid

pressure at the calibration data location, resulting in a corresponding decrease in hydraulic head. Sensitivity coefficients are negative for these configurations.

It thus follows directly that:

3. *Model cells intersected by flowlines forming a streamtube passing through the calibration point* are the most sensitive parameters to the flow response at that specific location.

4. *Geologic "features" or* geobodies *of relatively high permeability are sensitive where they are connected to a fluid source or sink* (Figure 5.2; geobodies 1-3). In this example, the flux node is a sink in the domain and the Dirichlet boundary nodes comprise fluid sources, since the hydraulic gradient at the interface between each boundary cell and the adjacent internal cell directs flow into the domain (Figure 5.1).

5. *Cells of lower permeability are sensitive where they form features that impede the flow through a streamtube* (Figure 5.2; geobodies 4-7). In other words, if we consider the permeability of model cells crossed by an arbitrary streamline, highest sensitivity cells are those having relatively low permeability, causing the greatest impedance to the flow through the calibration location (Figure 5.2).

Criteria 4 and 5, related to high- and low-permeability geologic features are described qualitatively; and indeed, the choice of permeability thresholds may be subjective. However, convergence to a calibrated model is not likely to be highly sensitive to the cutoffs used in the definition of the geobody categories as long as they do not become overly restrictive or all-inclusive. Model cell sensitivity corresponds to locations of geologic features that are relatively important fluid transmitters and those that tend to impede flow. For example, Geobody 1 (Figure 5.2a) meets criterion 4 above. It is a high-permeability feature that is connected to the boundary of the model and directs flow through Calibration Point 1. Other features meeting this criterion are identified as Geobodies 2 and 3 (Figure 5.2b,c). Geobody 4, on the other hand, is a moderate permeability feature interrupting an otherwise continuous high-transmissivity pathway originating at the boundary, passing through Calibration Point 1, and terminating at the flux node (Figure 5.2a). Other baffle-like geobodies are numbered 5-7 (Figure 5.2b,d), and correspond to model cells meeting criterion 4 above.

Clearly the selection of appropriate cutoff(s) for geobody definition is a model-specific consideration. In the case of a bimodal permeability distribution or a categorical distribution, one could simply assign population-specific cutoffs or use the categories directly to define potentially important fluid-transmitting and flow-impeding facies.

As a second example: consider the case of well-defined channel deposits, with a high permeability channel fill and a lower permeability interchannel facies (Figure 5.4a). The permeability distribution is bimodal, with a continuous lognormal histogram in the interchannel facies and a single value assigned to the channel facies, one order of magnitude higher than the highest value in the interchannel facies (Figure 5.4b). A single $\ln(k)$ cutoff of 0.0 was used for high and low-flow geobody definition. This cutoff defines: (1) a low-$\ln(k)$, flow-retarding category within the interchannel facies, (2) relatively transmissive pathways, above the cutoff, in the interchannel facies, and (3) the high-permeability channel fill facies. This results in two geobody categories that are important to the head response (Figure 5.4c). As in the previous example, there is an outward flux specified at the centre of the domain (i.e., a pumping well) and there are four calibration points for which sensitivities are required. The steady-state head solution was computed with flowpaths delineated by particle tracking from the calibration locations, both forward to the well and backward to the boundaries (Figure 5.5). According to criterion 3 above, sensitive regions should be concentrated along these flowpaths.

Maps of sensitivity coefficients for the four calibration points do indeed reveal predictable patterns of sensitivities in light of criteria 1 to 5 (Figure 5.6). In every map, sensitive cells correspond to geobody definitions (Figure 5.6e) described by criteria 3-5. In some cases cells are sensitive, consistent with criteria 3 and 4, but are not intersected by flowpaths passing through the calibration point (e.g., Figure 5.6a). These correspond to geobodies that are sensitive to supplying or restricting the specified flux at the centre of the domain. This is because model cells/geobodies that are most important to supplying the specified flux to the well will impart some non-negligible effect on the hydraulic head response at a calibration point anywhere else in the well capture zone (Figure 5.6e). In this sense, these particular sensitivities may be regarded as an artifact of the strong specified flux in the domain, although they are real. They are called "artifact" for clarity of explanation; these sensitivities are a global phenomenon due to the flux condition rather than indicators of sensitivity with respect to the response at one of the calibration data locations. These "artifact" sensitivities are also observed in the first example (Figure 5.2).

### 5.2.2 Approximation of sensitivity coefficients

The sensitivity criteria outlined in the previous section appear to be comprehensive. Despite being quite intuitive, they have probably rarely been utilized. It is apparent that we have enough information from solving the forward flow problem to formulate a simple rules-based approach for obtaining an approximate system of sensitivity coefficients.

The basic steps needed to compute approximate sensitivity coefficients are: (1) solve the flow problem; (2) map out connected bodies of high and low permeability cells; and (3) calculate particle tracks (i.e., flowlines) from the calibration data locations. By these relatively simple steps it is possible to obtain an approximation to the structure of the Jacobian matrix. The potential then exists to use such an approximate system of sensitivities as a proxy to the information obtained by calculating the Jacobian.

#### *Rules-based algorithm*

The permeability distribution is separated into high and low classes according to the permeability histogram (Figure 5.4b). The idea is to re-classify the possibly continuous permeability distribution in terms of a binary categorical variable to define two classes of geobodies — one category having permeability above and the other, below a specified cutoff — in order to establish criteria 3 and 4 above (Figure 5.4b,c). Geobodies are determined by scanning through the model for face-connected cells belonging to a specific categorical code (i.e., high or low); the code used for this paper is described in Deutsch (1998). A particle tracking step follows, based on pore velocities obtained from solving the flow solution on the current parameter field. Particle tracking is performed using the method developed by Pollock (1988). This is a simple analytical formulation which is the basis for modern three-dimensional streamline simulation (Thiele, 2001). Tracking particles is equivalent to tracing streamlines in the flow field and this is necessary to establish the sensitivity criteria identified thus far.

The rules that designate a cell as sensitive are based on the criteria outlined in the preceding section, and are as follows:

**Rule 1**: Sensitive cells, with respect to a given calibration location, must be intersected by a particle track that defines a streamtube containing that calibration data location. The streamtube has a user-specified cross-sectional area — this is described further below.

**Rule 2**: Geobodies above the cutoff contain sensitive cells if they are (i) connected to a source or sink in the model, *and* (ii) intersected by a particle track. This is because a transmissive geobody is sensitive only if it draws fluid into or out of the model.

**Rule 3**: Cells with permeability below the cutoff are sensitive along any streamtube intersecting a calibration point.

**Rule 4**: Sensitivity has a negative sign for a model cell that is located downgradient of the calibration location

The particle tracking step defines streamtubes of arbitrary cross-sectional area around the calibration data locations. Streamtube area is defined by particle "sources" of user-specified dimensions at the calibration data locations (Figure 5.7). Cells intersected by a pathline are assigned a sensitivity indicator if they meet the criteria addressed by Rule 2 or 3. By this rationale, only cells within a streamtube containing the calibration point are potentially sensitive to that location.

This simple approach results in a sensitivity matrix of zeros and ones, where the non-zero elements correspond to sensitive cells with the appropriate sign for a given calibration data location. A visual comparison shows that the method does approximate the structure of the analytical sensitivities (Figures 5.8 and 5.9). Specifically, most regions of significant sensitivity are identified and they have the appropriate sign for any given calibration location. As a result of Rule 1, there are some sensitive zones excluded from the approximation. As noted previously, this is due to the specified flux at the well in the centre of the model, and the exclusion of the flux well from the calibration data set. This missing information can be included in the approximation. If the missing sensitivities are accounted for by using the well location as a calibration point, the approximation will include the effects of the zones rendered globally-sensitive by the flux at the well. The difference between the structure of the approximate and analytical sensitivities in this regard is that the approximate sensitivities may exclude some (less important) sensitivity information from the sensitivity matrix.

### 5.2.3 Validation of approximate sensitivities

Thus far we have demonstrated the criteria that govern sensitive regions of the model with respect to a specific configuration of calibration data. Assessing whether the approximate sensitivities can be used as a proxy to the Jacobian matrix in calibration routines remains to be shown.

In order to allow a computationally-feasible parameter optimization, an approximate function evaluation may be substituted for the expensive computation of the model response. One approach is to linearize the model response about the parameters as follows:

$$h(p) = h_0 + \mathbf{J}\left(p^* - p\right) \tag{5.3}$$

where $h(p)$ is the hydraulic head response to the set of parameter changes, $h_0$ is the modeled head at the calibration locations, obtained by solving the flow equations on the current parameter set ($p$), $p^*$ is the vector of proposed updates for the parameters, and **J** is the Jacobian matrix (Carrera et al., 2005). Equation (5.3) can be rewritten as

$$h^{(lin)} = h^{c} + \sum_{i=1}^{N} \left[ s \cdot \Delta p_i \right], \tag{5.4}$$

where $h^{(lin)}$ and $h^c$ are the linearized and model-calculated hydraulic heads at the calibration points, $s$ is the matrix of sensitivity coefficients (Equation 5.1) and $\Delta p$ is a vector of perturbations to the log transform of permeability.

We hypothesized: if the approximate sensitivities do as well as the analytical coefficients in approximating the true model response by Equation (5.4), this should indicate a reasonably accurate approximation to the structure of the Jacobian matrix. In this case the approximate sensitivity matrix should have the correct form for the automatic calibration of flow models based on parameter optimization.

The difference between a reference permeability field (Figure 5.1) and each of $L = 20$ alternative realizations was calculated to obtain an ensemble of perturbation vectors, $\{\Delta p\}_l$, to be applied in Equation (5.4) (Figure 5.10). The perturbation fields mimic proposed perturbations of the permeability field during an optimization routine, without regard to whether they improve the model or not. The full flow solution was computed on each realization to obtain 20 vectors of actual model heads, $\{h^m\}_l$, which could be considered an expanded, rather than a truncated Taylor series, as in Equation (5.4).

Figure (5.11) compares the ensemble of linearized heads $\{h^{(lin)}\}$ against the corresponding model heads $\{h^m\}$. The approximate sensitivities perform as well as the analytical sensitivities in approximating the model response by Equation (5.4) based on a comparison of the correlation coefficients for the scatterplots (Figure 5.11). Because the approximate sensitivity coefficients are simple binary indicators with the appropriate sign (Figure 5.8), a constant multiplicative scaling factor equal to the mean of the absolute values of the analytically-calculated sensitivities was applied to the approximate system of coefficients. The magnitude of sensitivity coefficients is a function of scale of the model, magnitude of prescribed fluxes, and the ranges of variation of the parameters and dependent variables. However, the absolute *magnitudes* are not particularly revealing[1]; what is important to identify are (1) the critical parameters (grid cells with non-negligible sensitivity) and (2) the correct sign to indicate the direction of the gradient of the model response. Consequently, comparable results (Figure 5.11) would not have been obtained if the critical (i.e., sensitive) model cells were not adequately identified, with the correct signs.

The bias in the crossplot between the true heads and the linearized approximation of hydraulic head (Figure 5.11a) [using the analytical sensitivities in Equation (5.4)] reflects the global effect of the prescribed flux. The artifact sensitivities that result from the numerical solution of the sensitivity equations, which are subject to the same boundary conditions and prescribed flux conditions as the flow equations, identify sensitive cells that are evidently less relevant than those identified by the criteria implemented in the rules-based approximation. The approximate system of sensitivities provides sensitivity information that pertains exclusively to the model response at the locations of the calibration data.

## 5.3 DISCUSSION

Most calibration/inversion methods in flow modeling are based on parameter optimization formulated as a function minimization problem. Minimization methods seek a parameter set that results in a minimum of an objective function that is typically formulated as a function of the errors at the calibration locations. Gradient-based methods require an evaluation of the gradient of the model response in order to determine the direction needed for the parameter updates. The Jacobian matrix, or the sensitivity coefficients are needed in most methods used in practice. A summary of minimization methods used in groundwater inverse modeling is found in Carrera et al. (2005).

---

[1] The magnitudes of the sensitivities are important in scaling the step size of parameter updates in minimization algorithms associated with inverse algorithms (see Chapter 6).

The fundamental information contained in the sensitivity coefficients are: (1) the critical parameters controlling the measured response variable (grid cells with non-neglible sensitivity) and (2) the correct sign, or the direction of the model response as a result of a perturbation to the parameters. We have shown that an approximate system of sensitivities based on empirically-derived physical criteria contains the information needed for permeability field inversion. Because the sensitivity indicators do not specify magnitudes, there would be instability problems associated with using them directly in parameter optimization routines, due to excessive noise in the calculation of the gradient of the model response. To use the sensitivity indicators directly, a tuning or relaxation factor should be selected to yield stable algorithm performance. An appropriate optimization technique could then be selected which can make use of the sensitivity indicators directly (see Chapter 6).

The immediate objective in calibrating a flow model is to match the values of hydraulic head at each calibration location. An effective way to do this is to adjust the hydraulic conductivity within streamtubes that envelope the calibration points. If the head must decrease at a calibration point for example, reduce the effective hydraulic conductivity upgradient and/or increase the conductivity downgradient from the calibration location. This is obvious, and it is exactly what the spatial structure of analytical (i.e., a full numerical implementation of) sensitivity coefficients reveal (Figure 5.2).

History matching production data using streamlines has been proposed before (e.g., Vasco et al., 1998; Wang and Kovscek, 2000, Wen et al., 2002). However, we have demonstrated an efficient method to predict the structure of sensitivity coefficients of the head ( or pressure) response; of which streamlines are only one component. Streamlines identify the sensitive zones of the heterogeneous parameter field to a first order; but the structure of sensitivities, within which is valuable information usually obtained by a full numerical computation of the Jacobian, is controlled by additional factors which have been demonstrated in this paper.

The value of this study is not only in demonstrating the possibility of using approximate sensitivities explicitly in inverse modeling/calibration codes, but in the understanding of these sensitivity coefficients in general. Visualizing the spatial structure of the Jacobian matrix shows that physically-intuitive criteria govern the structure of the sensitivity coefficients, and exactly which criteria affect the sensitivity of the model response to the permeability field.

For the modeler, it should be easy to assess the potential of inverse modeling to improve parameter estimates, and ultimately, the reliability of the model. The modeler should ask, for example: What is the potential of a given set of calibration data to infer important geological features affecting flow and reservoir recovery? Which regions of the model are going to be most strongly influenced by calibrating to a given dataset, and what changes to the model parameters are going to be needed to achieve calibration? What is the impact of a certain type of boundary condition on this process? Sensitivity coefficients contain this information. Being able to easily predict model sensitivities without actually having to calculate them using expensive numerical techniques and specialized computer code is useful. We have shown that it is possible to devise relatively straightforward and inexpensive ways to substitute an approximate system of sensitivities for the technically-involved and computationally-expensive calculation of the Jacobian in parameter inversion codes.

## 5.4 CONCLUSIONS

Sensitivity of pressure or hydraulic head response at specific model locations to grid block permeability is predictable once the head solution has been obtained and some means of accounting for the flowpaths, such as particle tracking, has been implemented. The permeability structure coupled with the model specifications, such as boundary conditions and internal sources/sinks (production/injection wells), controls sensitivities. The criteria defining grid block sensitivity with respect to model response at specific locations are as follows: (1) cells that occur along flowpaths which intersect the locations of calibration data will be the most sensitive cells within the model, (2) High-transmissivity geobodies are sensitive if they are connected to a source or sink in the domain, (3) sensitive regions will also coincide with cells of relatively lower permeability that impede flow, and (4) the sign of the sensitivity coefficient is related to whether the parameter (model cell) is located up- or down-gradient from the observation location along a flowpath.

These criteria can be used within a standard flow code to obtain an approximation of the sensitivity matrix with minimal computational cost. This indicator matrix approximates the structure of the Jacobian matrix and thus contains information on: (1) which parameters in the spatially-distributed parameter field are sensitive with respect to the calibration data; and (2) the sign on the parameter sensitivity. This is the critical information needed to calibrate the permeability field to hydraulic head data. Understanding the controls on the magnitude and sign of sensitivity coefficients used in flow model calibration provides the modeler or practitioner with significant insight into the calibration process.

## 5.5 REFERENCES

Ahmed, S., de, M.G., (1989) Co-kriged estimates of transmissivities using jointly water level data. In: M. Armstrong (Ed.), *Geostatistics; Proceedings of the Third international geostatistics congress; Volume 2.* (Ed. by M. Armstrong), Kluwer Acad. Publ., Dordrecht, Netherlands. pp. 615-628.

Carrera, J., Neuman, S.P., (1986a) Estimation of aquifer parameters under transient and steady state conditions; 1, Maximum likelihood method incorporating prior information. *Water Resources Research*, 22(2), pp. 199-210.

Carrera, J., Neuman, S.P., (1986b) Estimation of aquifer parameters under transient and steady state conditions; 2, Application to synthetic and field data. *Water Resources Research*, 22(2), pp. 228-242.

Carrera, J., Neuman, S.P., (1986c) Estimation of aquifer parameters under transient and steady state conditions; 2, Uniqueness, stability, and solution algorithms. *Water Resources Research*, 22(2), pp. 211-227.

Carrera, J., Navarrina, F., Viues, L., Heredia, J., Medina, A., (1990) Computational aspects of the inverse problem. In: G. Gambolati, A. Rinaldo, C.A. Brebbia, W.G. Gray, F. Pinder George (Eds.), *Computational methods in subsurface hydrology*, Comput. Mech. Publ., Southampton, United Kingdom. pp. 513-522.

Carrera, J., Medina, A., Axness, C., Zimmerman, T., (1997) Formulations and computational issues of the inversion of random fields. In: G. Dagan, S.P. Neuman (Eds.), *Subsurface Flow and Transport: A Stochastic Approach, International Hydrology Series*, Cambridge University Press. pp. 62-79.

Carrera, J., Alcolea, A., Medina, A., Hidalgo, J., Slooten, L.J., (2005) Inverse problem in hydrogeology. *Hydrogeology Journal*, 13(1), pp. 206-222.

Chu, L., Reynolds, A.C. and Oliver, D.S., (1995) Computation of sensitivity coefficients for conditioning the permeability field to well-test pressure data. *In Situ*, 19(2), pp.179-223.

Cooley, R.L., (1977) A method of estimating parameters and assessing reliability for models of steady state groundwater flow; 1, Theory and numerical properties. *Water Resources Research*, 13(2), pp. 318-324.

Cooley, R.L., (1979) A method of estimating parameters and assessing reliability for models of steady state groundwater flow; 2, Application of statistical analysis. *Water Resources Research*, 15(3), pp. 603-617.

Cooley, R.L., (1982) Incorporation of prior information on parameters into nonlinear regression groundwater flow models; 1, Theory. *Water Resources Research*, 18(4), pp. 965-976.

Cooley, R.L., (1983) Incorporation of prior information on parameters into nonlinear regression ground-water flow models; 2, Applications. *Water Resources Research*, 19(3), pp. 662-676.

Dagan, G., (1985) Stochastic modeling of groundwater flow by unconditional and conditional probabilities; the inverse problem. *Water Resources Research*, 21(1), pp. 65-72.

Dagan, G., Rubin, Y., (1988) Stochastic identification of recharge, transmissivity, and storativity in aquifer transient flow; a quasi-steady approach. *Water Resources Research*, 24(10), pp. 1698-1710.

de Marsily, G., Delhomme, J.P., Coudrain-Ribstein, A., Lavenue, A.M., (2000) Four decades of inverse problems in hydrogeology. *Geophysical Society of America*, Special Paper 348, pp. 1-28.

Deutsch, C.V., (1998) FORTRAN programs for calculating connectivity of 3-D numerical models and for ranking multiple realizations. *Computers & Geosciences*, 24(1), pp. 69-76 (see http://www.iamg.org/ for code).

Dietrich, C.R., Newsam, G.N., Anderssen, R.S., Ghassemi, F. and Jakeman, A.J., (1989) A practical account of instabilities in identification problems in groundwater systems. *BMR Journal of Australian Geology and Geophysics*, 11, pp. 273-284.

Dogru, A.H. and Seinfeld, J.H., (1981) Comparison of sensitivity coefficient calculation methods in automatic history matching. *Society of Petroleum Engineers Journal*, pp. 551-557.

Emsellem, Y. and Marsily, G. de, (1971) An automatic Solution for the inverse problem. *Water Resources Research*, 7(5), pp. 1264-1283.

Ginn, T.R., Cushman, J.H., (1990) Inverse methods for subsurface flow. *Stochastic Hydrology and Hydraulics*, 4, pp. 1-26.

Gomez-Hernandez, J.J., Sahuquillo, A. and Capilla, J.E., (1997) Stochastic simulation of transmissivity fields conditional to both transmissivity and piezometric data; I, Theory. *Journal of Hydrology*, 203(1-4), pp. 162-174.

Gutjahr, A., Wilson, J.L., (1989) Co-kriging for stochastic flow models. In: G. de Marsily (Ed.), *The stochastic approach to subsurface flow., 4; 6, Transport in Porous Media* (Ed. by G. de Marsily), D. Reidel Publishing Company, Dordrecht, International. pp. 585-598.

Kitanidis, P.K. and Vomvoris, E.G., (1983) A geostatistical approach to the inverse problem in groundwater modeling (steady state) and one-dimensional simulations. *Water Resources Research*, 19(3), pp. 677-690.

Landa, J.L. and Horne, R.N., (1997) A procedure to integrate well test data, Reservoir Performance History and 4-D Seismic Information into a Reservoir Description, SPE Annual Technical Conference and Exhibition. Society of Petroleum Engineers, San Antonio, TX, pp. 177-192.

Loaiciga, H.A., Marino, M.A., (1986) On solution of the inverse problem for confined aquifer flow via maximum likelihood. *Mathematical Geology*, 18(7), pp. 677-692.

Loaiciga, H.A., Marino, M.A., (1987) Parameter estimation in groundwater: classical, Bayesian, and deterministic assumptions and their impact on management policies. *Water Resources Research*, 23(6), pp. 1027-1035.

McLaughlin, D., Townley, L.R., (1996) A reassessment of the groundwater inverse problem. *Water Resources Research*, 32(5), pp. 1131-1161.

Medina, A. and Carrera, J., (2003) Geostatistical inversion of coupled problems: dealing with computational burden and different types of data. *Journal of Hydrology*, 281(4), pp. 251-264.

Neuman, S.P., (1973) Calibration of distributed parameter groundwater flow models viewed as a multiple-objective decision process under uncertainty. *Water Resources Research*, 9(4), pp. 1006-1021.

Oliver, D.S., (1994) Incorporation of transient pressure data into reservoir characterization. *In Situ*, 18(3), pp. 243-275.

Pollock, D.W., (1988) Semianalytical computation of path lines for finite-difference models. *Ground water*, 26(6), pp. 743-750.

RamaRao, B.S., LaVenue, A.M., de Marsily, G., and Marietta, M.G., (1995) Pilot point methodology for automated calibration of an ensemble of conditionally simulated transmissivity fields; 1, Theory and computational experiments. *Water Resources Research*, 31(3), pp. 475-493.

Sun, N.Z., Yeh, W.W.G., (1992) A stochastic inverse solution for transient groundwater flow; parameter identification and reliability analysis. *Water Resources Research*, 28(12), pp. 3269-3280.

Sun, N.Z., Jeng, M.C., Yeh, W.W.G., (1995) A proposed geological parameterization method for parameter identification in three-dimensional groundwater modeling. *Water Resources Research*, 31(1), pp. 89-102.

Sykes, J.F., Wilson, J.L. and Andrews, R.W., (1985) Sensitivity analysis for steady state groundwater flow using adjoint operators. *Water Resources Research*, 21(3), pp. 359-371.

Thiele, M.R., (2001) Streamline simulation, *6th International Forum on Reservoir Simulation*, Schloss Fuschl, Austria.

Townley, L.R., Wilson, J.L., (1985) Computationally efficient algorithms for parameter estimation and uncertainty propagation in numerical models of groundwater flow. *Water Resources Research*, 21(1), pp. 1851-1860.

Vasco, D.W., Yoon, S. and Datta-Gupta, A., (1999) Integrating dynamic data into high-resolution reservoir models using streamline-based sensitvity coefficients. *SPE Journal*, 4(4), pp. 389-399.

Wang, Y. and Kovscek, A., (2000) A streamline approach for history-matching production data, *SPE Paper 59370* presented at SPE/DOE Improved Oil Recovery Symposium, Tulsa, Oklahoma, pp. 1-8.

Wen, X.H., Capilla, J.E., Deutsch, C.V., Gomez-Hernandez, J.J., Cullick, A.S., (1999) A program to create permeability fields that honor single-phase flow rate and pressure data. *Computers & Geosciences*, 25, pp. 217-230.

Wen, X.-H., Deutsch, C.V. and Cullick, A.S., (2002) Construction of geostatistical aquifer models integrating dynamic flow and tracer data using inverse technique. *Journal of Hydrology*, 255, pp. 151-168.

Woodbury, A.D., Smith, L., Dunbar, W.S., (1987) Simultaneous inversion of hydrogeoloic and thermal data; 1, Theory and application using hydraulic head data. *Water Resources Research*, 23(8), pp. 1586-1606.

Yeh, W.W.G., (1986) Review of parameter identification procedures in groundwater hydrology: The inverse problem. *Water Resources Research*, 22(2), pp. 95-108.

Yeh, T.C.J., Zhang, J., (1996) A geostatistical inverse method for variably saturated flow in the vadose zone. *Water Resources Research*, 32(9), pp. 2757-2766.

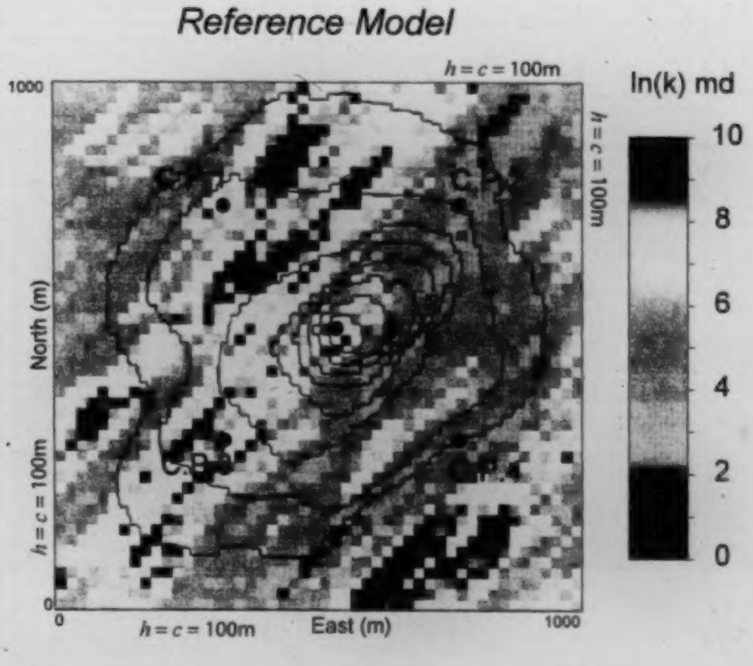

Figure 5.1. Flow model domain and flow solution for Model I. Calibration data locations are numbered C.P. 1-4. Specified flux at the centre of the domain produces a heterogeneous drawdown cone due to heterogeneous permeability field. Hydraulic head contours are labeled in metres (interval of 5 m). Head at well is -3.0 m.

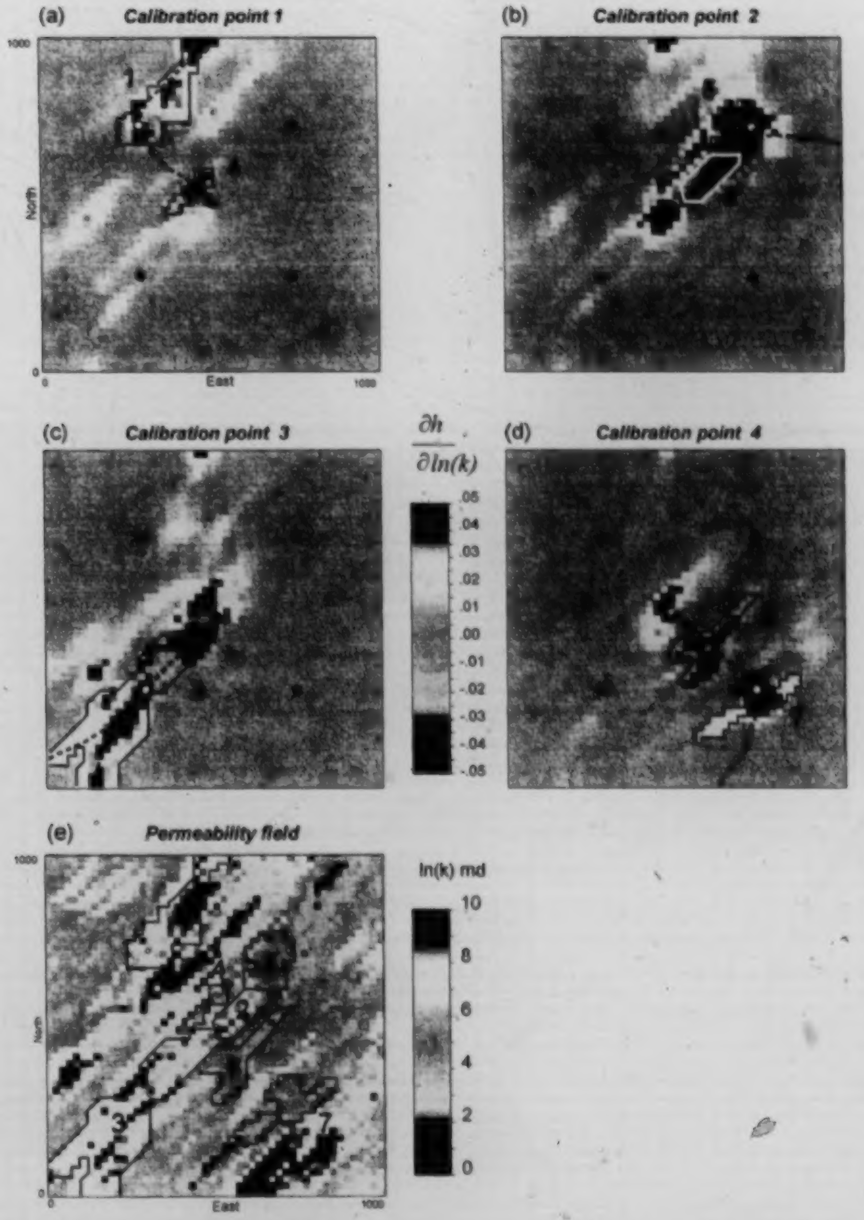
(a) Calibration point 1
(b) Calibration point 2
(c) Calibration point 3
(d) Calibration point 4
(e) Permeability field
1000
North
0
East
1000
∂h/∂ln(k)
.05
.04
.03
.02
.01
.00
-.01
-.02
-.03
-.04
-.05
ln(k) md
10
8
6
4
2
0
1
3
7

Figure 5.2. (a-d) Map displays of analytical sensitivity coefficients (i.e., rows of the Jacobian matrix) corresponding to the four calibration points in Model I. Reds indicate positive sensitivity coefficients and blues are negative sensitivities. Selected areas of high sensitivity are numbered 1-7 as referenced in the text. Dashed arrows indicate flowpaths tracking the centre of streamtubes passing through the calibration points; (e) Permeability field used in flow model with numbered geobodies corresponding to the sensitive bodies in (a-d).

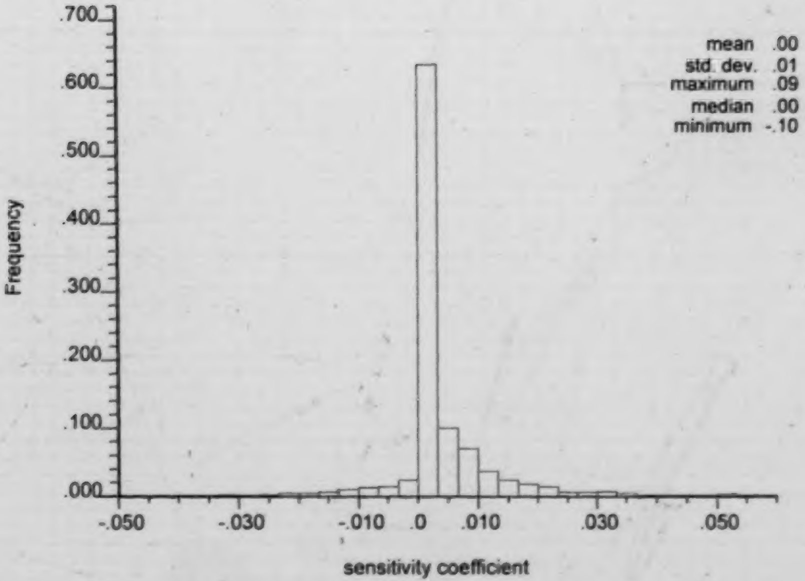

Figure 5.3. Frequency histogram of sensitivity coefficients for the entire Model I domain with respect to a single calibration point.

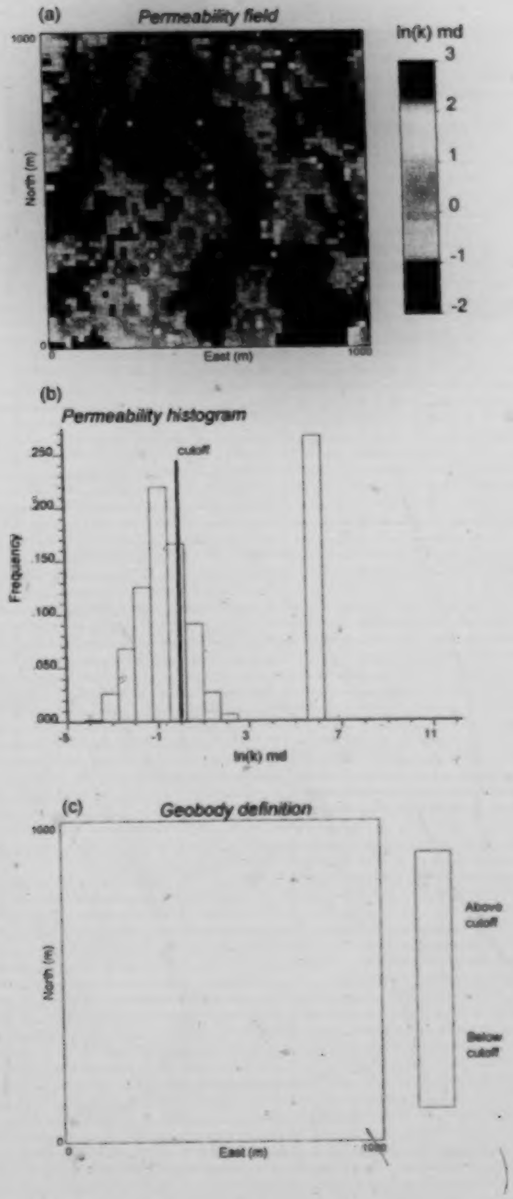

Figure 5.4. (a) Model II: bimodal permeability field comprised of high-permeability channel deposits and lower permeability heterogeneous interchannel facies having a continuous lognormal distribution. Calibration data locations are numbered C.P. 1-4; (b) permeability histogram with a single cutoff selected such that two geobody categories are defined: (i) high-transmissivity channel fill facies and conduits within the interchannel facies and (ii) low-transmissivity interchannel facies; (c) geobody map produced by this categorical definition.

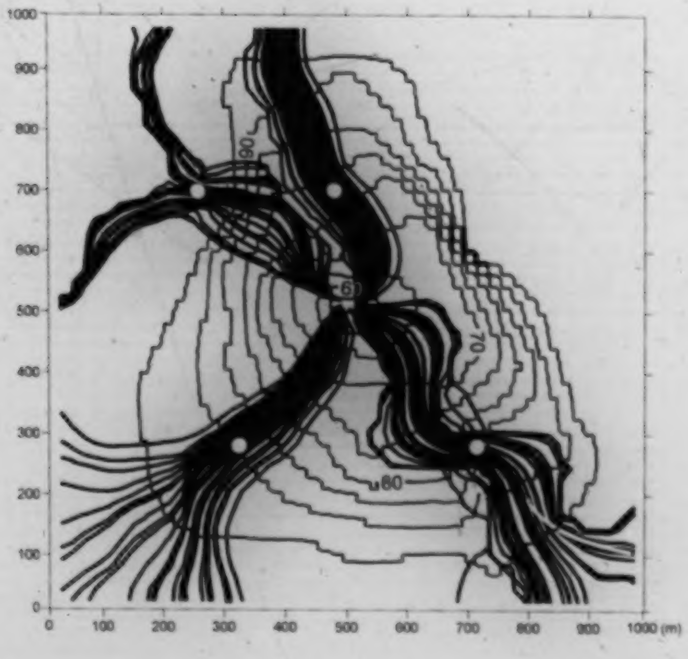

Figure 5.5. Hydraulic head solution (contour interval of 5 m) computed on Model II with particle tracks intersecting the locations of the calibration data.

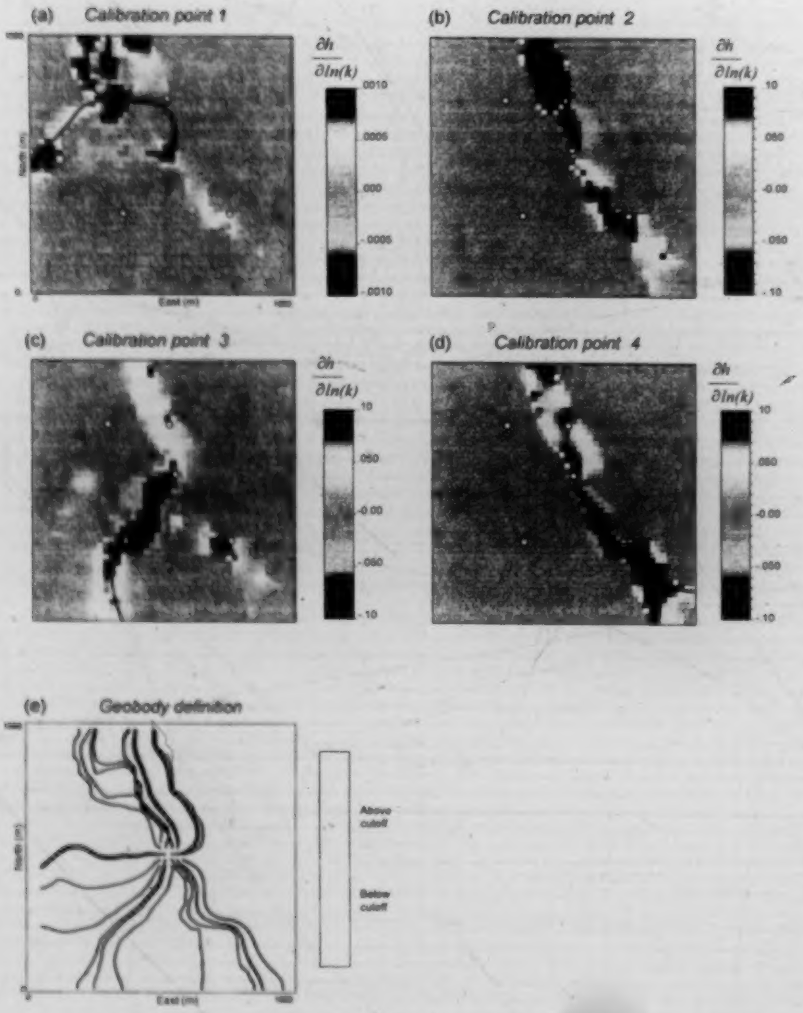
(a) Calibration point 1
(b) Calibration point 2
(c) Calibration point 3
(d) Calibration point 4
(e) Geobody definition
$\frac{\partial h}{\partial ln(k)}$
.0010
.0005
.000
-.0005
-.0010
10
.050
-0.00
-.050
-.10
North (m)
East (m)
1000
0
Above cutoff
Below cutoff

Figure 5.6. (a-d) Map displays of sensitivity vectors corresponding to the four calibration points in Model II. Black flowlines indicate focus of flow through calibration locations and delineate sensitivities most relevant to each calibration location. Other sensitive regions are global (i.e., not related to a particular calibration data location) due to the specified flux at the centre of the domain; (e) Geobody definition outlining important flow features in model with the well capture flowpaths overlain. Compare the well flowpaths with the locations of artifact sensitivities in (a-d).

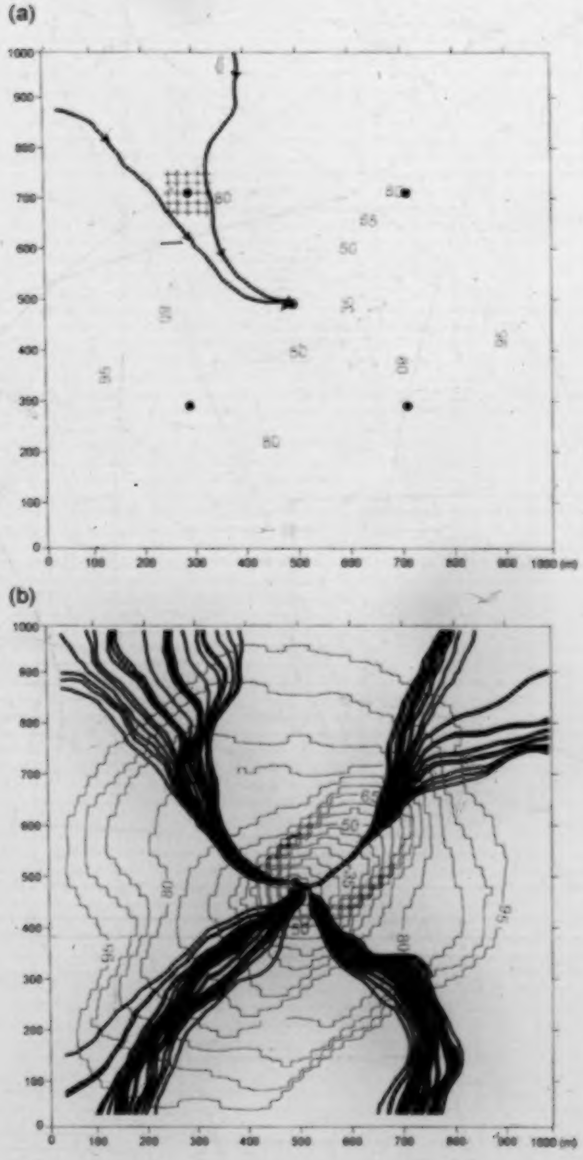

Figure 5.7. (a) Depiction of the definition of a streamtube for the computation of approximate sensitivity coefficients by seeding a particle source template around a calibration data location; (b) the result delineates streamtubes encompassing potentially sensitive zones of the model for a specific calibration data configuration.

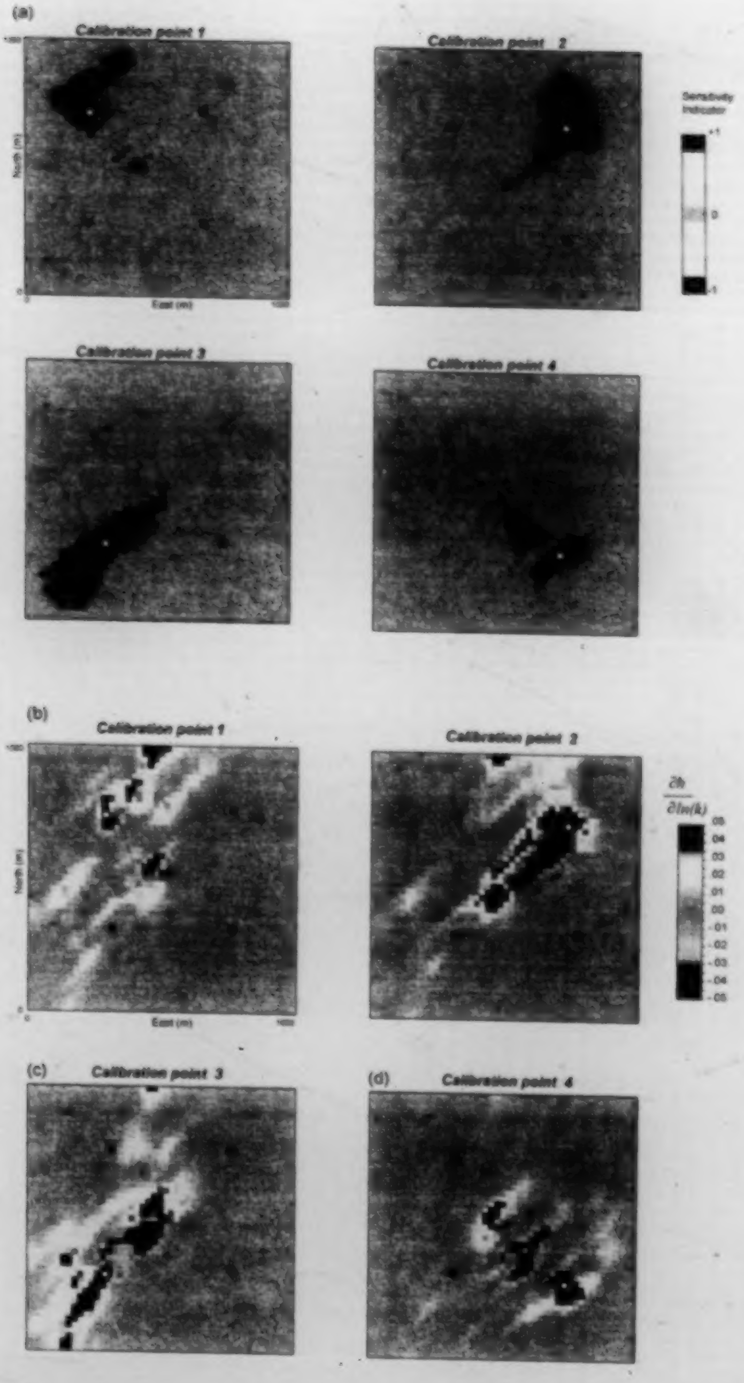

Figure 5.8. (a) Approximate sensitivity indicators displayed as sensitivity maps corresponding to (b) the analytical sensitivity coefficients calculated for Model I.

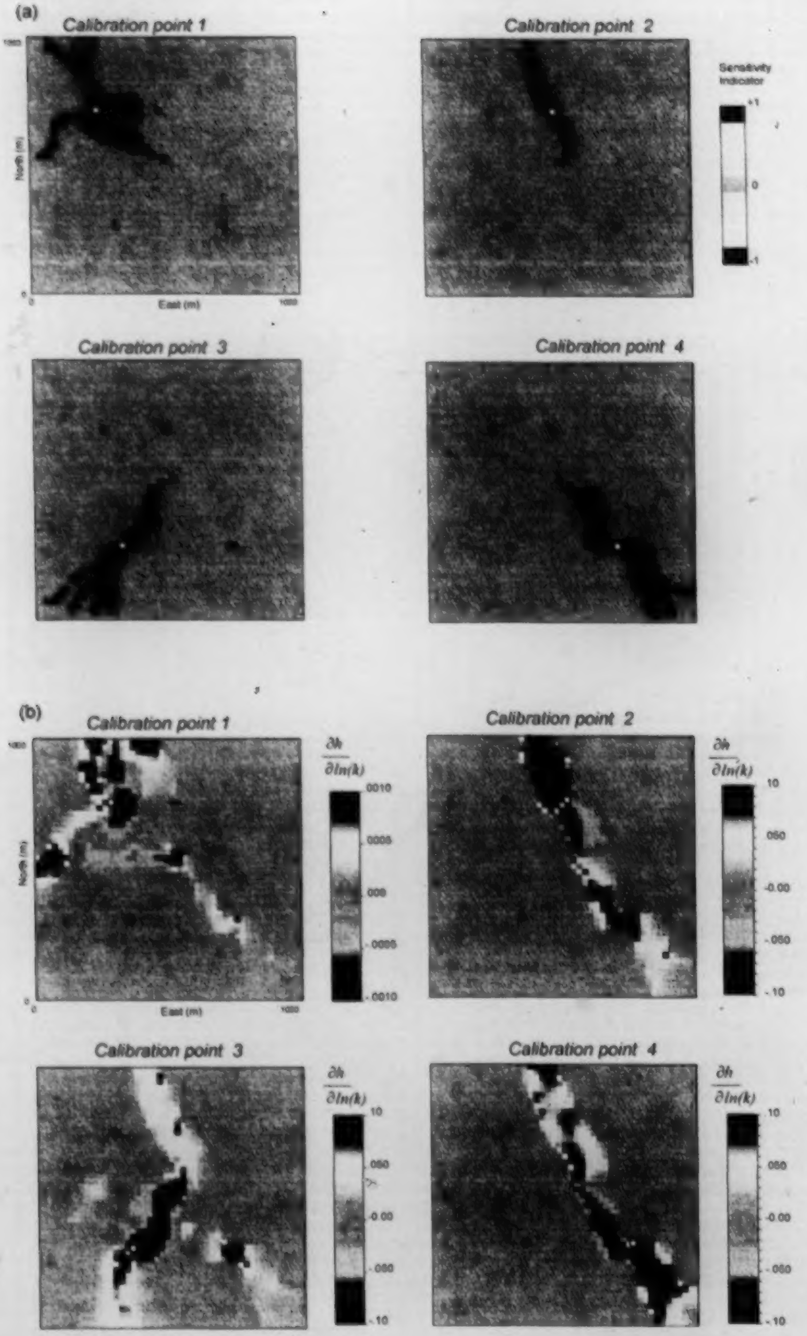

(a)
Calibration point 1
Calibration point 2
Sensitivity indicator
+1
0
-1
North (m)
East (m)
1000
0
Calibration point 3
Calibration point 4
(b)
Calibration point 1
Calibration point 2
Calibration point 3
Calibration point 4
∂h/∂ln(k)
.0010
.0005
.000
-.0005
-.0010
10
.050
-0.00
-.050
-.10

Figure 5.9. (a) Approximate sensitivity indicators displayed as sensitivity maps corresponding to (b) the analytical sensitivity coefficients calculated for Model II.

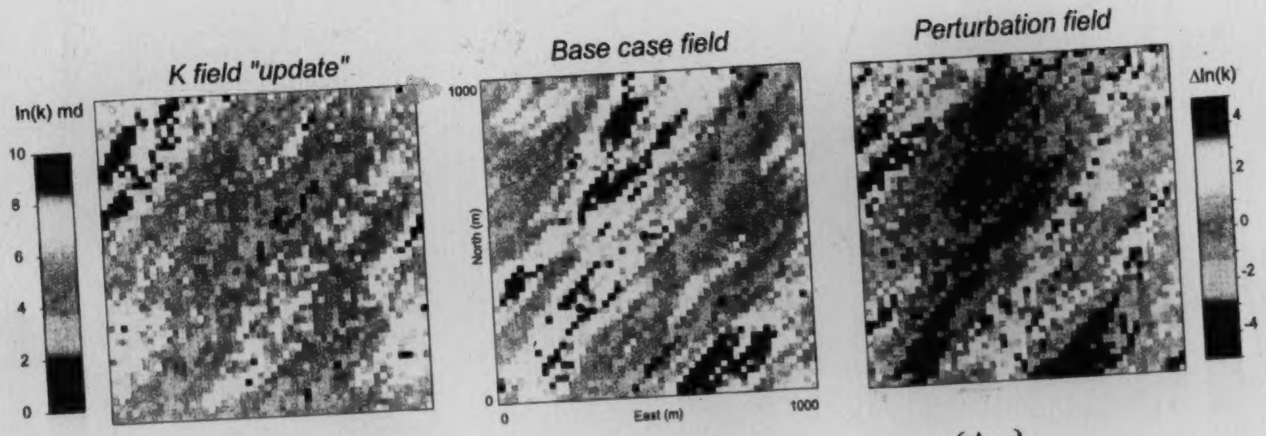

$$\{p^*\}_L \quad - \quad \{p\} \quad = \quad \{\Delta p\}_L$$

Figure 5.10. Graphical description of the generation of ln(k) perturbation vectors for the validation of approximate sensitivities using Model I.

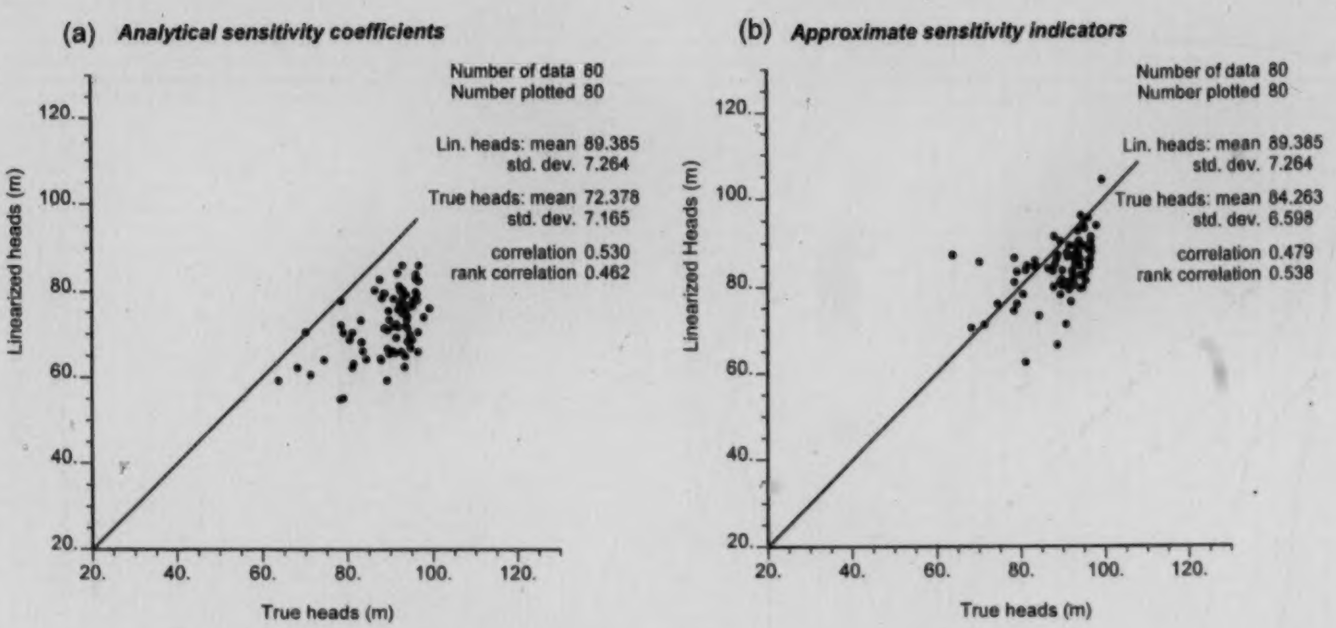

Figure 5.11. (a) Scatterplot comparing the linear approximation of hydraulic head about 20 ln(k) perturbation vectors against model-calculated heads using the analytically-derived sensitivity coefficients (b) The same comparison using the approximate sensitivities scaled to the same magnitude as the mean of the absolute value of the analytical sensitivities. Note the comparable results in the statistics which are plotted on the diagrams. Despite the scaling, comparable results would not have been obtained if the critical (i.e., sensitive) model cells were not adequately identified, including the correct sign.

# 6.0 A GRADIENT-FREE APPROACH TO INVERSE CONDITIONING OF HETEROGENEOUS AQUIFER MODELS TO HYDRAULIC HEAD DATA

## 6.1 INTRODUCTION AND BACKGROUND

Inverse modeling generally refers to identifying a model which adequately represents the system under analysis. Model identification is a broader and less frequently approached topic than parameter estimation (Draper, 1995), so most often, inverse modeling involves estimating the model parameters subject to the constraint that the chosen model reproduces measurements of the system response. In particular, for aquifer and petroleum reservoir characterization, inverse modeling refers to estimating the model parameters based on measurements of fluid pressure, flow rates at wells, tracer concentrations over time, and so on. These measurements of state variables serve as model calibration data, and are distinct from measurements of the properties represented by the parameters.

The problem of integrating measurements of hydraulic head into geological models for aquifer characterization (the groundwater inverse problem) remains an important area despite decades of research. Techniques for solving the inverse problem in hydrogeology have been developed by (Emsellem and de Marsily, 1971; Cooley, 1977; 1979; 1982; 1983; Kitanidis and Vomvoris, 1983; Dagan, 1985; Townley and Wilson, 1985; Carrera and Neuman, 1986; Loaiciga and Marino, 1986; 1987; Woodbury et al., 1987; Dagan and Rubin, 1988; Ahmed and de Marsily, 1989; Gutjahr and Wilson, 1989; Sun and Yeh, 1992; RamaRao et al., 1995; Sun et al., 1995; Yeh and Zhang, 1996; Gomez-Hernandez et al., 1997; Medina and Carrera, 2003) among numerous others. Integrating hydraulic head data into the process of modeling the geological heterogeneity of an aquifer requires solving an inverse problem, where the solution consists of model parameter estimates that are constrained by measurements of the system response. The ultimate goal of inverse flow modeling in this context is to identify important heterogeneities of the distributed parameter field, most often the permeability, of a heterogeneous aquifer or reservoir in order to increase the predictive ability of the model by narrowing the spaces of uncertainty of the response variables.

A major challenge of inverse modeling is related to non-uniqueness of the solution — where the solution is some parameter set that reproduces the measured response — and instabilities associated with this non-uniqueness, or more generally, with an ill-posed mathematical problem (Neuman, 1973, Deitrich et al, 1989; Carrera et al., 2005). Early research tended to focus on understanding and dealing with these difficulties and is summarized in reviews by Carrera and Neuman, (1986a), Yeh (1986), Ginn and Cushman (1990), McLaughlin and Townley (1996), and de Marsily et al. (1999), among others. More recent research has focused on technological advances, or ways to make the computations more efficient (e.g., Wen et al., 2002; Medina and Carrera, 2003).

### *Scope of Present Contribution*

The gradient-free method presented in this chapter utilizes and builds upon the concepts of Sequential Self Calibration (SSC) (Sahuquillo et al., 1992; Gomez-Hernandez et al., 1997), and pilot points (RamaRao et al., 1995). These simulation-based geostatistical inverse methods have addressed difficulties associated with obtaining satisfactory solutions to the generally ill-posed inverse problem (Gomez-Hernandez et al., 1997; de Marsily et al., 2000).

In particular, the problem of *regularization* to obtain valid solutions to the aquifer inverse problem has been addressed through Geostatistics-based approaches (de Marsily et al., 2000). The need for regularization is a direct consequence of the ill-posed nature of the inverse problem, for which an effectively infinite number of solutions may exist. This is obvious considering the number of unknowns (e.g., thousands) compared to the number of independent head data (e.g., tens) typical of inverse problems where the distributed parameter field representing heterogeneous aquifer permeability is being estimated[1].

---

[1] The case of a distributed parameter field in a discretized flow model is in contrast to the inverse problem dealing with only a few parameters, where the number of unknowns is comparable to the number of head data.

Thus there is a need to somehow algorithmically reduce the number of unknowns to solve the problem. The most straightforward approach is "zonation" (Yeh, 1986), which simply reparameterizes the problem by considering subdomains of the model and assigning a constant parameter value to each "zone". More realistic models of heterogeneity require more complex designs to reduce the degrees of freedom of the parameter space.

The pilot points method (RamaRao et al., 1995) represented a forward leap in that: (i) an objective means was employed for the selection of a location in the model (i.e., a pilot point) where the aquifer permeability was to be perturbed, with that perturbation being optimally-located so as to effect the largest reduction in the head mismatch produced by the model, and (ii) the initial fields were generated by conditional sequential simulation (Journel and Huijbregts, 1978; Goovaerts, 1997; Deutsch, 2002), thus a representation of the spatial patterns of permeability variation was available from the outset. With respect to the first point, a well-designed parameterization should render an initially ill-posed problem well-posed (Zimmerman et al., 1998). The pilot points method, and shortly afterwards, the SSC approach (Gomez-Hernandez et al., 1997), which opted to used multiple "master points" in place of a single optimized location in the model, focused on a well-designed parameterization for the heterogeneous aquifer identification problem.

The gradient-free method developed here is based on an approximate prediction of the sensitivity of hydraulic head response to perturbations in the permeability field (Chapter 5). Typically these sensitivity coefficients are obtained through expensive numerical procedures based on analytical formulations for parameter sensitivity (Dogru and Seinfeld, 1981; Sykes et al., 1985; Carrera et al., 1990; 2005; Oliver, 1994, Chu et al., 1995, Carrera et al., 1997; Landa et al., 1997; Medina and Carrera, 2003) and others. In the gradient-free approach, parameter sensitivities are predicted in advance, approximately, based on a set of physical criteria. This allows optimal selection of any desired number of parameters for optimization, thus combining the best elements of previous parameterization schemes (RamaRao et al., 1995; Gomez-Hernandez et al., 1997). The sensitivity approximation and an approximation of the associated gradient of the model response with respect to the parameters constitute a simplified methodology that offers several advantages over traditional gradient-based approaches. These advantages include: (1) a reduction in computational expense and computer code development effort; and (2) a clear understanding of the calibration process and the effects of conditioning to a given spatial configuration of calibration data.

## 6.2 METHODOLOGY

Synthetic examples are used to illustrate the gradient-free algorithm and to demonstrate the amount of information that can, in general, be expected from specific configurations of calibration head data with respect to identification of key heterogeneities. Synthetic examples assume a reference permeability field to be the "geological truth" and the calibration data are taken as a subset of the model response on that true field. The value of synthetic modeling studies is in the controlled experimental conditions, which permit the study to focus on key aspects of the modeling in order to illustrate foundational concepts.

### *Assumptions*

The inversion problem to be solved is that of estimating the value of absolute permeability at each model cell in a two-dimensional flow system by calibration to a set of steady-state heads. Steady-state flow in a two dimensional domain of uniform thickness is considered. The flow model is expressed as:

$$\frac{\partial}{\partial x}\left(k\frac{\partial h}{\partial x}\right)+\frac{\partial}{\partial y}\left(k\frac{\partial h}{\partial y}\right)=\frac{\mu}{\rho g}bQ, \qquad (6.1)$$

where $h$ is the total hydraulic head, which for a horizontal model, taking the value at the centre of the grid cells, is interchangeable with fluid pressure, but for generality, we use hydraulic head from this point; $k$ is isotropic absolute permeability, Q is the sum of fluid sources and sinks over the domain; $\mu$ and $\rho$ are dynamic viscosity and density of the single fluid phase, respectively; and $g$ is gravitational acceleration. The flow model is discretized by finite differences. The consideration of two dimensions is purely for convenience and simplicity. Neither the calibration algorithm, nor the concepts discussed are limited to two-dimensional applications. The assumption of steady state is made for simplicity and clarity of analysis and presentation.

The synthetic calibration data are obtained by solving the flow equations on a reference permeability field with the boundary conditions known exactly. The forward flow problem that is solved during the iterative calibration procedure uses exactly the same boundary conditions[2], internal fluxes, grid discretization, iterative solver parameters, and so on. The spatial discretization of the model is assumed to be adequate with respect to resolving the heterogeneity that is relevant to the model response.

The spatial structure of the permeability field is assumed to be known insofar as the random function model that characterizes it. Thus, the only effective source of uncertainty is the parameter uncertainty due to the heterogeneity of the permeability field. The initial permeability realizations are unconditional. No static data is assumed available. This allows us to isolate the effects of conditioning to the head data.

The parameter perturbations are based on a multi-Gaussian model. The propagation of optimal parameter perturbations throughout the domain is done by kriging. These assumptions are made for convenience. The focus of this paper, with respect to the calibration algorithm, is the gradient-free method. Any stochastic model could be implemented for the generation of initial parameter field realizations with a consistent mechanism used for the generation and propagation of parameter perturbations.

### 6.2.1 Gradient-free calibration

The algorithm structure is based on the SSC concept (Gomez-Hernandez et al., 1997) (Figure 6.1). It is an indirect calibration procedure that iteratively updates the parameter field until a satisfactory match to the head data is achieved. An outer loop consists of solving for head on the current realization and calculating the head mismatch between the model and the measured data. Unless the head mismatch is smaller than a specified tolerance, the algorithm proceeds with an inner parameter optimization routine (Figure 6.1).

---

[2] Note that specified heads do not comprise perfectly known boundary conditions because the fluxes are not constrained. However, the results did not change significantly when exact reference fluxes were used (other than getting absolute magnitudes of permeability that were closer to the reference field values).

In the gradient-free method, the calibration process begins by efficiently mapping sensitive areas of the model domain with respect to the calibration data locations. This step substitutes a system of sensitivity indicators for the calculation of sensitivity coefficients (see Chapter 5) and constrains the randomized drawing of a parameter subset for optimization. For each calibration data location, a subset of model cells is drawn within sensitive regions of the model (Figure 6.1). The gradient-free optimization routine calculates perturbations to this parameter subset that will minimize the mismatch between the model-predicted head response and the measured data at the calibration locations. An inexpensive function evaluation is used which is based on a linear approximation of the model response about the proposed parameter changes (Gomez Hernandez et al., 1997). The perturbations are then propagated through the domain by a kriging of the optimal values. The permeability field is finally updated by addition of the resultant perturbation field to the current realization of the permeability field (Figure 6.1).

The elements that differentiate this gradient-free algorithm from SSC and other gradient-based approaches in general are:

(1) The calculation of the full matrix of sensitivity coefficients is done by a simple approximation.

(2) The parameterization scheme for the optimization is based on prior sensitivity information, which results in a "smart" selection of a subset of parameters to use in the optimization.

(3) The optimization routine is based on the Simultaneous Perturbation Stochastic Approximation (SPSA) method (Spall, 1992; 2003). The algorithm uses an

approximation of the gradient of the objective function that is directly compatible with the approximate system of sensitivity indicators replacing the calculation of Jacobian matrix.

These three elements comprise the gradient-free approach and are explained in detail next.

*Approximate sensitivities*

Sensitivity coefficients are the partial derivatives of the model response at a location, *j*, with respect to a parameter change at model cell, *i*. We consider the sensitivity of head to the logarithm of permeability. The complete matrix of sensitivity coefficients, otherwise called the Jacobian matrix, may be expressed as:

$$\mathbf{J} = \{s_{i,j}\} = \frac{\partial h_j(t)}{\partial \ln(k)_i}, \qquad i = 1,\ldots N; j = 1,\ldots m \tag{6.2}$$

where *h* is hydraulic head at a specific calibration data location and *k* is the effective permeability specified at a model cell.

Sensitivity coefficients are used to determine the search direction within the parameter space that results in an improved match between the calibration data and the model response (Carrera et al., 2005). However, the computational burden of calculating sensitivity coefficients has always been a limiting factor in the practicality of automated calibration algorithms (Carrera et al., 1990, 2005; Medina and Carrera, 2003).

As an alternative to calculating the Jacobian matrix, an approximate system of sensitivity indicators may be obtained immediately following the head solution (see Chapter 5). The permeability structure coupled with the model specifications control the sensitivity of the model response at specific locations to perturbations of the permeability field. Sensitivity at a given calibration location is greatest to perturbations of permeability along streamlines intersecting that response location; particularly within relatively high transmissivity geobodies or features forming relatively low permeability barriers to flow (Figure 6.2). In order to quantify important permeability contrasts, a binary geobody classification scheme can be defined based on the selection of appropriate threshold permeability values[3] (Figure 6.2b,c).

The criteria to predict sensitivity are: (1) cells that occur along flowpaths which intersect the locations of calibration data will be the most sensitive cells within the model (Figure 6.2d), with the additional constraints that; (2) they constitute geobodies of *relatively* high-transmissivity which are connected to a source or sink in the domain [Figure 6.2e; geobodies (ii-v)], or; (3) they are cells of relatively low permeability, forming hydraulic barriers [Figure 6.2e; geobody (i)]. Lastly, (4) the sign of the sensitivity coefficient is related to whether a model grid cell is located up- or downgradient from the observation location along a flowpath. Cells that are downgradient will always have a negative sign (Figure 6.2e).

A simple rules-based algorithm based on the above criteria is used to obtain a sensitivity indicator matrix comprised of zeros and 1's, where non-zero elements indicate sensitive parameters. This indicator matrix approximates the form of the Jacobian matrix and can be used in place of the Jacobian in an appropriately-designed optimization routine (see Chapter 5). From this indicator matrix we obtain: (1) grid blocks with permeability values that are sensitive to the model response at a particular calibration location, and (2) the sign on the sensitivity (Figure 6.2e), which is critical to establishing the updating direction in the parameter optimization.

---

[3] **Remark:** When defining the categorical variable for modeling geobodies it may be better to use an upper and a lower cutoff, resulting in three categories: (i) above the upper threshold, (ii) below the lower threshold, and (iii) between the two cutoff values. Only cells of categories (i) and (ii) will be potentially sensitive. In addition, for transient flow problems, it may be effective to define a different (pair of) threshold value(s) at given times in the simulation. For example, as time progresses and the flow response approaches equilibrium, increasingly low permeability values will be needed to constitute sensitive flow barriers. But the performance of the algorithm in the synthetic examples was not found to be highly sensitive to the cutoffs used in the definition of the geobody categories (as long as they do not become overly restrictive or all-inclusive).

*Parameterization*

Given the extremely large number of parameters in the distributed parameter fields that populate flow model grids or meshes, an appropriate parameterization is needed for a well-posed optimization. The original SSC method utilizes a parameterization technique whereby a randomly-sampled subset of parameters is used in the optimization. This set of "master points" is also used in the calculation of a parameterized Jacobian matrix, which is a clever way of reducing the computational burden of obtaining the full matrix of sensitivity coefficients. However, this parameterization scheme is not based on any sensitivity information, making it a "blind" approach.

The original SSC algorithm draws a set of master points using a random stratified sampling scheme in order to cover all of the zones or sub regions of the model, regardless of whether the head response at the calibration locations is sensitive to permeability at the master point locations or not (Figure 6.3a). In the gradient-free approach, a prior prediction of sensitivity of head to permeability, as described above, constrains the random drawing of a subset of parameters to use in the optimization (Figure 6.3b). This ensures that each of the optimized permeability perturbations will effect a response at the calibration data locations. This parameterization scheme is a critically-important element of the gradient-free method — parameters with maximum sensitivity information are always selected, and each parameter carries information about the gradient of the model response, which leads directly to the gradient-free optimization method described next.

*Gradient-free optimization*

Gradient-based optimization methods are based on the evaluation of the gradient, $g(\theta)$ of a loss function, $L$ with respect to the parameters, $\theta = [k_1, k_2, \ldots, k_M]^T$ such that

$$g(\theta) \equiv \frac{\partial L}{\partial \theta} = \begin{bmatrix} \partial L / \partial k_1 \\ \partial L / \partial k_2 \\ \vdots \\ \partial L / \partial k_M \end{bmatrix}. \tag{6.3}$$

In Equation (6.3), $\partial L/\partial\theta$ corresponds to a *direct* measurement, with or without noise (Spall, 2003, p.127) of the (unknown) true gradient, $g(\theta)$. The evaluation of $g(\theta)$ depends on the calculation of the Jacobian matrix.

*Gradient-free* methods, however, do not depend on direct computation of the gradient, $g(\theta)$. Stochastic approximation techniques are a group of gradient-free methods that are based on an *approximation* to the gradient formed from measurements of $L$ (Spall, 2003). Simultaneous Perturbation Stochastic Approximation (SPSA) is one such technique (Spall, 1992; 2003). The form of the SPSA gradient approximation is well-suited to an optimization using the sensitivity indicator matrix described previously.

The SPSA gradient approximation is typically evaluated using only two measurements of $L$ about a simultaneous perturbation of the parameters. However, there is a one-sided approximation that may be suitable for certain applications, which makes use of only one loss function measurement (Spall, 2003). The one-sided gradient approximation has the form,

$$\hat{g}_l(\hat{\theta}_l)=\begin{bmatrix} \dfrac{L(\hat{\theta}_l \pm c_l\Delta)}{c_l\Delta_1} \\ \vdots \\ \dfrac{L(\hat{\theta}_l \pm c_l\Delta)}{c_l\Delta_M} \end{bmatrix}, \tag{6.4}$$

where $c_l$ is a positive scalar whose value at iteration $l$ is given by a gain sequence satisfying certain well-known stochastic approximation conditions (Spall, 1992; 1998; 2003) and $\Delta$ is a mean-zero perturbation vector with a distribution that should satisfy certain specific conditions requiring bounded inverse moments for the elements of $\Delta$ (Spall, 2003, p.184). One commonly-used distribution which satisfies these conditions is a symmetric Bernoulli ±1 distribution. Most of the rows of the sensitivity indicator matrix — where a row constitutes the vector of sensitivities for one calibration location (e.g., Figure 6.2e) — tend to follow this distribution[4].

The gradient approximation in Equation (6.4) is designed to perform a stochastic search of the gradient space of a noisy loss function, or one that is costly to evaluate. However, for the problem of calibration to head data, Equation (6.4) can be used in a deterministic sampling of the gradient space. The sampling is deterministic in the sense that it is known in advance from the head mismatch at a given calibration location whether an increase or a decrease in the elements of $\theta$ are needed to reduce the value of $L(\theta)_j$, where $L$ is evaluated for each $j^{th}$ calibration data location.

The loss function is constructed based on the form of the SPSA gradient approximation and an expression for the linearization of the model response about the parameter perturbations. The gradient-free loss function is evaluated as

$$L(\theta)_j = \left| h_j^{lin} - h_j^{o} \right|. \tag{6.5}$$

where $h_j^0$ is the value of the observed head at the $j^{th}$ calibration point, and $h_j^{lin}$, a linear approximation of hydraulic head, is calculated as a truncated series about the model-calculated head, $h_j^c$, on the current permeability field:

$$h_j^{lin} = h_j^c + \sum_{i=1}^{M} \left[ \ln(k)_i \pm c_i \Delta_{ij} \right]. \tag{6.6}$$

Note that in Equation (6.6), the term in the summation has the same form as the argument in the numerator of the elements of the SPSA gradient approximation[5]

---

[4] Even if some do not (i.e., the histogram of ±1 sensitivities to a given calibration location is very asymmetric with non-zero mean due to all negative or all positive sensitivities) this did not appreciably degrade the performance of the SPSA optimization.

[5] The numerator is the same for all the elements in Equation (6.4); it is the value of the loss function at the current inner optimization iteration.

(Equation 6.4). The ± 1 sensitivity indicators at the locations of the parameters to be optimized comprise the perturbation vector, $\Delta$, and the scalar gain coefficient, $c$, acts as a relaxation factor such that the products, $c\Delta$, in Equation (6.6) behave like traditional sensitivity coefficients[6]. This approach to approximating the Jacobian is really quite intuitive. Recall that what is obtained from the sensitivity indicator matrix is a binary map of sensitivities with respect to each calibration location (Figure 6.2e), indicating the sensitive areas of the model and the correct sign on the sensitivity of model response with respect to the parameters. The precise values of these approximate sensitivities are not critical in the evaluation of the loss function by Equations (6.5) and (6.6); only approximately-correct magnitudes are needed since the most critical sensitivity information is already established (Chapter 5).

The parameter vector $\theta$ is updated at each iteration using the general recursive form:

$$\theta_{l+1} = \theta_l - a_l \hat{g}_l\left(\hat{\theta}_l\right), \qquad (6.7)$$

where $a_l$ is a nonnegative scalar gain coefficient (Spall, 1992; 1998; 2003), which behaves like a relaxation factor, limiting the updating step size. More details on gain coefficients $c_l$ and $a_l$ and the formulation of the gradient-free minimization step are included in Appendix B.

The main reason for using a multi-objective formulation (Equation 6.5) is that the parameter update direction is based on the sensitivity information and the head mismatch at each respective calibration location.

As an example, consider the case where the head mismatch ($h^c$ - $h^o$) at a single calibration location is equal to -11.0 m, indicating that the calculated model response, $h^c$, is below the observed value, $h^o$, at that location (Figure 6.4). In order to reduce the mismatch, permeability must be reduced in areas of negative sensitivity coefficients and/or increased at locations having positive sensitivity with respect to this calibration location (Table 6-1). The subset of permeability values selected for optimization (Figure 6.4) are the initial $M$ elements corresponding to $\hat{\theta}_0$ in Equation (6.4), and the elements of the perturbation vector, $\Delta$, correspond to the ±1 sensitivity indicators at those locations (Table 6-1). The term in brackets in Equation (6.6) represents the proposed parameter updates for the $l$th iteration (Table 6-1). In the opposite case of a positive head mismatch at the calibration data location, Table (6-2) summarizes the direction of required changes to the parameters and the corresponding expression for the loss function evaluation considering the same parameterization (Figure 6.4).

---

[6] Aside from setting the seed value of this gain sequence following SPSA guidelines, you can check the optimization results after one outer iteration (a single SPSA run) to help tune an appropriate magnitude to the approximate sensitivities, $c\Delta_{ij}$ by checking for reasonable magnitudes of the optimized perturbations.

Upon converging to a minimum loss function tolerance or reaching a maximum number of inner iterations, the optimal parameter perturbation vector is propagated through the domain by kriging (Figure 6.1).

## 6.3 RESULTS AND DISCUSSION

This section has two parts: (1) a demonstration of the algorithm working to condition prior realizations of the permeability structure of two synthetic reservoirs; and (2) a discussion of the identification of the key heterogeneities through inverse conditioning to head data. The second part, on identification, is a general topic of importance to inverse modeling of heterogeneity using dynamic data. The elements of the gradient-free method make clear what to expect in this regard from the inverse conditioning process.

The first example consists of a 1000 x 1000 m square domain that is discretized as a 50 x 50 grid using a uniform cell size of 20 x 20 m. Reference field (I), taken as the "true field" (Figure 6.5), and all other permeability field realizations to be conditioned to the head data obtained on the reference field were generated by unconditional sequential Gaussian simulations using an anisotropic semivariogram consisting of a single spherical structure with maximum and minimum range parameters of 600 m and 160 m, respectively maximum continuity at an azimuth of 45 degrees. The permeability histogram was lognormally distributed with a ln($k$) mean and variance of 6.0 and 3.0, respectively.

Dirichlet boundaries are used with a hydraulic head of 100 m specified at each boundary cell. The flow equations were solved in steady state on reference field (I) in order to obtain the values for head at the five well locations to be used as the calibration data set (Figure 6.5). A constant withdrawal flux is specified at the center of the domain, plus four calibration points (C.P.'s) spaced equidistant from the "production well" (Figure 6.5) forming a five-spot pattern.

### 6.3.1 Conditioning a single realization

A single permeability realization was selected as an initial parameter field to be conditioned (Figure 6.6a). The initial field was selected from an ensemble of realizations such that the effective permeability in the near production well zone was similar to the reference field so there would be relatively small initial head mismatch at the flux well (Figure 6.6a). This was to ensure that near pumping-well effects did not dominate the calibration process in the first few iterations. In addition, during the calibration run, perturbations to the permeability field were frozen within a restricted zone around the flux well[7] in order to prevent an artificial convergence of the calibration due to near-well effects. This would occur as a result of a large reduction in the effective permeability in the near-well zone, constricting the head response throughout the domain.

The initial head mismatch (Figures 6.6a, 6.7a) was reduced to 30% of the initial global calibration error at the second iteration (Figure 6.7b). The global objective function is the performance measure assessed at the outer calibration iterations (Figure 6.1) after solving for head on the updated permeability field. The global objective function at the $l^{th}$ outer iteration was specified as:

---

[7] **Remark:** If the pressure at the flux well was not included in the calibration data it was possible to get a good match at the other four points largely by reducing the effective permeability near the flux well. In this case, there would be a large negative pressure mismatch at the flux well. Both of these effects are undesirable.

$$F(\theta)_l = \frac{\sum_{j \in (n_p)} \left(h_j^o - h_j^c\right)^2}{F(\theta)_1}. \tag{6.8}$$

After nine iterations the calibration converged to the specified objective function tolerance (Figure 6.7).

### 6.3.2 Conditioning an ensemble of realizations

This example was rerun over an ensemble of 20 unconditional realizations. The constraint of having the correct effective permeability within the zone near the flux well was removed since there was no prior conditioning of the permeability fields (i.e., no conditioning to static data). The optimal permeability perturbations were also propagated freely over the domain, with no freezing of perturbations near the flux well.

More than half (13/20) of the calibration runs show a reduction of the global objective function (Equation 6.8) to a tight convergence (Figure 6.8). A few realizations are somewhat unstable and/or unable to converge to better than 40% of the initial calibration error. This indicates some sensitivity to the initial field, in particular, the effective permeability in the zone near the extraction well. The results indicate good performance of the algorithm by this somewhat unfair test. That is, in practice the effective permeability near production wells would be constrained, with the initial fields being conditioned to honour effective permeability from well-tests, for example. As an aside: if this were not the case, and a real study was to proceed as in this example, the success in achieving a satisfactory calibration to the head data would be a good plausibility measure. Those realizations for which a satisfactory calibration was not possible could be excluded from the final ensemble of conditioned realizations.

### 6.3.3 Identification of the reference field

It is apparent from the shape of the drawdown on the potentiometric surface (Figure 6.6a,b,d) that calibration to only a few wells improves the identification of important features of the permeability field. In particular, the conduit of increased drawdown between the central flux well and C.P.3 is identified, and the overall shape of the head drawdown (Figure 6.6d) is much closer to the reference solution (Figure 6.6b) than the initial field (Figure 6.6a). Note that there is poor identification of the correct magnitudes of permeability structures defining features that effect the requisite pressure response to achieve calibration to the head data (Compare Figure 6.6b and d) . The specified flux at the centre of the domain does not provide sufficient flux data to arrive uniquely at correct effective permeability values which characterize important heterogeneities. The actual identification of geological features, based on a visual comparison between the reference field (Figure 6.6b) and the single calibrated field (Figure 6.6d), is fair. Indeed, we should not necessarily expect anything more from looking at a single realization conditioned to a set of pressure data.

The non-uniqueness of the solution to this inverse problem is well-known. Yet, there is potentially valuable information available from inverse conditioning to head data. The aim of conditioning is to reduce uncertainty in the flow response variables. In order to ensure a meaningful impact on global uncertainty through a reduction in parameter uncertainty, where the parameters are the values of permeability distributed throughout the model, key heterogeneity features that affect the flow response in the real system should be identified. Inverse conditioning to head data may or may not achieve this objective. An important question then, is: How much information can we expect from conditioning to a given configuration of head data?

From the sensitivity criteria listed previously, high-transmissivity conduits should be consistently identifiable where they are connected to a source or sink of fluid and intersected by streamlines passing through a calibration data location. High permeability features will not be reliably identified from head data in any other configuration. We should also expect to identify low permeability barriers along flowpaths coincident with any calibration head data location. The following examples illustrate these points.

### *Identification of flow barriers*

The second example (Figure 6.9) considers a reference permeability field (reference field II) in a reservoir zone with good productivity near the production well and a high permeability conduit leading from near the production well to the SW boundary (Figure 6.9). Two of the observation wells (1 and 4) are completed in effectively poor reservoir quality zones because of the adjacent low permeability lenses. The flow solution is calculated on the reference field using the same model specifications as used in the previous example. Steady state heads are obtained from the four observation wells (1-4) for the calibration data set. The reason for the exclusion of the head at the production well from the calibration data set for this example is to isolate the conditioning effect of the calibration data that should identify the low permeability lenses; namely, C.P. 1 and 4.

The gradient-free algorithm was applied to the same 20 initial unconditional realizations used in the previous example. Note, however, that now a different reference field (II) is used as "truth" and to generate the calibration data. Compared to the initial realizations, the conditioned realizations quite consistently identify the two low permeability barriers between the central flux well and C.P.'s 1 and 4 (Figure 6.10)[8].

The ensemble average, or E-type map (i.e., the point-by-point average) of the calibrated realizations[9] (Figure 6.11) shows that good local accuracy can be expected in identifying low permeability barriers that are important in controlling the system response (i.e., the real system) as long as they are "sampled" by the calibration data. The swath of streamlines intersecting a calibration data location defines, to a first order, the effective zone of the model that the calibration data location informs. In order for a calibration point to inform a permeability barrier, that data location must be intersected by streamlines which also intersect the barrier (Figure 6.12a,b). Without this condition, it should not be possible to identify a permeability barrier, as is apparent by the effect of moving the location of C.P. 1 (Figure 6.12c,d); the low permeability lens in the NW quadrant of the domain is not identified. The basic criterion is that the anomaly in the head response that is produced by an important heterogeneity must be sampled by a calibration datum in order to identify the heterogeneity feature through an inverse approach.

---

[8] Remark: Note how some features in the initial fields are completely changed, whereas others noticeably "seed" heterogeneities that result in a good calibration (Figure 6.10). This latter characteristic indicates that the algorithm preserves the initial field structure as much as possible. This is known as a "plausibility criterion" (Neuman, 1973) and it is an important aspect of regularizing the inverse problem (de Marsily, 2000). This is implicit to the SSC method in general; and it provides an example of how the SSC concept tackles the problem of obtaining a solution to the aquifer identification problem.

[9] This is the best measure of the impact on the space of uncertainty by conditioning to the pressure data without actually assessing that space — which is too large an undertaking to fit into the discussion. It suffices here to point out that if the most important heterogeneities are identified consistently in the realizations then this will result in a significant impact on the global uncertainty through conditioning to head data.

*Identification of high-transmissivity conduits*

The same reference field (II) and flow model specifications are utilized in the following example, but this time including the head at the central flux well as a calibration point (C.P. 5) in order to take necessary advantage of the available flux constraint.

High-transmissivity conduits will be reliably identified between calibration head data and a source or sink in the domain. A source or sink represents valuable flux data, which constrain an otherwise non-unique head response. For example, the high permeability band in reference field II, located between the central well and C.P. 3 (Figure 6.9), is identified consistently in the calibrated fields (Figure 6.13). However, the connection between C.P. 3 and the SW boundary is not identified across all (or most) conditioned realizations (Figure 6.13). With only head specified at the boundary, there is no constraint on the flux passing through the zone where this conduit should be identified between C.P. 3 and the SW boundary. As is evident from the ensemble average calibrated field, low permeability between the boundary and C.P. 3 is equally plausible (Figure 6.13b).

However, the specification of an additional boundary condition, an arbitrary flux at the SW boundary cells forming the "inlet" to the conduit (Figure 6.14a), results in a complete identification of the feature across all calibrated realizations (Figure 6.14b). In this case, the total inflow from the subset of boundary cells selected along the inlet to the conduit was made equal to the outflow at the well (Figure 6.14). From a practical modeling perspective, this is an inappropriate choice of boundary conditions for this system which has been assumed to have open boundaries, since the rest of the domain boundary now contributes a negligible amount of fluid to the production well; but it serves to illustrate the point. This is like reducing the model to a "quarter five spot", considering only the SW corner of the domain, and replacing the corner flux boundary by an injection well with a comparably high injection rate to the production rate at the producer. A high-transmissivity conduit between the injector and the producer will be consistently identified (e.g., Wen et al., 2005). The constraint to the solution set provided by the flux data coupled with head data which sample the anomaly produced by a high transmissivity feature uniquely identifies the heterogeneity.

### 6.3.4 Technological contribution

The key simplification that leads to the gradient-free approach — a sufficiently complete, yet fast assessment of parameter sensitivity — eliminates the need for specialized numerical procedures used to calculate sensitivity coefficients. This has been an area of extensive research for decades (e.g., Dogru and Seinfeld, 1981; Carrera et al., 1990; Oliver, 1994, Chu et al., 1995, Carrera et al., 1997; Landa et al., 1997). The rules-based method for sensitivity prediction that is at the heart of the gradient-free approach provides the modeler with a complete vector of sensitivity for each calibration location in the model (e.g., Figure 6.2e).

Obtaining the sensitivity indicator matrix permits an effective parameterization of the optimization (Figure 6.4). In general, it is advantageous to have ready access to a complete assessment of sensitivity prior to approaching a model calibration. The manual trial-and-error approach would benefit from a quick assessment of sensitivity for the entire model. A quick look at "sensitivity maps" (e.g., Figure 6.2e) at various iterations during a calibration procedure would offer the modeler insights into the calibration process that are not otherwise easily accessible.

With respect to savings in CPU time, it would be a major endeavor, that is beyond the scope of this study, to compare different methods given the number of variables involved, and the plethora of highly-specialized research codes. However, it is apparent that the elimination of the calculation of the Jacobian matrix, yet still utilizing sufficiently detailed sensitivity information in its place, is a major advantage in terms of computational efficiency over other sensitivity-based methods, with the possible exception of the Adjoint-state method[10] (Medina and Carrera, 2003). However, the method of Adjoint-states is a technically-involved procedure to implement, and the efficiency of the method depends on the number of observations (Medina and Carrera, 2003). The gradient-free method is relatively insensitive to the number of observations.

The gradient-free approach could be considered a streamline or streamtube approach to inverse conditioning. Streamline-based history matching approaches have been proposed before (Wang and Kovscek, 2000; Caers et al., 2002; Wen et al., 2002). An important distinction that sets the gradient-free method apart from previous streamline-based methods for matching pressure data is that it is based on an understanding of the sensitivity process[11] and an explicit account of sensitivities that can substitute directly for the calculation of the Jacobian. It is not only a bulk change along the streamlines/streamtubes that is proposed in order to obtain a match to the flow response (Wang and Kovscek, 2000; Caers et al., 2002); rather, spatially precise perturbations are made. This is because the selection of parameters to optimize is based on an assessment of the sensitivity structure of the field, of which streamlines are only one component. The method of Caers et al. (2002) also honours the geostatistical model of spatial uncertainty[12], but because of the second point, will not guarantee local precision in identifying important heterogeneities. Caers et al. (2002) emphasize histogram and variogram reproduction though a Gauss-Markov iterative procedure; but the SSC approach, in general, will adequately reproduce these statistics without hard constraints, by preserving the structure of the prior model (Gomez-Hernandez et al., 1997; Xue and Datta-Gupta, 1997).

---

[10] Even the clever concept of master points in SSC, which, for a small number of master points is on-par with the gradient-free method in efficiency, is at a disadvantage for two reasons: (1) CPU time is quite sensitive to the number of master points (this is not the case in the gradient-free approach), and (2) the parameterization offered by the original SSC sampling scheme is "blind" because of a lack of incorporation of prior sensitivity information (Figure 3), so if a small number of master points is used, you will generally not get a maximum amount of conditioning information from the inverse calibration to a pressure data set.

[11] It is only after a clear understanding of what controls the structure of sensitivity coefficients for pressure in reservoir models, that a streamtube approach is adopted here.

Seeding the perturbations from sensitive locations in the model, not simply using a bulk change along a relevant streamtube, is critical to obtaining a good solution to the inversion problem; in particular, for preserving the prior permeability field structure, and more importantly, for identification of key heterogeneities affecting the flow response. There is important information contained in pressure or head data which may allow spatially-accurate identification of permeability heterogeneity features if the calibration data sample them, and the approach of modifying effective permeability along streamlines cannot guarantee the identification of such features. Perhaps the best approach to date has been to combine a bulk streamline approach for rate and concentration data, and a traditional sensitivity method (i.e., SSC) to explicitly account for the pressure response (Wen et al., 2002). The simplified methodology presented in this paper solves the sensitivity problem for pressure such that an expensive numerical procedure is not needed to account for the pressure, thus simplifying the problem of integrating pressure, rate and concentration data, by a unified streamline approach that explicitly accounts for the information contained in the pressure data.

## 6.4 CONCLUSIONS

The gradient-free method is a relatively intuitive approach to calibrating the distributed parameter fields representing heterogeneous permeability in aquifer or reservoir models to hydraulic head data.

---

[12] They emphasize histogram and variogram reproduction though a Gauss-Markov iterative procedure; but the SSC approach, in general, will adequately reproduce these statistics without hard constraints. Moreover, the reproduction of these statistics is less critical than obtaining local precision in the calibrated realizations.

The method is based upon the procurement of a system of parameter sensitivities which replaces the need to calculate the Jacobian matrix. A rules-based approach for determining the required parameter sensitivity information is based upon: (1) delineation of flowpaths relevant to the calibration head data, (2) transforming the permeability field into a categorical variable in order to define relatively high-transmissivity and low-permeability geobodies, and (3) some connectivity measures identifying geobody connections to fluid sources or sinks in the model.

This results in identifying the sensitive grid cells to the response at the calibration data locations. The approximate direction of the gradient of the model response is determined from the sign on the sensitivity coefficients at selected parameters and the head mismatch at calibration locations. This information is used to construct the optimization problem for the calibration.

Parameter optimization is based on the deterministic gradient information inferred from the sign on the sensitivity coefficients and the head mismatch. The optimization algorithm uses an approximation of the gradient of the model response with respect to the parameters that is adapted from a proven gradient-free optimization technique (SPSA). Results from synthetic examples indicate good performance of the gradient-free algorithm under a reasonable suite of tests, including varying the reference and initial fields.

The method is partly based on a streamtube approach, whereby the conditioning effect of each calibration data point is seeded within the area covered by the locus of streamlines that intersects the calibration data location, with sensitive areas predicted by additional structural criteria coupled with the model specifications. From these insights, a framework is constructed to illustrate the effects of inverse conditioning to head data with respect to the information content that can be expected from the conditioning. Specifically: key heterogeneities which impact the flow response must be sampled by the calibration data. A calibration data point "samples" a heterogeneity feature when it occurs along a flowline that intersects the feature. By this approach, the permeability field can be adjusted within sensitive areas, seeding spatially precise perturbations to produce a head match at that calibration data location which results in an improvement in the local precision of the spatial uncertainty model from the conditioning process.

These general observations related to inverse conditioning to head data are not specific to the gradient-free approach. However, the constitutive elements of the gradient-free method lead to their clarification by adding a degree of transparency to the calibration process.

## 6.5 REFERENCES

Ahmed, S., de, M.G., (1989) Co-kriged estimates of transmissivities using jointly water level data. In: M. Armstrong (Ed.), *Geostatistics; Proceedings of the Third international geostatistics congress; Volume 2.* (Ed. by M. Armstrong), Kluwer Acad. Publ., Dordrecht, Netherlands. pp. 615-628.

Caers, J., Krishnan, S., Wang, Y. and Kovscek, A.R., (2002) A geostatistical approach to streamline-based history matching. *Society of Petroleum Engineers Journal*, 7(3), pp. 250-266.

Capilla, J.E., Gomez-Hernandez, J.J. and Sahuquillo, A., (1997) Stochastic simulation of transmissivity fields conditional to both transmissivity and piezometric data; 2, Demonstration on a synthetic aquifer. *Journal of Hydrology*, 203(1-4), pp. 175-188.

Capilla, J.E., Rodrigo, J. and Gomez-Hernandez, J.J., (1999) Simulation of non-gaussian transmissivity fields honoring piezometric data and integrating soft and secondary information. *Mathematical Geology*, 31(7), pp. 907-927.

Carrera, J. and Neuman, S.P., (1986a) Estimation of aquifer parameters under transient and steady state conditions; 1, Maximum likelihood method incorporating prior information. *Water Resources Research*, 22(2), pp. 199-210.

Carrera, J. and Neuman, S.P., (1986b) Estimation of aquifer parameters under transient and steady state conditions; 2, Uniqueness, stability, and solution algorithms. *Water Resources Research*, 22(2), pp. 211-227.

Carrera, J. and Neuman, S.P., (1986c) Estimation of aquifer parameters under transient and steady state conditions; 3, Application to Synthetic and Field data. *Water Resources Research*, 22(2), pp. 228-242.

Carrera, J., Navarrina, F., Viues, L., Heredia, J. and Medina, A., (1990) Computational aspects of the inverse problem. In: G. Gambolati, A. Rinaldo, C.A. Brebbia, W.G. Gray and F. Pinder George (Editors), *Computational methods in subsurface hydrology*. Comput. Mech. Publ., Southampton, United Kingdom, pp. 513-522.

Carrera, J., Medina, A., Axness, C. and Zimmerman, T., (1997) Formulations and computational issues of the inversion of random fields. In: G. Dagan and S.P. Neuman (Editors), *Subsurface Flow and Transport: A Stochastic Approach*. International Hydrology Series. Cambridge University Press, pp. 62-79.

Carrera, J., Alcolea, A., Medina, A., Hidalgo, J. and Slooten, L.J., (2005) Inverse problem in hydrogeology. *Hydrogeology Journal*, 13(1), pp. 206-222.

Chu, L., Reynolds, A.C. and Oliver, D.S., (1995) Computation of sensitivity coefficients for conditioning the permeability field to well-test pressure data. *In Situ*, 19(2), pp. 179-223.

Cooley, R.L., (1977) A method of estimating parameters and assessing reliability for models of steady state groundwater flow; 1, Theory and numerical properties. *Water Resources Research*, 13(2), pp. 318-324.

Cooley, R.L., (1979) A method of estimating parameters and assessing reliability for models of steady state groundwater flow; 2, Application of statistical analysis. *Water Resources Research*, 15(3), pp. 603-617.

Cooley, R.L., (1982) Incorporation of prior information on parameters into nonlinear regression groundwater flow models; 1, Theory. *Water Resources Research*, 18(4), pp. 965-976.

Cooley, R.L., (1983) Incorporation of prior information on parameters into nonlinear regression ground-water flow models; 2, Applications. *Water Resources Research*, 19(3), pp. 662-676.

Dagan, G., (1985) Stochastic modeling of groundwater flow by unconditional and conditional probabilities; the inverse problem. *Water Resources Research*, 21(1), pp. 65-72.

Dagan, G., Rubin, Y., (1988) Stochastic identification of recharge, transmissivity, and storativity in aquifer transient flow; a quasi-steady approach. *Water Resources Research*, 24(10), pp. 1698-1710.

de Marsily, G., Delhomme, J.P., Coudrain-Ribstein, A., Lavenue, A.M., (2000) Four Decades of Inverse Problems in Hydrogeology. *Geophysical Society of America*, Special Paper 348.

Deutsch, C.V., (2002) *Geostatistical Reservoir Modeling*. Oxford University Press. 384p.

Dietrich, C.R., Newsam, G.N., Anderssen, R.S., Ghassemi, F. and Jakeman, A.J., (1989) A practical account of instabilities in identification problems in groundwater systems. *BMR Journal of Australian Geology and Geophysics*, 11, pp. 273-284.

Dogru, A.H. and Seinfeld, J.H., (1981) Comparison of sensitivity coefficient calculation methods in automatic history matching. *Society of Petroleum Engineers Journal*, pp. 551-557.

Draper, D., (1995) Assessment and propagation of model uncertainty. *Journal of the Royal Statistical Society Series B*, 57, pp. 45-97.

Emsellem, Y. and de Marsily, G., (1971) An automatic Solution for the inverse problem. *Water Resources Research*, 7(5), pp. 1264-1283.

Ginn, T.R., Cushman, J.H., (1990) Inverse methods for subsurface flow. *Stochastic Hydrology and Hydraulics*, 4, pp. 1-26.

Gomez-Hernandez, J.J., Sahuquillo, A. and Capilla, J.E., (1997) Stochastic simulation of transmissivity fields conditional to both transmissivity and piezometric data; I, Theory. *Journal of Hydrology*, 203(1-4), pp. 162-174.

Goovaerts, P., (1997) *Geostatistics for Natural Resources Evaluation*. Oxford University Press. 496p.

Gutjahr, A., Wilson, J.L., (1989) Co-kriging for stochastic flow models. In: G. de Marsily (Ed.), *The stochastic approach to subsurface flow., 4; 6, Transport in Porous Media* (Ed. by G. de Marsily), D. Reidel Publishing Company, Dordrecht, International. pp. 585-598.

Journel, A.G., Huijbregts, C.J., (1978) *Mining Geostatistics*. Academic Press, London. 600p.

Kitanidis, P.K. and Vomvoris, E.G., (1983) A geostatistical approach to the inverse problem in groundwater modeling (steady state) and one-dimensional simulations. *Water Resources Research*, 19(3), pp. 677-690.

Landa, J.L. and Horne, R.N., (1997) A procedure to integrate well test data, reservoir performance history and 4-D seismic information into a reservoir description, *SPE Paper 38653 presented at SPE Annual Technical Conference and Exhibition*. Society of Petroleum Engineers, San Antonio, TX, pp. 177-192.

Loaiciga, H.A., Marino, M.A., (1986) On solution of the inverse problem for confined aquifer flow via maximum likelihood. *Mathematical Geology*, 18(7), pp. 677-692.

Loaiciga, H.A., Marino, M.A., (1987) Parameter estimation in groundwater: classical, Bayesian, and deterministic assumptions and their impact on management policies. *Water Resources Research*, 23(6), pp. 1027-1035.

McLaughlin, D., Townley, L.R., (1996) A reassessment of the groundwater inverse problem. *Water Resources Research*, 32(5), pp. 1131-1161.

Medina, A. and Carrera, J., (2003) Geostatistical inversion of coupled problems: dealing with computational burden and different types of data. *Journal of Hydrology*, 281(4), pp. 251-264.

Neuman, S.P., (1973) Calibration of distributed parameter groundwater flow models viewed as a multiple-objective decision process under uncertainty. *Water Resources Research*, 9(4), pp. 1006-1021.

Oliver, D.S., (1994) Incorporation of transient pressure data into reservoir characterization. *In Situ*, 18(3), pp. 243-275.

RamaRao, B.S., LaVenue, A.M., de Marsily, G., and Marietta, M.G., (1995) Pilot point methodology for automated calibration of an ensemble of conditionally simulated transmissivity fields; 1, Theory and computational experiments. *Water Resources Research*, 31(3), pp. 475-493.

Sahuquillo, A., Capilla, J.E., Gomez Hernandez, J.J., Andreu, J., (1992) Conditional simulation of transmissivity fields honoring piezometric data. In: B.a. Cabrera (Ed.), *Hydraulic Engineering Software IV, Fluid Flow Modeling, II, Elsevier Applied Science* (Ed. by B.a. Cabrera), Elsevier. pp. 201-214.

Sykes, J.F., Wilson, J.L. and Andrews, R.W., (1985) Sensitivity analysis for steady state groundwater flow using adjoint operators. *Water Resources Research*, 21(3), pp. 359-371.

Spall, J.C., (1992) Multivariate stochastic approximation using a simultaneous perturbation gradient approximation. *IEEE Transactions on Automatic Control*, 37, pp. 332-341.

Spall, J.C., (1998) Implementation of the simultaneous perturbation algorithm for stochastic optimization. *IEEE Transactions on Aerospace and Electronic Systems*, 34, pp. 817-823.

Spall, J.C., (2003) Simultaneous Perturbation Stochastic Approximation, *Introduction to Stochastic Search and Optimization: Estimation, Simulation, and Control, Wiley-Interscience series in discrete mathematics*. John Wiley and Sons, Inc., Hoboken, New Jersey. pp. 177-230

Spall, J.C., (2003) *Introduction to Stochastic Search and Optimization: Estimation, Simulation, and Control*. John Wiley and Sons, Inc., Hoboken, New Jersey. 525p.

Sun, N.Z., Yeh, W.W.G., (1992) A stochastic inverse solution for transient groundwater flow; parameter identification and reliability analysis. *Water Resources Research*, 28(12), pp. 3269-3280.

Sun, N.Z., Jeng, M.C., Yeh, W.W.G., (1995) A proposed geological parameterization method for parameter identification in three-dimensional groundwater modeling. *Water Resources Research*, 31(1), pp. 89-102.

Townley, L.R., Wilson, J.L., (1985) Computationally efficient algorithms for parameter estimation and uncertainty propagation in numerical models of groundwater flow. *Water Resources Research*, 21(1), pp. 1851-1860.

Wang, Y. and Kovscek, A., (2000) A streamline approach for history-matching production data, *SPE Paper 59370 presented at SPE/DOE Improved Oil Recovery Symposium*, Tulsa, Oklahoma, pp. 1-8.

Wen, X.H., Capilla, J.E., Deutsch, C.V., Gomez-Hernandez, J.J. and Cullick, A.S., (1999) A program to create permeability fields that honor single-phase flow rate and pressure data. *Computers & Geosciences*, 25, pp. 217-230.

Wen, X.H., Deutsch, C.V. and Cullick, A.S., (2002) Construction of geostatistical aquifer models integrating dynamic flow and tracer data using inverse technique. *Journal of Hydrology*, 255, pp. 151-168.

Wen, X.H., Deutsch, C.V., Cullick, A.S. and Reza, Z.A., (2005) Integration of production data in generating reservoir models. *Centre for Computational Geostatistics Monograph Series*, 1. Centre for Computational Geostatistics, pp. 85-93.

Woodbury, A.D., Smith, L., Dunbar, W.S., (1987) Simultaneous inversion of hydrogeoloic and thermal data; 1, Theory and application using hydraulic head data. *Water Resources Research*, 23(8), pp. 1586-1606.

Xue, G. and Datta-Gupta, A., (1997) Structure preserving inversion: An efficient approach to conditioning stochastic reservoir models to dynamic data, *SPE Paper 38727* *presented at 1997 SPE Annual Technical Conference and Exhibition*. SPE, San Antonio, TX, pp. 101-113.

Yeh, W.W.G., (1986) Review of parameter identification procedures in groundwater hydrology: The inverse problem. *Water Resources Research*, 22(2), pp. 95-108.

Yeh, T.C.J., Zhang, J., (1996) A geostatistical inverse method for variably saturated flow in the vadose zone. *Water Resources Research*, 32(9), pp. 2757-2766.

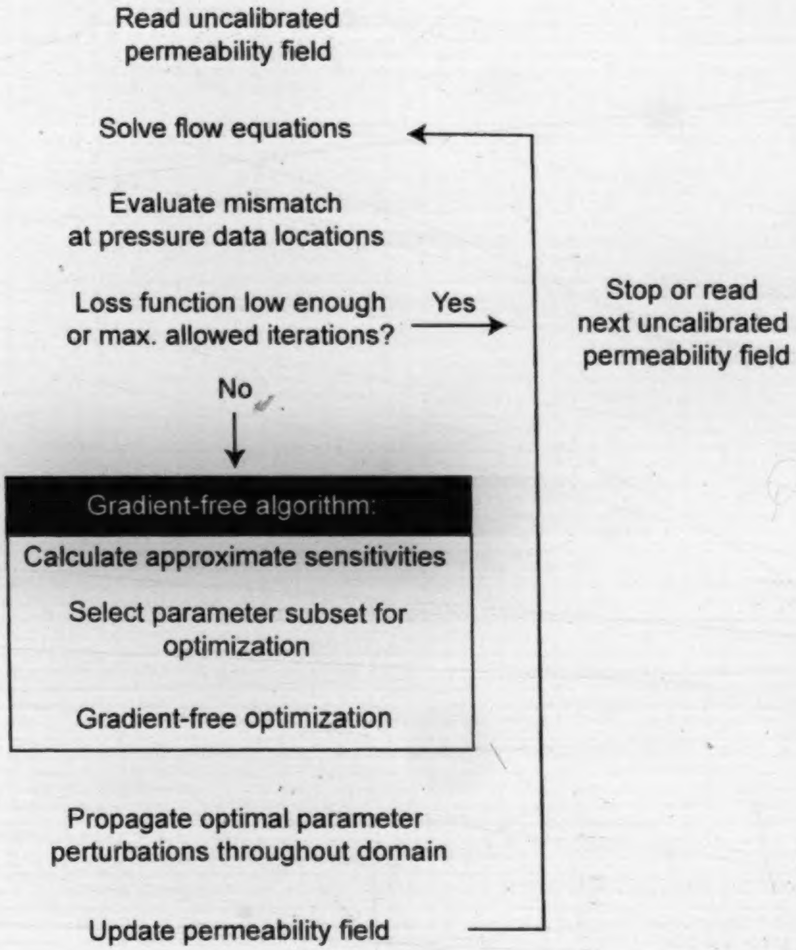
Read uncalibrated permeability field
Solve flow equations
Evaluate mismatch at pressure data locations
Loss function low enough or max. allowed iterations?
Yes
Stop or read next uncalibrated permeability field
No
Gradient-free algorithm:
Calculate approximate sensitivities
Select parameter subset for optimization
Gradient-free optimization
Propagate optimal parameter perturbations throughout domain
Update permeability field

Figure 6.1. General flow chart depicting the Sequential Self Calibration (SSC) algorithm with gradient-free method (boxed) incorporated.

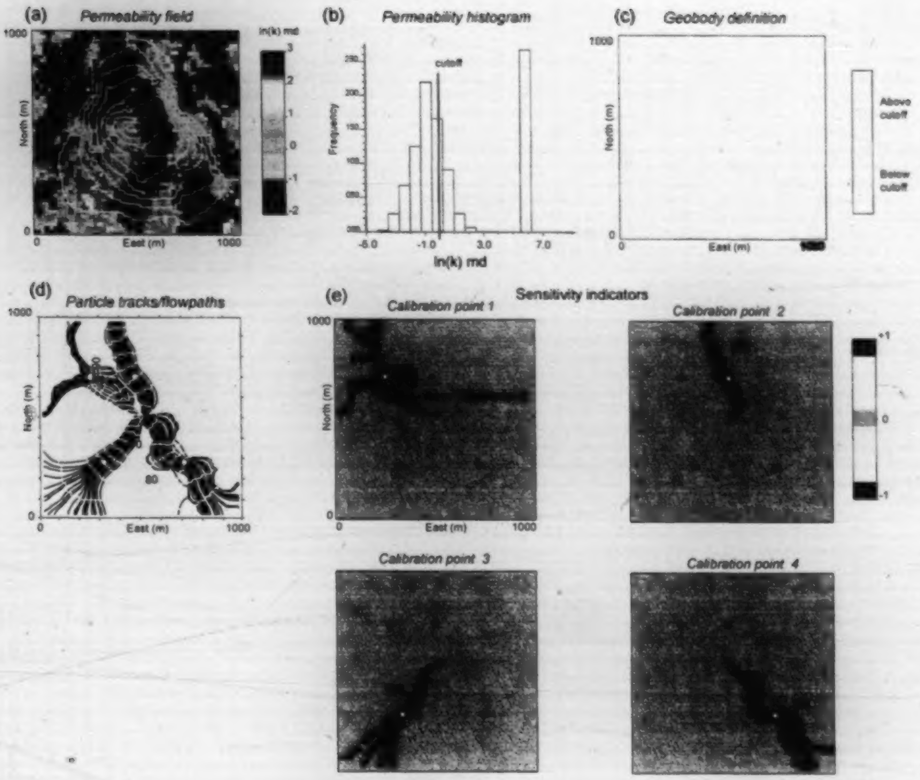

Figure 6.2. The process of obtaining approximate sensitivity indicators of head response at four calibration locations to the permeability field. (a) Permeability field structure, locations of calibration data, and contours of head due to pumping well at centre of model; (b) histogram of lognormal transform of permeability with ln(k) cutoff of 0.0 used to define two classes of geobodies; (c) binary geobody classification defining relatively transmissive and flow-retarding geobodies; (d) streamline tracks intersecting the four calibration data locations; (e) sensitivity indicator maps corresponding to the vector of sensitivity for each calibration location. Numbered geobodies are referenced in text.

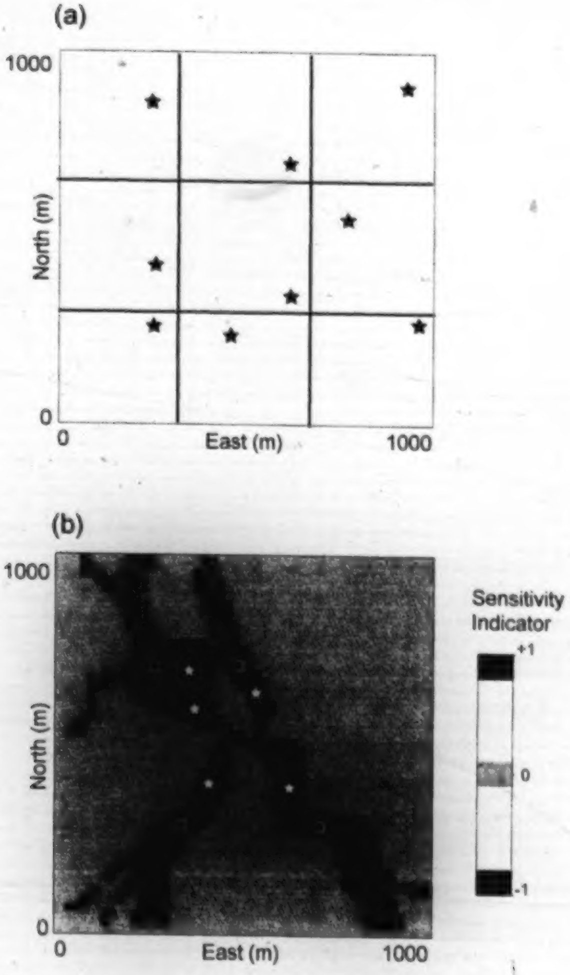
(a)
1000
North (m)
0
0
East (m)
1000
(b)
1000
North (m)
0
0
East (m)
1000
Sensitivity Indicator
+1
0
-1

Figure 6.3. Comparison of the parameterization scheme preceding the optimization routine in (a) the original SSC method, which uses a random stratified sampling scheme; and (b) the gradient-free approach which uses the prior prediction of sensitivities to constrain the random drawing of a parameter subset (stars) to sensitive areas of the model given a specific configuration of calibration data (circles).

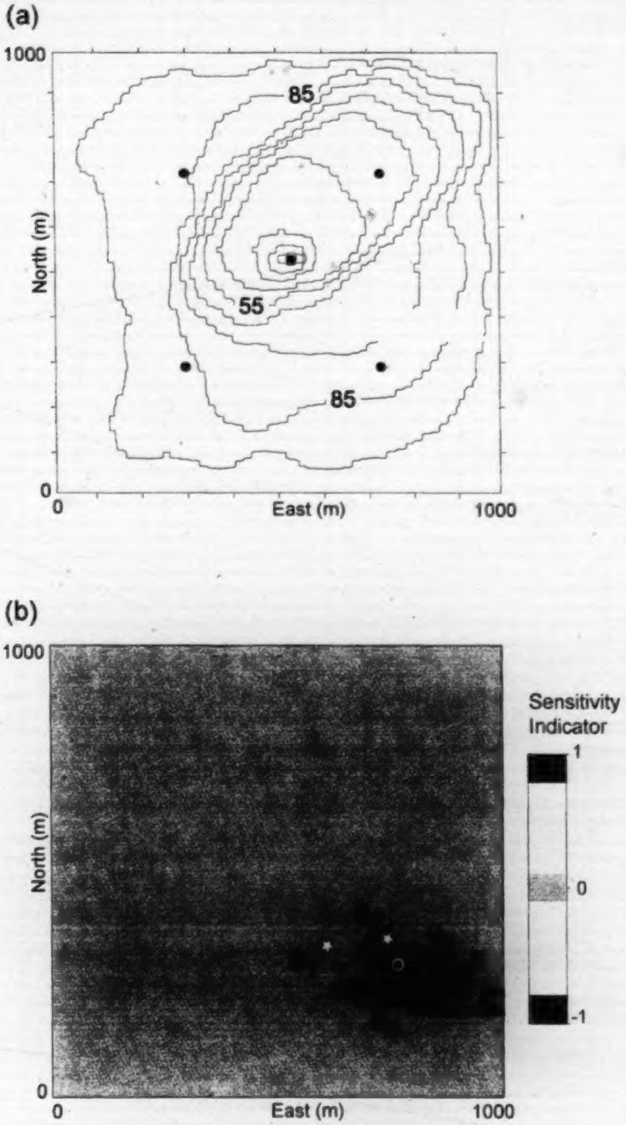

Figure 6.4. An example of the parameterization of the optimization to reduce the head mismatch at a specific calibration location. (a) The initial head solution and the head mismatch at a calibration data location; (b) the vector of sensitivity indicators and a selected parameter subset $\{\theta\}$ corresponding to sensitive grid cells to the response calibration data location.

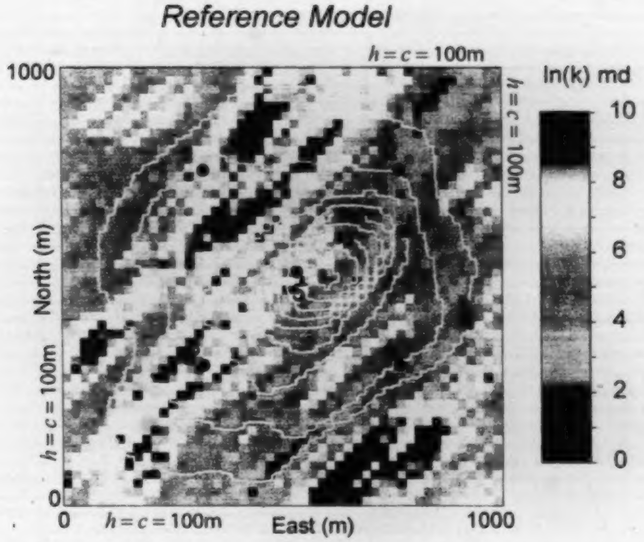
Reference Model
h = c = 100m
1000
ln(k) md
10
8
6
4
2
0
h = c = 100m
North (m)
h = c = 100m
0
0
h = c = 100m
East (m)
1000

Figure 6.5. Reference permeability field (I) and steady state head solution. Calibration points are numbered 1-5. The specified flux at the centre of the domain produces a heterogeneous drawdown pattern as indicated by hydraulic head contours labeled in units of metres.

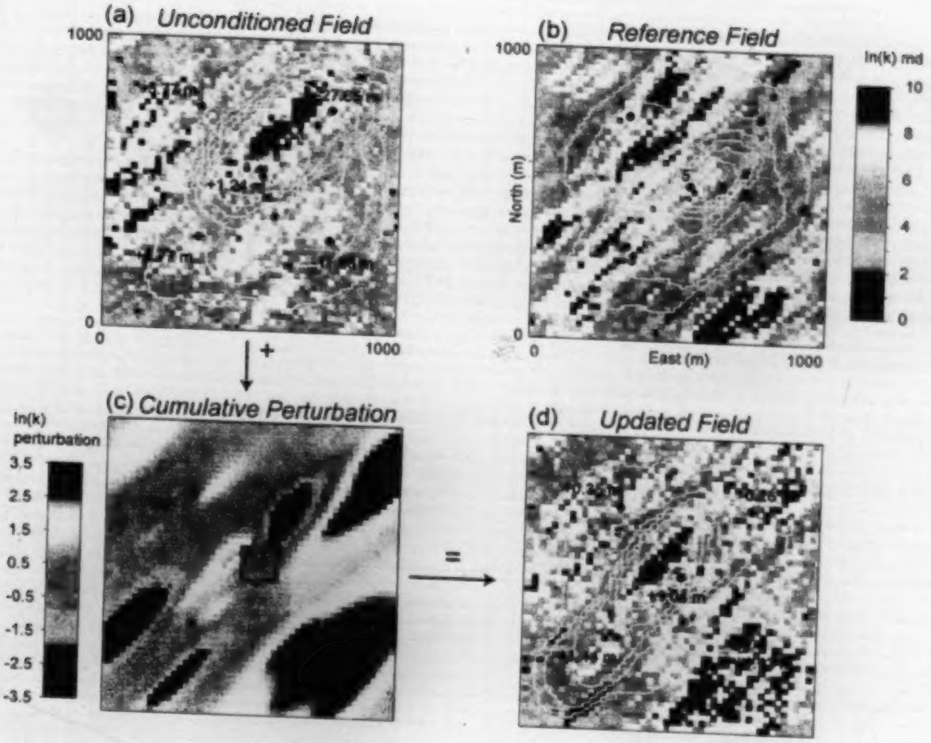
(a) Unconditioned Field
1000
0
0
1000
+
(b) Reference Field
1000
North (m)
5
0
0
East (m)
1000
ln(k) md
10
8
6
4
2
0
(c) Cumulative Perturbation
ln(k) perturbation
3.5
2.5
1.5
0.5
-0.5
-1.5
-2.5
-3.5
=
(d) Updated Field

Figure 6.6. Results of a synthetic calibration using the gradient-free method: (a) initial ln(k) field with steady-state head solution contours and initial head mismatch at calibration points 1-5; (b) reference model (I); (c) cumulative ln(k) perturbation field to arrive at calibrated permeability field; (d) calibrated ln(k) field with head solution and final head mismatch. Square region in (c) was frozen to prevent propagation of parameter perturbations near the central flux well.

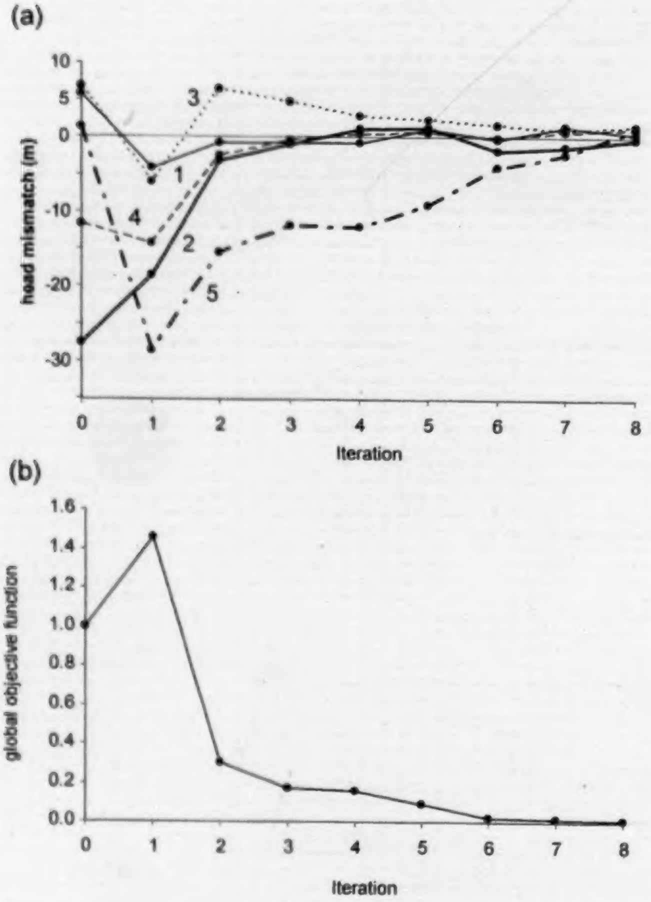

Figure 6.7. Gradient-free calibration progress for a single initial permeability field realization: (a) plot of absolute head errors versus outer iteration for calibration points 1-5; (b) plot of global objective function versus iteration number.

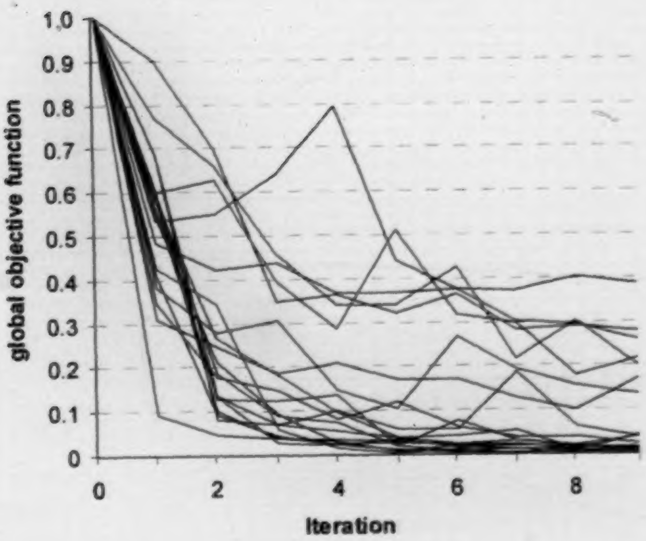

Figure 6.8. Convergence behaviour of gradient-free conditioning for an ensemble of 20 realizations.

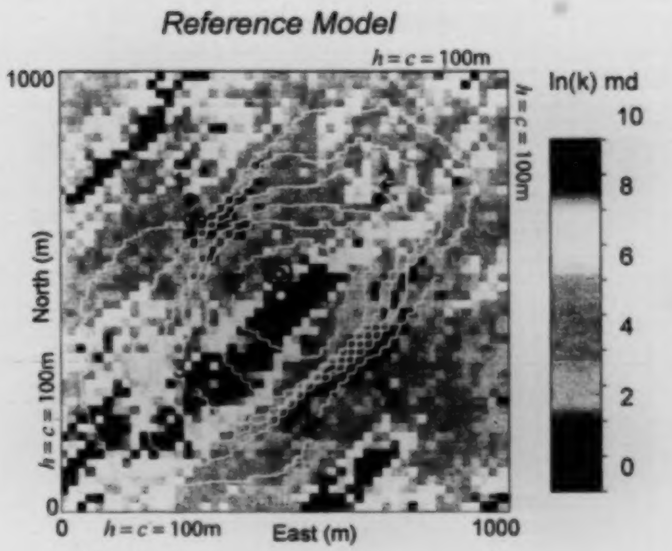

Figure 6.9. Reference permeability field (II) used for the demonstration of the types of features that can be consistently identified from a set of calibration head data.

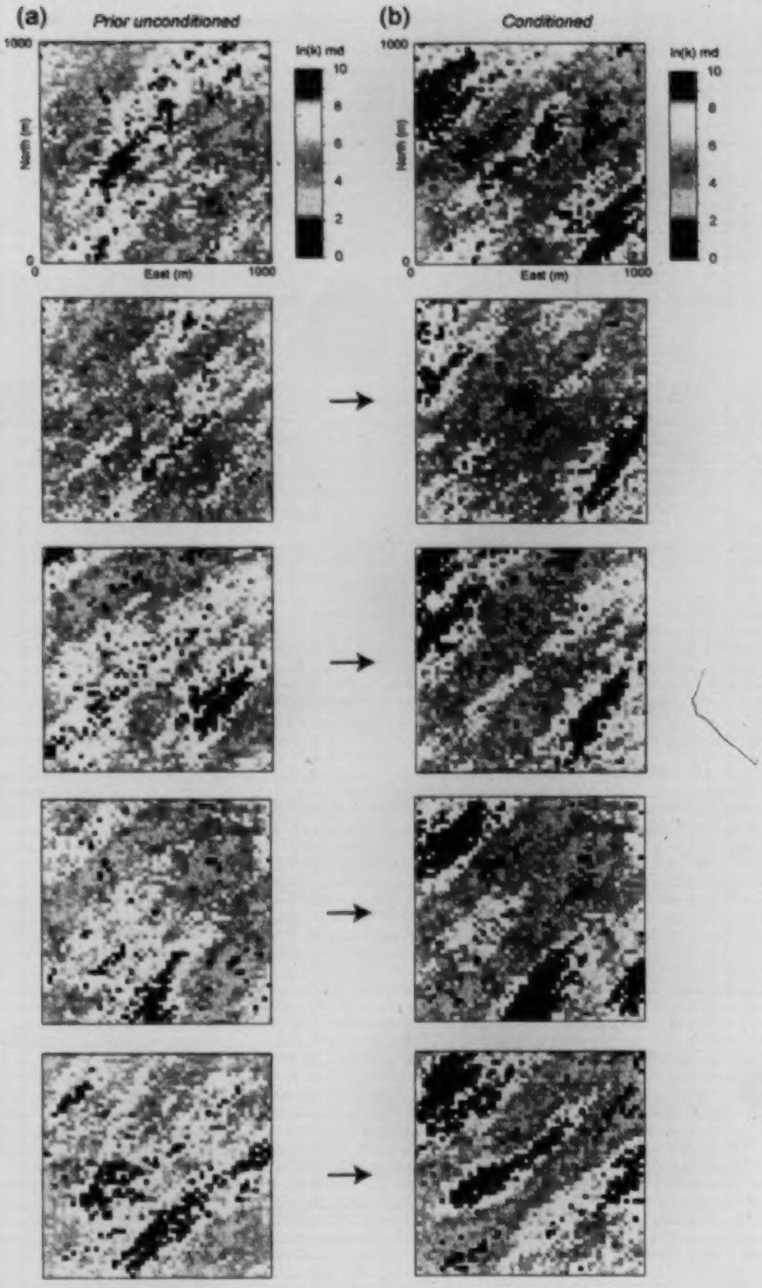

Figure 6.10. Gradient-free calibration results shown on five realizations: (a) initial unconditional fields; (b) corresponding calibrated fields conditioned to calibration head data 1-4.

(a) *Reference Field*

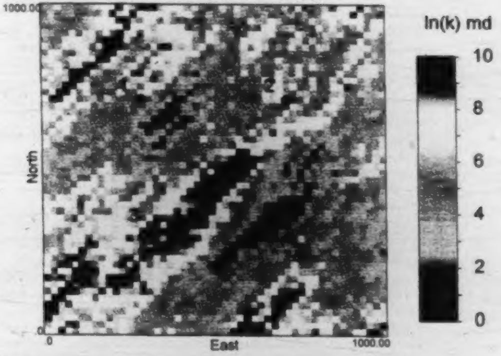
1000.00
North
0
0
East
1000.00
2
3
ln(k) md
10
8
6
4
2
0

(b) *E-Type: Prior unconditioned*

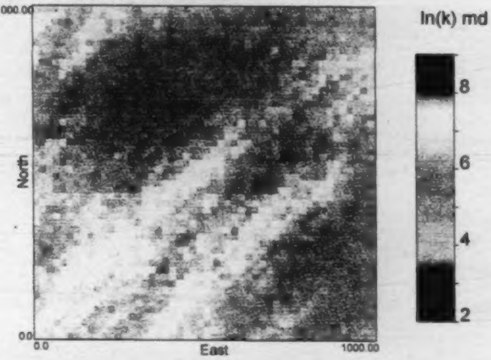
1000.00
North
0.0
0.0
East
1000.00
ln(k) md
8
6
4
2

(c) *E-Type: Conditioned*

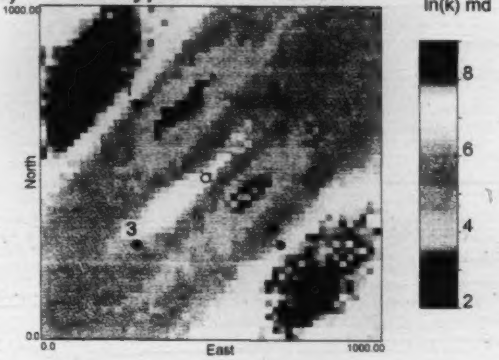
1000.00
North
0.0
0.0
East
1000.00
3
ln(k) md
8
6
4
2

Figure 6.11. Identification of low-permeability features: (a) Reference permeability field (II) on which calibration data at C.P. 1-4 are collected; (b) Ensemble average (E-Type map) of 20 initial unconditional realizations; (c) E-type of calibrated realizations conditioned to calibration head data.

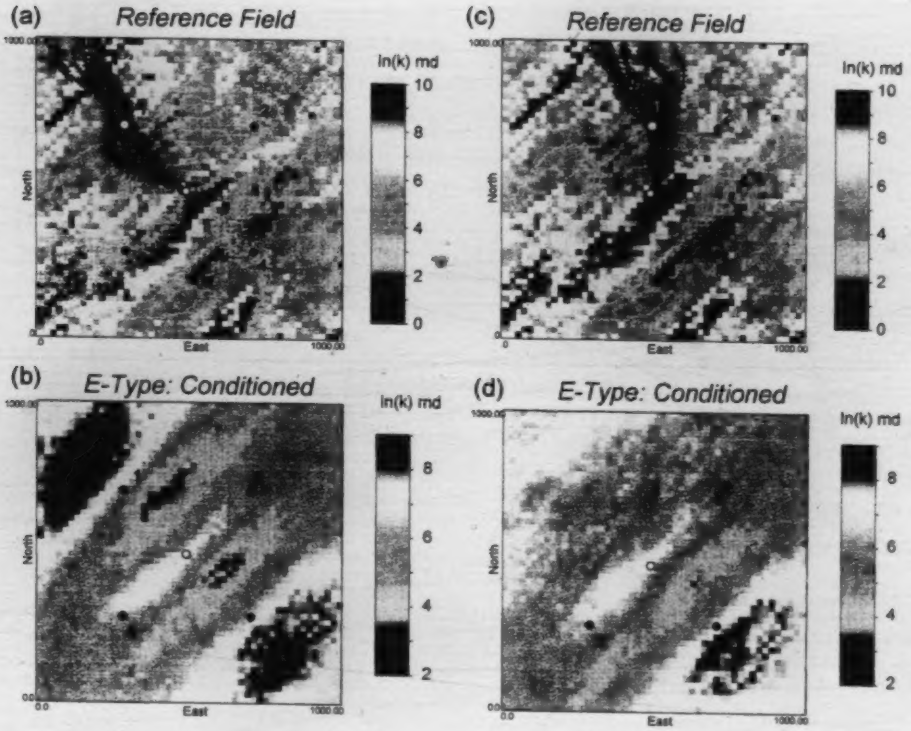
(a)
Reference Field
ln(k) md
10
8
6
4
2
0
North
East
1000.00
0
(c)
Reference Field
ln(k) md
10
8
6
4
2
0
North
East
1000.00
0
(b)
E-Type: Conditioned
ln(k) md
8
6
4
2
North
East
1000.00
0.0
(d)
E-Type: Conditioned
ln(k) md
8
6
4
2
North
East
1000.00
0.0

Figure 6.12. Controls on the identification of low permeability features by inverse conditioning: (a) Reference permeability field II with head solution, calibration data locations, and "swaths" of flowlines intersecting effective zone of information of each calibration data location -- note that all of the important heterogeneities controlling the flow response are "sampled" by the calibration data in this configuration; (b) E-type map of 20 calibrated realizations showing reasonably good local precision in identifying the key features; (c) Reference field II with calibration point C.P. 1 moved 220 m east of original location. The corresponding flowlines indicate that the low permeability feature identified by the original position of calibration point 1 is bypassed; (d) E-type map of 20 calibrated realizations showing the effect of the alternate calibration data configuration -- the low permeability feature is not identified.

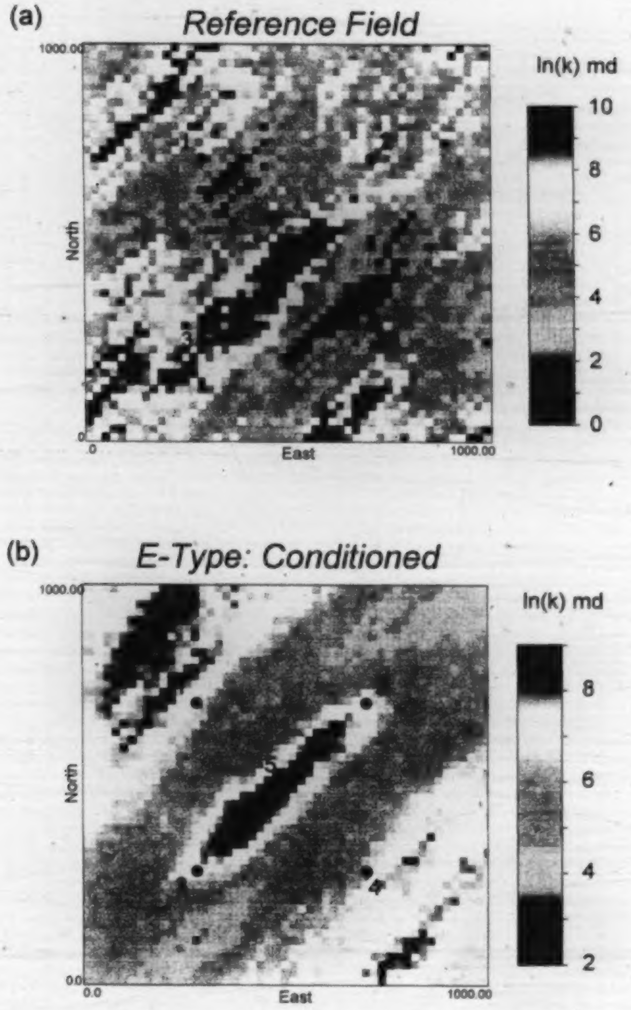

Figure 6.13. Partial identification of a high-transmissivity conduit: (a) Reference permeability field II showing calibration data 1-5; (b) E-type of calibrated realizations conditioned to calibration head data.

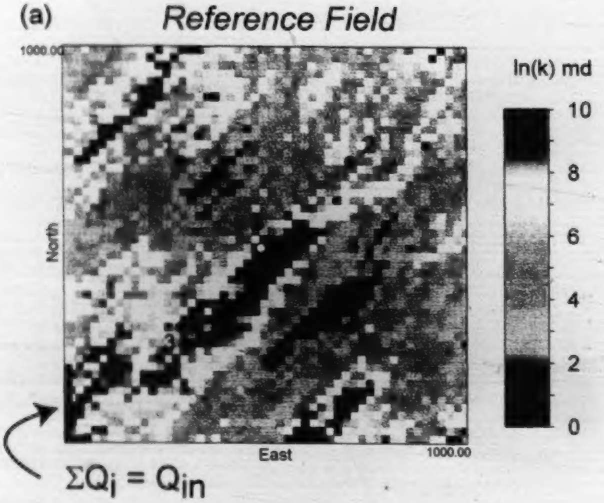
(a)
Reference Field
1000.00
North
East
1000.00
ln(k) md
10
8
6
4
2
0
2
3
ΣQi = Qin

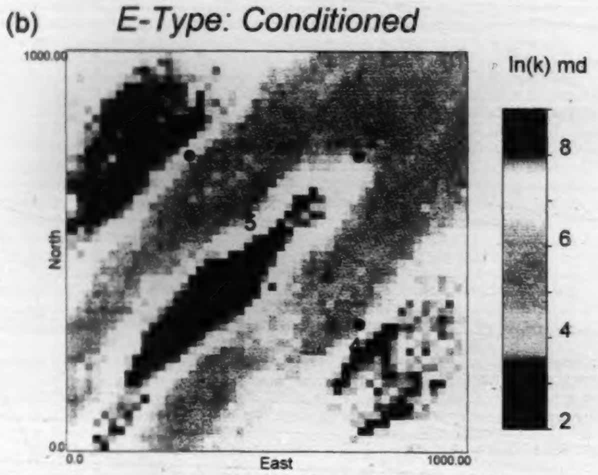
(b)
E-Type: Conditioned
1000.00
North
0.0
0.0
East
1000.00
ln(k) md
8
6
4
2
5

Figure 6.14. Complete identification of a high-transmissivity conduit: (a) Reference permeability field (II) with the addition of additional flux boundary condition in the SW; (b) E-type of calibrated realizations conditioned to calibration head data.

| $\theta_M$ | sens. indicator | $\Delta$ | $\Delta\ln(k)$ direction | $\left(\hat{\theta}_l \pm c_l \Delta\right)$ |
|---|---|---|---|---|
| $\theta_1$ | -1 | -1 | decrease | $\left(\hat{\theta}_l + c_l \Delta\right)$ |
| $\theta_2$ | -1 | -1 | decrease | $\left(\hat{\theta}_l + c_l \Delta\right)$ |
| $\theta_3$ | +1 | +1 | increase | $\left(\hat{\theta}_l + c_l \Delta\right)$ |
| $\theta_4$ | +1 | +1 | increase | $\left(\hat{\theta}_l + c_l \Delta\right)$ |

Table 6-1. Explanation of relationship between sign of sensitivity indicator at selected parameter locations (Column 2); the perturbation vector Δ (Column 3); the required direction of parameter change needed to reduce the head mismatch at a calibration data location (Column 4); and the appropriate ± expression for the loss function evaluation (Column 5). The negative head mismatch necessitates the updates to the parameters specified by columns 4 and 5.

| $\theta_M$ | sens. indicator | $\Delta$ | $\Delta\ln(k)$ direction | $\left(\hat{\theta}_l \pm c_l \Delta\right)$ |
|---|---|---|---|---|
| $\theta_1$ | -1 | -1 | increase | $\left(\hat{\theta}_l - c_l \Delta\right)$ |
| $\theta_2$ | -1 | -1 | increase | $\left(\hat{\theta}_l - c_l \Delta\right)$ |
| $\theta_3$ | +1 | +1 | decrease | $\left(\hat{\theta}_l - c_l \Delta\right)$ |
| $\theta_4$ | +1 | +1 | decrease | $\left(\hat{\theta}_l - c_l \Delta\right)$ |

Table 6-2. In the case of a positive head mismatch at the calibration data location, columns 4 and 5 are opposite to the values shown in Table (6-1).

# 7.0 CONCLUSIONS

## 7.1 WEYBURN AREA HYDROGEOLOGICAL CHARACTERIZATION

The north-central Williston Basin is an area where the confluence of the three major groups of formation waters found within the basin, and within the world's sedimentary basins, is observed: (1) fresh waters with dominant major ionic constituents other than Na and Cl, (2) Na-Cl brackish waters to brines, and (3) halite-saturated brines with Ca as a dominant cationic species. Within any given Paleozoic aquifer in the Williston Basin, and within the current study area, all three of these major compositions are present.

There are five principal water types, all belonging to the three major compositions mentioned above. Type (1) waters represent a plume of fresh Ca-$SO_4$ water recharging Williston Basin aquifers. Type (2) waters represent evolved Na-Cl brines. Type (3) waters are Ca-Cl brines that are found exclusively within the pre-Mississippian Paleozoic aquifers. Type (4) waters have a low TDS Na-$HCO_3$ composition and are only found in the Mesozoic aquifers. Type (5) waters are brackish to saline, have a Na-$SO_4$ composition, and are formed by mixing between Type (1) recharge waters and Na-Cl brines (Type 2).

The absence of Type (3) brines in the Mississippian aquifers is an important observation because there is no hydrogeological reason that the compositions of the hypersaline brines should be different between the pre-Mississippian and Mississippian aquifers. This invokes the debated hypothesis of secular variation of global seawater chemistry through geological time.

Hydraulic heads in the Deep Paleozoic aquifers drive formation waters across the study area in a generally northeasterly direction. Fluid flow is primarily parallel to aquifer confining surfaces with potentiometric surfaces of the aquifers indicating little dependence between fluid potentials and depth. Within the Mississippian aquifers, hydraulic heads exhibit similar large-scale trends to the underlying Deep Paleozoic aquifer group. Patterns of brine migration suggest that the current hydrodynamic regime of the Williston Basin is in a transient relaxation from a period of peak energy which resulted in hydraulic gradients significantly higher than those observed at present. High formation-water densities in the Paleozoic aquifers result in large areas characterized by down-dip, basin-inward flows where "sinking" formation waters tend to oppose the updip-directed driving force due to the potentiometric gradients. The fact that the dense brines occur at locations where they are gravitationally unstable indicates that such locations have been positions where the brines were in positions of gravitational equilibria, when hydraulic gradients were sufficient to displace the brines updip and overcome the tendency to sink back toward lower elevations in the basin. In other areas where the present hydraulic gradient is sufficient to counter, or balance this tendency to flow back down dip to a position of static equilibrium, the brines continue to move slowly updip, or stagnate in place, respectively.

Hydraulic heads in the Mesozoic aquifers imply significant differences in the hydraulics of the Mesozoic aquifer group from the deeper systems. High transmissivity aquifers and associated underpressuring reflect efficient pressure drainage due to Mesozoic aquifer outcrops along the Manitoba escarpment to the northeast of the study area. Although vertical pressure versus depth profiles indicate predominantly hydrostatic pressures and horizontal formation water flow though the entire hydrogeologic section within the study area, notable exceptions include large-scale underpressuring and upward cross-formational flow in the northeast due to the pressure drainage initiated in the Mesozoic aquifer system, and cross-formational flow in the west of the study area at the interface between a regional plume of recharging fresh water and Williston Basin brines. The absence of brines within the Mesozoic aquifer system and the unique hydrochemical signature of the Type (5) waters suggest that the Mesozoic aquifer system is hydraulically separated from the underlying Mississippian system within most of the current study area.

Mississippian hydrodynamics and hydrochemistry indicate that there are significant differences between individual Mississippian aquifers, thus showing that the common assumption made in all previous studies that the Mississippian system may be treated as a single aquifer is an unwarranted oversimplification. The majority of the Mississippian subcrop between the Alida to Midale Beds is a barrier to formation water flow, as indicated by flow directions inferred from potentiometric surfaces, and a lack of a vertical component to flow, as determined from vertical pressure-depth profiles. However, leakage across the (lower) Mississippian subcrop in the northeast of the study area is apparent. Detailed mapping of the hydrochemistry of the Mississippian aquifers delineates the position and extent of the plume of Type (1) waters recharging this aquifer system, and is useful for understanding trends in crude oil gravity along the Mississippian subcrop.

The oil reservoirs along the Mississippian subcrop are likely not filled to capacity. The anhydritic seal rock facies underlying the subcrop is unlikely to leak via capillary failure to a separate hydrocarbon phase. However, during periods of elevated paleo-fluid pressures, such as at the onset of the Laramide Orogeny, the sealing lithofacies would have likely failed hydraulically via the wedging-open of pre-existing fractures.

Storage of injected $CO_2$ in the oil reservoirs along the Mississippain subcrop appears to be feasible given the high capillary breakthrough pressures calculated for the sealing lithofacies at the location of the Weyburn Field (Li et al., 2005). However, given that fracturing is known to exist in the Weyburn reservoir, and, by extension, the Midale caprock, a hydraulic seal model, where breakthrough pressures are governed by capillary leakage through fractures may be a better (and more conservative) model.

### 7.1.1 Scientific and technological contributions

The detailed hydrogeological characterization contained in Chapters 2, 3, and 4 is unprecedented in the Williston Basin. The hydrostratigraphic resolution was achieved by diligent assignment of hydrogeological data within the framework delineated by a consistent dataset of formation tops picked by a small team of Geologists for the Weyburn Project (Whittaker et al., 2004). Density-dependent flow was considered in conjunction with potentiometric mapping, which was critical for evaluating the local hydrodynamic force regime. Vertical integration through pressure-depth profiles and hydraulic and hydrochemical cross-sections enabled an understanding of the system in three-dimensions. A location-specific classification scheme for formation waters which encompassed both global observations (e.g., Hanor, 1994) and local compositional variations enabled the interpretation of the formation fluid history on multiple time scales. Future regional hydrogeological studies in sedimentary basins may adopt the methods and synthesis of the mapping components presented in this work for successful results elsewhere. In this respect this work is exemplary.

The scope of the hydrogeological characterization led to two specific interpretations which redefine and update the conceptual model for paleo-hydrogeology in the Williston Basin:

1. A marked contrast in the brine chemical compositions between the deep Paleozoic (Cambrian to Upper Devonian) and the Mississippian aquifers in the study area support the hypothesis of secular oscillations in global seawater chemistry. To date some of the strongest evidence supporting this hypothesis has come from fluid inclusion studies (Lowenstein et al., 2001; Horita et al., 2002), but evidence from variations in formation water samples has not been postulated prior to this work.

2. The quantification of brine migration patterns including the effects of density are interpreted as a direct indication of the magnitude of the Laramide hydrodynamic event in the Williston Basin, and defines the nature of the transience in the basin flow system.

### 7.1.3. Recommended areas of future research

The Williston Basin appears to be an important area for the study of the controls on the stratigraphic and thus age-related distribution of primary brine compositions. There is good reason, based on hydrodynamics observed within the study area, to speculate that the bulk hydrochemistry of brines in the basin has largely remained stratigraphically confined, such that, to a first order, connate chemical compositions are reflected in the brine compositions observed today[1]. Williston basin hydrochemistry provides further support for the position that $CaCl_2$ brines observed in sedimentary basins represent primary seawater compositions formed during periods of rapid seafloor spreading and associated high influxes of mid-ocean-ridge brines (Hardie, 1996; Stanley and Hardie, 1998; Lowenstein et al., 2003). It will be of interest to continue to sample and map the distributions of brine compositions beyond the study area of this work to confirm consistency in the interpreted results on a basin-wide scale.

There is evidence of an unmixed $Ca\text{-}Cl_2$ brine end member in the Williston Basin (Chapter 3; Jensen et al., 2006) which is rare, if not unique to the Williston Basin. Considering the compositions from Silurian fluid inclusions (Lowenstein et al., 2003) as a starting point, the samples observed in Williston Basin aquifers will enable testing alternative evolutionary models, including the effects of mineral-buffered reactions (Hanor, 1994; Hanor and McIntosh, 2006). Williston Basin brine samples will enable a more meaningful comparison of modeling results that assume a modern seawater composition as a starting point, with the results from models that consider $CaCl_2$ marine compositions as a starting point (Lowenstein et al., 2003), since it is now evident that formation water samples from other (North-American) intra-continental basins differ from what is observed in the Williston Basin.

## 7.2 GRADIENT-FREE INVERSE CONDITIONING

The gradient-free method works without the need for expensive or technically-involved computations of sensitivity coefficients and the associated gradient of the model response with respect to the parameters. A simple and effective approximation procures a matrix of sensitivity indicators as a substitute for the computation of the Jacobian matrix. A rules-based approach for determining the required parameter sensitivity information is based upon: (1) delineation of flowpaths relevant to the calibration head data, (2) transforming the permeability field into a categorical variable in order to define relatively high-transmissivity and low-permeability geobodies, and (3) identification of geobody connections to fluid sources or sinks in the model. Parameter optimization is based on the deterministic gradient information inferred from the sign on the sensitivity coefficients and the head mismatch at each calibration point. The optimization algorithm uses an approximation of the gradient of the model response with respect to the parameters that is adapted from a proven gradient-free optimization technique (SPSA).

---

[1] The term connate is used in its proper sense here, although loosely. Connate formation waters have remained within the pore spaces of the sediments in which they were deposited. Williston basin brines have undoubtedly been displaced, but have most likely remained largely within the aquifer systems in which they were deposited.

The gradient-free method solves the inversion problem in a similar manner as proven gradient-based calibration methods, but with a much more transparent approach. In particular, a multi-objective formulation of the optimization that is based on prior sensitivity information allows a deterministic sampling of the gradient space of the objective function with respect to each calibration location. This means that for a given calibration head data location, the direction of change in the permeability at any sensitive location that will result in a better calibration to the observed data is known. The basis for this deterministic knowledge of the gradient direction is in the sign on the parameter sensitivity and the sign of the head mismatch.

The gradient-free method is partly based on a streamtube approach, whereby the conditioning effect of each calibration data point is seeded within the area covered by the locus of streamlines that intersects the calibration data location, with sensitive areas predicted by additional structural criteria, coupled with the model specifications. From these insights, we are able to elucidate some key points with respect to the inverse conditioning to head data, including the controls on the information available from a given configuration of head data in identifying important heterogeneity features controlling the flow response. Specifically: key heterogeneities which impact the flow response must be sampled by the calibration data. A calibration data point "samples" a heterogeneity feature when it occurs along a flowline that intersects the feature. By this approach, the permeability field can be adjusted within sensitive areas, seeding locally precise perturbations to produce a head match at that calibration data location which results in an improvement in the local precision of the spatial uncertainty model from the conditioning process.

### 7.2.1 Scientific and technological contributions

Chapter 5 presents a straightforward concept with rather far-reaching implications. An understanding of the controls on the spatial structure of the sensitivity process for head — as contained in the Jacobian matrix — leads to the following technological elements:

1. A rules-based approach to obtaining a complete assessment of sensitivity of the modeled hydraulic head response at a subset of calibration locations to the parameters representing a discretized heterogeneous permeability field can be used in place of procedures to compute the Jacobian matrix.

2. The resultant system of sensitivities, which is comprised of binary sensitivity indicators for each parameter with the correct sign, leads naturally to a gradient approximation formulation for the minimization problem of finding the optimal parameter perturbations which reproduce a set of calibration data (the thesis of Chapter 6).

3. This gradient-free method — so named because the gradient of the objective function is obtained through an approximation rather than a direct computation — simplifies gradient-based formulations for inverse conditioning by reducing the need for specialized computer code and eliminates the CPU-intensive steps involved in minimization procedures requiring the Jacobian matrix.

4. The transparency of the gradient-free method, which results from a direct translation of the physical rules governing the sensitivity process to the constitutive elements of the algorithm, makes clear what to expect from inverse procedures in terms of identifying key heterogeneities in geological models from measurements of hydraulic head.

### 7.2.2 Recommended areas of future research

A comparison of the gradient-free method to other inverse-conditioning approaches was beyond the scope of Chapter 6. It would be of interest to do a comparison with other geostatistical inversion methods to test two hypotheses: (i) The gradient-free method offers a significant computational advantage when a large number of parameters is considered for parameter optimization (i.e., a significant percentage of the number of flow model grid blocks or elements) and for large numbers (i.e., greater than 10) of observation locations; (ii) Key heterogeneity features in synthetic fields, or real aquifers having a sound geological conceptual model, are better identified by the gradient free approach than other methods. The paper by Zimmerman et al. (1998) offers a framework for the comparison of different methods that could be adopted for such a study.

Although the gradient-free algorithm is built upon a deterministic assessment of the gradient direction (Chapter 6, Section 6.2.1; Appendix B), the SPSA optimization engine is designed for, and most powerful when measurements of the loss function are corrupted by noise (Spall, 2003). The introduction of stochastic approximation techniques that are designed to deal with noise in the minimization routines at the core of many inverse techniques used in groundwater modeling is itself a significant research contribution. A particular recommendation for future research follows directly from this: An *adaptive* SPSA optimization routine would be very powerful for complex inversion problems with large (time variant) data sets with possibly conflicting gradient information. Conflicting information may result from errors in the data or in the conceptual model such that the sensitivity information is misleading/incorrect, and thus confounds convergence of the algorithm. Although non-convergence is a good indication of model problems (Chapter 6, Section 6.3.2), it may be desirable to promote a convergent solution since the errors are often too difficult to filter out of the data, or the results of the solution will indicate the nature of model errors. An adaptive SPSA formulation that switches between the one-sided approach (Equation 6.4) and the standard two-sided formulation (Spall, 2003, p. 178) for problematic calibration points would be a simple, yet powerful, adaptation of the calibration algorithm developed in Chapter 6.

Extending the gradient-free approach to inversion problems dealing with multiple data types sampling system response variables is also an area that is ripe for exploration[2]. Stochastic minimization techniques would enable the integration of data types for which the sensitivity coefficients are not available because of a lack of a computationally-feasible method to obtain them[3], or ambiguity in the sensitivity process (e.g., to seismic attributes).

Finally, simply applying the gradient-free approach to a real aquifer with a rich dataset, such as any of the aquifers characterized in Chapters 2 and 4 for the Weyburn $CO_2$ project, would be a noteworthy contribution. This is an extension of Chapter 6 already slated for publication.

## 7.3 REFERENCES

Hardie, L.A., (1996) Secular variation in seawater chemistry: An explanation for the coupled secular variation in the mineralogies of marine limestones and potash evaporites over the past 600 m.y. *Geology*, 24(3), pp. 279-283.

Hanor, J.S., (1994) Origin of saline fluids in sedimentary basins. In: *Geofluids: Origin, Migration and Evolution of Fluids in Sedimentary Basins* (ed. J. Parnell)
Geological Society Special Publication 78, pp. 151-174.

Hanor, J.S., McIntosh, J.C., (2006) Are secular variations in seawater chemistry reflected in the compositions of basinal brines? *Journal of Geochemical Exploration*, 89(1-3), pp. 153-156.

Horita, J., Zimmerman, H., Holland, H.D., (2002) Chemical evolution of seawater during the Phanerozoic: Implications from the record of marine evaporites. *Geochimica et Cosmochimica acta*, 66(21), pp. 3733-3756.

---

[2] The most straightforward application would be to incorporate the gradient-free method for hydraulic head data into streamline-based sensitivity techniques for flow rate and concentration data (Wen et al., 2002).

[3] In comparison to the efficiency of the sensitivity process used in the gradient-free approach

Jensen, G.K.S., Rostron, B.J., Duke, M.J.M., Holmden, C., (2006) Bromine and stable isotopic profiles of formation waters from potash mine-shafts, Saskatchewan, Canada. *Journal of Geochemical Exploration*, 89(1-3), pp. 170-173.

Li, S., Dong, M., Li, Z., Huang, S., Qing, H., Nickel, E., (2005) Gas breakthrough pressure for hydrocarbon reservoir seal rocks: implications for the security of long-term $CO_2$ storage in the Weyburn field. *Geofluids*, 5(4), pp. 326-334.

Lowenstein, T.K., Timofeeff, M.N., Brennan, S.T., Hardie, L.A., Demicco, R.V., (2001) Oscillations in Phanerozoic seawater chemistry: Evidence from fluid inclusions. *Science*, 294, pp. 1086-1088.

Lowenstein, T.K., Hardie, L.A., Timofeeff, M.N., Demicco, R.V., (2003) Secular variation in seawater chemistry and the origin of calcium chloride basinal brines. *Geology*, 31(10), pp. 857-860.

Spall, J.C., (2003) Simultaneous Perturbation Stochastic Approximation, Introduction to Stochastic Search and Optimization: Estimation, Simulation, and Control. Wiley-Interscience series in discrete mathematics. John Wiley and Sons, Inc., Hoboken, New Jersey, pp. 177-230.

Stanley, S.M., Hardie, L.A., (1998) Secular oscillations in the carbonate mineralogy of reef-building and sediment-producing organisms driven by tectonically forced shifts in seawater chemistry. *Palaeogeography, Palaeoclimatology, Palaeoecology*, 144, pp. 3-19.

Wen, X.H., Deutsch, C.V. and Cullick, A.S., (2002) Construction of geostatistical aquifer models integrating dynamic flow and tracer data using inverse technique. *Journal of Hydrology*, 255, pp. 151-168.

Whittaker, S., Rostron, B.J., Khan, D., Hajnal, Z., Qing, H., Penner, L., Maathuis, H., Goussev, S., (2004) IEA GHG Weyburn CO2 Monitoring & Storage Project Summary Report 2000-2004. In: *Seventh International Conference on Greenhouse Gas Control Technologies, 1* (Ed. M. Wilson, M. Monea), Petroleum Technology Research Centre. pp. 15-69.

Zimmerman, D.A., de Marsily, G., Gotway, C.A., Marietta, M.G., Axness, C.L., Beauheim, R.L., Bras, R.L., Carrera, J., Dagan, G., Davies, P.B., Gallegos, D.P., Galli, A., Gomez-Hernandez, J.J., Grindrod, P., Gutjahr, A.L., Kitanidis, P.K., Lavenue, A.M., McLaughlin, D., Neuman, S.P., RamaRao, B.S., Ravenne, C., Rubin, Y., (1998) A comparison of seven geostatistically based inverse approaches to estimate transmissivities for modeling advective transport by groundwater flow. *Water Resources Research*, 34(6), pp. 1373-1414.

# APPENDIX A

## Additional details on methodologies for calculating driving forces on formation waters

## APPENDIX A: Details on Methodologies

### Potentiometric Analysis

Equivalent freshwater hydraulic heads are derived from point measurements of pore pressures by the relation

$$EFWH = h = (p/\rho_0 g) + z \tag{A.1}$$

where the term in parentheses is the pressure head, which is calculated by dividing the fluid pressure, *p*, by the weight of the reference fluid, where $\rho_0$ is the density of the reference fluid (freshwater in this case). The second term, *z*, is the elevation of the point measurement with respect to mean sea level.

### Estimation of in-situ formation water densities

Formation water densities were calculated using an equation developed by Chierici (1994):

$$\begin{aligned}\rho_w &= 730.6 + 2.025T - 3.8\times10^{-3}T^2 \\ &+ \left[2.362 - 1.197\times10^{-2}T + 1.835\times10^{-5}T^2\right]p \\ &+ \left[2.374 - 1.024\times10^{-2}T + 1.49\times10^{-5}T^2 - 5.1\times10^{-4}p\right]C,\end{aligned} \tag{A.2}$$

where:

$\rho_w$ is formation water density

*p* is pressure (in MPa) with range of validity 0-50 MPa,

*T* is temperature (K) applicable over 293-373 K

*C* is salinity, valid between 0-300 kg m$^{-3}$

The state equation developed by Chierici (1994) was selected because it was determined to be better suited to the estimation of formation water densities in the Williston Basin. Adams and Bachu (2002) reviewed and compared various equations of state for formation waters and provided some guidelines toward their applicability. An important consideration with respect to the accuracy of the estimates of formation water densities is the specific cationic composition of the brines due to the effects of cations heavier than $Na^{+}$ which are abundant in Williston Basin brines (Benn and Rostron, 1998; Iampen and Rostron, 2000; Khan and Rostron, this issue). The algorithm of Batzle and Wang (1992) would therefore have been most suitable of those reviewed by Adams and Bachu (2002).

The results from equation (A2) were compared to the estimates calculated by the algorithm of Batzle and Wang (1992). The comparison was made by estimating densities based on discretized grids of TDS, formation temperature and pore pressures from a selected aquifer in the study area and cross plotting the density estimates from the two algorithms. The agreement between the density estimates is quite good below densities of approximately 1100 kg $m^{-3}$, above which the equation of Chierici estimates higher values (Figure A-1). To determine which of the two algorithms, if any, would better approximate the specific relationship between formation- water density and TDS in the study area, the density estimates calculated by both algorithms were compared to a linear regression of measured sample densities from our dataset, corrected to in-situ conditions (Figure A-2). The correction of the lab measurements to in-situ conditions was done using the correction of Rowe and Chou (1970). It was found that both algorithms apparently underestimate densities above approximately 1050 kg $m^{-3}$, with the state equation of Chierici of course underestimating by less (Figure A-2). The underestimation is most likely due to the high concentrations of $Ca^{2+}$ ions in the halite saturated brines in the area as well as the occurrence of formation water salinities in excess of 300 kg $m^{-3}$, which is beyond the strict range of validity of the state equation of Chierici (1994). The resultant error in the mapped formation water driving force directions caused by this apparent underestimation of in-situ formation water densities by the state equation of Chierici (1994) was not deemed significant.

**Estimation of density-dependent driving forces**

Darcy's Law for variable density flow systems in three-dimensions aligned along the coordinate axes may be expressed as

$$q_i = \frac{-k_{ij}}{\mu_0}\frac{\mu_0}{\mu}\left[\nabla h + \frac{\rho-\rho_0}{\rho_0}\nabla z\right],\quad i=1,2,3 \tag{A.3}$$

where:

| | |
|---|---|
| $q$ | is specific discharge in the $i^{th}$ direction; |
| $k$ | is the rock absolute permeability tensor; |
| $\mu$ | is dynamic fluid viscosity; |
| $\rho$ | is fluid density; |
| $h$ | is hydraulic head; |
| $z$ | is elevation. |

Subscript $_0$ refers to the reference state at standard pressure and temperature conditions.

For confined flow in a sloping aquifer (Davies, 1987; Bachu, 1995), Equation (A3) can be rewritten as

$$q(x,y) = \frac{-k}{\mu_0}\frac{\mu_0}{\mu}\left[\nabla h + \frac{\rho-\rho_0}{\rho_0}\nabla E\right], \tag{A.4}$$

where *E(x,y)* is the elevation of the confining surface forming the aquifer base. The term in brackets of Equations (A3 and A4) represents the addition of two vectorial terms which give the net driving force acting on formation water at a point. The Water Driving Force (WDF) is calculated by addition of these two vectors (Figure A-3)

$$WDF = \nabla h + \frac{\Delta\rho}{\rho_{fw}}\nabla E \tag{A.5}$$

where:

| | |
|---|---|
| $h$ | is freshwater hydraulic head; |
| $\Delta\rho$ | is density difference between in-situ brine and freshwater; |

$\rho_{fw}$ is density of freshwater;

$E$ is the elevation of the aquifer base.

In situ brine density was calculated over the area using the state Equation (A2), which computes density as a function of total dissolved solids (TDS) and formation temperature. The TDS maps shown in Chapter 2 and Chapter 3 were used, and temperature grids were interpolated from long-duration drill stem test measured values over the study area.

The vectorial addition of Equation (A5) was used to resolve the driving force vector field within each aquifer using discretized grids of the of in-situ formation water density and hydraulic gradients calculated from freshwater hydraulic heads. A computer program developed by Alkalali and Rostron (2003) was used to perform this task.

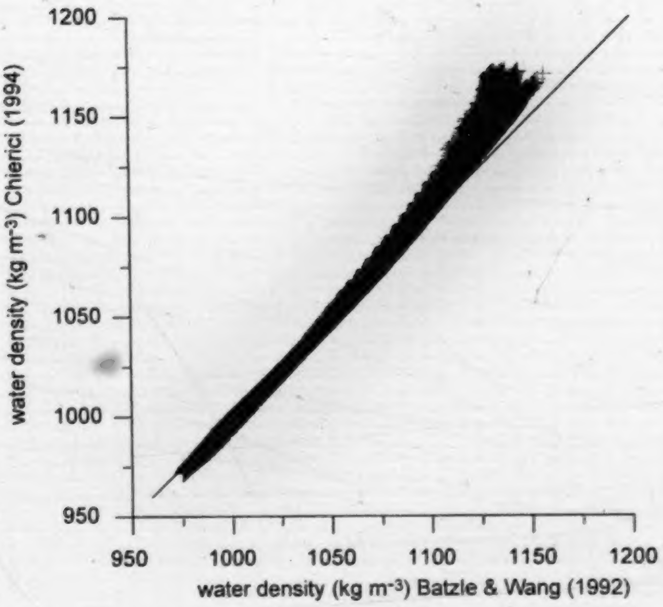

Figure A-1. Crossplot of water density estimates for comparing equations of state

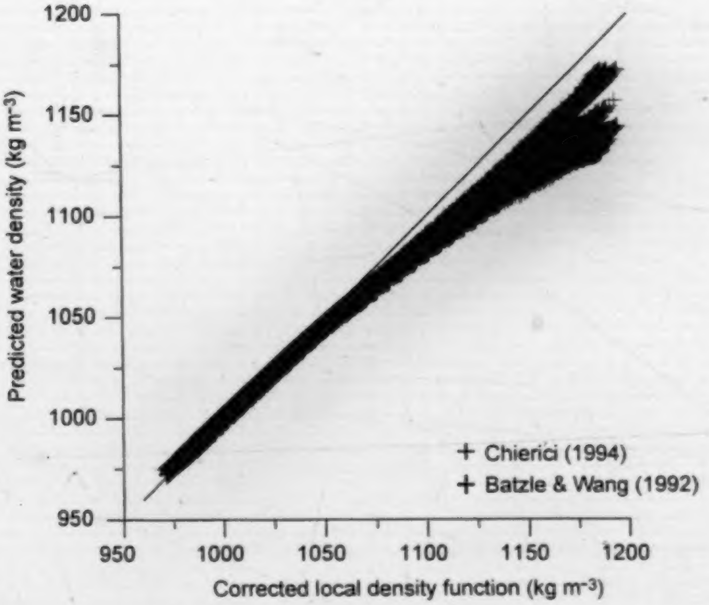

Figure A-2. Crossplots of water density estimates from the two equations of state versus an empirical relation describing density as a function of TDS.

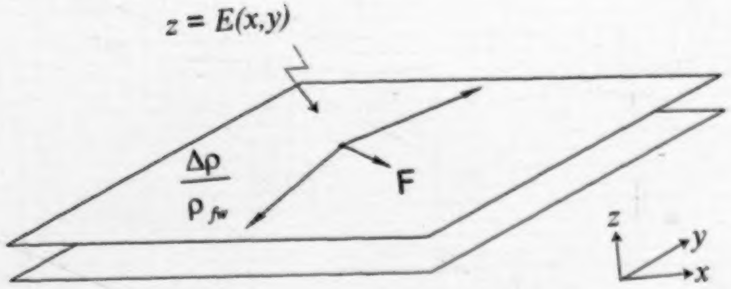
z = E(x,y)
Δρ
ρ_fw
F
z
y
x

Figure A-3. Schematic depicting the analytical calculation of formation water driving force

# APPENDIX B

## Additional details on the construction and implementation of the gradient-free algorithm

## APPENDIX B: Additional details on the construction and implementation of the gradient-free algorithm

Gradient-based optimization methods are based on the evaluation of the gradient, $g(\theta)$ of a loss function, $L$ with respect to the parameters, $\theta = [k_1, k_2, \ldots, k_M]^T$ such that

$$g(\theta) \equiv \frac{\partial L}{\partial \theta} = \begin{bmatrix} \partial L/\partial k_1 \\ \partial L/\partial k_2 \\ \vdots \\ \partial L/\partial k_M \end{bmatrix}, \tag{B.1}$$

where $M$ is the number of parameters.

In the original SSC formulation of Gomez Hernandez et al. (1997), $g(\theta) = \partial L/\partial \theta$ is evaluated based on a linear approximation of the model response about the parameters, such that the following global minimization problem is formulated:

$$L(\theta) = \sum_{j \in (n_p)} w_j \left(h_j^0 - h_j^{lin}\right)^2, \tag{B.2}$$

where the vector $\{h^{lin}\}$ is computed as a truncated series about the parameter perturbations,

$$\left\{h^{(lin)}\right\} = \left\{h^c\right\} + \sum_{i=1}^{N} \left[ \frac{\partial}{\partial \Delta \ln(k)_i} \{h\} \cdot \Delta \ln(k)_i \right]. \tag{B.3}$$

The evaluation of $g(\theta)$ thus depends on the calculation of the Jacobian matrix.

The two key elements of the gradient-free formulation are: (1) the approximation of the elements of the Jacobian matrix,

$$\hat{s}_{l,j} \approx \partial\{h\} / \partial\Delta\ln(k)_i, \tag{B.4}$$

and (2) a corresponding approximation of the model gradient:

$$\hat{g}_l\left(\hat{\theta}_l\right) = \begin{bmatrix} \dfrac{L\left(\hat{\theta}_l \pm c_l\Delta\right)}{c_l\Delta_1} \\ \vdots \\ \dfrac{L\left(\hat{\theta}_l \pm c_l\Delta\right)}{c_l\Delta_M} \end{bmatrix} \tag{B.5}$$

The numerator in the elements of Equation (B5) represents the value of the loss function at the $l^{th}$ iteration of the SPSA optimization routine. The form of the loss function used for the gradient-free approach is:

$$L(\theta)_j = \left|h_j^{lin} - h_j^{o}\right| \tag{B.6}$$

where

$$h_j^{lin} = h_j^{c} + \sum_{i=1}^{M}\left[\ln(k)_i \pm c_l\Delta_{ij}\right] \tag{B.7}$$

Note that the loss function is minimized for each $j^{th}$ calibration location rather than globally, as in Equation (B2).

Equations (B5) and (B6) parallel equations (B1) and (B2) with the exception that a multi-objective formulation (Equation B6) is adopted in the gradient-free algorithm. The relationship between Equations (B3) and (B7) is explained in the text of Chapter 6.

The basis of the gradient-free approach is the Simultaneous Perturbation Stochastic Approximation (SPSA) optimization routine. SPSA is a stochastic approximation technique[1], which is a class of algorithms suited to measurements of loss functions corrupted by noise, or those that are too expensive to evaluate (Spall, 2003). In the present context, the loss function (Equations B6 and B7) is inexpensive, and although the loss function may contain noise[2], it is assumed to be noise-free in the development of the gradient-free method for inverse conditioning. This is because the approximate direction of the gradient, $\hat{g}_l\left(\hat{\theta}_l\right)_j$, is always known when a multi-objective formulation is adopted, as explained in the text (Figure 6.4; Tables 6-1 and 6-2).

In the original SPSA formulation, $\Delta$ is a vector of $M$ mutually independent random variables $\{\Delta_1, \Delta_2, \Delta_3, \ldots, \Delta_M\}$ following a probability distribution that satisfies certain convergence-dependent conditions related to finite inverse moments for the elements of $\Delta$, as given in Spall (1992, 2003). The recommended choice of distribution of $\Delta$ is symmetric Bernoulli (±1). Note that this is approximately the form of the row vectors of the approximate sensitivity matrix, and the sensitivities play the role of the SPSA perturbation vector, $\Delta$..

SPSA may use one or two function evaluations at each iteration to approximate the gradient, $\hat{g}_l\left(\hat{\theta}_l\right)$, depending on whether a one-sided SPSA gradient formulation is adopted (Equation B5) or the standard two-sided form (Spall, 2003; p. 178) is used, respectively.

The key algorithmic "trick" in the present implementation is that: based on the sign of the head mismatch at the calibration location for which we are evaluating $L(\theta)_j$, the approximate direction of the gradient, $g(\theta)$, is known. It follows that the appropriate (binary) choice of the function evaluation, $L\left(\hat{\theta}_l \pm c_l\Delta\right)$, is selected based on the additional information contained in the sign of the vector of (±1) sensitivity indicators, which comprise the vector $\Delta$.

---

[1] Although the gradient-free method for inverse conditioning does not take advantage of the stochastic element of SPSA, since it is not needed in the present context, the flexibility of the approach is enticing, for example, in integrating large data sets of differing quality, and different types of measurements. Taking advantage of the stochastic element of SPSA would simply involve the adoption of the standard two-sided gradient approximation (Spall, 2003) for some (but preferably not all) of the loss function evaluations.

[2] Sources of noise include data errors, discretization errors and other modeling-related errors.

A critical consideration for convergence[3] is the specification of appropriate gain sequences for $c_l$ and $a_l$ (with the context of $a_l$ given in Equation (6.7) in the text). As stated in the text, these positive scalar sequences of coefficients behave like relaxation factors: $c_l$ relaxing the integer-valued elements of $\hat{s}$ to similar magnitudes of the elements of the Jacobian matrix, and $a_l$ limiting the updating step size. The critical sensitivity information: the identification of the parameters with non-negligible sensitivity and the sign on the sensitivity coefficients, is established with reasonable accuracy in the approximation, as shown in Chapter 5. No automated calibration algorithm is free of user-specified tuning parameters to ensure convergence. The choice of appropriate values for the parameters specifying the gain sequences ($c_l$ and $a_l$) should be based upon the recommendations in Spall (1992, 2003). This should be followed by an examination of the final values of the parameter perturbations, $\{\Delta\theta\} = \left(\hat{\theta}_L \pm c_L \Delta\right)$, where $L$ is the counter value at the final SPSA optimization iteration. It is then possible to adjust one or more of the parameters controlling the gain sequences to achieve appropriately-sized perturbations to the parameters for a given problem.

In addition to the control offered on the magnitude of the parameter perturbations described above, it is generally necessary for plausibility considerations to impose hard constraints on the minimum and maximum allowed perturbations. The approach taken here was to simply define constraint intervals based on the histogram of ln($k$), such that

$$\Delta\theta_{\min} \leq \Delta\theta \leq \Delta\theta_{\max} \qquad \text{(B.8)}$$

with

---

[3] There are other specifications that will affect performance of the algorithm, but, in general, will have much less of an effect on convergence than the specification of appropriate gain sequences.

$$\Delta\theta_{\min} = m_{\ln(k)} - \alpha_1\sigma_{\ln(k)}\,;\ \Delta\theta_{\max} = m_{\ln(k)} + \alpha_2\sigma_{\ln(k)} \tag{B.9}$$

where $m_{\ln(k)}$ and $\sigma_{\ln(k)}$ are the mean and standard deviation of the ln(*k*) histogram, respectively, and $\alpha_1$ and $\alpha_2$ are factors defining the widths of the constraint intervals. In the case that static conditioning data are used to construct a conditional ln(*k*) model for the initial fields, the kriged estimate and local kriging standard deviations would be used (Gomez-Hernandez et al., 1997) instead of the global statistics.